PREFACE

I would like to offer the reader the following report on the scientific activity of the Frank Laboratory of Neutron Physics (FLNP) of the Joint Institute for Nuclear Research (JINR) in 1999. The report consists of two parts. The first is a brief review of the results of experimental and theoretical investigations in condensed matter physics, nuclear physics and applied research. The second contains experimental reports with more information about particular studies. The list of the 1999 publications closes the book.

In 1999 the IBR-2 reactor operated according to the approved working schedule, all of the 8 planned IBR-2 cycles were conducted. In the autumn cycles of the IBR reactor a physical startup of a solid methane-based cryogenic moderator was accomplished and all its rated regimes tested. This completed successfully many-year work of the technical departments of the laboratory.

In 1999 we succeeded in carrying out the IBR-2 modernization project to a large extent. A JINR-MINATOM (Ministry of Atomic Energy of Russia) agreement was signed. Following its terms MINATOM will take part in the reactor modernization project. A new working schedule of the project is elaborated.

A positive tendency in the financing of the IREN project is noted.

V.L.Aksenov

Director

1 March 2000

1.1. CONDENSED MATTER PHYSICS

Late in 1998 the Condensed Matter Physics Department (CMPD) was reorganized with the aim of concentrating effort on scientific activity itself. Diffraction, small angle scattering, inelastic scattering, and neutron optics continued to be the basic neutronographic methods used by CMPD members to carry out experiments with the IBR-2 spectrometers. During the year there were eight reactor cycles at a mean power of 1.5 MW. As in the past few years the beam time was distributed on experts' recommendation based on submitted proposals and long-term agreements for cooperation. The 1999 list of spectrometers operating in the user mode included 10 instruments: HRFD, DN-2, DN-12, SKAT, YuMO, SPN, REFLEX-P, KDSOG, NERA, and DIN. Several experiments were conducted with the spectrometer TEST in channel 6B.

By spring 1999 laying of a neutron-guide for carrying out diffraction measurements of residual stresses in large-volume products on the new Fourier diffractometer FSD had completed. In May 1999 neutron beam profiles were measured at the exist of the mirror neutron guide and at the sample position. The obtained absolute fluxes appeared to be close to expected. In 1999, a biological shielding was laid and a Fourier chopper manufactured using an improved technology was installed on FSD. In April 2000, the first stage of the FSD detector system and the FSD correlation electronics will start operation. After that regular measurements with FSD will begin.

A smooth transition of the detecting and control electronics of the neutron spectrometers to VME standard continued. During the year the new electronics of another two spectrometers, FHRD and YuMO, was commissioned. It allows essential automation of the experiment, including remote control. In particular, the new software for YuMO is a multiwindow system that controls motors, temperature, and experimental data acquisition.

1. Methodological. In the operating Fourier diffractometer HRFD (IBR-2 channel 5) the rotor and stator of the Fourier chopper were replaced by new ones analogous to those installed in FSD. Contrast measurements of the new system showed that the contrast had grown to a value of 20 (about 3 times). This improves considerably the quality of the registered diffraction spectra. In the high pressure diffractometer DN-12 a closed-cycle refrigerator-based cryostat is put into operation to conduct measurements under simultaneous action of low temperatures down to 12 K and high pressures up to 7 Gpa. The first scientific experiments were carried out.

On the polarized neutron reflectormeter REFLEX-P test experiments of the inelastic scattering mode were performed. The mode is designed to carry out investigations of the inelastic interaction of neutrons with surface excitations in thin films. The spectrometry of the scattered neutrons is conducted in the direct geometry with a fast chopper in front of the sample for the monochromatization of the incident beam (Dl/l=0.04/l). Experiments to investigate a Ni/Ti thin film and a FeCo/TiZr supermirror showed that this direction of the physics of thin films is a promising field of research with the reflectometer REFLEX-P.

For the spectrometer DIN-2PI, assembling of control systems for the thermostat TS3000 which will make it possible to investigate materials at temperatures to 3000 K started.

In the reported year most important was the testing of a cryogenic methane moderator (CM) which was installed in October 1999 on the side of beams 4 (YuMO), 5 (DN-2), and 6 (HRFD). During the followed three reactor cycles information about the CM parameters was obtained. **Figure 1** illustrates the obtained spectra of scattering on vanadium for three different states of the moderator: with methane at 30 K or 60 K, with an empty chamber and a water premoderator, T=300 K. In addition to the shifting of the maximum in the spectrum in the direction of larger wavelengths with decreasing temperature, it is characteristic of the CM spectrum to have a strong eating-away in the region of the Be-boundary (l=3.96, 3.58, and 3.46 E) due to the moderator design. In the warm state, i.e. without methane, CM is inferior to a standard grooved moderator (GM) especially at wavelengths lower than 4 E where the score is 1 to 3. In the cold state CM gives a considerable gain in comparison with GM: at T=70 K starting from l=2 E and at T=30 K starting from l=3 E (**fig. 2**).

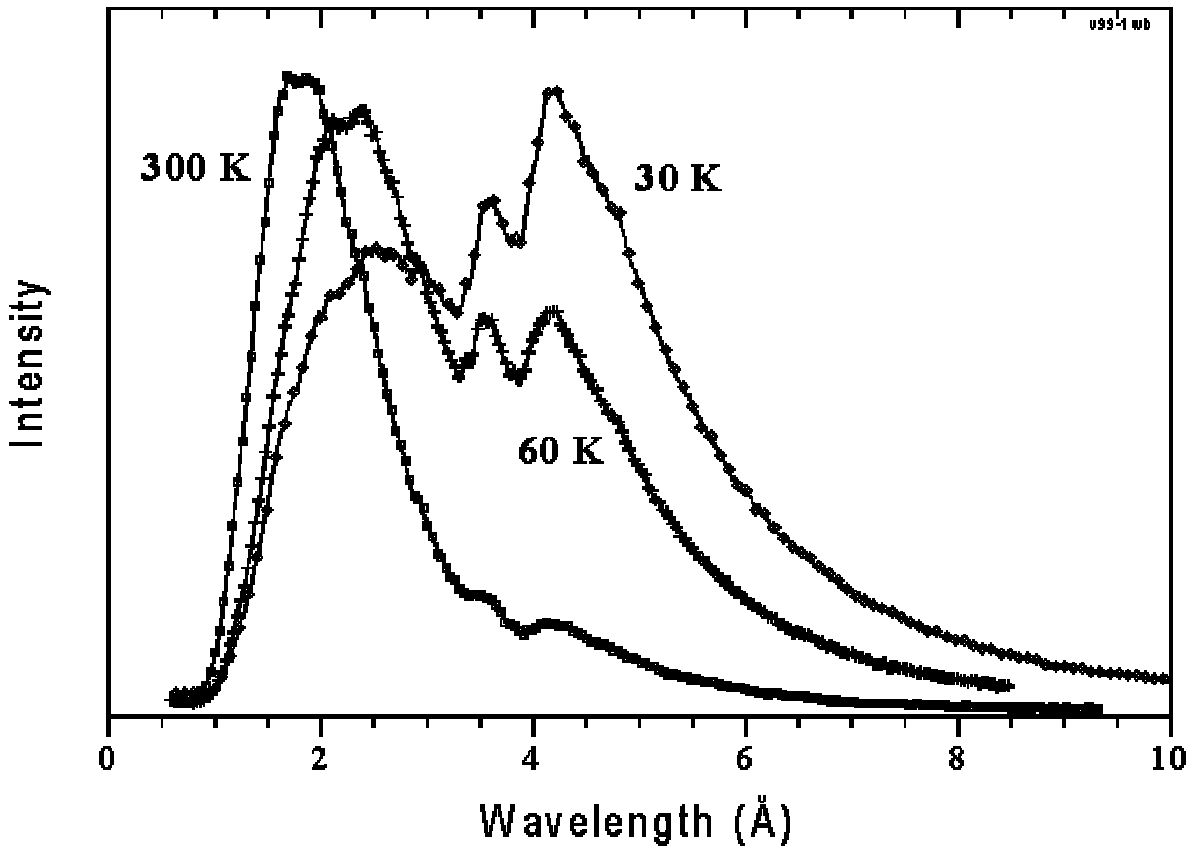

Fig.1. *The spectra registered with HRFD using the detector D1 for three different states of the moderator: T=60 K, 30 K, and 300 K (empty chamber, water premoderator).*

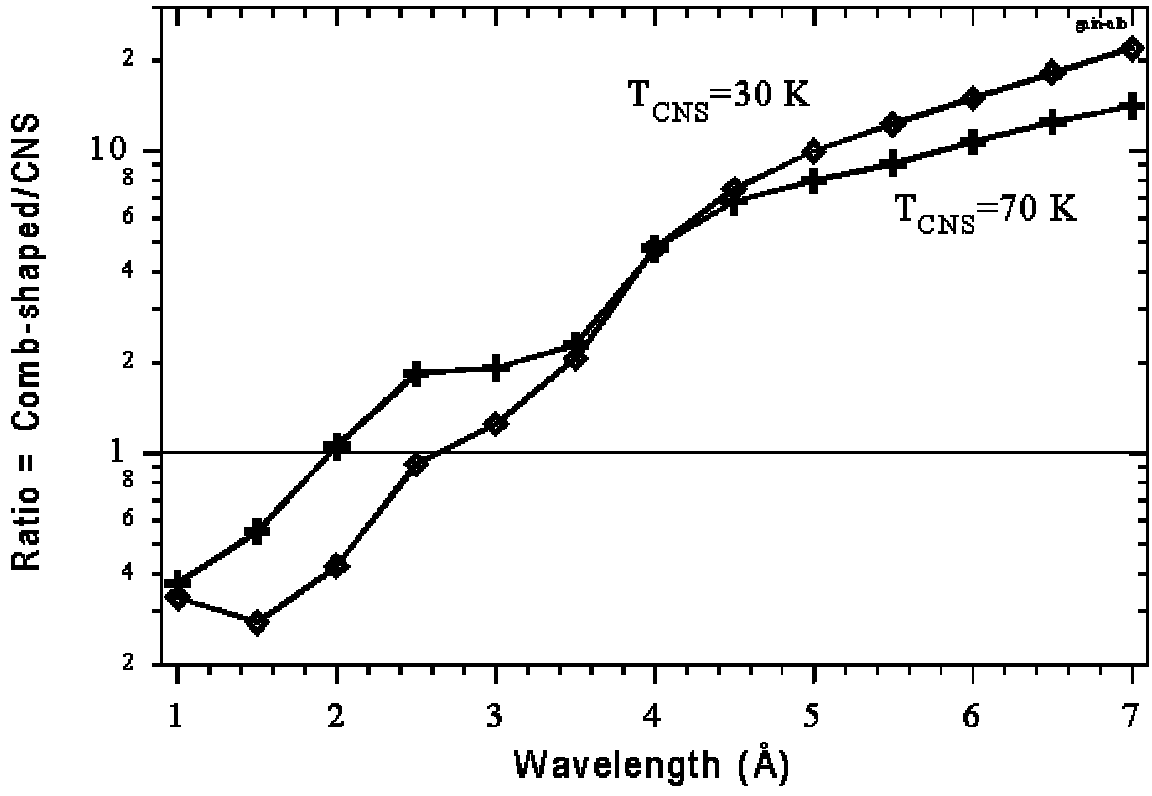

Fig.2. *The coefficient of gain (loss) at transition from a grooved moderator (300 K) to CM (30 K or 70 K) as determined from scattering on Al_2O_3 or V.*

The most detail data on CNS parameters were obtained with HRFD. Their analysis prompted the following conclusions.

- Problems solved with the diffractometer HRFD or DN-2 can be **optimally divided** between experiments with the moderator in the warm or cold mode.
- **The cold moderator makes it possible** to study effectively low-symmetry structures with a unit cell volume of ~500 E as well as magnetic and long-period structures using HRFD.
- The moderator temperature 70 K **is optimal** for the solution of the enumerated problems.

As to small angle neutron scattering investigations of macromolecular systems in solutions (e.g., ribosomes) the cold moderator will also make it possible to start experiments that have been thought unfeasible at IBR-2 so far.

2. Scientific. In the 1999 scientific program for the IBR-2 spectrometers many of the performed investigations continued the themes that had become traditional for the Laboratoryr. In the past three years a program of investigations of a $HgBa_2CuO_{4+}$d (Hg-1201) mercury-containing superconductor was carried out on the diffractometers HRFD and DN-12. It was precision investigations of the structure of the compound and how it changes under the action of high pressure at varying d or substitution of stoichiometric oxygen by fluorine atoms. In 1999 on HRFD a third member in a series of mercury-containing superconductors, $HgBa_2Ca_2Cu_3O_{8+d}$ (Hg-1223), was investigated in the condition when the main part of superstoichiometric oxygen was replaced by fluorine. The synthesis and certification of Hg-1223 were made in E. V. Antipov's laboratory of the Chemistry Chair of MSU. It is shown that a record temperature of the superconducting transition of 134 K obtained in oxygen-containing compounds increases to 138 K as fluorine is implanted. Another effect of fluorine doping is a noticeable decrease of the distance between copper and oxygen atoms in the conducting planes (CuO_2) without any increase in their corrugation. Finally, a neutronographic experiment made it possible to determine reliably the existence of atoms of stoichiometric fluorine in the center of the basis plane (HgO) and on the sides (*a*, *b*) of the cell. The latter may be related to partial substitution of mercury by copper atoms. (See Experimental Reports).

In 1998, a RRC Kurchatov Institute-MSU-FLNP collaboration conducted a series of experiments to determine the magnetic structure of a series of compounds, $(La_{1-y}Pr_y)_{0.7}Ca_{0.3}MnO_3$, in which earlier there was observed a giant isotopic effect exhibiting itself as a change of the transport state (metal-dielectric) at low temperatures on substitution of oxygen isotopes (^{16}O by ^{18}O). In 1999, systematic structural data depending on the temperature and the mean radius of the A-cation were obtained for the series. An analysis of the data showed that mean values, such as the volume of a unit cell, the length of the bond <Mn-O>, and the valence angle <Mn-O-Mn> are linear functions of the Pr content or the mean radius of the A-cation, which is the same. The transition temperature to the metallic ferrmomagnetic state is also a linear function of the angle <Mn-O-Mn> (**Fig. 3**). One of the main goals of the work was to determine the structure of two samples with y=0.75 (LPCM-75) and different concentrations of ^{16}O and ^{18}O isotopes. A HRFD precision experiment made it possible to demonstrate that over the interval from room temperature to the transition temperature of samples with ^{16}O to the metallic ferromagnetic phase, $T_{FM,\ O\text{-}16}$, the investigated samples are identical not only in the parameters of the unit cell but also in the structure parameters, such as interatomic bond lengths and valence angles (**Fig. 4**). Reliable evidence of the fact that an essential difference in the transport and magnetic properties of the isotopically enriched samples LPCM-75 at $T < T_{FM,\ O\text{-}16}$ is due to different dynamics of oxygen atoms and as a result, unusually strong electron-phonon interaction was first obtained. (See Experimental Reports).

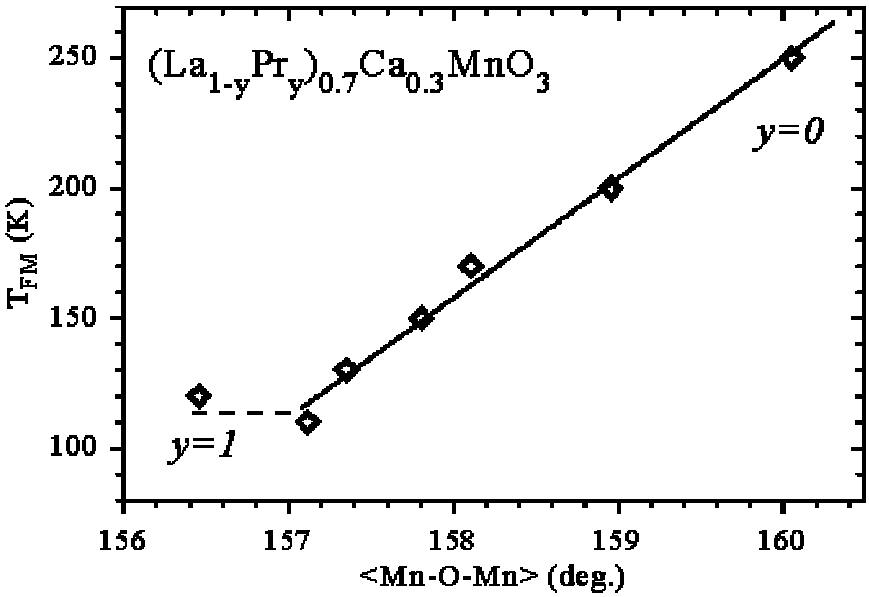

***Fig. 3**. The dependence of the temperature of the establishment of the far-range order FM on the mean value of the valence angle Mn-O-Mn.*

As soon as materials with a colossal magnetic resistance effect are interesting from the viewpoint of both fundamental and applied research, seeking new manganese oxide-based compounds is topical. In 1999 in E.V.Antipov's laboratory (Chemistry Chair, MSU) a Ca_2GaMnO_{5+}d compound with a layered structure was first synthesized. In a neutronographic experi-ment conducted with the diffractometer DMC (SINQ) it was shown that compounds with the oxygen index 5.04 experience antiferromag-netic ordering below 150 K (**Fig. 5**) and the direction and value of the magnetic moments of Mn atoms were determined.

Helicoidal magnetic ordering in a Tb monocrystal was studied with the diffractometer DN-2. The aim was to investigate the influence of external axial of stretching on the spiral period and the intensity of satellite diffraction peaks. First, the temperature dependence of the magnetic structure was studied. **Figure 6** illustrates the temperature dependence of the vector of the spiral at normal pressure and it is seen that helicoidal ordering in Tb exists just in a narrow interval of temperatures, between 225 K and 231 K. Further measurements of the dependence of magnetic ordering on external axial stretching showed that the spiral disappears as the stretching gets larger than 400 bar. It is a strong argument for the assumption that the ordering depends on the form of the Fermi surface in metals which can be modified by external action.

On the diffractometer DN-12 there continued experiments to investigate the effect of high pressures on the structure of ammonium halides, particularly ND_4I, and search a possible structural transition at high pressure in SmB_6 In the latter case, experimentalists managed to observe anisotropic broadening of some diffraction peaks and even splitting of them which confirms the existence of the phase transition. To obtain more detail information, an experiment was conducted with the diffractometer POLARIS at the ISIS source. In the experiment to investigate the «electron» high temperature superconductor Nd_2CuO_4 structural changes and an accompanying interlayer transition of the charge at an external pressure up to 5Gpa were studied. A comparison of the contraction of separate interatomic distances in Nd_2CuO_4 with the contraction in «hole» superconductors revealed noticeable diffferences (See Experimental Reports).

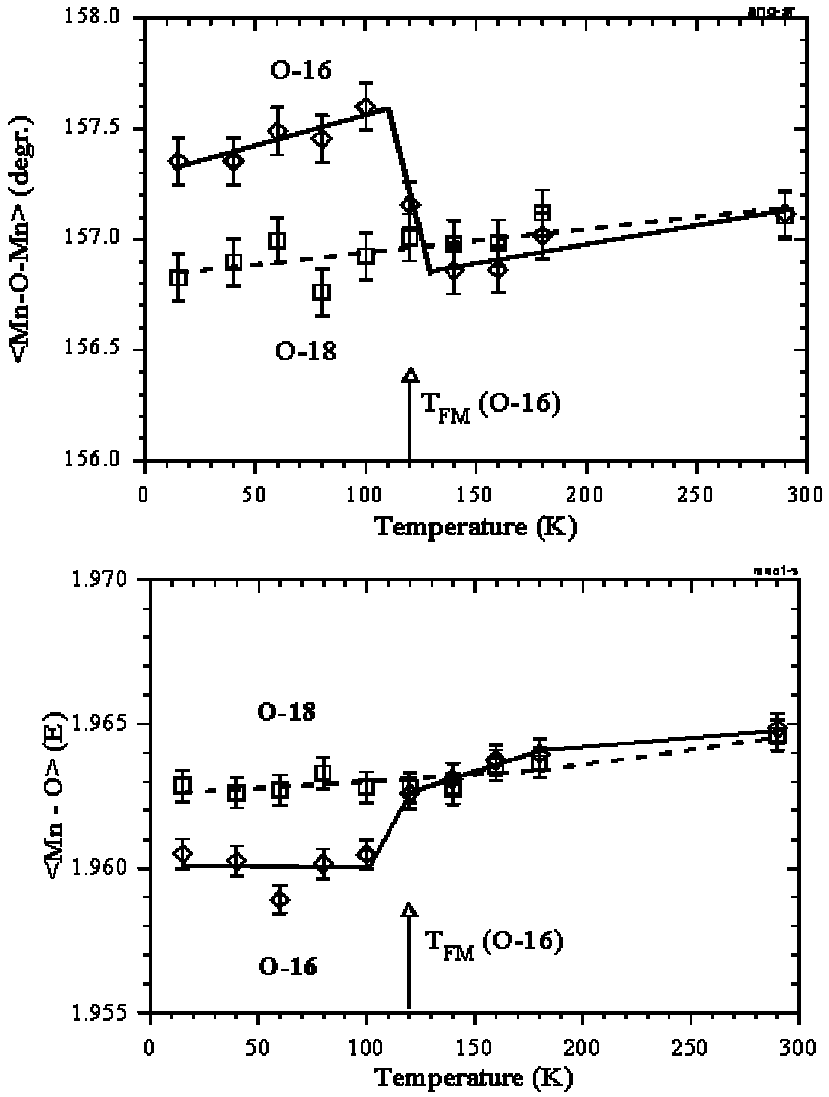

Fig.4. *A comparison of the temperature dependence of the mean length of the bond <Mn-O> (bottom) and of the mean valence angle <Mn-O-Mn> (top) for the samples* $(La_{0.25}Pr_{0.75})_{0.7}Ca_{0.3}MnO_3$ *with* ^{16}O *or* ^{18}O *isotopes. The arrow marks the transition temperature of the sample with* ^{16}O *to the FM-state.*

In 1999 the small angle diffractometer YuMO was intensely used to conduct investigations in different fields of biology, physics and physical chemistry. Also, experiments to study colloidal systems, polymers and solve problems in materials science were conducted. In particular, investigations of the behavior of surface-active substances under different conditions continued. In collaboration with Bayreuth University (Germany) the behavior of rod-like micelles in TMDMAO molecules was studied at different pressures and temperatures. Pressure-induced phase transitions at 280 K and 249.9 K were discovered. The difference between the chemical potentials of monomers in the edge and cylindrical parts of spherical-cylindrical micelles was determined. The difference between the chemical potentials of the monomers was determined.

Another example is a collaboration with the University of Utrecht (The Netherlands) for the investigation of a triple system, monoglyceride/dicedylphospate/water (MSG/DCP/water). It is of interest from the viewpoint of biology, the physics of accidental surfaces, and applied purposes (monoglycerides are basic alimentary emulsifiers). It is shown that even small amounts of charged lipid dicedylphosphate destroy an «infinite» bicontinuous minimal surface organized in an ordered cubic structure of the two-component system MSG/water. Topological and phase transitions were discovered in a wide temperature range of 10°C to 90°C for different mole ratios, MSG/DCP (19:1, 9:1,4:1), and lipid concentrations (DCP) in water (1, 10, 20, or 30 weight percent). An interesting effect was discovered:
polydispersion samples transformed into monodispersion ones. The influence of an air-sample interface on the properties of the given colloidal system was first proved.

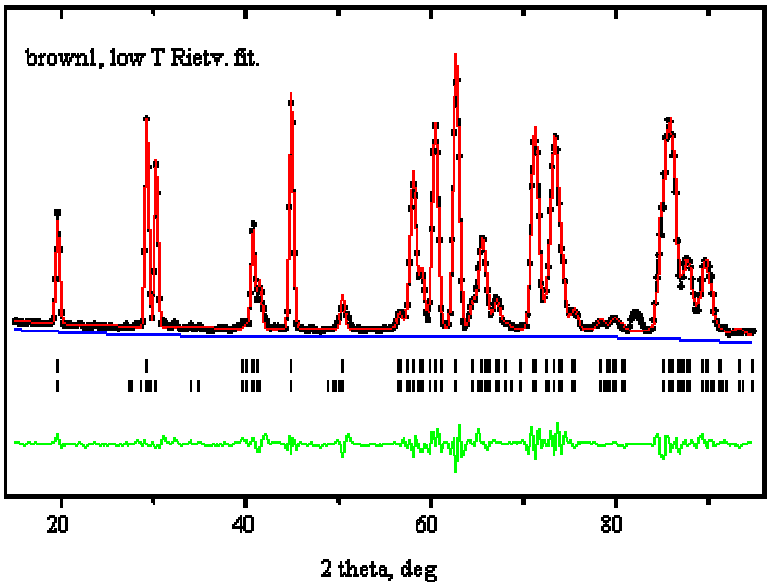

Fig. 5. *The diffraction spectrum of a* $Ca_2GaMnO_{5.04}$ *powder measured at T=12 K. Processing by the Rietveldt method is carried out taking into account the AFM-phase (the lower row of lines).*

An example of small angle neutron scattering investigations of biological systems is the study of purple membranes of (PM) of *Halobium Salinarium* bacteria. In experiments conducted together a research center in Juelich (Germany) there were discovered photo-induced changes in the structure of dopcyne (BR) protein, the only protein in PM. It is the very protein that catches a quantum of light and uses its energy to transport proton in an anti-electric potential gradient direction. The proton transport whose mechanism is not quite clear yet is a key element in the bioenergetics of cells. The conducted small angle scattering investigations showed that the polar part (loop) of BR is involved in proton transport-accompanying structural changes of the protein.

Systematic small angle neutron scattering studies of the properties of polymer systems started for the first time with YUMO. They were performed in collaboration with A. P. Khokhlov's laboratory of MSU. In particular, polymer gels with implanted surface-active substances were studied. For example, fractal arrangement of sodium dodecylsulphate (SDS) in a grid polymer from diallyldimethylammoniumchloride was discovered.

Investigations of layered structures continued on the spectrometer of polarized neutrons SPN using new experimental techniques - the observation of neutron standing waves and of neutron beam splitting at magnetization direction noncolinear with the interface of media. As a result, in the system Fe(1000 E)/Gd(50 E) there was observed triple spin-flip of the reflected neutrons (**Fig. 7**) and this was interpreted as neutron spin-flip at transmission through two domain walls enveloping the magnetic domain. To verify the hypothesis, model calculations will be carried out.

The most interesting result obtained with the reflectometer of polarized neutrons REFLEX was a new estimate of the upper limit of the neutron coherent wavelength manifesting itself in the process of neutron specular reflection from thin films. The experiment consisted of precision measurements of the reflection curve R(l) from a thin film of Cu (~1800 E) on a glass substrate and its description with an analytical function. It appears that the quality of the reflection curve description improves essentially as one introduces in the formula for R - parameter which in particular, can be interpreted as a quantity related to the coherent properties of the neutron wave. In this interpretation the estimate of the neutron coherent wavelength is 1.5 mm which is approximately 8 times larger than published earlier in the literature. In any case, the experiments showed that the description of precision reflectometric data should be modified and this may be important for their interpretation in a number of cases.

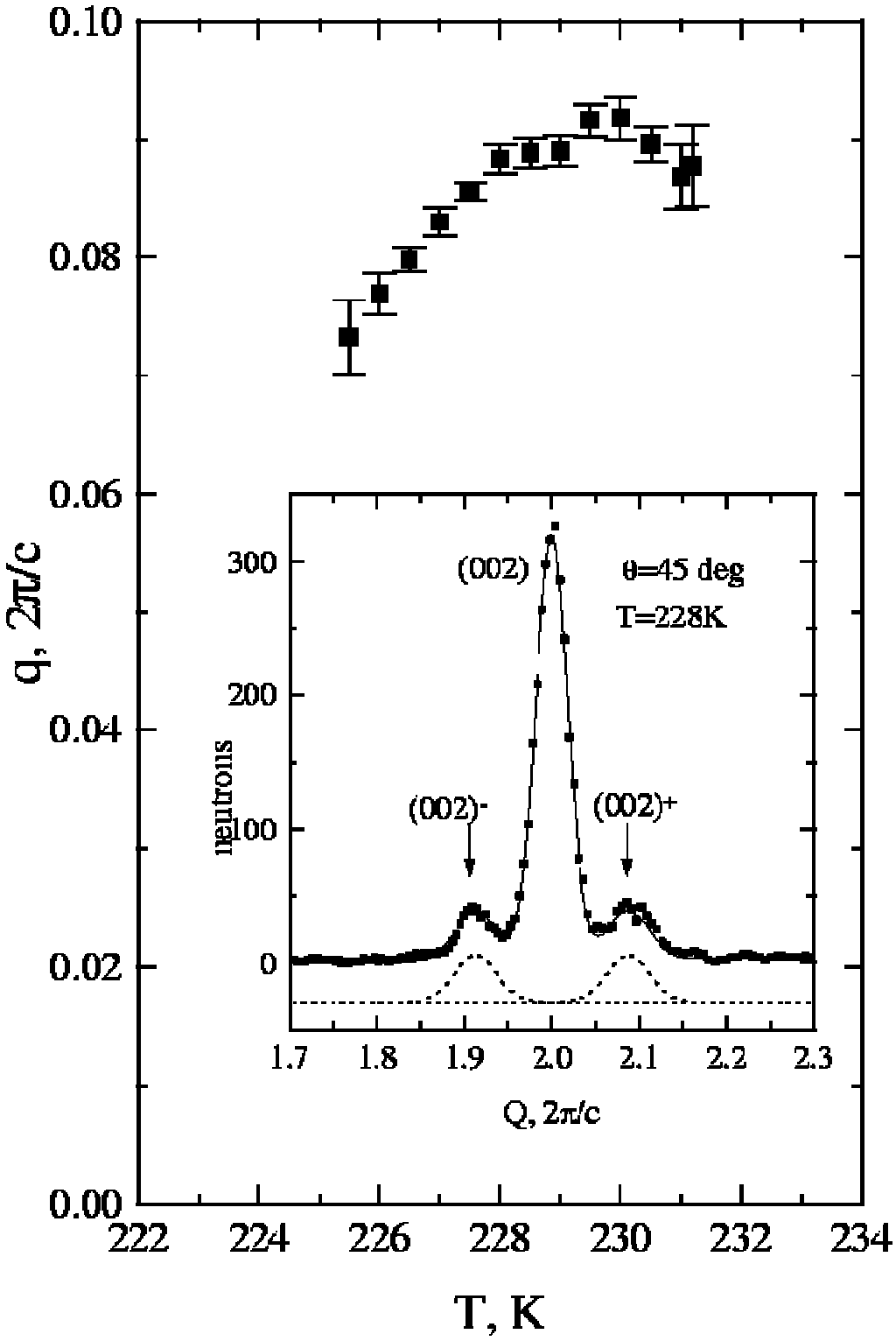

Fig.6. *Temperature dependence of helicoid magnetic structure in Tb. Helicoid arrangement exists only in narrow temperature diapason from 225 to 231 K. A typical part of diffraction spectra are shown in the inset.*

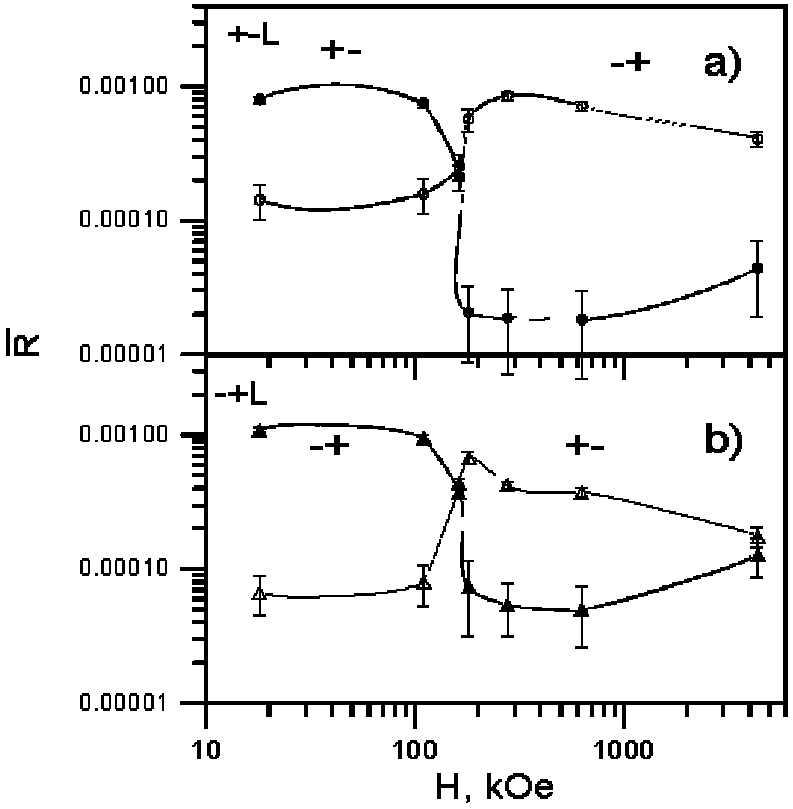

Fig. 7. *The dependence of the neutron reflection coefficient R on the external magnetic field H for «+-« and «-+» spin transitions, «+-L» and «-+L» spin transitions in a local surface magnetic field.*

The main direction of research on the inverse-geometry spectrometer NERA-PR was the investigation of the dynamics of ammonium groups and their influence on structural phase transitions in ammonium salts. In particular, in 1999 there continued experiments to study $Rb_{1-x}(NH_4)_xI$, $K_{2-x}(NH_4)_xSeO_4$, $LiRb_{1-x}(NH_4)_xSO_4$, and $Rb_{1-x}(NH_4)_xMnF_3$. Transitions to a proton (orientational) glass phase at low temperatures and a transition to the ordering of ammonium groups with increasing concentration of ammonium were investigated. The crystalline-to-glass phase transition in solid methanol phases CH_3OH, CH_3OD, and CD_3OH, i.e., for different numbers of deuterium atoms in the molecule, were also investigated.

An extended program of experiments was carried out with the DIN-2PI spectrometer. In particular, investigations of water solutions to reveal the effect of dissolved particles on the microdynamics of water molecules entering into the hydrate spheres of the particles continued. Detail knowledge of the phenomenon which has been given the name of hydration is essential in the physics of solutions lying in the basis of the most important directions of chemistry, biology, and related sciences. Constantly growing interest in hydrophobic effects is practical and comes from the role they play in the organization and functioning of the most important biological structures (cell membranes, proteins, etc.) and of surface-active substances (micelles, emulsions). An analysis of DIN-2PI experiments shows that in contrast to small ions (Li^+ and Cs^+) large apolar particles do not destroy the grid of hydrogen bonds in their surrounding water. The next step to the understanding of the discussed phenomena is to search a relationship between the obtained microscopic information and the known macroscopic thermodynamic hydrophobic effects.

Also, low-frequency vibrational modes of atoms in the normal and superionic phases of PbF_2 at T=293 or 823K were investigated with DIN-2PI. The obtained data provide evidence in favor of a liquid-like state of the anion sublattice in the superionic phase of PbF_2 the nature of collective excitations of which is different from classical liquids. At the same time, investigations of hydrates, including the system $Zr\text{-}H_x$ (x=0.38-0.80) in particular, continued. In samples with a low hydrogen content in the energy transfer interval 2-10 meV the system exhibits low-frequency excitations possibly connected with tunneling or resonance effects in the dynamics of hydrogen atoms in a-Zr.

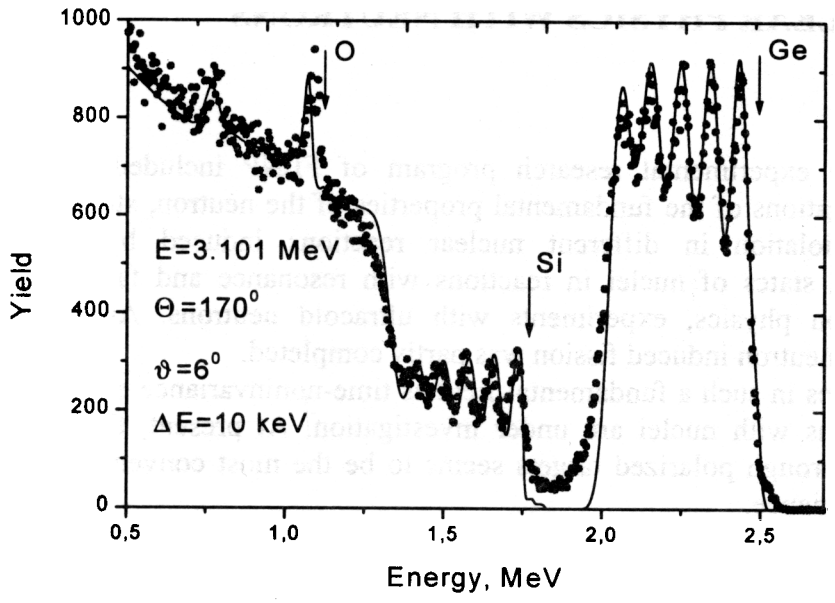

Fig. 8. The experimental (points) and calculated (line) RBS spectra for a 10-layer Si/Ge structure. The layer thickness: Si-23nm, Ge-13nm. The presence of oxygen in the layers is also detected (13 atomic %).

The conducted applied research was mainly the investigation of internal stresses in large-volume products with the spectrometers HRFD and EPSILON, of rock textures with the spectrometer SKAT, and the application of diagnostic methods at an ion accelerator (see Experimental Reports). The important feature of the 1999 year is the beginning of real cooperation with several industrial plants in Russia which approached the Laboratory on the matter of conducting internal stress investigations of key parts in different machines. Investigations of Ge/Si layered structures aimed, in the main, at the determination of the amount and positions of oxygen in the layers continued at the accelerator EG-5 under the auspices of the program «Ion Beams for the Certification of Semiconducting Materials» with the support of IAEA (fig.8).

Scientific program of the Condensed Matter Physics Division in 1999 was executed in cooperation with the following institutes and organizations

Bulgaria	University; Institute for Nuclear Research and Nuclear Energy (Sofia)
Czech Republic	Polytechnical Institute (Prague)
Egypt	Atomic Energy Authority of Egypt (Cairo)
Finland	Technical Center (Espoo)
France	Laboratoire Leon Brillouin (Saclay); Institut Laue-Langevin (Grenoble)
Georgia	University (Tbilisi)
Germany	Hahn-Meitner Institute (Berlin); Research Center (Rossendorf); University (Bayreuth); Technical University (Kemnitz); Research Center (Darmstadt); GKSS (Geesthacht); Fraunhofer Institute for Nondestructive Testing (Dresden-Saarbruecken)
Hungary	Research Institute for Solid State Physics (Budapest)
D.P. Republic of Korea	University (Pyongyang)
Poland	Institute of Nuclear Physics (Cracow); University (Poznan)
Romania	Atomic Physics Institute (Bucharest)
Russia	Kurchatov Institute; Institute of Solid State Physics; Institute of Theoretical and Experimental Physics; Petersburg Nuclear Physics Institute; Institute of Physics of Metals; Moscow State University; Institute of Crystallography; Physical Energetical Institute (Obninsk); Institute of Nuclear Physics RAS
Slovakia	University (Bratislava)
Sweden	University (Goteborg)
Switzerland	Paul Scherrer Institute (Villigen); ETH Zentrum (Zurich)
U.K.	Rutherford Appleton Laboratory (Abingdon)
Uzbekistan	Institute of Nuclear Physics (Tashkent)
Vietnam	Institute of Physics (Hanoi)

1.2. NUCLEAR PHYSICS WITH NEUTRONS

1. Introduction

In the reported period, the experimental research program of FLNP included traditional directions: experimental investigations of the fundamental properties of the neutron, studies of the processes of spatial parity violation in different nuclear reactions induced by neutrons, investigations of highly excited states of nuclei in reactions with resonance and fast neutrons, astrophysical aspects of neutron physics, experiments with ultracold neutrons. An extensive program of studies in resonance neutron induced fission was partly completed.

Also, experimental approaches in such a fundamental field as time-noninvariance effects in the interaction of resonance neutrons with nuclei are under investigation. At present, the study of polarized neutron propagation through polarized targets seems to be the most convenient way of direct tests of time-reversal invariance.

Applied research in the field of neutron activation analysis (NAA) and also, a methodological development of neutron and gamma detectors of different types were conducted.

The main part of these investigations was carried out on seven neutron beams of the IBR-30 booster, the first and eleventh beam of the IBR-2 reactor, and the experimental facility "Regata" for neutron activation analysis at IBR-2. At the same time, a number of works were conducted in collaboration with the nuclear centers of Russia (RRC KI, ITEP, MEPI, PNPI, PEI, RSRIEP), Ukraine (INR NU, Kiev), Bulgaria (INRNE, Sofia), Poland (UL, Lodz; INP, Krakow), Germany (FZK, Karlsruhe; Tubingen Univ.; THD, Darmstadt; FRM, Garching), Republic of Korea (PAL, Pohang; KAERI, Taejon), France (ILL, Grenoble; CEC CEA, Cadarache), Belgium (IRMM, Geel), USA (LANL, Los Alamos), China (Peking University) and Japan (Kyoto University; KEK, Tsukuba) at their neutron sources. It is necessary to note that the new opportunities which opened after Russia had jointed ILL, Grenoble have been effectively used: some measurements with cold and ultracold neutrons were successfully performed.

Very interesting possibilities for investigations are opening now in the framework of a wide international collaboration PS-213 based on a new n-TOF facility which starts operation in late May 2000 in CERN.

The research program for IBR-30 was written taking into account the working schedule of the creation of the new Intense REsonance Neutron source for nuclear physics investigations — the IREN project. In accordance with the recently revised schedule approved in March 1999 by the JINR directorate, the IREN source is to start operation by the end of 2002. So, the complex IBR-30+LUE-40 has to be dismounted in the second half of 2001. A very important reason why the IBR-30 scientific program has continued to present and will continue in nearest future is to preserve the research team able to carry out investigations on the basis of the IREN source and prepare new experimental techniques for such investigations.

2. Experimental Researches

2.1. Parity Violation in the Interaction of Resonance Neutrons with Nuclei

2.1.1. TRIPLE collaboration results

The Frank Laboratory of Neutron Physics participates in the Time Reversal Invariance and Parity at Low Energy (TRIPLE) collaboration studying Parity NonConservation (PNC) in compound-nuclear states. The experiments are conducted at the Los Alamos pulsed neutron source LANSCE by the transmission of longitudinally polarized neutrons through isotopically pure targets. The directly measured quantities are the longitudinal asymmetries of the cross sections for p-wave resonances defined as $\sigma_p^{\pm} = \sigma_p(1 \pm p)$, where $\sigma_p^{\pm}$ is the resonance cross section for positive and

negative neutron helicities, σ_p is the resonance part of the p-wave cross section. In the statistical approach, a set of PNC matrix elements obtained for many resonances determines the mean square matrix element M^2 of the effective weak interaction of nucleons in nuclei provided that complete spectroscopic information about resonances is obtained in addition to longitudinal asymmetries. Dividing the level spacing by D one obtains the weak spreading width $\Gamma_w = 2\pi M^2/D$ which is a global measure of the strength of the effective parity violation interaction in nuclei; it has a typical value of ~10^{-7} eV. In 1999 the Γ_w results were published for ^{93}Nb, ^{103}Rh, ^{107,109}Ag $^{106;108}$Pd and ^{133}Cs. They are shown in Table 1.

Table 1

Nuclei	^{93}Nb	^{103}Rh	^{106}Pd	^{107}Ag	^{108}Pd	^{109}Ag	^{133}Cs
$\Gamma_w(10^{-7}$ eV)	**≤ 0.11**	$1.4^{+1.2}_{-0.6}$	$34.0^{+47.0}_{-28.0}$	$2.7^{+2.6}_{-1.2}$	**≤ 12.0**	$1.3^{+2.5}_{-0.7}$	$0.006^{+0.154}_{-0.003}$

The data indicate possible existence of local fluctuations in the mass dependence of the weak interaction in compound nuclei contrary to an earlier conclusion about the mass independence of the weak interaction spreading width [FLNP Annual Report 1998, p.17].

2.2. *Experimental Approaches to Time-Noninvariance Effects in the Interaction of Resonance Neutrons with Nuclei*

2.2.1. Comparative analysis of experimental proposals on T-, P-invariance tests in nuclear reactions with neutrons.

An analysis of different proposed experiments to investigate CP-violation in nuclear reactions induced by resonance neutrons was carried out. The formalism of spin density matrices and special methods of the nuclear reaction theory were used to analyze the CP-violating quantities suggested for measurement in various experiments. The dependence of the effects and their relative errors on the neutron energy and target thickness was studied. The necessity to compensate strong pseudo-magnetic precession by an external magnetic field is shown. Being completely compensated some of the above effects show an additional enhancement of 3 orders of magnitude while the total enhancement reaches 6 orders of magnitude. In this case, neutron spin reverse essential for the effect occurs due to precession caused by the CP-violating interaction while the beam absorption is caused by the strong nuclear interaction. The enhancement appears due to the dynamical and resonance mechanisms caused by a complicated (chaotic) structure of compound resonances. An analysis of some other relevant quantities shows that, although their values themselves do not show resonance enhancement, their relative errors decrease sharply in the vicinity of the p-wave resonance.

To avoid some problems mentioned above, one can use a two-stage scheme with just one neutron polarization device proposed in FLNP.

Nowadays, there are two possible target designs for the proposed experiment. The first is the Dynamical Nuclear Polarization technique for the polarization of ^{139}La nuclei in a $LaAlO_3$ compound. It requires extra-low temperatures and a high magnetic field. The second is the optical polarization of ^{131}Xe in exactly the same manner as ^{3}He. The latter is precisely the experimental approach that is now under investigation within the KaTRIn project.

2.2.2. Recent results of the KaTRIn project

The ability to create a long-lived high nuclear spin polarization in dense noble gases (^{3}He, ^{129}Xe, ^{131}Xe) opens wide perspectives in new fundamental and applied research and medicine applications. We propose to use a spin-polarized ^{3}He nuclear target as a neutron

polarizer and analyzer of neutron polarization in the KaTRIn project for an experimental test of time-reversal invariance in nuclear reactions. A high polarization in the neutron beam can be reached by the use of the dense ($3 \cdot 10^{20}$) highly polarized (~50%) prolonged Ø3x30 cm^3 ^3He target. The spin exchange technique allows the creation of high nuclear polarization directly in dense noble gases by transferring the electron spin of optically pumped alkali (Rb, K, Cs) atoms. As nuclear polarization cannot be higher than electron polarization and the growing rate of nuclear polarization is proportional to the alkali atom number density, a powerful circularly polarized laser beam tuned to the atomic resonance line is required. In 1999, an experimental setup for creating a ^3He neutron target (Figure 1) was built. To have high polarization values, P_{Rb}, the laser should provide no less than 0.2 W per every cm^3 of Rb vapor at density $n_{Rb} \approx 10^{15}$ cm^{-3}. In recent years, powerful diode laser arrays with the power up to 30 W became available. We used 15 W 23, a diode laser array, tuned to the D1 Rb resonance line (795 nm). The laser spectrum was thoroughly investigated using a spectrograph.

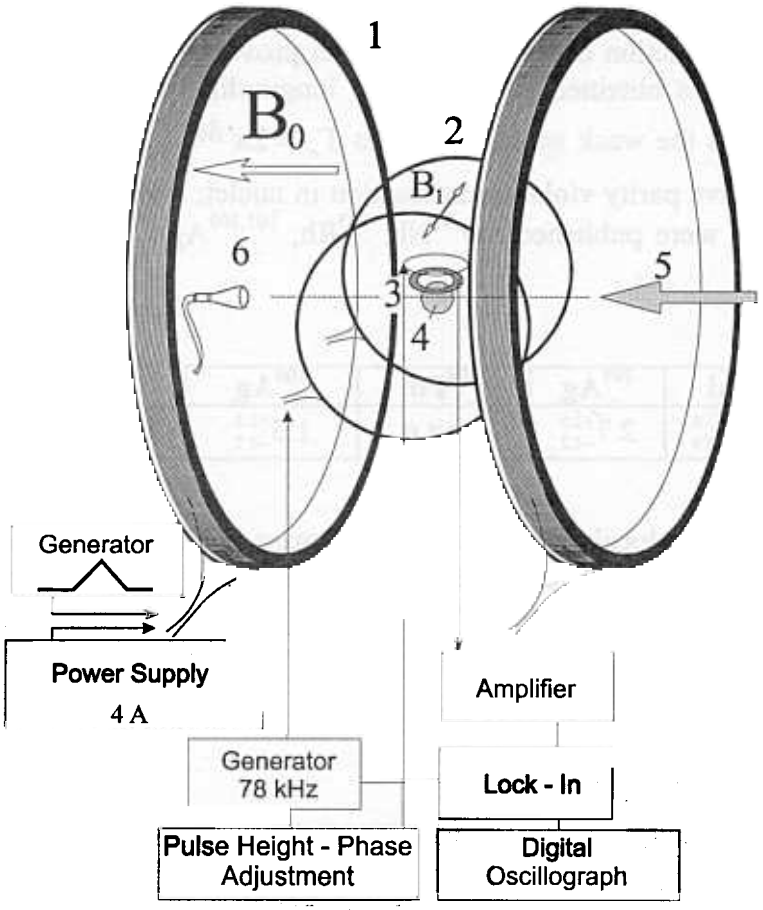

Fig. 1. NMR system: 1- Helmholz coils, 2- RF-coils, 3- Pick-up, 4- ^3He Cell, 5- Laser beam, 6- Photodiode

We investigated three spherical cells with the diameters 2 cm (A), 4 cm (B), and 3 cm (C) filled with at 2, 8.5, and 13 atm, respectively. The cells were heated up to 200 C° and the averaged polarization was determined from the absorption spectra using the spectroscopic technique by switching the stabilizing magnetic field on and off. The experimental data are supported by the calculations based on the numerical solution of the equations describing broadband light propagation through an optically dense medium.

The ^3He nuclear polarization, P_{He}, was determined by a standard technique of NMR adiabatic fast passage. Helmolz Ø1400 mm coils produced an axial stabilizing magnetic field of 22.4 Gauss along the laser beam direction with a homogeneity not worse than in the middle and variations in time being at the same level. A pair of radio frequency (RF) coils 700 mm in diameter produced a 78 kHz transverse field.

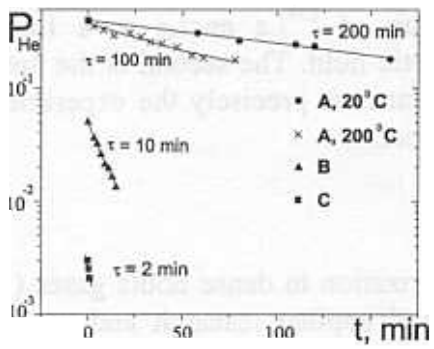

Fig. 2. ^3He nuclear polarization decay curves

A saw-like pulse of 3 Gauss was applied to the stabilizing field to create resonance conditions for ^3He nuclei. NMR pick-up coils were incorporated into a cell holding platform. Their axis was orthogonal to the stabilizing and RF-field. The induced NMR signal was guided to lock-in the amplifier and then to the digital oscilloscope. The sensitivity of the system was about

$5 \cdot 10^4$ V/Gauss. The RF - interference and vibrations, set the noise level at about 100 mV. The value of P_{He} was indirectly determined by the calculation of the filling factor and is shown in Figure 2. Rather low decay constants, τ, can be attributed to cell wall relaxation and paramagnetic impurities in ^{3}He. Nevertheless, the efficiency of polarization transfer happened to be rather high, about 10^{18} of ^{3}He atoms/s for a B cell. Generally, Helmholz coils and the related equipment are necessary for the NMR measurement of the ^{3}He polarization. On the other side, it can be extracted from measurements in the neutron beam. The μ-metal magnetic shields can provide a homogeneous magnetic environment for the ^{3}He target. Now, this activity is underway and the first experimental tests on an IBR-30 neutron beam will be conducted in 2000.

2.3. *Theoretical and experimental approaches to studies of the amplitude of the n-e interaction and the electric polarizability of the neutron*

Methodological experiments and MC calculations have been carried out at IBR-2 to optimize the scheme of the experiment to study the neutron elastic cross section on noble gases with the aim of extracting the neutron-electron scattering length. It was observed that the neutron beam from the IBR-2 reactor passing through a mirror neutron guide becomes inhomogeneous in energy. This fact causes serious experimental difficulties in the measuring of the angular anisotropy of the scattered neutrons on a Xe target. However, computations show the possibility of the extraction of the (n, e) scattering length from measurements of the elastically scattered neutron intensity in the 4π-geometry if one uses a gaseous Ar target. The advantage of Ar is its relatively small nuclear scattering cross section resulting in a relative contribution of the (n, e) scattering equal to Xe's.

In the year 2000 a high-pressure Ar-filled gaseous chamber with ^{3}He proportional counters around it will be constructed and the first measurements of the Ar scattering cross section will be carried out.

A new method to study the neutron polarizability and neutron–electron scattering was proposed. It is based on the fact that the real part of the s-wave scattering amplitude changes its sign near the s-wave neutron resonance at $E = E^* = E_0 - \frac{\Gamma_n}{2kR_0'}$ (here E is the neutron energy, E_0 is the energy of the resonance, k and Γ_n are the resonant values of the neutron wave number and width, R_0' is the s-wave scattering radius). The method consists of the observation of the energy behavior of the forward–backward scattering asymmetry $\omega_1 = \frac{\sigma(\vartheta_1) - \sigma(\vartheta_2)}{\sigma(\vartheta_1) + \sigma(\vartheta_2)}$ that experiences a jump at $E=E^*$, here $\sigma(\vartheta)$ is the differential scattering cross section. Approximate expressions for the differential cross section are presented by the equation $\sigma(\vartheta) = (f_0 + f_1 \cos\vartheta + a_{ne} Zf(q))^2$, where f_0 is the s- wave scattering amplitude, $f_1 = f_1^N + f_1^{pol}$ is the sum of nuclear and polarizability contributions to the p-wave amplitude, $a_{ne} = (1.3-1.6) \cdot 10^{-3} fm$, $f(q)$ is the atomic formfactor, $q = 2k \sin\frac{\vartheta}{2}$ is the transferred momentum. Thus, in the expression for $\sigma(\vartheta)$ we have the interference terms $2f_0 f_1 \cos\vartheta$ and $2f_0 a_{ne} Zf(q)$. The calculations show that the latter term for $Z \geq 70$ and $1\text{eV} \leq E \leq 10eV$ exceeds $2f_0 f_1$ ~100 times. It makes ω_1 be always negative at energies below E^* and positive at energies higher than E^*. It is supposed that this phenomenon will serve as a new method for the observation of a_{ne}. More detailed calculations of possible experiments to investigate a_{ne} will be done.

2.4. *Interference Effects in Resonance Neutron Induced Nuclear Fission and Delayed Neutron Yields at Thermal Energy*

2.4.1. Angular correlations of fission fragments in the resonance neutron induced fission of the ^{235}U nucleus

Spontaneous and induced nuclear fission has been under investigation for over 50 years but we do not have a complete understanding of its mechanism and dynamics yet. This is because nuclear fission is one of the most complicated nuclear transformations connected with deep rearrangement of the mass and charge of initial nuclei, production of extremely deformed and excited fragments with high spin and excitation energy sufficient for the emission of several neutrons and about ten gamma quanta. Another basic circumstance is the fact that in most cases, nuclear fission is studied in the conditions when it is impossible to obtain information on basic amplitudes of the process. Such amplitudes are characterized by the parity π of the system, its spin J and the projection on the fission axis K. Resonance s- or p-neutron induced fission only permits one to obtain information on $J^{\pi}K$ fission amplitudes because in the total cross section of the (n, f) reaction and in the energy dependence of the angular distribution of fission fragments there appears the interference of $J^{\pi}K$ amplitudes of different compound states. The possibility of the extraction of fission amplitudes from the experiment with an aligned ^{235}U target is determined by the existence of a complete set of experimental data on differential and total cross sections for this nucleus.

In 1999, data taking in the experiment to measure the fission fragment angular anisotropy of the ^{235}U resonance neutron induced fission with an aligned ^{235}U target in the energy region 0.5–30 eV finished. The value of the anisotropy coefficient A_2 (E) was extracted. The energy dependence of the A_2 coefficient, which characterizes the angular anisotropy of fission fragments, is shown in Fig.3.

For a combined analysis, the experimental cross sections for ^{235}U available from the National Nuclear Data Center (NNDC) at BNL were used. All other cross sections are also well reproduced. The dashed line is calculated using a set of resonance parameters from the ENDF/B-VI library, which also describes all other cross sections quite well, but obviously

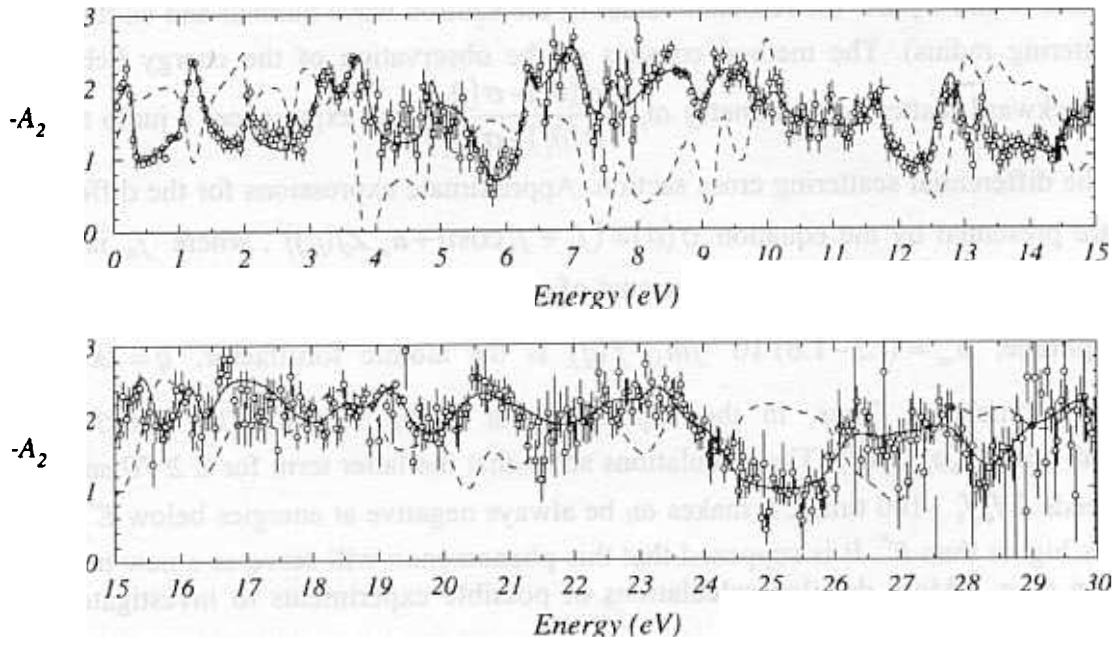

Fig. 3. The results of the fit (solid curve) for A_2 (E), circles are the experimental data. The dashed line is calculated using the resonance parameters from ENDF/B-VI.

fails to reproduce the A_2 energy dependence. It is necessary to note that the latter set of resonance parameters was obtained in the two-channel approximation without taking into account the information on A_2 (E).

The data were analyzed assuming that three channels are open for the spin group $J=3$ ($K=0,1,2$) and two for the spin group $J=4$ ($K=1,2$). According to a commonly used assumption the $J^{\pi}K=4^{-}0$ state is forbidden by parity conservation. We can expect no or a very small contribution from higher K states ($J^{\pi}K=3^{-}3$, $4^{-}3$, and $4^{-}4$) as the geometrical factors defining the value of the anisotropy coefficient for these fission channels have a positive sign while the observed anisotropy coefficient A_2 is negative over the whole measured energy range. The fission barriers for these states should be much higher. So these fission channels are not taken into account. The integral distributions of the partial fission widths for the spin group $J=4$ obtained in such approximation turned out to be not consistent with the Porter-Thomas distribution with one degree of freedom (see Fig. 4, right column). An additional fission channel seems to be open for this spin group. It is necessary to note that the conclusion about an absolute forbiddeness of the $4^{-}0$ channel was based on A.Bohr's hypothesis in its simplest variant. However, a more careful examination of the problem leads to a conclusion that the $4^{-}0$ channel has a higher first fission barrier and a relatively low second one for asymmetric fission modes. Thus, one would expect the $J^{\pi}K=4^{-}0$ channel to be at least partially open in our case. So, we reanalyzed the data assuming that all three channels are open for both spin groups.

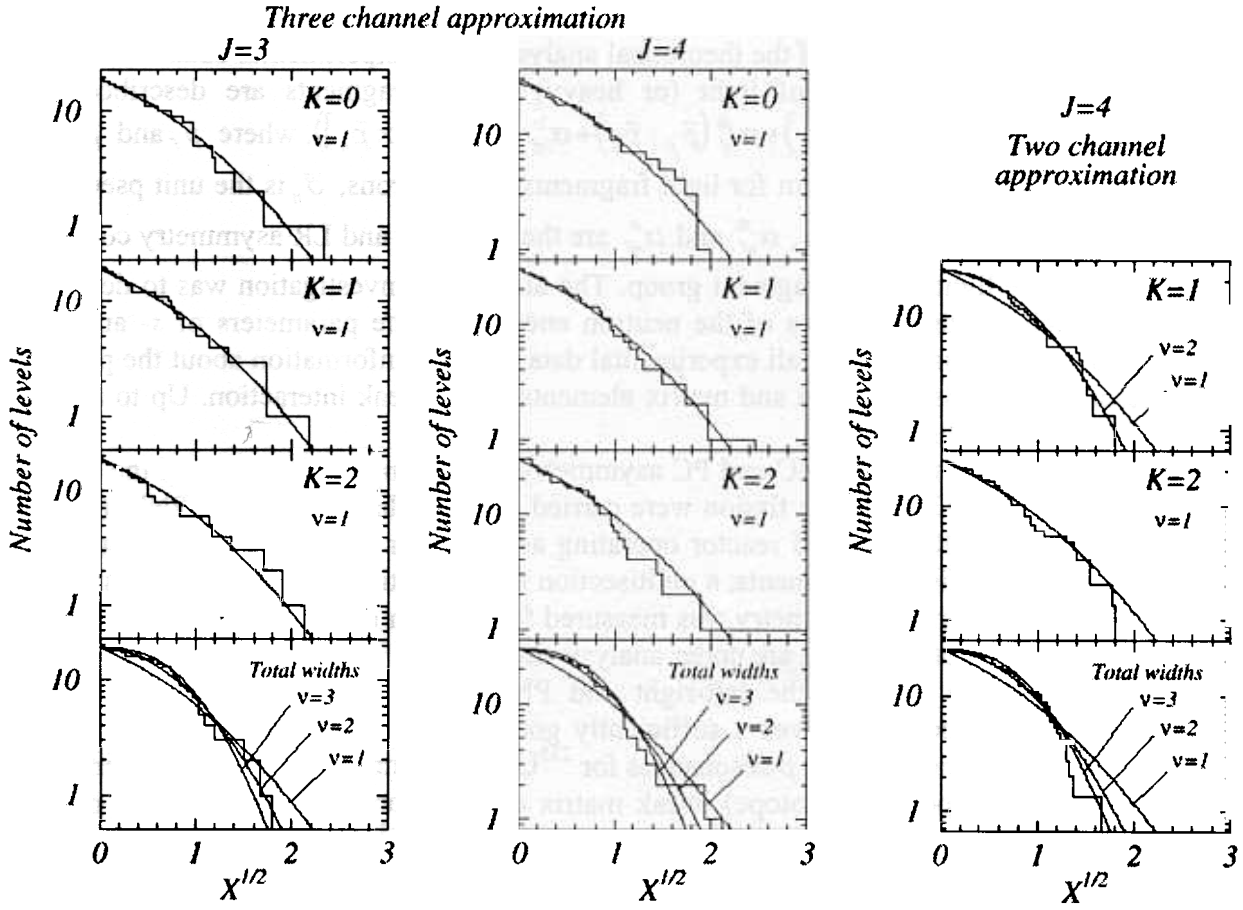

Fig. 4. Integral distributions of partial and total fission widths (number of resonances with $\Gamma_{\lambda f}/\langle\Gamma_{\lambda f}\rangle > X$*). Solid lines are the* χ^2 *distributions with* ν *degrees of freedom.*

For more details see the section of scientific publications: "Angular Anisotropy of Fission Fragments from the Resonance Neutron Induced Fission of an Aligned ^{235}U Target and the Role of $J^{\pi}K$ Fission Channels".

In 2000, experiments to study the angular anisotropy of fission fragments for different mass groups will continue. Also, experiments to determine the temperature dependence of the anisotropy coefficient will be done aiming at an increase of the accuracy of the absolute value of the anisotropy coefficient.

2.4.2. Parity violation and other effects caused by the interference of *s*- and *p*- wave neutron induced fission

To explain PNC effects in nuclear fission, theoreticians used an assumption about neighboring compound-states with opposite parities mixed by the weak nucleon-nucleon interaction. As it is well known, an analogous assumption was used earlier to explain the PNC-effect arising in the (n, γ) - reactions.

As a result of such a mixing, the interference between the fission channels with equal values of ***JK*** and opposite parities may arise. In turn, this interference leads to the asymmetry of light (heavy) fragment emission relative to the spin direction of the polarized neutrons initiating the nuclear fission.

Recently on the basis of a consistent theory of neutron-induced fission it was shown that parity conserving (PC interference effects such as the left-right (LR) and forward-backward (FB) asymmetry of fission products emission could be expressed through the same fission amplitudes as the PNC effect. As a result, complementary investigations of PNC and PC interference effects can essentially extend the capabilities of the theoretical analysis of the experimental data.

The angular distributions of light (or heavy) fission fragments are described by the expression: $W(\vec{p}_f)=1+\alpha_{nf}(\vec{\sigma}_n\cdot\vec{p}_f)+\alpha_{nf}^{fb}(\vec{p}_f\cdot\vec{p}_n)+\alpha_{nf}^{lr}\cdot(\vec{p}_f\cdot[\vec{\sigma}_n\times\vec{p}_n])$, where $\vec{p}_f$ and $\vec{p}_n$ are the unit vectors of the linear momentum for light fragments and neutrons, $\vec{\sigma}_n$ is the unit pseudovector of the neutron polarization, and α_{nf}, α_{nf}^{fb} and α_{nf}^{lr} are the PNC, FB and LR asymmetry coefficients, respectively, for the light fission fragment group. The aim of the investigation was to determine α coefficients which are the functions of the neutron energy and the parameters of *s*- and *p*-wave resonances. Simultaneous fitting of all experimental data can give information about the parameters of the *p*-resonances of fissile nuclei and matrix elements of the weak interaction. Up to now, such information is entirely absent.

All measurements of the PNC and PC asymmetry coefficients as functions of the resonance neutron energy in ^{233,235}U and ^{239}Pu fission were carried out in collaboration with PNPI (Gatchina) on the beams of the IBR-30 pulsed reactor operating as a booster with a LUE-40 electron linear accelerator. To register fission fragments, a multisection fast ionization chamber was constructed.

In 1999, the left-right asymmetry was measured for ^{239}Pu in the energy region from thermal neutron to 70 eV. The obtained data are under analysis now.

For ^{233,235}U, the data on the left-right and PNC effects were analyzed. Simultaneous processing of the obtained data gives a sufficiently good description of the observed effects. In doing so, tentative parameters of 29 *p*-resonances for ^{235}U and 18 ones for ^{233}U were obtained. For 6 uranium resonances (3 per each isotope), weak matrix elements are estimated and the mixing of states with different parities is obtained. The value appears to be $10^{-4} - 10^{-3}$ eV.

2.4.3. Delayed neutron yields

It is well known that the existence of delayed neutrons (DN) has a fundamental significance for the realization of a controllable chain fission reaction. The yields and time characteristics of DN from the main reactor isotopes, ^{235}U, ^{239}Pu and ^{233}U, are some of the most important nuclear reactor constants used in kinetic calculations. An accuracy of 3% for ^{235}U, 4% for ^{239}Pu and 6% for ^{233}U

has now been achieved for DN yields. Nevertheless, the requirements for the accuracy of the parameters have continued to increase.

The measurements of the $\beta_0 = \frac{\nu_d}{\nu_d + \nu_p}$ values for the thermal neutron induced fission of ^{233}U, ^{235}U, ^{239}Pu and ^{237}Np isotopes were performed with an ISOMER facility at IBR-2. Here, ν_d is the number of DN, and ν_p is the number of prompt neutrons. The IBR-2 operation mode, the pulse rate 5 Hz, permits one to register neutrons in a 200 ms time period. The system of a chopper synchronized with the reactor pulses allows one to extend the time interval to 800 ms by rejecting one or two reactor pulses and irradiating the sample with neutrons from a selected energy region.

The DN yields from ^{233}U, ^{235}U, and ^{239}Pu were measured after samples irradiation with neutrons of the energy 3 meV, 23 meV, or 40 meV. In the experiment the yields were measured relative to the DN yields at thermal neutron irradiation. The results on β_0 for 3 meV and 23 meV energies are presented in Table 2.

Table 2

β_0 values (in %) and ratios to standard DN yields (from ^{235}U thermal neutron induced fission)

Isotope	En = 0.003 eV	En =0.023 eV
^{235}U	0.683 ± 0.021 (1.004 ±0.009)	0.680 ± 0.021 (1.000)
^{233}U	0.274 ± 0.009 (0.403 ± 0.006)	0.267 ± 0.009 (0.393 ± 0.006)
^{239}Pu	0.227 ± 0.011 (0.334 ± 0.016)	0.234 ± 0.008 (0.344 ± 0.004)

There is no energy dependence of β-values in the energy range between cold and thermal neutrons.

One can see that the accuracy of relative measurements is on the level of 1%. The errors of absolute values are determined by uncertainty in the DN yield from ^{235}U which serves as a standard. The same experimental setup allows one to obtain the time dependence of the DN yield in short periods of time (up to 800 ms).

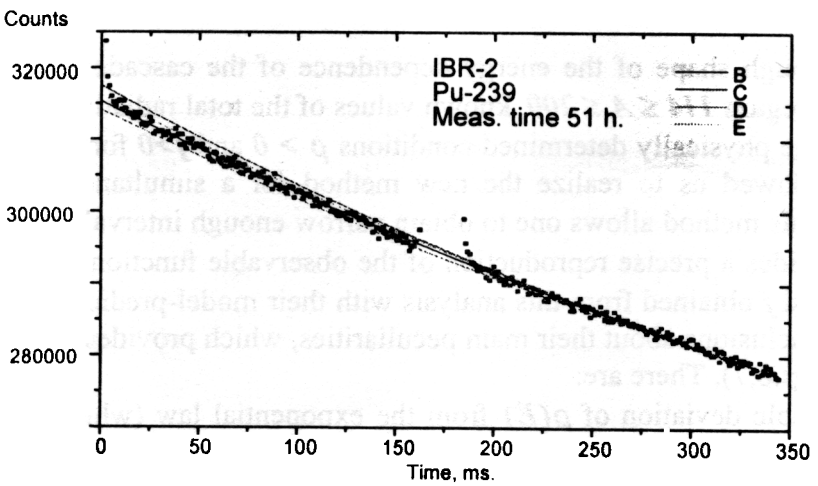

Fig. 5. DNs from the ^{235}U experimental points and calculations in the 6-group approach.

Figure 5 represents the experimental results for the ^{235}U DN yield time dependence. The statistical accuracy is 0.2 - 0.3% in a 1 ms time interval. The experimental data are compared with the calculation using the 6-group approach with group constants from different authors.

For ^{237}Np, two different methods of β_0 determination were used. The results for ν_d are 1.25±0.11 and 1.14±0.09. One should mention that measurements of the ν_d value for ^{237}Np in the thermal energy region were performed for the first time thanks to using a unique combination of a large high purity Np sample and the neutron beam cleaned from fast neutrons.

2.4.4. Studying of fission modes and their correlations with the quantum numbers of compound states

A method of precise measurements of the kinetic energies of fission fragments was developed and realized for actinide isotopes. The method is based on a double ionization chamber with Frish grids. Using the method TKE were measured for low lying ^{235}U resonances with a statistical accuracy of one order of magnitude better than in previous works. This enabled measurements of TKE in narrow energy bins of 0.2 eV in the energy region up to 10 eV. An analysis of the experimental results could give information on variations of fission mode weights as a function of excitation energy of the fissioning system.

2.5. Highly Excited States of Nuclei

2.5.1. Studying of the (n, 2γ) reaction

The acquisition, analysis and systematization of the experimental data on the properties of heavy enough (first of all, deformed) nuclei at the excitation energy $E_{ex} \leq B_n$ continued. Detailed and reliable information is necessary for a better understanding of the process of nuclear transition in this energy region from simple, well-studied structures to extremely complicated compound states. An analog of this process for a macroscopic system is a transition from order" to chaos". At present, maximum possible information on this process in any nucleus is only provided by the study of two-step γ-cascades proceeding between the compound state of the nucleus and its low-lying levels. The intensity of two-step cascades measured in the experiment equals the product of the radiative strength functions f of the primary and secondary $E1$ and $M1$ transitions and the density ρ of the states excited by them in the energy interval $\leq B_n$. A detailed study of nuclear parameters requires the measurement of these parameters with a high enough accuracy. This has stimulated the development of a new technique for the extraction of such data because all the algorithms of analysis used for this aim earlier have irremovable systematical uncertainties of an unknown magnitude.

A detailed enough shape of the energy dependence of the cascade intensity observed for nuclei from the mass region $114 \leq A \leq 200$, known values of the total radiative widths of compound states together with the physically determined conditions $\rho > 0$ and $f>0$ for any of excitation or γ-transition energies allowed us to realize the new method for a simultaneous estimation of the parameters ρ and f. This method allows one to obtain narrow enough intervals of variations of the ρ and f values and provides a precise reproduction of the observable functionals of cascade γ-decay. A comparison of ρ and f obtained from this analysis with their model-predicted values allows us to make quite certain conclusions about their main peculiarities, which provides a precise reproduction of the experiment (Figs.6,7). There are:

1. A considerable deviation of $\rho(E)$ from the exponential law (which is characteristic for pure fermion systems) at the excitation energy of about 2 MeV. It is not excluded that $\rho(E)$ at this energy can have a constant value or even decrease with increasing excitation energy. The corresponding energy regions of this effect in nuclei of different types shift by approximately a value of the neutron pairing energy. The strongest demonstration of the effect of the "stepwise" structure is observed in deformed nuclei.

The conclusion about the existence of a serious deviation of ρ from the exponential law in the excitation energy interval mentioned above is confirmed by an additional independent analysis. In this analysis, the distributions of random (due to their physical nature) deviations were approximated by some functions over a given excitation energy interval around the detection threshold L_c of individual cascades with a further extrapolation of the result to the value $L_c = 0$. The density of the cascade intermediate levels unambiguously determines the shape of this distribution in the excitation energy interval under consideration. These results are shown in Fig.6, as well.

2. The sums of the strength functions $f(E1)+f(M1)$ which allow the description of all the measured functionals of the cascade γ-decay process deviate noticeably from the model predictions. The least discrepancy between theory and experiment is observed for low-energy transitions in near-magic nuclei provided a modified giant electric dipole resonance model in which the width of the resonance depends on the nuclear temperature and quantum energy is used. The majority of deformed nuclei demonstrate a considerable enhancement of the RSFs of high-energy transitions. An abrupt increase in the discrepancy is observed in the vicinity of double-magic nuclei (N = 126; Z = 82).

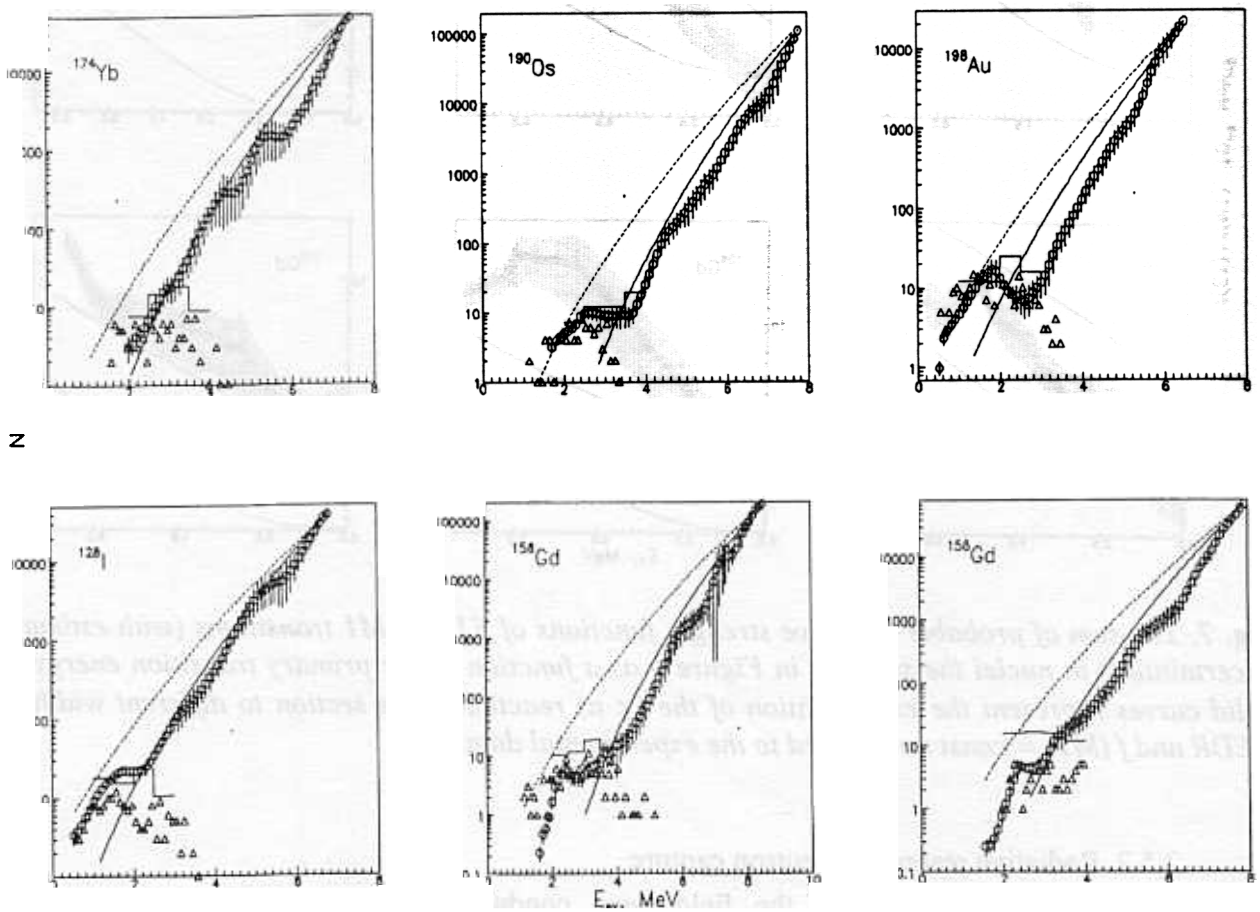

Fig. 6. The number of levels of both parities excited by primary dipole transitions in 100 keV energy intervals as a function of the excitation energy E_{ex}. Triangles represent the experimental data, histogram is the estimation of the level density for a zero detection threshold, $L_c = 0$; points with bars are the most probable ρ values reproducing both cascade intensities and total radiative widths. Dashed and solid curves correspond to the Fermi-gas model and generalized model of a superfluid nucleus, respectively. The model parameters are chosen to reproduce the resonance spacing

At present, the simplest qualitative explanation of the observed effects can be made under the assumption that the observed energy dependence of the level density above 3-4 MeV corresponds to the theoretical approach of the generalized model of the superfluid nucleus in its

early variant. This means that the structure of states in the excitation energy interval 1-2 to 3-4 MeV (and, probably, higher) must be mainly determined by vibrational (boson) components. The structures of levels at higher energies must be under dominant influence of quasiparticle (fermion) components.

This conclusion is confirmed by the observation of the regularity in the excitation spectra of the intermediate levels of the most intense cascades (equidistant period between 3, 4 and more levels equals some hundred keV).

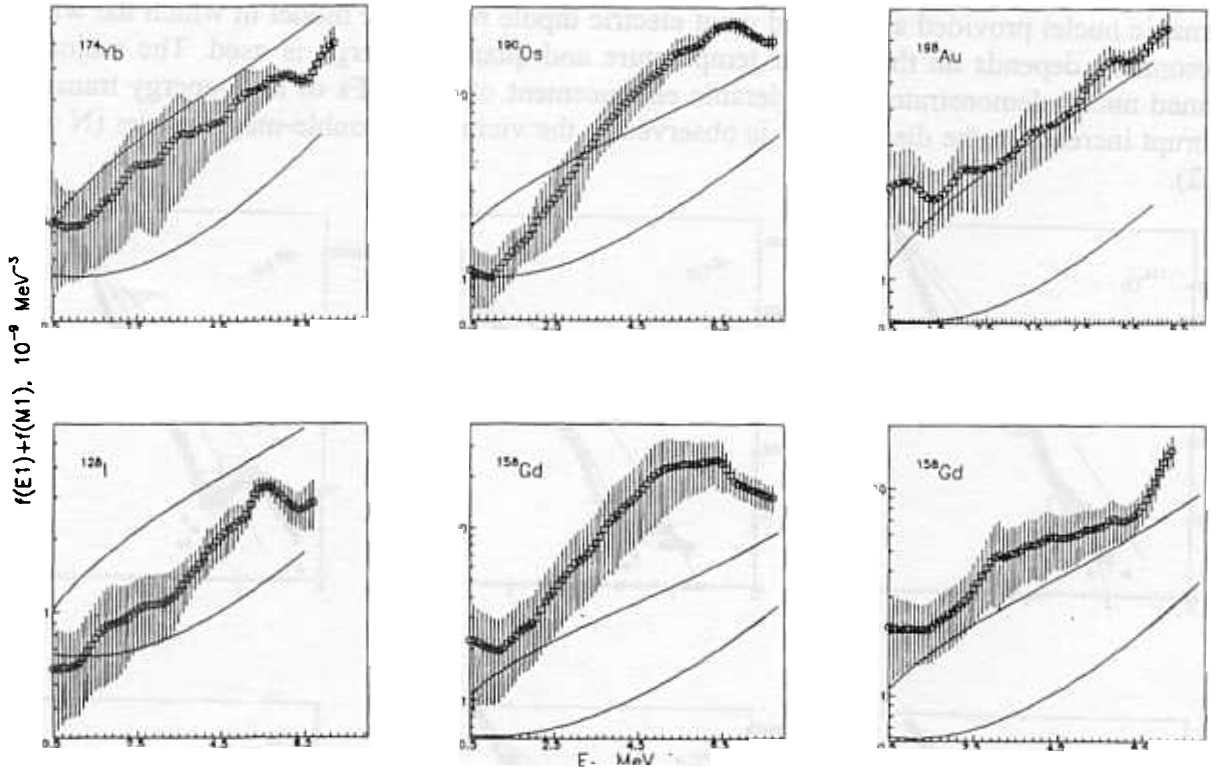

Fig. 7. The sum of probable radiative strength functions of E1 and M1 transitions (with estimated uncertainties) in nuclei the same as in Figure 6 as a function of the primary transition energy E_γ. Solid curves represent the extrapolation of the (γ, n) reaction cross section to different widths of GEDR and f (M1) = const normalized to the experimental data.

2.5.2. Radiative resonance neutron capture

In 1999, investigations in the field were conducted in several directions using the ROMASHKA and PARUS multidetector facilities. On the ROMASHKA facility the measurements of gamma-quanta multiplicities and the determination of the parameters of neutron resonances: spins, radiative widths and neutron strength functions, and the mean gamma-ray multiplicity after resonance capture in ^{149}Sm, ^{117}Sn, ^{187}Re, ^{232}Th, ^{48}Ti and after the fission of ^{235}U and ^{239}Pu isotopes over the energy interval from 20 to 300 eV were conducted. On the PARUS spectrometer similar measurements of the same isotopes plus ^{238}U and Pb were done in the energy region from 4 to 160 eV.

Incomplete data on spins and radiative widths and a practical lack of information about gamma-spectra from the resonance neutron capture and fission of the mentioned nuclei determined the importance of the measurements. The radiative capture cross section of Hf, Sn, and In isotopes in the resonance neutron energy range is interesting from the point of view of the understanding of the process of nucleosynthesis. At the same time, these investigations have a certain applied

importance. Some of the above mentioned isotopes are used in reactor construction where new, more exact and reliable data are now necessary in connection with an increasing accuracy of nuclear reactor calculations. The data on the spectra of capture γ-rays are important for shielding calculations.

Pioneering experiments to measure the effects of resonance self-shielding and the value of $\alpha = \sigma_\gamma / \sigma_f$ for ^{235}U target nuclei in the 20-2000 eV energy region were performed. Multiplicity spectra were also measured for the ^{239}Pu target to refine the α- value for ^{239}Pu in the 0.007-20 keV energy region. As a result, α- values were obtained for 80 resonances and several energy groups.

In collaboration with Pohang Accelerator Laboratory (PAL, Pohang, Republic of Korea) group total cross sections were obtained. Transmission experiments were performed on the PARUS spectrometer with samples-filters of different thickness made from ^{232}Th and ^{237}Np.

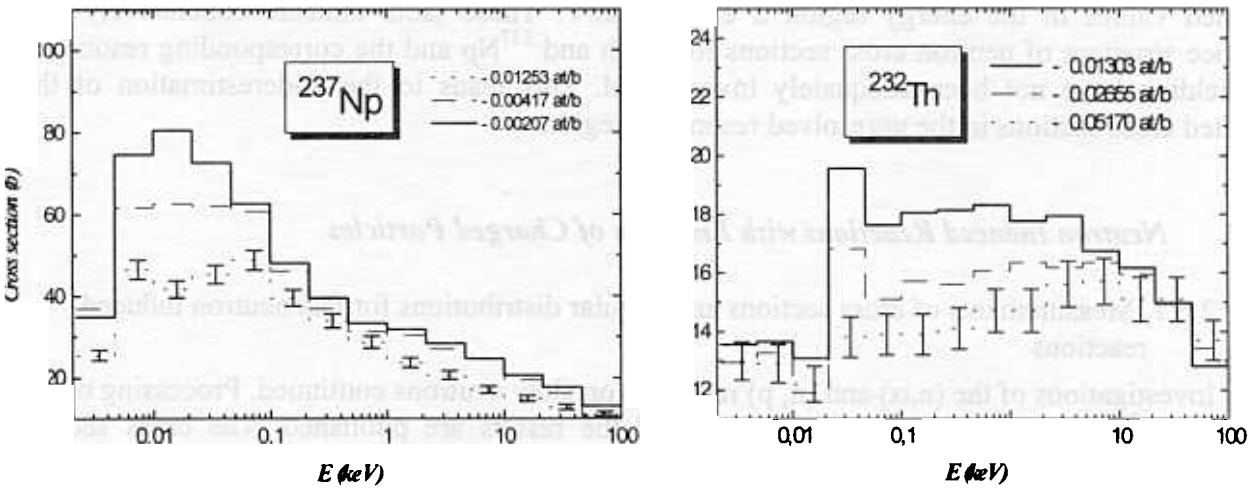

Fig.8. The experimental total group cross-sections of ^{237}Np and ^{232}Th for different thickness of the sample.

Figure 8 represents experimentally observed total group cross sections for ^{232}Th and ^{237}Np. Figure 9 show a comparison between the experimental total cross section for the thickest samples and the calculated with the GRUKON code using the ENDF/B-6 and JENDL-3 libraries. The experimental uncertainties of the transmission coefficients range from 0.2% to 0.5% and the corresponding uncertainties of the total cross sections are from 2% to 10%. Total transmissions are typically measured at $n\sigma x = 0.2 \div 0.4$ and result in the underestimating of the averaged group cross sections by 20% – 40% in the region of unresolved resonances. To avoid such errors, one has to take into account corrections due to resonance self-shielding effects in the averaged cross sections. The thickness of the filter-sample reduces the effects of resonance self-shielding.

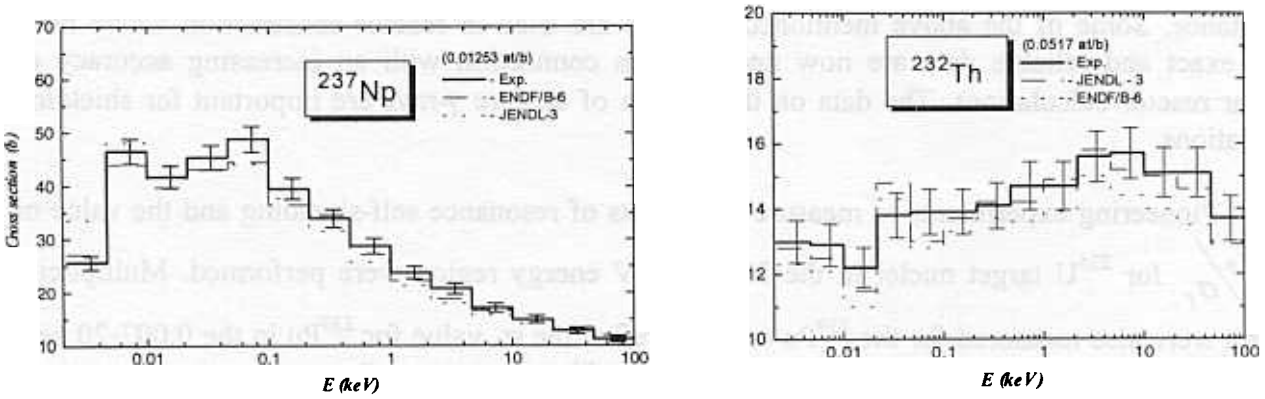

Fig.9. The observed experimental and calculated total cross-sections of ^{237}Np and ^{232}Th

The total cross sections calculated for thick samples are in good agreement with the experimental ones as it could be seen from Fig. 9. For thin filter-samples the observed cross sections are significantly larger than for thick samples and are systematically higher than the calculated values in the energy region 2 eV–100 keV. These facts indicate conclusively that resonance structure of neutron cross sections for ^{232}Th and ^{237}Np and the corresponding resonance self-shielding have not been adequately investigated. This leads to the underestimation of the calculated cross sections in the unresolved resonance region.

2.6. Neutron Induced Reactions with Emission of Charged Particles

2.6.1. Measurements of cross sections and angular distributions for fast neutron induced reactions

Investigations of the (n,α) and (n, p) reactions on slow neutrons continued. Processing of the data on the $^{14}N(n, p)^{14C}$ reaction completed and the results are published. The cross section measurements of the $^{35}Cl(n, p)^{35}S$, $^{36}Cl(n, p)^{36}S$, $^{36}Cl(n,\alpha)^{33}P$ reactions induced by thermal neutrons were performed using gaseous and solid targets. The processing of the angular distributions and cross sections of the $^{58}Ni(n,\alpha)^{55}Fe$ reaction at 5.1 MeV were accomplished in collaboration with Beijing and Tsinghua Universities (Beijing). The $^{64}Zn(n,\alpha)^{61}Ni$ reaction was measured for the neutron energies 5 and 6.5 MeV.

Systemizing of the (n, α) and (n, p) reaction cross-sections in the neutron energy interval from 2 to 16 MeV for the wide range of atomic weights A=19-197 was carried out. The dependence of cross sections on the (N-Z)/A parameter was obtained.

2.7. Astrophysical Aspects of Neutron Physics

For a long time it has been known that abundance of elements heavier than iron in the solar-system has been produced by neutron-capture reactions. However, neutron capture is also of the relevance to abundance of isotopes lighter than iron especially to neutron-rich isotopes, even though the bulk of these elements has been synthesized in charged-particle-induced reactions. Examples of such neutron-rich isotopes that are bypassed by charged-particle reactions and are produced by neutron-induced nucleosynthesis are ^{32}Si, ^{36}S, ^{40}Ar, and the calcium isotopes ^{46}Ca and ^{48}Ca. Attempts to understand neutron-induced nucleosynthesis are necessary to be made to obtain important ingredients of the knowledge of neutron-capture rates. The influence of shell effects on neutron capture is one of the most interesting aspects of neutron capture, especially because neutron capture in the vicinity of magic numbers is often a bottleneck in neutron-induced nucleosynthesis. This is also the case in the neutron capture on neutron-rich isotopes close to the magic proton and

neutron numbers Z=20 and N=28, i.e., in the vicinity of the double-magic nucleus ^{48}Ca. In particular, the reaction rate of neutron capture for Ti isotopes is of relevance to isotopic abundance anomalies in silicon carbide (SiC) grains occurring in carbonaceous meteorites. Contrary to most other solar system solids this type of grain has not been reprocessed and/or homogenized. Therefore, they can be potentially associated with their stellar origin. The main part of presolar SiC grains has an isotopic composition implying that they are most likely condensed in the winds of a variety of asymptotic giant branch (AGB) stars.

2.7.1. Neutron capture of ^{46}Ca at thermonuclear energies

The nucleus ^{46}Ca is produced and destroyed as a result of neutron-induced nucleosynthesis in hydrostatic helium, carbon, and neon burning through the reaction chain ^{45}Ca(n, γ)^{46}Ca(n, γ)^{47}Ca. At the Karlsruhe and Tübingen 3.75 MeV Van de Graaff accelerators the thermo-nuclear ^{46}Ca(n, γ)^{47}Ca cross section was measured by the activation technique via the 1297.09 keV γ-ray line of ^{47}Ca decay. Samples of $CaCO_3$ enriched in ^{46}Ca to 5% were irradiated between two gold foils serving as capture standards using the ^{7}Li(p, n) and T (p, n) reactions. The capture cross section was measured at the mean neutron energies 30, 104, 149, 180, and 215 keV. The Maxwellian averaged capture cross sections were measured at the quasithermal neutron energies kT=25 and 52 keV. It was found that the ^{46}Ca(n, γ)^{47}Ca cross section in the thermonuclear energy region and at thermal energy there dominates the s-wave resonance at 28.4 keV with the neutron width $\Gamma_n = (17.4^{+3.8}_{-2.6})$ keV and the radiation width $\Gamma_g = (2.4 \pm 0.3)$ eV. The stellar reaction rate is determined in the temperature range from kT=1 to 250 keV and is compared with previous investigations using Hauser-Feshbach calculations or experimental cross section data.

2.7.2. Neutron capture in ^{48}Ca at thermal and thermonuclear energies

The neutron capture cross section of ^{48}Ca was measured relative to the known gold cross section at kT=52 keV using the fast cyclic activation technique. The experiment was performed at the Van de Graaff accelerator of Tubingen University. The new results are in good agreement with the calculation based on a direct capture model. The $1/v$ behavior of the capture cross section at thermonuclear energies is confirmed and the adopted reaction rate which is based on several previous experimental investigations remains unchanged.

2.7.3. Measurement of neutron capture on ^{50}Ti at thermonuclear energies

At the Karlsruhe and Tübingen 3.75 MeV Van de Graaff accelerators the thermonuclear ^{50}Ti(n, γ)^{51}Ti cross section was measured by the fast cyclic activation technique via the 320.852 and 928.65 keV γ-ray lines of ^{51}Ti decay. Metallic Ti samples of natural isotopic composition and samples of TiO_2 enriched in ^{50}Ti to 67.53% were irradiated between two gold foils that served as capture standards. The capture cross section was measured at the neutron energies 25, 30, 52, and 145 keV. The direct capture cross section was determined to be (0.387 ± 0.011) mbn at 30 keV. We found evidence of a bound state s-wave resonance with an estimated radiative width of 0.34 eV that destructively interferes with a direct capture. The strength of the suggested s-wave resonance at 146.8 keV was determined. In addition to directly measured Maxwellian averaged capture cross sections at 25 and 52 keV, the present data served to calculate an improved stellar ^{50}Ti(n, γ)^{51}Ti rate in the thermonuclear energy region from 1 to 250 keV. At low temperatures the new stellar rate leads to much higher values than the previously recommended rate; e.g., at kT 58 keV the increase amounts to about 50%. The new reaction rate, therefore, reduces the abundance of ^{50}Ti due to s processing in asymptotic giant branch stars.

2.8. Investigations with Ultracold Neutrons

2.8 Precise experimental test of the UCN dispersion law

In the frame of an FLNP-Kurchatov Institute-ILL-Melbourne University collaboration, a precise experiment to verify the neutron wave dispersion law was performed using an original method. It is based on a search for the resonance line shift in an interference filter, the Fabri-Perrot interferometer, accompanied with a change in the neutron velocity component parallel to the filter surface. The parameters of the spectrometer permit one to measure the shift of the resonance line ($6.5 \cdot 10^{-9}$ eV width) with the accuracy 10^{-11} eV.

Deviations from the dispersion law were not observed on such a level.

2.8.2. Observation of the new mechanism of UCN losses

UCN can be confined in material traps for a long time making possible their usage in experiments aimed at studying the fundamental properties of the neutron. It is well known that, in particular UCN losses in traps are due to β-decay, upscattering and capture on the trap walls. In the reported study an additional mechanism of UCN escape from traps was observed. It is associated with an approximately two-fold increase of UCN energy with a probability of about 10^{-6} per collision for the stainless steel surface and it is lower for other studied materials (Cu, Be). The observed effect does not reduce to known UCN upscattering that leads to an increase in the neutron energy to approximately thermal energy.

3. Theoretical Researches

3.1. Nuclear Fission

A theory of nuclear fission induced by resonance neutrons was developed. The new and sufficiently natural interpretation of A. Bohr's fission channels follows from this theory. A unified description of P-even and P-odd angular correlations of fission fragments has been made. Part of the predicted new effects found confirmation in the experimental works performed in FLNP (see sections 2.4.1, 2.4.2). This theoretical approach was used for an analysis of the experimental data on the resonance neutron induced fission of aligned ^{235}U target nuclei.

3.2. Neutron optics

The reflection of neutrons from multilayer magnetic systems was considered numerically and analytically. The magnetization of adjacent layers was supposed to be noncollinear. Two methods were compared. The first one, analytical, uses infinitesimal splitting of layers and multiple reflections in the infinitesimal gaps. It is analytical and is called the recursion method (RM).

The second one uses matching of the wave function at the interfaces of layers. The wave function is represented as a two-dimensional vector, $\psi = \begin{pmatrix} \psi_0 \\ \rho\psi_0 \end{pmatrix}$, or $\psi = \begin{pmatrix} \tau\psi_0 \\ 0 \end{pmatrix}$ with both components being spinors. Here ψ_0 is the incident spinor wave, and ρ, τ are the reflection and transmission amplitudes, respectively. The upper component is related to the wave going right and the lower one is the wave going left. Matching at the i-th interface is described with a generalized 2x2 matrix (GM) M_i: $\psi_i = M_i\psi_{i-1}$, with the matrix elements of M_i being 2x2 matrices. The GM provides the continuity of the wave function and its derivative. Successive matching at different interfaces gives the resulting matrix from which the reflection spinorian amplitude can be evaluated. This method, called the generalized matrix method (GMM), is appropriate for numerical calculations.

A comparison of two methods in numerical calculations has shown that GMM is less time consuming. It is nearly 10 times faster than RM. However, RM has an advantage if we only need to find the positions and width of resonances in a multilayer system.

3.3. Neutron-electron interaction

The neutron-electron scattering amplitude a_{ne} is usually extracted from transmission experiments where the transmission exponent *exp (-Nσ$_t$L)* of the sample is measured. Here, *N* is the atomic density, *L* is the thickness of the sample, and σ_t is the total transmission cross section which contains the coherent elastic scattering cross section σ_{el}^c. It is the latter which is most important for a_{ne}, because $\sigma_{el}^c = \int d\Omega |a_c - Z a_{ne} f(q)|^2$, where a_c is the coherent neutron-nucleus scattering amplitude, *Z* is the atomic number, *f (q)* is the atomic form factor which depends on the momentum transfer *q*, and the integration should be performed over all scattering angles *Ω*. Since the amplitude a_{ne} is small, the last expression can be approximated as $\sigma_{el}^c = \sigma_0^c \left[1 - 2Z\left(a_{ne}/a_c\right)\langle f(k)\rangle\right]$, where $\sigma_0^c = 4\pi|b_c|^2$, *k* is the wave number of the incident neutrons, and $f(k) = \int d\Omega \, f(q)/4\pi$ is the form-factor averaged over all angles. Thus, to find a_{ne}, we need to measure σ_{el}^c, the dependence $\sigma_{el}^c(k)$ on *k* and also, know <*f (k)*>.

However, it is shown that at small *k* the coherent cross section σ_{el}^c does not enter into σ_t at all, and in the case of polycrystalline media, at large *k* this cross section enters into the Placek correction, i.e. σ_t contains $\sigma_{el}^c\left(1 - C/a^2k\right)$, where *C* is the constant calculated by Placek and *a* is the interatomic distance. It is seen that the Placek correction C/a^2k^2 increases as *k* decreases, but it is not clear how it completely eliminates σ_{el}^c at small *k*.

It was shown that:

1. the contribution of σ_{el}^c taking into account the Placek correction can be represented in the form $\sigma_{el}^c\left[1 - 1/\left(1 + a^2k^2/C\right)\right]$, which is acceptable for all *k*.
2. the magnitude of the Placek constant has some uncertainty which depends on the form of the atomic correlation function and leads to an uncertainty in the a_{ne} magnitude of the order of 10\%.
3. the correction to σ_{el}^c at large *k* also contains the term $\approx \left(4/ka\right)\left(l/a\right)\left(b_c/a\right)$, where *l* is an average dimension of crystallites.

Some corrections which can modify the amplitude related to the neutron polarizability were also considered.

3.4. Ultracold neutrons

Attempts were made to explain the anomaly of ultracold neutrons fom the fundamental viewpoint. An assumption was made that a non-spreading wave packet can describe the neutron and a reduction of the wave function takes place both in the coordinate and momentum space. It has also been noticed that a particle and its wave function are a non-local object whose coordinates and momentum demand an exact mathematical determination and can be determined unambiguously

and simultaneously without coming in contradiction with the uncertainty principle which appears to have no relation to quantum mechanics. In the frame of the canonical approach, one fails to describe anomalous losses. In the frame of de Broglie representations, a singular wave packet can be ascribed to the neutron. In this case, the anomaly can be explained by over-barrier leakage. As a result, the packet width is determined, the future of the neutron is predicted, and the possibility of experimental verification of this prediction is hoped for.

Experiments to verify the hypothesis started in 1998 and continued in 1999 in collaboration with Kyoto University (Japan) and Institute Laue-Langevin (France).

4. Methodological Researches

4.1. The anticompton gamma spectrometer HPGe-BGO for nuclear physics experiments at pulsed neutron sources

Pioneer investigations to observe the neutron standing waves using the TOF technique with a high precision gamma-spectroscopy were performed on channel 8 of the IBR-2 reactor.

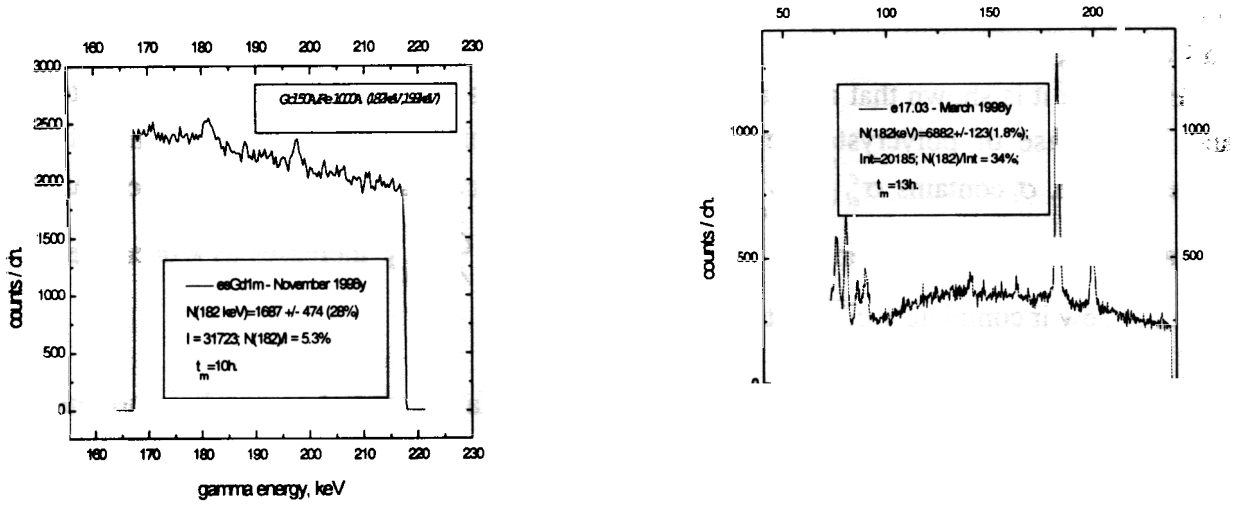

Fig.10. Gamma- spectra from ^{158}Gd in a multilayer structure without anticompton spectroscopy (left) and with anticompton spectroscopy (right)

The technique determines the success in the studying of the long wave dependence of the neutron density in layers with an extremely high capture cross section (Gd, Sm, Cd) and a several angstrom thickness. This permits one to discover such elements in a multilayer structure and determine their spatial position.

Figure 10 demonstrates improvements in the use of the technique after applying a high precision gamma- spectroscopy with an anticompton active shielding.

4.2. Construction of the KOLHIDA instrument

To carry out investigations of the paramagnetic neutron resonance and nuclear pseudomagnetism on the IBR-2 pulsed reactor, an experimental complex "Kolkhida" is being built which consists of a polarized neutron spectrometer and a polarized nuclear target installation. The spectrometer for investigations with polarized neutrons has been completed and measurements of its parameters have been carried out.

The spectrometer of polarized neutrons is located on the first channel of IBR-2. The general scheme of the spectrometer is shown in Fig. 11. The Co(92%)-Fe(8%) single crystals (1 and 2) are used for neutron polarization and polarization analysis.

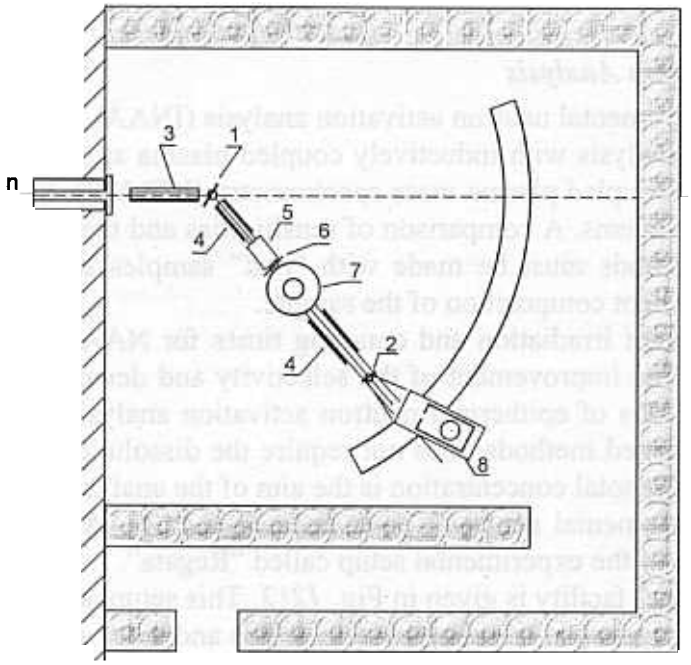

Fig.11. A schematical view of the Kolkhida setup. 1,2 – Co-Fe crystals; 3 - collimator; 4 – magnet; 5 – spin flipper; 6 – fission chamber monitor; 7 – polarized target; – neutron detector

The thickness of the crystals is 3 mm and the surface areas are 34x34 mm^2 and 35x53 mm^2, respectively. The crystals are placed between the poles of the electromagnets which produce a magnetic field of H=0.4T.

The spectrometer is assembled on a massive arm. It comprises guide field magnets (4), a flipper (5) for polarization reversal, a polarized target holder (7), a polarization analyzer (2) with a magnet, and a platform with a neutron detector (8). The arm on a circular rail can be rotated about the same axis as the neutron polarizer. The rotation axis of the detector platform coincides with the axis of the neutron analyzer. The ^{3}He counter is used as a neutron detector and the ^{235}U fission chamber (6) is used to monitor the primary neutron beam.

The parameters of the polarized neutron beam are given in Table 3.

Table 3

The parameters of the polarized neutron beam

Angle θ (degree)	19	12	6	4	3
Wavelength λ (Å)	1,15	0,74	0,37	0,25	0,19
Energy E_n (eV)	0,062	0,15	0,60	1,3	2,3
Counting rate of the detector behind the polarizer, n_1 (sec^{-1})	800	270	65	33	22
Intensity of polarized neutrons I_1 (n/sec cm^2)	430	200	80	60	50
Counting rate of the detector after analysis n_2 (sec^{-1})	70	23	3,1	0,6	0,2

The completed tests of the spectrometer showed that it could be used conveniently to carry out investigations with polarized neutrons over a range from thermal energy to several eV.

5. APPLIED RESEARCH

5.1. Neutron Activation Analysis

At the present time, instrumental neutron activation analysis (INAA) is one of the most sensitive methods for multielement analysis with inductively coupled plasma atomic emission spectrometry (ICP-AES) and inductively coupled plasma mass spectrometry (ICP-MS). Each of these techniques has their own merits and problems. A comparison of sensitivities and the quantity of elements to be determined for various methods must be made with "real" samples because the analysis result depends strongly on the element composition of the sample.

A combination of different irradiation and counting times for NAA technique is necessary to achieve an optimal result. The improvement of the selectivity and detection power of this method can be also achieved by means of epithermal neutron activation analysis (ENAA). Besides NAA, just one of the above mentioned methods does not require the dissolution of the sample. This is a great advantage of NAA if the total concentration is the aim of the analysis.

Applications of the instrumental neutron activation analysis (INAA) at the IBR-2 fast pulsed reactor are based on the use of the experimental setup called "Regata".

The layout of the "Regata" facility is given in Fig. *1*212. This setup consists of four channels for irradiation (Ch1-Ch4), the pneumatic transport system (PTS) and three gamma-spectrometers. It is located in three special rooms on the ground floor of the reactor IBR-2 building. The main parameters of the irradiation channels are presented in Table 4. The channels Ch3, Ch4 are cooled with water and the channels Ch1 and Ch2 connected with the pneumatic transport system are cooled with air. That is why the temperature in channels Ch3 and Ch4 is less than the temperature in channels Ch1 and Ch2 with the greater fluxes of neutrons. The time of sample irradiation in channels Ch3, Ch4 depends on the operation cycle duration of the reactor and is equal to 10-12 days, as a rule.

Table 4

Irradiation channel parameters

Irradiation site	Neutron flux density ($n/cm^2 s$)$\times 10^{12}$			T°C	Channel diam., mm	Channel length, mm
	Thermal	Resonance	Fast			
Ch1	Cd coat	0.23±0.03	1.4±0.16	70	28	260
Ch2	0.54±0.06	0.12±0.01	0.64±0.04	60	28	260
Ch3	Cd coat	4	7.0±0.5	30-40	30	400
Ch4	13.0±0.5	0.9±0.10	7.0±0.5	30-40	30	400
Ch0	$n_o \cong 0$	1.25±0.1	150	400	16	180
		<0.1				

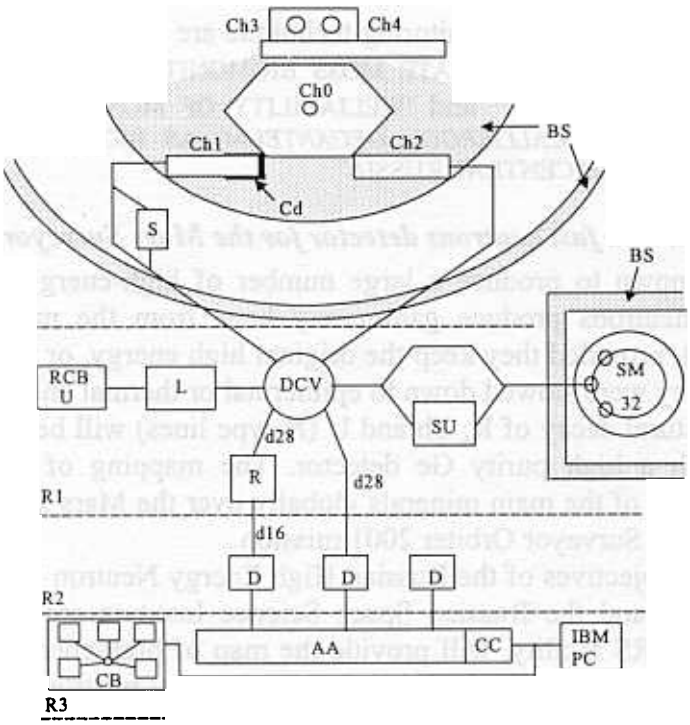

Fig. 12. The scheme of the "Regata" experimental setup. Ch0-Ch4 –irradiation channels, S- intermediate storage, DCV- directional control valves, L- loading unit, RCB- radiochemical box, U- unloading unit, SU- separate unit, SM- storage magazine, R- repacking unit, D- Ge(Li) detector, AA- amplitude analyzer, CB- control board, CC- controller CAMAC, R1-R3- The rooms where the system is located.

The irradiation channels Ch1 and Ch2 are the same, but Ch1 has a Cd coating. Each channel consists of two concentric tubes made from stainless steel. Both are placed into an aluminum box with a biological shield. One of the tubes is a flight tube 28 mm in diameter, and compressed air flows through the second tube. In order to prevent a hard shock of a capsule with the irradiated sample at the end of the channel there is an additional valve to let the compressed air out.

In the reported period most experience in applying the activation analysis involves air pollution studies in some industrial areas of Russia (the South Ural, Tula, Moscow region) and in member-states of JINR (Poland, Romania). The application of the neutron activation analysis with epithermal neutrons (ENAA) allows improving of the selectivity and detection power of the method. The technique is based on the fact that some elements have isotopes with resonances in the epithermal neutron region. The ratio of resonance activation integral/thermal neutron cross-section (I_o/σ_o) is of the order of 0.5 for nuclides without resonance in the epithermal neutron region and it may be as high as 100 in other cases. This means that the radionuclide distribution originating from epithermal activation may deviate strongly from the apparent when the whole reactor spectrum is employed. This forms the basis of ENAA.

The dominant part of air pollution studies is based on the use of the moss biomonitoring technique. Mosses have no developed root system that is why they take nutrients almost exclusively from the atmosphere. This technique has been applied to study air pollution with heavy metals and other trace elements in combination with the atomic absorption spectrometry of the elements Pb, Cd, Cu and Ni. The results of the investigations are presented in the form of tables, diagrams, graphs and, using the geographical information system (GIS) technology, in the form of colored contour maps for each element. The technique of multivariant statistical analysis (factor analysis) is applied to obtain information on the character and origin of pollution sources.

In more detail, the NAA and biomonitoring technique are presented in the section of scientific publications: "SELECTION OF APPROPRIATE MOSS BIOMONITORS FOR STUDYING ATMOSPHERIC ELEMENTAL DEPOSITION IN CHINA" and "RELIABILITY OF MOSSES *(HYLOCOMIUM SPLENDENS, PLEUROZIUM SCHREBERI* AND *CALLIERGON GEGANTEUM)* AS BIOMONITORS OF HEAVY METAL ATMOSPHERIC DEPOSITIONS IN CENTRAL RUSSIA"

5.2. Development of a fast neutrons detector for the Mars Surveyor 2001 space program

Cosmic rays are known to produce a large number of high-energy neutrons in the Martian surface layer. These neutrons produce gamma-ray lines from the nucleus either via inelastic scattering (I-type lines), provided they keep the original high energy, or via capturing reactions (C-type lines), provided they were slowed down to epithermal or thermal energies. These lines together with the lines of the natural decay of K, Th and U (N-type lines) will be measured by the Gamma-Ray Spectrometer with a high purity Ge detector. The mapping of these lines will allow to determine the distribution of the main minerals globally over the Mars surface, which is one of the primary goals of the Mars Surveyor Orbiter 2001 mission.

The main scientific objectives of the Russian High Energy Neutron Detector HEND created by a collaboration of JINR and the Russian Space Science Institute are consistent with this goal. HEND, as part of the GRS facility, will provide the map of high-energy neutrons albedo, which will allow (together with a complementary map of low energy neutrons albedo from the Neutron Spectrometer NS) the distinguishing of I-type, C-type and N-type lines from a "forest of lines" from the GRS spectrometer.

To achieve these goals, HEND is integrated into GRS. The HEND detector scheme was developed, modeled, and tested in FLNP. It has three ^{3}He-based neutron counters with polyethylene moderators and one stylben scintillator with an active anti-coincidence shielding around it. The ^{3}He-based detectors with thin and medium moderators will ensure the complementary measurement verification in the Neutron Spectrometer at low energies below 1 keV, and will provide data for the cross-calibration of HEND and NS. The ^{3}He-based detector with a thick moderator and a stylben scintillator will provide data for high energy neutrons at 1 keV–10 MeV to build a map of the elemental composition of the Martian surface and determine regions with an increased abundance of hydrogen on a shallow subsurface.

Also, the data of high-energy neutrons from HEND will characterize the radiation environment on the interplanetary cruise and on the Martian orbit to provide information about radiation-related risks to human explorers. Special data formats with time profiles will be used to measure, with a fine time resolution, the fluxes of high-energy neutrons and gamma rays during strong solar flares and gamma ray bursts.

The numerical computation of the detectors sensitivity was performed in FLNP to optimize the thickness of the moderators around the ^{3}He-counters for the expected energy spectra of albedo neutrons on the Martian orbit. The instrument will be calibrated in the neutron beams of the Van de Graaf accelerator and the pulsed neutron reactors of FLNP. The cross-calibration of the HEND and NS in the overlapping range of neutron energies will be performed by means of numerical computations.

2. NEUTRON SOURCES

2.1. THE IBR-2 PULSED REACTOR

In 1999, the reactor IBR-2 operated in accordance with the approved schedule. The details are given in Tables 1 and 2. The reactor operated for physical experiment a total of 8 cycles (1984 hr) at W=1.5 MW, including 3 cycles with a cryogenic moderator (CM).

As scheduled, the plan of reactor maintenance PMW-99 was executed from June to September. In the period, radioactive elements of MR-1 (movable reflector-1) were removed from a working storage by explosive techniques.

Work to improve control of a number of important systems of safety was conducted, including the formation of independent reference signals (5 Hz) in the channels of side pulses, introduction of a system of permanent control of the position of the emergency shutdown block (ESB) during power operation, upgrading of some measuring and control devices (MCD).

In October 1999, a license for the operation of the IBR-2 reactor was obtained from the State Atomic Inspection (SAI).

The main achievement of the year is the completion of work to build CM.

In the period from October 18 to December 17, 1999 the physical startup of the solid methane-based cryogenic moderator CM was carried out. The designing and manufacturing of CM were executed by the Scientific Research and Design Institute of Power Engineering in Moscow under the scientific guidence and with participation of FLNP JINR in Dubna.

The CM of IBR-2 is a third in the world solid methane moderator. The first two in Japan and USA, work in much less intense fields of radiation, however.

In accordance with the schedule of physical startup operations all three rated modes of CM were tested. Both technical and neutron-physical characteristics of the moderator proved to be as expected. In particular, it was shown that a small addition of ethylene reduces considerably the rate of the formation of radiolytic hydrogen which causes major difficulties in the use of solid methane as a moderator. For $\lambda \geq$ Å and the methane temperature 30 K, the neutron yield was 10-20 as much as from a usual water moderator (see Figs. 1, 2).

The flux from CM of IBR-2 exceeds that of the recently best source of cold neutrons at ISIS (England) having liquid methane as a moderating agent.

In 2000, CM IBR-2 will be operated in a regular mode.

In 1999, the concept of the reactor modernization underwent considerable changes. As a result, the improvement continues under the auspices of the program "Concept of the IBR-2 Modernization in the Period to the Year 2010".

In accordance with it work was carried out along the lines:

1) working drawings of MR-3;
2) preparations to start manufacturing of a new fuel loading. The technical and working design of TVEL is completed and manufacturing of the new elements of TVEL started;
3) work on the technical project of IBR-2 modernization started. Technical assignments for the modernization of control and emergency systems (CES) are prepared and technical requirements for the electronic equipment of CES are specified.

In 1999, the financing of the operation and modernization of IBR-2 improved considerably as compared to 1998 (see Table 3).

The main 2000 objectives.

Provide the physical program of beam measurements with a beam time in the volume of 2000 hr (8 cycles a year, including 3 cycles with CM).

2. Start manufacturing of MR-3.
3. Continue work to prepare a new fuel loading.
4. Technical project of the IBR-2 modernization, including CES of the reactor.

Table 1

IBR-2 operation parameters in 1999

Cycle	Dates	Time of operation for physical experiment Tph.ex.	Time of operation of movable reflector T_{MR}	Energy production E, MW*hr	Number of emergency shutdowns N_{ES}	Causes of emergency shutdowns (classified as in РД-04-10-94)				Number of beams in operation
						Voltage drops (PO8)	Equipment malfunctioning (PO7)	Electronic equipment malfunctioning (PO7)	Human factor (PO5)	
1	18.01 - 29.01	267	273	403	0	0	0	0	0	11
2	15.02 - 26.02	247	263	376	3	2	0	1	0	11
3	15.03 – 26.03	244	270	370	3	1	1	0	1	11
4	12.04 – 20.04	171	198	257	4	0	3	1	0	11
5	17.05 – 01.06	323	356	494	6	1	3	2	0	11
6	18.10 – 29.10	227	252	264	2	1	1	0	0	11
7	15.11 – 26.11	252	273	406	1	1	0	0	0	11
8	06.12 – 17.12	253	271	385	2	1	0	0	1	11
TOTAL:		**1984**	**2156**	**2955**	**21**	**7**	**8**	**4**	**2**	

Table 2

Current IBR-2 parameters

	Parameter	December 1999	Rated
1	Operation for physical experiment (th.hr)	36. 984	44
2	Generated energy (th.MWhr)	68.216	85
3	Operation of MR-2P(th.hr)	11.676	18*
4	Maximum fluence on the jacket in the center of the active zone (10^{22} n/cm^2):		
	$E_n > 0.5$ MeV	1.845	2.3
	$E_n > 0.1$ MeV	2.98	3.72
5	Maximum burn of fuel (%)		
	Brick-like TVEL	5.19	6.5
	rod-like TVEL	5.51	8.2
6	Number of emergency shutdowns	424	550

Note:

* *The resource is established in the process of reactor operation as a function of the MR state. The expected resource is indicated by analogy with MR-2.*

Table 3

IBR-2 expenditures in 1999 in k$ (paid to outside organizations)

	Budget	Non-budget
Operation and maintenance	67	18
Modernization	156	–
TOTAL:	**223**	**18**

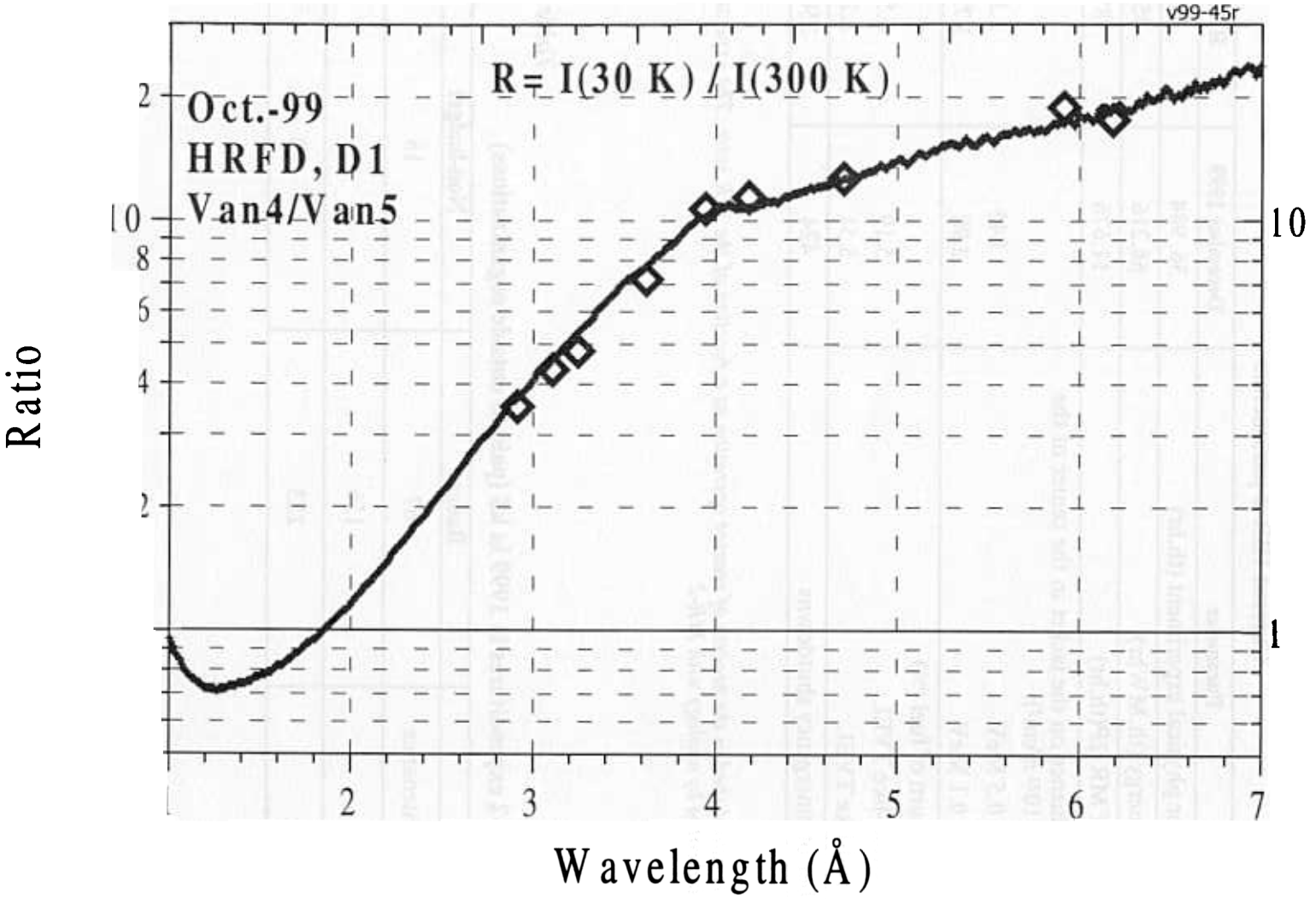

Fig.1. Relative changes of the initial spectra generated by the cryogenic and water moderators

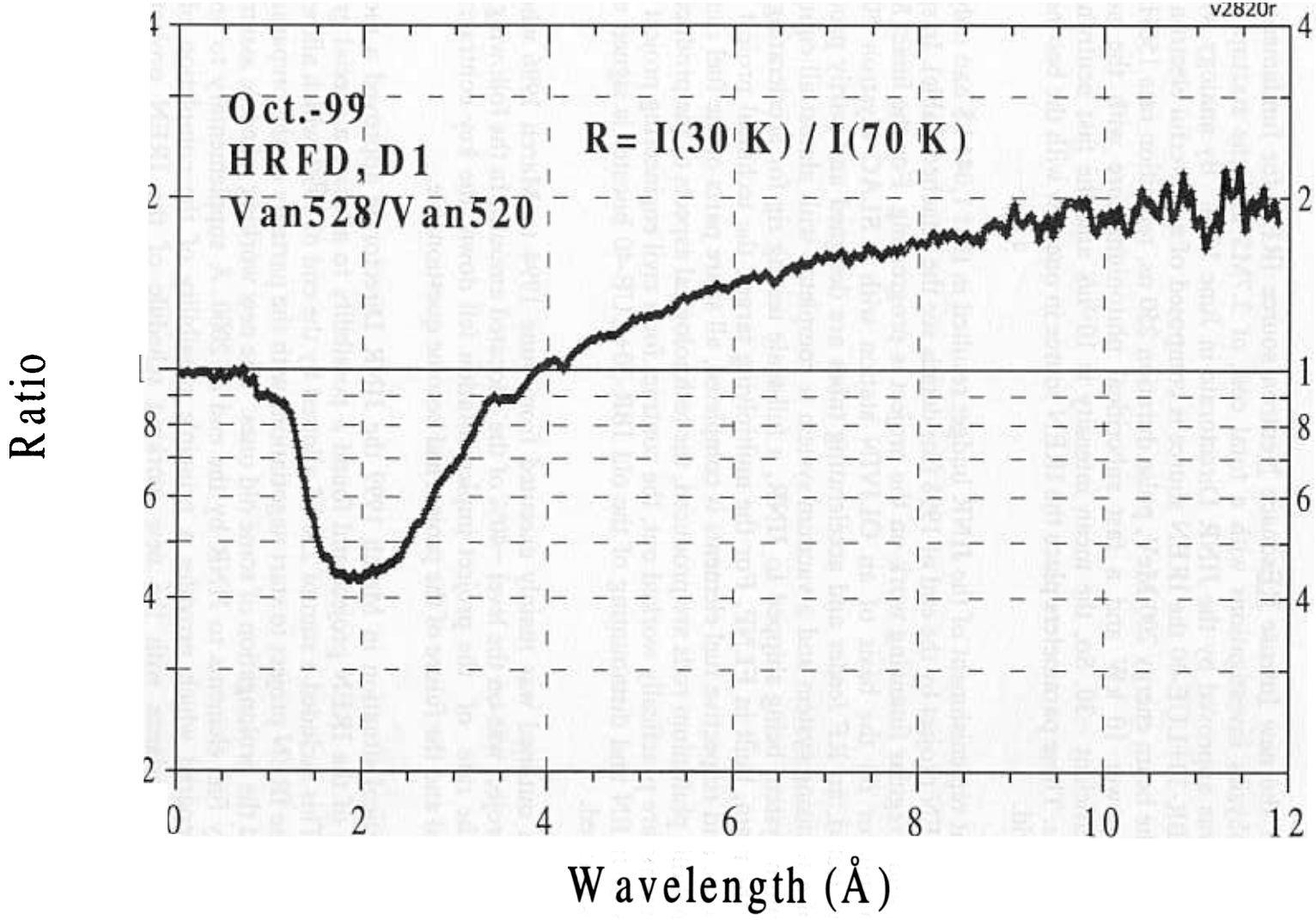

Fig.2. Relative changes of the initial neutron spectra generated by the cryogenic moderator at different temperatures

2.2. THE IREN PROJECT

The project of the new Intense REsonace Neutron source IREN for fundamental and applied nuclear physics investigations with a total cost of 3.7M$ and the startup date in December 1997 was approved by the JINR Directorate in June 1994. By analogy with the existing booster IBR-30+LUE-40 the IREN source is composed of a powerful electron linac, LUE-200, with the beam energy 200 MeV, pulse duration 250 ns, repetition rate 150Hz, and the mean beam power 10 kW and a fast subcritical plutonium core with the neutron multiplication coefficient ~30. So, the mean intensity is 10^{15}n/s and the fast neutron pulse duration is ~400ns. These parameters place the IREN source in one row with the best neutron sources in the world.

Insufficient replenishment of the JINR budget resulted in that 1,044 k$ had only been invested in the IREN project by the end of 1998 (for details see the attached Table). In spite of insufficient and irregular financing work on the project is progressing. For the linac: M-350, the first modulator on the basis of an OLIVIN station with a SLAC klystron 5045, is successfully tested, an RF feeder and accelerating tubes are designed and partly produced, designing of a focusing system and a vacuum system is completed with almost all equipment for the vacuum system being shipped to JINR, a full-scale testing rig for accelerating tubes trials is, in the main, built in FLNP. For the multiplying target: the technical project of the subcritical core and respective fuel elements is completed, all spare parts of the fuel elements, including metallic plutonium rods are produced, the technological aspects of the production of the fuel elements are practically worked out, the contract for a civil engineering project of the installation of IREN and dismounting of the old IBR-30+LUE-40 booster is signed and its first stage is realised.

The above outlined was mainly executed from June 1994 to March 1996 when the financing of the project was on the level ~40% of the allocated amount. In the following three years, however, the rate of the project implementation fell down, the key contracts were frozen or cancelled and the future of the project had become questionable.

In this critical situation in March 1999 the JINR Directorate approved a modified working schedule of the IREN project and found a possibility to allocate a special grant to save the project. This included a sum of 250 k$ allotted by the end of 1999, which allowed the management of the IREN project to start negotiations with the partners on the preparation of new contracts and the prolongation of some old ones. The new working schedule assumes the shipment of ready fuel elements to JINR by the end of 2000. A supplementary to previous agreements is prepared which provides a principle possibility of the completion of linac construction in accordance with the new working schedule of the IREN project. The implementation of financial plans in 1999 is illustrated in Table 4.

The modified working schedule of the IREN project, realized and planned investments in 1999-2002 are shown in Table 5. It is necessary to emphasise that the implementation of the new working schedule with a startup date at the end of 2002 requires the investment of not less than 560 k$, including the financing for the resuming of work in JINR laboratories, in 2000. However, increased financing in the coming years will not compensate for the delay in the project implementation as soon as each stage needs a definite time and should be included in the annual plans of partner-institutions.

Table 4

Financing of the IREN project in 1999

№	Activity	Contract №	Executing Institution	Initially scheduled payments in 1999	Modified payments schedule in 1999	Paid in the first half of 1999	To be paid by the end of 1999	Paid in the second half of 1999	Total payments in 1999
1	Design and manufacture of $W(^{10}B)_2$ reflectors for fuel elements	400/485	"Tyazhimpex"	1.5 k$	1.5 k$	1.5 k$	----	----	1.5 k$
2	Design and construction of fuel elements	400/482 400/483 400/612	Mayak plant VNIINM Tyazhimpex	300 KR 150 KR 3010 KR	300 KR 150 KR 3010 KR	---- ---- 1964 KR	300 KR 150 KR 1046 KR	250 KR 150 KR 1046 KR	250 KR 150 KR 3010 KR
3	Multiplying target Technical project Project of technical provision of safety Civil engineering project	 400/193 400/643 400/644 400/196 400/645	 NIKIET NIKIET RECON GSPI ECOPROECT	 12.7 k$ 45 k$ 27.9 k$ 66 k$ 65.6 k$	 12.7 k$ --- 5 k$ --- 5 k$	 12.7 k$ --- --- --- 	 --- --- 5 k$ --- 5 k$	 --- --- --- --- ---	 12.7 k$ --- --- --- ---
4	Design and construction of accelerating system of LUE-200	400/299	BINP, Novosibirsk	110 k$	80 k$	46 k$	34 k$	40 k$	86 k$
5	Construction of RF feeder	400/251	MEPI	15 k$	10 k$	---	10 k$	10 k$	10 k$
6	Equipment of full scale RF testing-rig	---	FLNP	15 k$	15 k$	----	15 k$	9.7 k$	9.7 k$
7	Stand of electron gun	---	FLNP, LHE, PPL	5 k$	5 k$	---	5 k$	---	---
8	Beam control system	---	FLNP, LHE	2.5 k$	2.5 k$	---	2.5 k$	---	---
	TOTAL			504.2k$	274.7 k$	139.2 k$	135.5 k$	117.9 k$	257.1 k$

Table 5

Time-table of the IREN project implementation in 2000-2003

Work	2000				2001				2002				2003			
Quarter	1	2	3	4	1	2	3	4	1	2	3	4	1	2	3	4
Civil engineering project of IREN facility, including technical provision of safety																
Production of accelerating tubes, buncher and SLED system and shipment to JINR																
Construction of main linac systems and their test at full scale testing facilities of JINR																
Fuel elements manufacture, licensing and shipment to JINR																
Technological project of multiplying target construction																
Manufacture of the multiplying target and its auxiliary systems																
Licensing of shut down and dismounting of IBR-30																
Production of equipment for IBR-30 dismounting																
Dismounting of IBR-30 and LUE-40																
Reconstruction of Bld. 43 and IREN infrastructure																
Mounting of IREN linac and multiplying target in Bld. 43																
Startup, tests and adjusting of IREN																
Required funding (k$)	576				920				699				300			

Approved total cost of the IREN project - *3740 k$*
Invested in 1994-1999 - *1302 k$*
To be invested in 2000-2003 - *2438 k$*

THE IBR-2 SPECTROMETERS COMPLEX AND COMPUTATION INFRASTRUCTURE

In the development of the IBR-2 spectrometers complex the main effort concentrated on the creation and introduction of new-generation electronics and software for VME-systems of data acquisition and control of experiment.

On HRFD, test experiments of a VME-system completed and it was commissioned. The system consists of several subsystems and provides:

- accumulation of low-resolution spectra,
- control of the spectrometer devices (goniometer, scanner, refridgerator, etc.),
- registration, computation, and accumulation of high-resolution spectra (RTOF-analyzers),
- control of the Fourier-chopper,
- network support (accumulation of data in central file-servers, remote control from an X-terminal).

The YUMO spectrometer was modernized. In place of old drivers, step-motors were installed to drive the sample displacement table (in two directions) and platforms for moving of scattering detectors inside the neutron guide. Also, new electronic blocks were developed to automate the moving mechanisms, which makes it possible to change the configuration of the setup in the manual and computer versions. The second collimator was replaced by a collimator with a sliding tube. This removed an air gap of 1 m on the way of neutrons. A second scatterer (polyethelene) in front of the scattering detector platform and an additional monitoring counter were installed. The system for regulating of the sample temperature was essentially improved.

On the YUMO spectrometer, VME-subsystems to automate control of the spectrometer devices and the first stage of electronics and software for the VME-subsystem of data acquisition were put into operation in October 1999. The software enables multiwindow control of data acquisition, temperature, motors, monitoring of parameters, and control of the experiment, including remote control from any point of the local network. For several months, test experiments of a ring position-sensitive detector in aggregate with a unified VME-electronic system of data acquisition were carried out with a neutron source. At present, the detector, electronics and the software are ready for the installation in the beam.

In the VME-system of data acquisition of the x-ray spectrometers DRON and SAX, electronics controlling the executive mechanisms is renewed and a new software analogous to the YUMO software in functional possiblities is developed.

On the DN-2 spectrometer, preparatory work to change the measuring systems and sample environment to VME-standard completed. The electronics of the goniometer (GKS-100, PS111, HUBER) and of moving the rotation table with a PSD using a position sensor were reconsructed and modernized. The electronics of a linear PSD was manufactured.

The two-axis position-sensitive detector is filled with a new gas mixture. Test measurements and tuning of the working modes of the detectors were conducted. The electronics of the detectors was modernized and work to optimize time and position resolutions was carried out. A new two-channel time-digital converter for data reading from PSD was developed.

Today, a complete set of VME-devices for the spectrometer is installed, the software is ready, and debugging is being done.

Under the auspices of the modernization project of the polarized neutron spectrometer SPN, the working drawings of the head part of the spectrometer were made and manufacturing started in Experimental Workshops. The electronics of the monitoring detector and 16 preamplifiers for the main detector were manufactured and debugged. Manufacturing of a unified VME system for data acquisition started.

A large volume of work was conducted to manufacture and assembly the elements of the FSD spectrometer in channel 11 of the IBR-2 reactor. Namely,

- a Fourier chopper was manufactured, assembled and tested in cooperation with PINP,
- a prototype of one element of the 90^{o}-detector was manufactured and tested,
- a mirror oven (to 10000^{o}C) was manufactured and tested in cooperation with LfZP (Rossendorf),
- test measurements of a tensor neutron scanner were conducted,
- VME equipment for the registration of low-resolution spectra and the system to control the executive mechanisms were manufactured and tested. Also, tuning of the RTOF analyzer for the detector MultiCon 5.2 began.
- the beam profile at the neutron guide entrance and transmission functions of the Fourier chopper were measured.

For the spectrometer DN-12, a complete set of detecting electronics and a VME-system for data acquisition were manufactured and debugged. Work to select He-counters and develop software is being completed.

In cooperation with HMI (Berlin) there was developed a data acquisition system for a PSD prototype based on microstrip-chambers with a Gd neutron converter. The central elements of the system are a TMS320C67XX digital signal processor with a performance of 1 Gfolps, two 8-channel time-digital converters, F1, with a picosecond resolution, a hystogram memory with a capacity of 256 Mb, two FIFO-buffers, and a PCI interface.

Also, in cooperation with HMI new programs were developed and they essentially extended the possibilities of the PV-Wave packet for visual express analysis of data from neutron scattering experiments.

Together with the Laboratory of Nuclear Problems a system of filmless registration and accumulation of data from a streamer chamber was created (DUBTO project). The basic elements of the system are two digital TV-cameras (a stereo-pair) on scientific-grade CCD matrices with the resolution 1300x1000. The data are accumulated in a PC with high-capacity removable hard disks. In 1999 the system was commissioned and the first physical results were obtained.

In 1999 a number of new unified blocks of analog electronics, including preamplifiers, amplifier-formers and discriminators for point detectors, power units and power amplifiers for executive mechanisms, etc., were created to replace outdated blocks in the equipment of the spectrometers.

During the reported year a lot of effort concentrated on repairing, modernization and maintenance of the measuring and control systems of the spectrometers and computers.

In 1999 the members of the Division published 5 papers and a Candidate of Science thesis was defended by E.I.Litvinenko.

4. EXPERIMENTAL REPORTS

4.1. CONDENSED MATTER PHYSICS

Diffraction

Structural and Magnetic Properties of $La_{0.85}Ca_{0.15}MnO_3$ CMR Perovskite
M.V.Lobanov, A.M.Balagurov, V.Yu.Pomjakushin, P.Fischer, M.Gutmann, A.M.Abakumov, O.G.D'yachenko, E.V.Antipov, O.I.Lebedev, G. Van Tendeloo

Enhancement of T_c in Hg-1223 by Fluorination
K.A.Lokshin, D.A.Pavlov, S.N.Putilin, E.V.Antipov, D.V.Sheptyakov, A.M.Balagurov

A-Cation Size and Oxygen Isotope Substitution Effects on $(La_{1-y}Pr_y)_{0.7}Ca_{0.3}MnO_3$ Structure
A.M.Balagurov, V.Yu.Pomjakushin, D.V.Sheptyakov, V.L.Aksenov, N.A.Babushkina, O.Yu.Gorbenko, A.R.Kaul

TOF Width of Diffraction Lines Measured with High Resolution Fourier Diffractometer
A.M.Balagurov, V.G.Simkin, M.Popovici

Helical Magnetic Structure in Tb Affected by Uniaxial Tension: Neutron Examination
A.V.Andrianov, A.I.Beskrovnyi, D.I.Kosarev

Structure Investigation of Rhenium Dioxide by Neutron Powder Diffraction at Ambient and High Pressure
K.G.Bramnik, H.Fuess, D.V.Sheptyakov

High Pressure - Low Temperature Structural Study of ND_4I
V.P.Glazkov, D.P.Kozlenko, B.N.Savenko, V.A.Somenkov

Investigation of Nd_2CuO_4 Crystal Structure at High Pressures
V.P.Glazkov, B.N.Savenko, V.A.Somenkov, D.V.Sheptyakov, S.Sh.Shilstein

Influence of Temperature and Long-Time Loading on Texture and Physical Property of Calcite
T.I.Ivankina, A.N.Nikitin, G.A.Sobolev, V.A.Sukhoparov, A.S.Telepnev, K.Ullemeyer, K.Walther

Laboratory Investigation of Elastic Anisotropy and Texture of Rocks from Kola Super Deep Borehole SG-3
A.N.Nikitin, T.I.Ivankina, K.Ullemeyer, T.Lokajicek, Z.Pros, K.Klima, Yu.P.Smirnov

Applied and Residual Strain/Stress Determination on Quartz Rocks Using Neutron TOF Diffraction
C.M.Scheffzuk, A.Frischbutter, K.Walther, R.A.Zhukov

Residual Stress Study by Neutron Diffraction in Perforator's Striker
G.Bokuchava, N.Shamsutdinov, A.Tamonov

Small-Angle Scattering

Light-Induced Long-Living Changes of Bacteriorhodopsin Structure
V.I.Gordeliy, N.Dencher, T.Hauss, A.Kuklin, A.Tougan-Baranovskaya, J.Teixeira, L.S.Yaguzhinsky, G.Bueldt

Microstructural Studies on Different Treated Aluminium Alloys by SANS
F.Haussler, A.I.Kuklin, G.Zouhar, H.Worch

Microstructural Studies on Hydrating Tricalcium Silicate by SANS
F.Haussler, A.I.Kuklin, S.Palzer, A.Eckart

A Structure of DMPC Vesicles in Surcose/Water Solutions
M.A.Kiselev, P.Lesieur, A.M.Kisselev, D.Lombardo, M.Killany, S.Lesieur

Determination of Structural Parameters and Hydration of Unilamellar Vesicles at High Water Excess from SANS Curves Using a Multiple-Strip Model
P.Jorchel, M.Kiselev, G.Klose, H.Schmiedel

SANS Study of Aggregates of the Gemini Surfactant 1,4-Butanediamonium-N,N'-Dihexadecyl-N,N,N',N'-Tetmethyl Dibromide in the Aqueous Solution
M.Dubnickova, M.Kiselev, I.Lacko, F.Devinsky, P.Balgavy

SANS Study of Block Copolymer Micelles with Coated Cores
J.Plestil, H.Pospisil, V.I.Gordeliy

Neutron Optics

Nuclear Potential of Glass Substrate Obtained from Spin-Flipped Neutron Transmission Through the Co Film
V.L.Aksenov, S.V.Kozhevnikov, Yu.V.Nikitenko

Magnetic Inequality of Film Interfaces Extracted by Polarized Neutron Refraction
V.L.Aksenov, S.V.Kozhevnikov, Yu.V.Nikitenko

Magnetic Regime of glass/Fe(1000Å)/Gd(50Å) Layered Structure Extracted by Neutron Polarization Methods
V.L.Aksenov, S.V.Kozhevnikov, Yu.V.Nikitenko, H.Lauter

First Experiments of Observation of Surface Phonons and Magnons at Polarised Neutron Reflectometer REFLEX-P
D.A.Korneev, V.I.Bodnarchuk, V.F.Peresedov, V.V.Zhuravlev, A.F.Schebetov, S.P.Yaradaikin

Reflectometry Studies of the Coherent Properties of Neutrons
D.A.Korneev, V.I.Bodnarchuk, S.P.Yaradaikin, V.F.Peresedov, V.K.Ignatovich, A.Menelle, R.Gaehler

Magnetic Off-Specular Neutron Scattering from Fe/Cr Multilayers
V.Lauter-Pasyuk, H.J.Lauter, B.Toperverg, O.Nikonov, E.Kravtsov, A.V.Petrenko, M.A.Milyaev, L.Romashev, V.Ustinov

Inelastic Scattering

Collective Dynamics of Liquid Gallium Studied by Inelastic Neutron Scattering
A.Beldiman, M.Ion, Zh.A.Kozlov, A.G.Novikov, I.Padureanu, A.Radulescu, V.V.Savostin

Some Results of Investigation of Liquid ^{4}He Dynamics
I.V.Bogoyavlenski, A.V.Puchkov, A.Skomorokhov

Neutron Spectroscopy and QC Modeling of the Low Frequency Internal Vibrations of Mesitylene
L.Cser, K.Holderna-Natkaniec, I.Natkaniec, A.Pawlukojc

Neutron Spectroscopy and QC Modeling of Methyl Dynamics in 1-and 2-Methyl-Naphtalene Crystals
K.Holderna-Natkaniec, I.Natkaniec, V.D.Khavryuchenko

Neutron Scattering Studies and Quantum Chemistry Modeling of Internal Vibration of Testosterone
P.Klodzinski, K.Holderna-Natkaniec, I.Natkaniec, A.Pawlukojc, A.Szyczewski

Neutron Scattering Study of the $Cs_5H_3(SO_4)_4 \cdot 0.5H_2O$ Crystal and its Deuterated Analog
S.G.Lushnikov, A.V.Belushkin, S.N.Gvasaliya, I.Natkaniec, L.A.Shuvalov, L.S.Smirnov, V.V.Dolbinina

Investigation of Disorder Degree Effect on Vibrational Spectra of the Relaxor Ferroelectrics $PbSc_{1/2}Ta_{1/2}O_3$
S.Lushnikov, S.Gvasaliya, I.Sashin, R.Blinc

Structure, IR, NQR and INS Spectra of Hydrogen Dichloromaleates
I.Majerz, L.Jerzykiewicz, A.Pawlukojc, I.Natkaniec, J.Kalenik, L.Sobczyk

Vibrational Analysis of Pentachlorophenol
I.Majerz, A.Pawlukojc, I.Natkaniec, L.Sobczyk

On Diffusion of Big Ions in Aqueous Solutions
A.G.Novikov, M.N.Rodnikova, O.V.Sobolev

Local Structure and Charge Distribution in Ionic Conductors $Ln_{1-x}Sr_xCoO_{3-\delta}$, Ln = La,Ho; x=0.6, 0.8; δ = 0, 0.1, 0.2
A.Podlesnyak, A.Mirmelstein, H.Chimid

Low-Frequency Collective Modes in the Superionic Phase of Lead Fluoride
A.Radulescu, I.Padureanu, S.N.Rapeanu, A.Beldiman, M.Ion, Zh.A.Kozlov, V.A.Semenov

Hydrogen Trapping by Solute Atoms in Nb-Mo Alloys as Observed by the Neutron Spectroscopy
V.V.Sumin, G.Chimid, F.Mazzolai

4.2. NEUTRON NUCLEAR PHYSICS

Nuclear Properties

Experiments on Neutron Spin Interferometry Using Spin-Echo Technique
A.I.Frank, A.V.Kozlov, P.Hoghoj, F.Pfeiffer, G.Ehlers

The Technique for Simultaneous Estimation of the Level Density and Radiative Strength Functions of Dipole Transitions at $E_{ex} \leq B_n$ - 0.5 MeV
V.A.Khitrov, A.M.Sukhovoj, E.V.Vasilieva

Experimental Indications of the Probable Abrupt Change in Nuclear Properties of Heavy Nucleus at $E_{ex} \cong 0.5B_n$
V.A.Khitrov, A.M.Sukhovoj, E.V.Vasilieva

New Method of Partial Radiative Capture Cross Section Measurements
Yu.P.Popov, A.V.Voinov, P.V.Sedyshev, S.S.Parzhitski, A.P.Kobzev, N.A.Gundorin, D.G.Serov, M.V.Sedysheva

Fission

Determination of the Forward-Backward Asymmetry Coefficient in $^{35}Cl(n,p)^{35}S$ Reaction
Yu.M.Gledenov, R.Machrafi, A.I.Oprea, P.V.Sedyshev, V.I.Salatski, P.J.Szalanski

Angular Anisotropy of Fission Fragments from the Resonance Neutron Induced Fission of Aligned ^{235}U Target and the Role of $J^{\pi}K$ Fission Channels
Yu.N.Kopatch, A.B.Popov, W.I.Furman, D.I.Tambovtsev, L.K.Kozlovsky, N.N.Gonin, J.Kliman

Applied Research

Reliability of Mosses (*Hylocomium Splendens, Pleurozium Schreberi* and *Calliergon Geganteum)* as Biomonitors of Heavy Metal Atmospheric Deposition in Central Russia
M.V.Frontasyeva, Ye.V.Yermakova, E.Steinnes

Selection of Appropriate Moss Biomonitors for Studying Atmospheric Elemental Deposition in China
O.A.Stan, Zh.H.Zhang, M.V.Frontasyeva, E.Steinnes

Structural and magnetic properties of $La_{0.85}Ca_{0.15}MnO_3$ CMR perovskite

M.V. Lobanov[1], A.M. Balagurov[2], V.Yu. Pomjakushin[2,3], P. Fischer[3], M. Gutmann[3], A.M. Abakumov[1,4], O.G. D'yachenko[1], E.V. Antipov[1], O.I. Lebedev[4], G. Van Tendeloo[4]

[1] *Department of Chemistry, Moscow State University, Moscow 119899, Russia*
[2] *Frank Laboratory of Neutron Physics, JINR, 141980 Dubna, Russia*
[3] *PSI, CH-5232, Villigen, Switzerland*
[4] *EMAT, University of Antwerp (RUCA), Groenenborgerlaan 171, B-2020 Antwerp, Belgium*

The CMR perovskites exhibit a large variety of phase transformations and lattice distortions determined by several structural factors including average size of A-cations and formal Mn valence. According to standard structural phase diagram [1], compositions belonging to the crossover between AFM-insulating and FM-metallic region are within the stability range of orthorhombic (space group Pnma) structure. The Sr-containing compositions corresponding to the crossover region have been recently studied in detail. It was shown by use of single crystal neutron and X-ray synchrotron diffraction for the particular composition $La_{0.88}Sr_{0.12}MnO_3$ that a sequence of temperature-induced structural transformations [2] occurs. Recently Cox et al. [3] showed that a phase separation into two phases occurs below 350 K with splitting of some majority-phase reflections indicative of monoclinic ($\beta \approx 90.1°$) distortion of the parent orthorhombic structure. Our recent HREM observation may indicate for the breakdown of orthorhombic symmetry for Ca-containing compositions as well at least on the microdomain scale. Thus we attempted to prepare stoichiometric compound with the composition $La_{0.85}Ca_{0.15}MnO_3$ belonging to the crossover region in order to clarify its structural and magnetic properties in neutron and electron diffraction experiments.

To avoid possible inhomogeneous cation distribution and also to reduce synthesis temperature to avoid anion vacancies formation we applied freeze-drying technique which is characterised by atomic-scale homogenisation. Single phase composition of the sample was confirmed by X-ray powder diffraction. The cation composition inferred from EDX corresponds to La:Ca:Mn ratio 0.84(2):0.149(3):1.00(1), indicating for absence of deviations from nominal cation stoichiometry. The ratio is virtually identical for different crystallites; numbers in parentheses are calculated statistical errors, their magnitudes are indicative of highly uniform cation distribution. The iodometric titration analysis revealed 15±5% of Mn^{4+} corresponding to the oxygen index 3.00(3). Thus, combination of EDX and chemical analysis confirmed complete stoichiometry of the compound and absence of significant deviations from the nominal composition.

Neutron data for magnetic structure refinement were collected with the powder diffractometer DMC at the SINQ spallation source at PSI in Villigen using neutron beam with wavelength λ=2.562 Å. A ferromagnetic contribution was clearly observed at low temperature and no additional antiferromagnetic peaks were detected at any temperatures. The atomic positions obtained from the high resolution neutron diffraction data (HRFD diffractometer at the IBR-2 reactor) for Pnma space group were fixed in the refinement of the DMC data. The refinements show best χ^2-square for Mn-spins directed along the c-axis, however, the refined value of the Mn-moment is not sensitive to the Mn-spin direction. The low temperature data obtained at HRFD shows that the main magnetic contribution is to the (200) peak, which means at least that μ_{Mn} is non-parallel to *a*-axis. Low temperature value of

the moment is μ=2.9(2) μ_B, and agrees well with Mn-moments measured for the same compositions earlier.

In order to determine the actual symmetry Selected Area Electron diffraction (SAED) and High-Resolution Electron Microscopy (HREM) were performed using Philips CM20 and Jeol 4000 EX instrument operating at 200 kV and 400 kV, respectively. Image simulations were made using MacTempas software. On the basis of these data it was concluded that the real-space symmetry is lower than Pnma. The data are consistent with either $Pmc2_1$ or $P2_1/c$ symmetry.

For choosing the correct model neutron powder diffraction (NPD) experiments were performed with high resolution TOF Fourier diffractometer HRFD (Fig.1). It was found that the diffraction patterns could be rather well described in average by the standard structural model with the orthorhombic Pnma symmetry. In this approximation the temperature behavior of average <Mn-O> bond length and <Mn-O-Mn> angle well before and below phase transition temperature was found regular and typical: <Mn-O> goes down with decreasing temperature and changes slope at T_c, <Mn-O-Mn> also goes down till T_C, but then

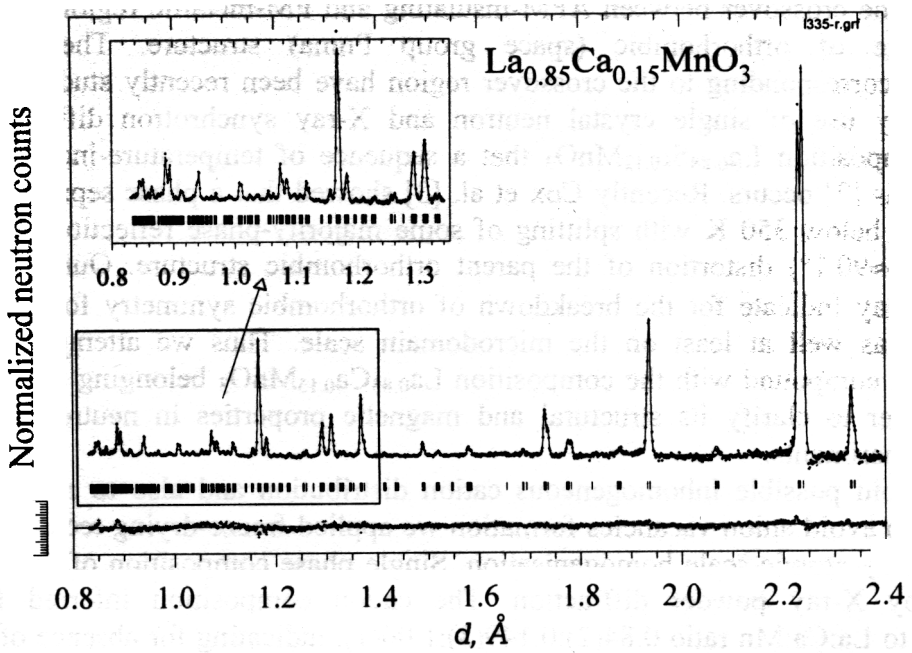

Fig.1. Neutron diffraction pattern of $La_{0.85}Ca_{0.15}MnO_3$ sample, measured at 200 K with the HRFD diffractometer. Experimental, calculated ($P2_1/c$ sp. gr.) and difference curves are shown. The difference curve is normalised on the mean square deviation.

starts to increase (Fig.2). However in some interval of spectra, especially around (220)/(022) doublet, coincidence between experimental and calculated patterns was unsatisfactory. Analysis showed that in the frame of Pnma space group variation of any parameters including atom occupancy factors does not give adequate description of that doublet. The general outlook of the diffraction pattern including the doublet region is only slightly affected by temperature variation (except for the appearance of ferromagnetic component below T_c), so the fit was performed for the data acquired with the best statistical accuracy at T=200 K.

The three possibilities (two $Pmc2_1$ and $P2_1/c$ models) were checked by the Rietveld refinement of NPD data. The refinement of the $Pmc2_1$ model with two A-cation sites yielded reliability factors (χ^2=1.58, R_P=0.116, R_w=0.078), atomic positions and interatomic distances almost identical with those for Pnma model. The refinement is not sensitive to the relative occupation of nonequivalent A-sites by La and Ca in spite of significant difference in their

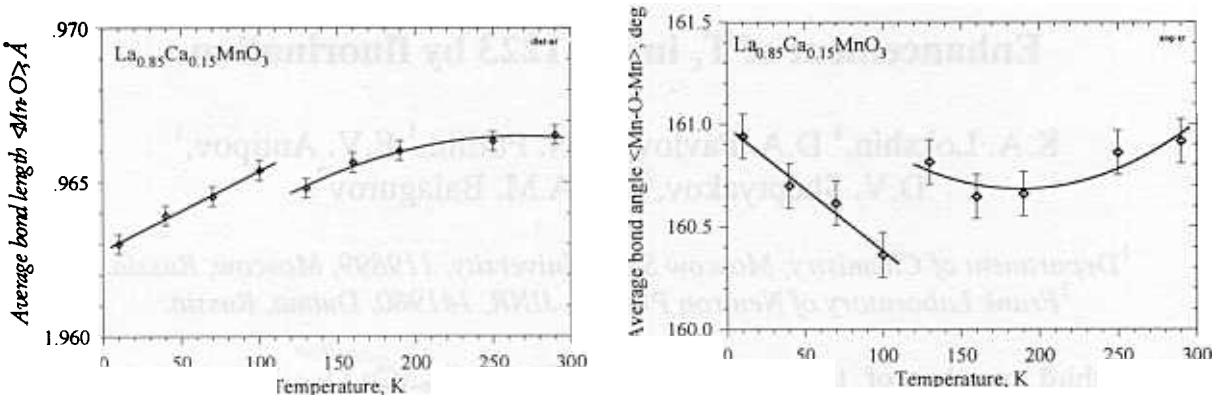

Fig.2. Temperature dependence of average Mn-O distance and Mn-O-Mn bond angle, calculated in Pnma model. The lines are guides to the eye.

atomic scattering factors (0.824 and 0.490 for La and Ca, respectively); the variation of occupation factors does not provide better profile description or χ^2 value lowering. On the other hand, $Pmc2_1$ model with two Mn-sites gives satisfactory description of the doublet, but the general fit is much worse compared with Pnma model (χ^2=3.21, R_P=0.139, R_w=0.111). Moreover, the refinement of thermal parameters for oxygen atoms fails to converge indicating for their incorrect location. The refinement in $P2_1/c$ space group leads to significantly better fit of experimental neutron diffraction pattern (χ^2=1.43, R_P=0.107, R_w=0.074); the main difference from Pnma case arising from the correct description of the (220)/(022) orthorhombic doublet.

The two Pnma phase model as another possibility for better fitting of high-resolution neutron diffraction pattern could not be rejected on the basis of neutron diffraction data only. The refinement in this model was performed with the positional parameters for two phases forced to coincide and yielded reliability factors comparable with the $P2_1/c$ model (χ^2=1.47, R_P=0.110, R_w=0.075). Refined lattice parameters for the two phases are a=5.4764(1), b=7.7488(2), c=5.5036(2) and a=5.4680(2), b=7.7383(4), c=5.5058(4), respectively; phase ratio is approximately 2:1. However, this possibility does not account for ED and HREM data available.

In conclusion, we performed detailed crystal structure investigation for the $La_{0.85}Ca_{0.15}MnO_3$ composition by a combination of electron diffraction, high resolution electron microscopy and neutron diffraction. Various possible crystal structure models allowed by ED were checked by Rietveld refinement of NPD data. On the basis of the entire set of data we claim that the actual crystal structure is monoclinic $P2_1/c$. The different oxygen environment for two nonequivalent Mn-atoms suggests the possibility of the treatment of observed structural distortion as a consequence of charge ordering. The ordered placement of Mn atoms can lead to a profound modification of physical properties. Since ordering has two-dimensional character, it would not necessarily lead to insulating behavior. Nevertheless, the existence of different Mn-O-Mn angles may lead to the complicated pattern of exchange interactions, different from those expected from Pnma model.

P. Schiffer, A.P. Ramirez, W. Bao, and S.-W. Cheong, Phys. Rev. Lett. **75**, 3336 (1995).
2. H. Kawano, R. Kajimoto, M. Kubota, and H. Yoshizawa, Phys. Rev. **B53**, R14709 (1996)
3. D.E.Cox, T.Iglesias, G.Shirane, K.Hirota, and Y.Endoh, Powder Diffraction, **14**, 147 (1999)

Enhancement of T_c in Hg-1223 by fluorination

K.A. Lokshin,[1] D.A. Pavlov,[1] S.N. Putilin,[1] E.V. Antipov,
D.V. Sheptyakov,[2] and A.M. Balagurov[2].

[1]*Department of Chemistry, Moscow State University, 119899, Moscow, Russia.*
[2]*Frank Laboratory of Neutron Physics, JINR, 141980, Dubna, Russia.*

The third member of the superconducting $HgBa_2Ca_{n-1}Cu_nO_{2n+2+\delta}$ homologous series exhibits a record $T_c \approx 135$ K at ambient conditions. Moreover, an application of external pressure promotes its increase up to 160 K. This result shows a principal possibility to achieve in Hg-1223 similar values of T_c at ambient pressure by proper modifying of its composition and, subsequently, crystal structure. Pressure effect can be simulated by an anion exchange. Fluorine has a lower formal valence than oxygen therefore the larger amount of fluorine should be incorporated into the structure to achieve the same carrier concentration. Moreover, it has slightly smaller radius than oxygen. Both factors can promote a variation of characteristic bond lengths. It was shown that fluorination of Hg-1201 resulted in a significant compression of the apical Cu–O distance, while the in-plane one did not vary in comparison with those in the oxygenated Hg-1201 samples exhibiting the same T_c values [1]. For this superconductor an anion exchange does not allow to enhance T_c and its optimal values for both series were 97 K. This fact allowed to conclude that compression of apical Cu-O bond could not be the main factor of T_c enhancement under high pressure. It was shown that the achievement of the same carrier concentration and T_c's requires a double amount of fluorine in comparison with oxygen.

The larger anion concentration can be also incorporated into the fluorinated Hg-1223 structure compared to the oxygenated one resulting in the Cu–O distances variation. The effect of oxygen – fluorine anion exchange may be different for Hg-1201 and Hg-1223 phases due to different coordination polyhedra for Cu cations. Therefore we suggested that it would be interesting to study an influence of such anion substitution on structural and superconducting properties of Hg-1223 phase.

Syntheses of Hg-1223 samples were carried out in a sealed silica tubes in two-temperature furnace. We found that an excess of copper in the starting mixture resulted in synthesis of Hg-1223 samples with the lower amount of impurity phases. This technique allowed to obtain samples with Hg-1223 content about 95%. Reduced Hg-1223 samples were subjected by fluorination or treatment in oxygen flow during 20 h at 300°C. Fluorination was performed with the use of XeF_2

The most important observation is that some samples after fluorination exhibit T_c = 138 K which was not reached on samples annealed in oxygen flow. This fact was carefully investigated. The Hg-1223 sample preliminary reduced to T_c = 100 K was divided on two parts. One of them was fluorinated while the other part was treated in oxygen flow. Fluorinated sample (a=3.8501(2) Å and c=15.773(3) Å) shows onset of the transition at 138 K, while the oxygenated sample exhibits T_c=134 K and has significantly larger lattice parameters: a=3.8524(4) Å and c=15.819(4) Å. So we can conclude that fluorine incorporation into Hg-1223 structure allows to increase T_c up to 3 – 4 K in comparison with oxygen-treated samples.

To understand the reason of this phenomenon one sample with the minimum of impurities was further investigated by NPD and XRD methods. The neutron powder diffraction spectrum

was measured at temperature T=7 K with the high-resolution Fourier diffractometer (HRFD) at the IBR-2 pulsed reactor. In our experiment the resolution of HRFD, Δd/d was near 0.0015, which allowed to obtain the precise structural information. In particular, the errors of the interatomic distances were about 0.005 Å. An example of the diffraction spectrum measured at the HRFD and treated with the Rietveld method is given in Fig.1. Remarkably that NPD pattern contains only one impurity phase of CaO with mass fraction less than 1%. This allowed us to obtain structural parameters with high precision, because incorrect handling in the refinements of impurity phases results in significant systematic errors especially for the occupancy parameters.

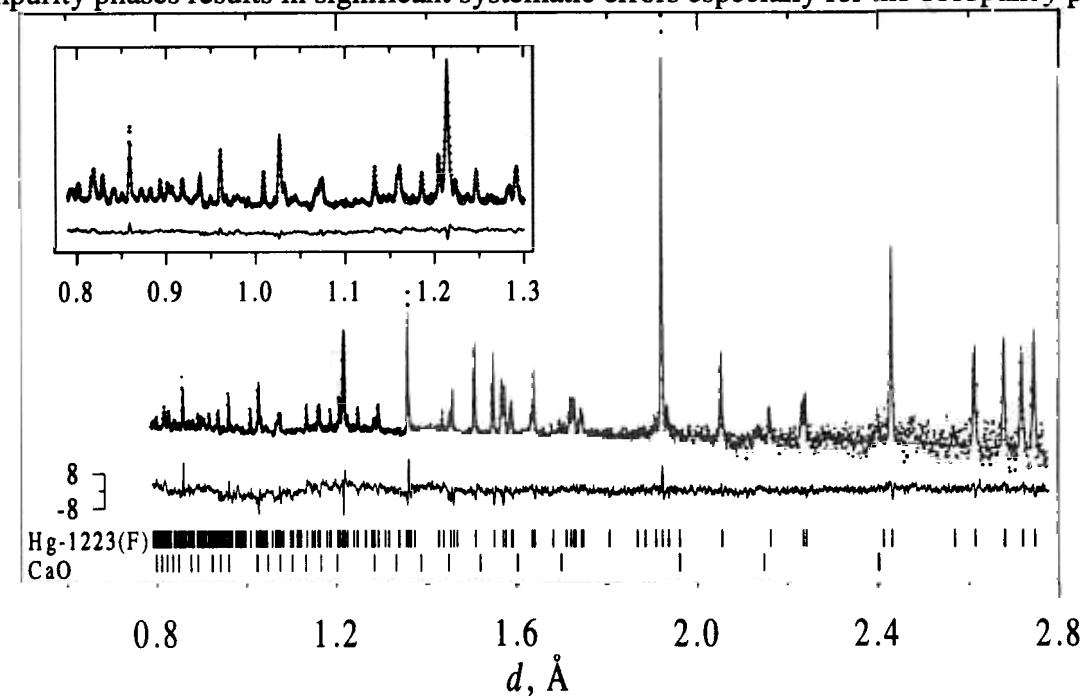

Figure 1. Rietveld refinement of neutron diffraction pattern of Hg-1223 fluorinated compound. Experimental points, calculated and difference profiles are shown. Tiks below the graph correspond to the positions of Hg-1223 and CaO impurity phase peaks. The inset shows the low d-spacings region.

We have found two types of positions of extra anion located in the (Hg) layer: A(1) in the middle of the mesh – (0.5, 0.5, 0) and A(2) in the middle of the edge – (0.5, 0, 0) with the occupancies 27(1)% and 10(1)% respectively. The latter value is close to Cu concentration in Hg site and may be attributed to additional bonding between Cu and anions. It is interesting to note that these values as well as positional parameters of atoms were practically insensitive to a variation of the Hg/Cu ratio in the Hg position in the range of 10 – 30%.

Incorporation of fluorine results in structure modifications reflected by a change in lattice parameters. The change of the *a*-parameter reflects a variation of the extra anion concentration in the structure. The dependencies of T_c vs *a*-parameter for oxygenated and fluorinated Hg-1223 samples are shown in Fig.2. The values of lattice parameters determined by XRD with internal standard were used to avoid possible systematic errors between data obtained by different techniques.

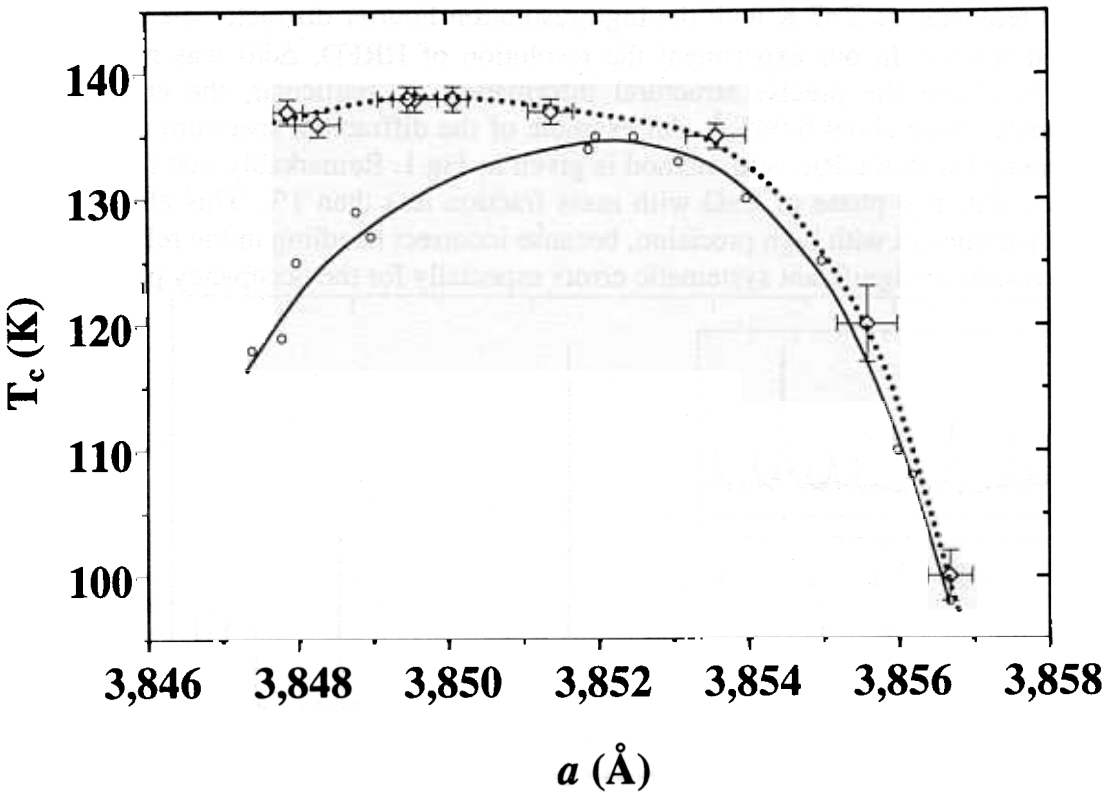

Figure 2. The T_c vs a-parameter dependence the fluorinated (◊) and oxygenated (O) Hg-1223 samples. Lines are guides to the eye.

The right part (underdoped range) of the $T_c(a)$ curve for fluorinated series is close to the oxygenated one up to a = 3.852 Å and $T_c \approx 134 - 135$ K. These values correspond to the optimally doped oxygenated Hg-1223 samples. However, further increase of extra anion concentration promotes an increase of T_c for the fluorinated series up to 138 K while oxygenated Hg-1223 exhibits a decrease of T_c due to overdoping. For the fluorinated series the optimal value of the a-parameter is smaller in comparison with the oxygenated series: 3.850 Å and 3.852 Å respectively. Therefore we can conclude that a partial exchange of extra oxygen by fluorine in (Hg) layer results in a compression of the structure in the *ab* plane which is accompanied by an increase of optimal T_c value. This fact is different from the data recently found for Hg-1201 where the $T_c(a)$ dependencies for oxygenated and fluorinated samples practically coincide and have the same values of optimal T_c = 97 K and in-plane parameter (3.880 Å).

[1] A.M. Abakumov, V.L. Aksenov, V.A. Alyoshin, E.V. Antipov, A.M. Balagurov, D.A. Mikhailova, S.N. Putilin, and M.G. Rozova, Phys. Rev. Lett. **80**, 385 (1998).

A-cation size and oxygen isotope substitution effects on $(La_{1-y}Pr_y)_{0.7}Ca_{0.3}MnO_3$ structure

A.M.Balagurov[1], V.Yu.Pomjakushin[1], D.V.Sheptyakov[1], V.L.Aksenov[1], N.A.Babushkina[2], O.Yu.Gorbenko[3], A.R.Kaul[3]

[1]*Frank Laboratory of Neutron Physics JINR, 141980 Dubna, Russia*
[2]*RRC "Kurchatov" Institute, 123182 Moscow, Russia*
[3]*Chemistry Department, Moscow State University, 119899 Moscow, Russia*

The new systematic structural data for the $(La_{1-y}Pr_y)_{0.7}Ca_{0.3}MnO_3$ series were obtained for y=0.5, 0.6, 0.7 and 0.75 as functions of temperature. One of the main goals of the work was to define the structure of the two samples with y=0.75 with different contents of the ^{16}O and ^{18}O (O-16 and O-18 samples hereafter) oxygen isotopes.

The samples of $(La_{1-y}Pr_y)_{0.7}Ca_{0.3}MnO_3$ with y=0.50, 0.60, 0.70 and 0.75 (LPCM-50 and so on, hereafter) were prepared as powders with the use of the so-called "paper synthesis". The LPCM-75 composition was additionally exposed to the process of oxygen isotopes enrichment. Their low-temperature magnetic structure was defined in the neutron-diffraction experiments, carried out with the DMC diffractometer in the Paul Scherrer Institute at the SINQ neutron source [1]. The structural neutron-diffraction experiments were carried out with the neutron diffractometer HRFD in the FLNP, JINR at the IBR-2 pulsed reactor.

At room temperature the dependencies of the LPCM unit cell parameters on the Pr content are monotonic, and the decrease of the unit cell volume with increasing Pr content is linear. The dependencies of the average values of the Mn-O distance and Mn-O-Mn angle (Fig.1) on y are also close to linear. The change of the angle in the extreme points is quite significant (about 2.5%), while the <Mn-O> distance is changed not more than by 0.15%.

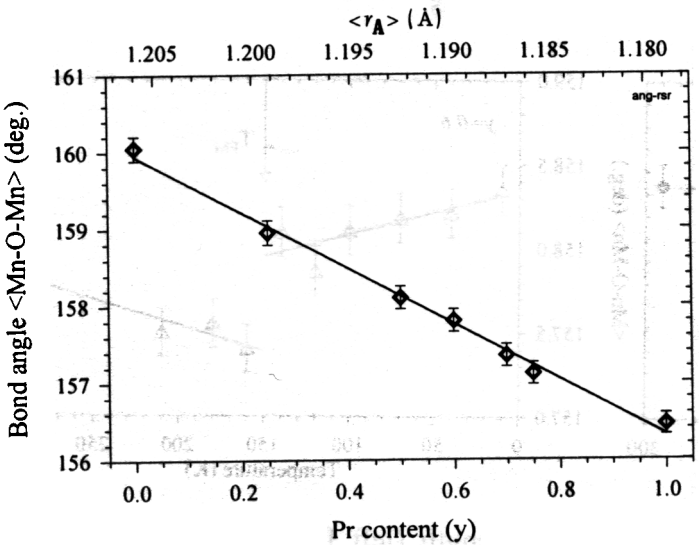

Fig.1. Dependencies of the average values for the <Mn-O-Mn> valence angle at room temperature on the Pr content. The points for y=0.5, 0.6, 0.7 and 0.75 were defined in the present paper, the points for y=0, 0.25 and 1 are taken from literature. The linear dependencies were obtained by the least-squares method. At the upper x-axis, the calculated average A-cation ionic radii corresponding to the Pr content are presented.

For all the compositions, the unit cell parameters changing with temperature has quite a complicated character, which reflects the changes of the atomic and magnetic structure in them (Fig.2). The most characteristic peculiarities are the lowering of a and b parameters near the transition to the FM phase and the characteristic minimum in the b-parameter temperature

dependence near 180 K is observed (practically absent for y=0.5 and very weak for y=0.6), which might be connected to the beginning of the charge ordering process.

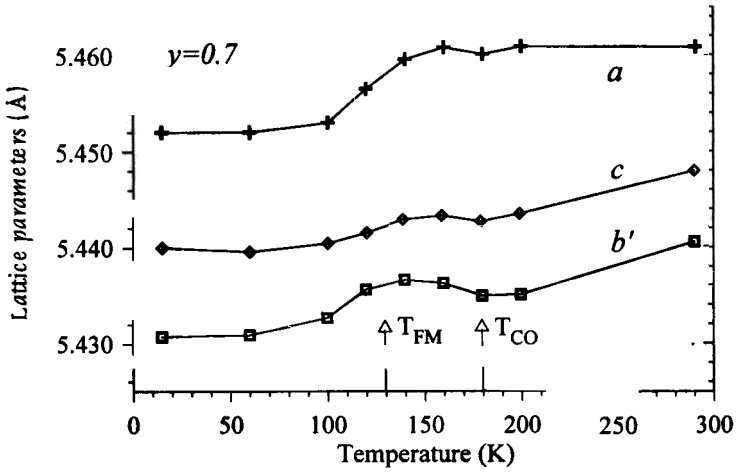

Fig.2. Temperature dependencies of *a*, *b*, and *c* unit cell parameters for the LPCM-70. The lines drawn through the experimental points are guides for the eye. The symbol sizes are larger than the experimental errors.

At room temperature the oxygen octahedra of LPCM-y are almost regular, i.e. all three independent bonds, Mn-O1 (along the *b* axis), Mn-O21 and Mn-O22 (in the *a*-*c* plane) have practically equal lengths. At approaching the temperature of the phase transition into the metallic FM state, the strong Jahn-Teller distortion appears. After reaching the saturated FM state, the "melting" of the orbital ordering occurs and the bond lengths become equal again. In the dependencies of the average values on temperature the peculiarity is also clearly observed at T_{FM}. In Fig.3, the temperature dependencies of the <Mn-O> and <Mn-O-Mn> values for LPCM-60 are shown. The characteristic jumps in <Mn-O-Mn> angle and in <Mn-O> distance are clearly seen at T=T_{FM}. The same dependencies are observed to some extent in the other compositions as well. The analysis shows that the jump in lattice parameters at T_{FM} is equally due to the jump-like change of distances and angles both in the (a,c) plane, and along the b axis.

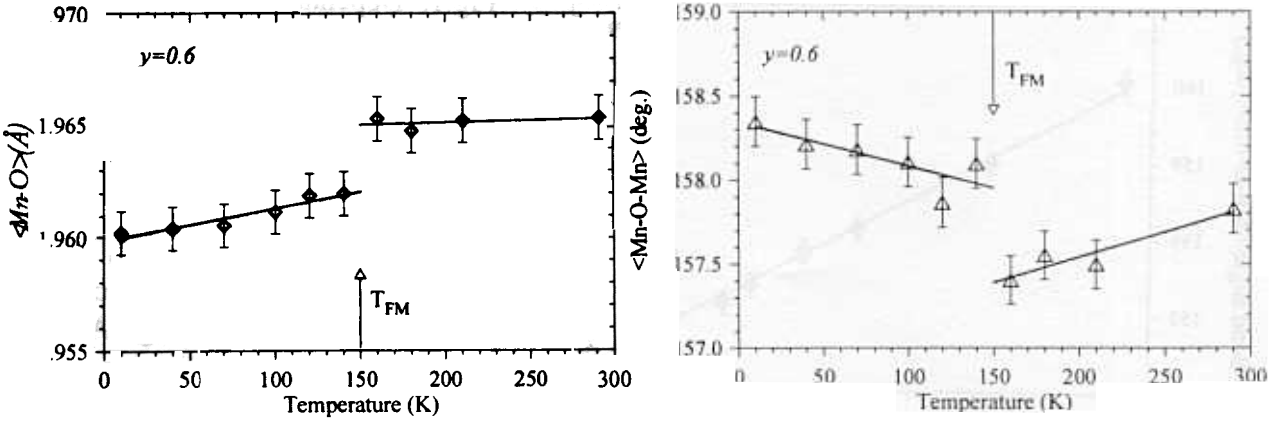

Fig.3. Temperature dependencies of the average bond length (left frame) and of the average valence angle (right frame) for LPCM-60. The arrows indicate the temperature of the transition into the FM state.

The differences in the structural behavior of O-16 and O-18 samples are more clearly seen from the temperature dependencies of the average Mn-O bond length and of the average Mn-O-Mn valence angles in them (Fig.4). It is obvious that at T≈110 K in the O-16 sample, the jump-like

(same as in LPCM-60) changes of the bond length (by ~0.003 Å) and of the valence angle (by ~0.7°) occur, while in the O-18 sample these values remain practically constant.

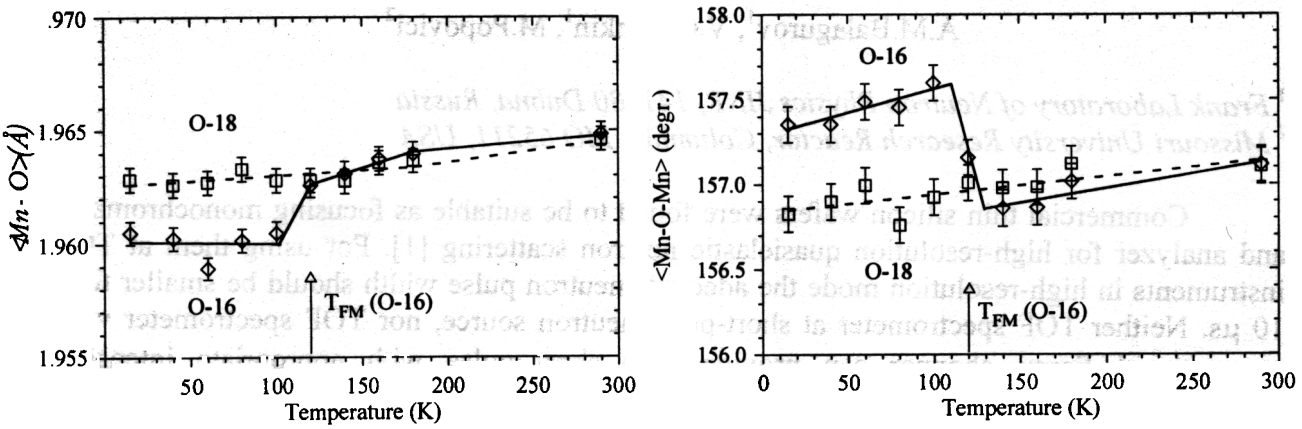

Fig.4. Comparison of the temperature dependencies of the average <Mn-O> bond length (left frame) and the average <Mn-O-Mn> valence angle (right frame) for the O-16 and O-18 samples. The arrow indicates the temperature of the ^{16}O sample transition into the FM-state.

Summary. We have shown that in $(La_{1-y}Pr_y)_{0.7}Ca_{0.3}MnO_3$, as in the other CMR perovskites, there exists the clear interplay between $\langle r_A \rangle$, atomic and magnetic structure, and transport properties. Decrease of $\langle r_A \rangle$ leads to the linear decrease of the mean <Mn-O-Mn> valence angle and, in turn, to the linear decrease of T_{FM}. The data obtained for the ^{16}O and ^{18}O enriched samples with y=0.75 have shown the structural identity of the samples in the interval between the room temperature and the temperature of the O-16 sample transition into the FM metallic phase. It means that their quite different transport and magnetic properties at $T \leq 110$ K are driven by the different oxygen atoms dynamics solely.

1 A.M.Balagurov, V.Yu.Pomjakushin, D.V.Sheptyakov, V.L.Aksenov, N.A.Babushkina, L.M.Belova, A.H.Taldenkov, A.V.Inyushkin, P.Fischer, M.Gutmann, L.Keller, O.Yu.Gorbenko, A.R.Kaul "Effect of oxygen isotope substitution on magnetic structure of $(La_{0.25}Pr_{0.75})_{0.7}Ca_{0.3}MnO_3$" Phys. Rev. B, 1999, v.60, pp.383-387.

TOF width of diffraction lines measured with High Resolution Fourier Diffractometer

A.M.Balagurov[1], V.G.Simkin[1], M.Popovici[2]

[1] *Frank Laboratory of Neutron Physics JINR, 141980 Dubna, Russia*
[2] *Missouri University Research Reactor, Columbia, MO 65211, USA*

Commercial thin silicon wafers were found to be suitable as focusing monochromator and analyzer for high-resolution quasielastic neutron scattering [1]. For using them at TOF instruments in high-resolution mode the adequate neutron pulse width should be smaller than 10 μs. Neither TOF spectrometer at short-pulse neutron source, nor TOF spectrometer with conventional Fermi chopper can provide such short pulse with appropriate intensity. Measurements confirming that it is possible with Fourier chopper are presented here.

Diffraction spectra from commercial 6″ diameter thin Si [111] plate have been measured with HRFD instrument at the IBR-2 pulsed reactor in Dubna for Fourier chopper velocities: V=4000, 6000, and 8000 rpm. Four orders of reflection are seen in diffraction patterns: 111, 333, 444, 555 (also peaks from Al jacket) (Fig.1).

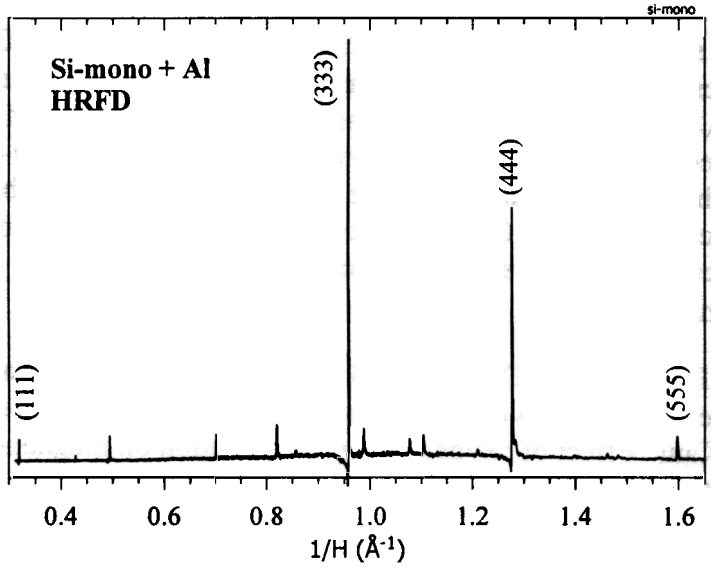

Fig.1. Diffraction pattern from Si-monochromator (hhh-plane) in Al-jacket.

In Table 1 the obtained diffraction peak widths are presented.

Table 1. Data for full diffraction peak widths (in TOF channels, τ=4 μs) for (111), (333), (444), and (555) orders at three Fourier-chopper velocities.

hkl	*d*, Å	4000 rpm	6000 rpm	8000 rpm
111	3.136	12.01	12.01	11.53
333	1.045	5.15	4.35	4.08
444	0.784	4.76	3.8	3.39
555	0.627	4.48	3.4	2.96

The general formulae for W(*d*) dependence is:

$$W^2 = (W_{TOF})^2 + (W_{ang})^2 \cdot d^2,$$

where W_{TOF} is the contribution connected with chopper velocity (W_{TOF}~1/V), W_{ang} is geometrical contribution (W_{ang}~$\Delta\theta/tg\theta$). In Fig.2 the width data are fitted by (1), without the width of the 1th order (111) which is disturbed by divergence of incident neutron beam.

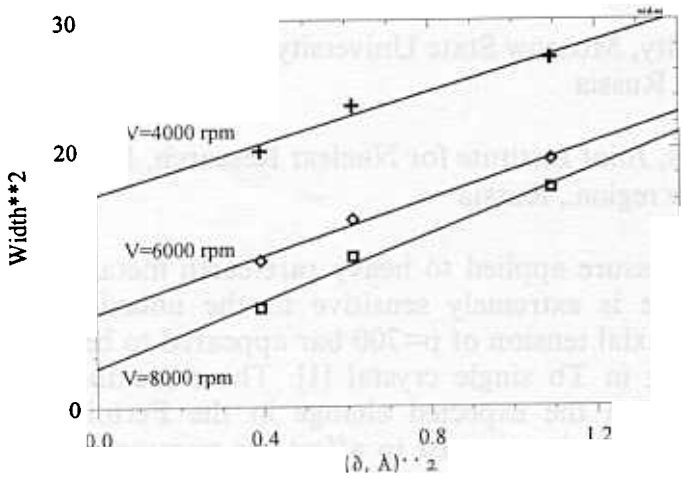

Fig.2. The full diffraction peaks width as a function of d_{hkl} for three chopper velocities.

W_{TOF} parameter determined from fits is presented in Table 3.

V, rpm	W_{TOF}^2	1/V	W_{TOF}	W_{TOF}, μs
4000	16.75	0.25	4.092676	16.3707
6000	7.73	0.1666667	2.780288	11.12115
8000	4.46	0.125	2.111871	8.447484

In Fig.3 W_{TOF} as a function of 1/V is shown. The LS line is indeed going to zero point if V=∞.

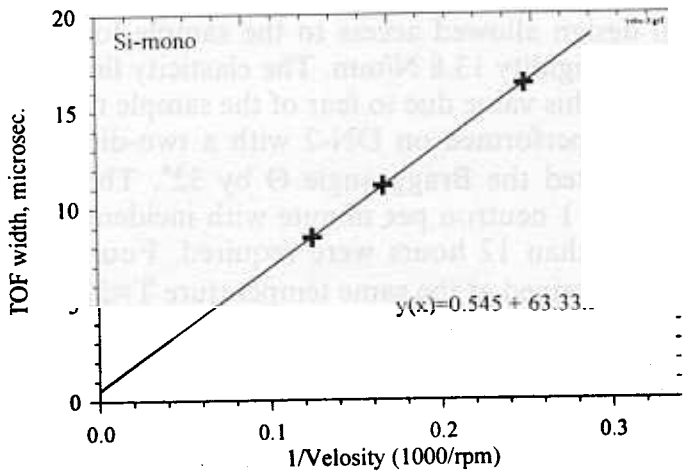

Fig.3. TOF contribution in the full width as a function of 1/V. The line is the least-square fit.

In conclusion, we have shown that equation (1) is a good approximation for the width of diffraction peaks measured with HRFD and the TOF contribution in full width is inversely proportional to chopper velocity. If Fourier chopper speed V>7000 rpm, TOF contribution is smaller than 10 μs, in particular for V=10000 rpm, W_{TOF} could be as small as 6.8 μs.

[M.Popovici et al., Physica B, 243 (1998) 216

HELICAL MAGNETIC STRUCTURE IN Tb AFFECTED BY UNIAXIAL TENSION: NEUTRON EXAMINATION

A.V.Andrianov[a], A.I.Beskrovnyi[b] and D.I.Kosarev[a]

[a] Low Temperature Dept., Physics Faculty, Moscow State University, 19899, Moscow, Russia

[b] Frank Laboratory of Neutron Physics, Joint Institute for Nuclear Research, Dubna, Moscow region., Russia

Recent experiments with uniaxial pressure applied to heavy rare-earth metal terbium revealed that its helical magnetic structure is extremely sensitive to the uniaxial elastic deformation. Namely, the relatively low uniaxial tension of p=700 bar appeared to be enough to suppress completely the helical ordering in Tb single crystal [1]. There are theoretical considerations that tie this phenomenon with the expected change in the Fermi surface topology caused by tension applied. This change is expected to affect the parameters of the RKKY interaction (that is responsible for the magnetic ordering in rare earth metals) and thus the type of the magnetic ordering [2]. The theory [2] predicts that the helical wavevector q shall depend on uniaxial tension p as a square root: $q \propto (p_{cr}-p)^{1/2}$, where p_{cr} is the critical tension value (p_{cr}=700 bar in our case). The neutron experiment was performed to validate this prediction.

The purity is declared as 99% of the Tb single crystal. The neutron scattering examination performed on DN-2 installation on IBR-2 pulse reactor confirmed the helical ordering in the sample. The sample of the shape of "capital I" *en face* was cut from this single crystal by spark erosion. Two holders of beryllium-copper were also cut by spark erosion as a fit to the sample shape. The c crystalline axis was parallel to load direction within ±1°. Operational fragment of the sample was of 3 mm length with crossection 0.57*3.87 mm^2; total length of the sample was 5.5 mm. The cell design allowed access to the sample for neutron beam. The load was produced by steel string of rigidity 13.8 N/mm. The elasticity limit for Tb is some 2 kbar, thus we newer exceed the half of this value due to fear of the sample rupture.

The neutron diffraction experiment was performed on DN-2 with a two-dimensional position sensitive detector. The cell design limited the Bragg angle Θ by 32°. The neutron output from the sample occured to be as low as 1 neutron per minute with incident beam of 10^7 neutrons/s/cm^2, hence expositions of more than 12 hours were required. Four scans at different tensions p=0, 160, 310, 470 bar were obtained at the same temperature T=229±0.2 K, or 2.5 K below magnetic ordering temperature (Neel point) T_N=231.5 K. The scan at the ambient pressure was taken before mounting the sample in the experimental cell, thus its noise level is much smaller than in the others. The remainder three were taken in the experimental cell without remounting.

The first three scans are presented on Fig.1. As the magnetic sattelites due to helical structure are weak compared with nuclear peak, 80 percent of the nuclear peak (taken in paramagnetic phase) were substracted for clarity. The sattelites are well observable but hardly resolved as their width appeared to be comparable with the helical wavevector. Under load increase the satellite width increases rapidly while nuclear peak width remains almost unchanged. Due to this broadening we failed to resolve the sattelites on the scan for the highest tension p=470 bar (not presented).

The helical wavevector values were obtained by fitting the scans with Gauss central peak accompanied with two equidistant Gauss satellites equal in amplitude and width. The fitting results are presented on Fig.1 as dashed curves, sattelites centers marked by arrows. In spite of the poor accuracy of these fits, the decrease in helical wavevector is clear. The numerical estimations of changes in lattice parameters under uniaxial tension revealed value of the order of 10^{-3}. Hence it has been confirmed that the helical ordering in terbium is rather

sensiyive to the uniaxial tension applied along c crystalline axis. This suggests that the role of crystalline lattice parameters in magnetic ordering in rare earth metal can be really crucial as was expected [2].

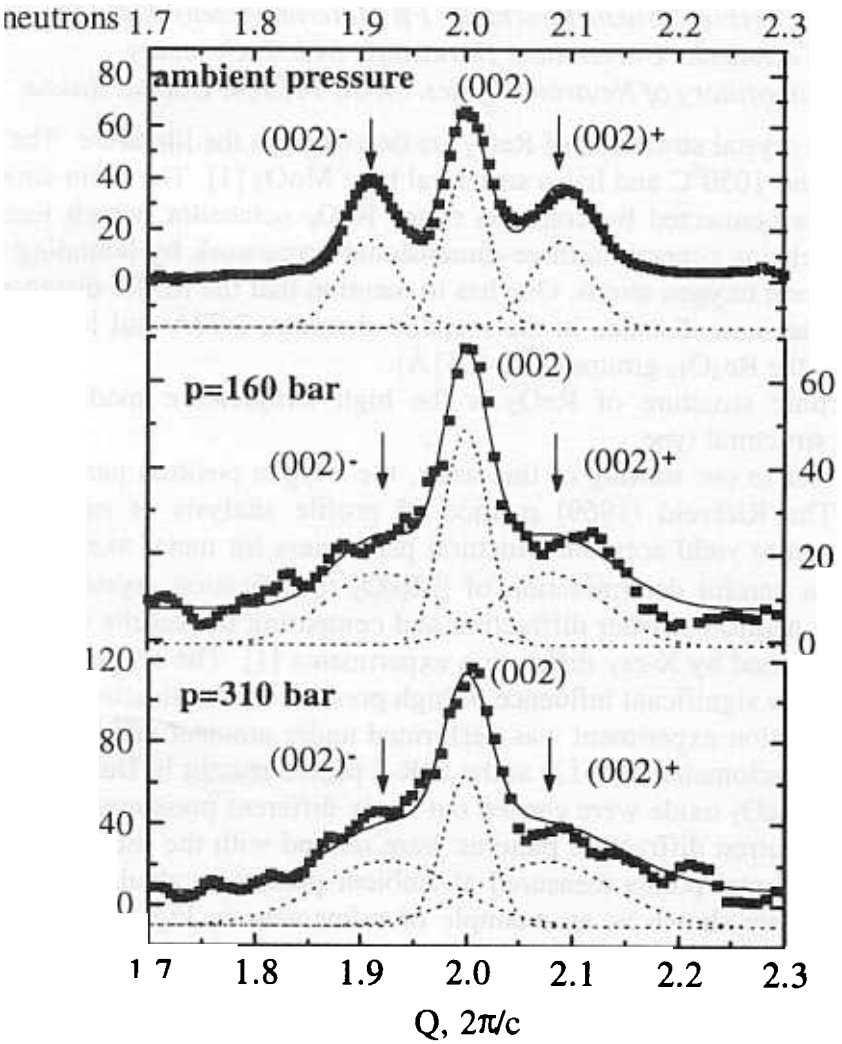

Fig.1. Neutron patterns at T=229K at ambient pressure (the top one), at p=160 and 310bar (the bottom one). 80 percent of the nuclear peak substracted for clarity. Fitting results presented as dashed curves, sattelite positions marked by arrows.

We are grateful to the late V.S.Zasimov for the X-ray examination of the sample. We are grateful to O.D.Chistiakov for the sample provided. The work was partially supported by Russian Foundaion for Basic Research (N98-02-17401).

References:

[1] A.Andrianov, D.Kosarev, A.Beskrovnyi, to be published.
[2] A.Andrianov, JETP Lett. **55** (11), 666 (1992); A.Andrianov, JMMM **140-144**, 749 (1995).

Structure investigation of rhenium dioxide by neutron powder diffraction at ambient and high pressure.

K.G. Bramnik[1], H.Fuess[1], D.V. Sheptyakov[2]

[1]*Fachgebiet Strukturforschung, FB Materialwissenschaft, Technische Universitaet Darmstadt, 64287, Germany*
[2]*Frank Laboratory of Neutron Physics, JINR, 141980, Dubna, Russia*

Two different crystal structures of ReO_2 are described in the literature. The first one is stable between 300 and 1050^{0}C and has a structural type MoO_2 [1]. The main structural units of this compound are connected by common edges ReO_6 octahedra, which form Re_nO_{4n+2} infinite chains. The chains generate a three-dimensional framework by bounding themselves together by the common oxygen atoms. One has to mention that the Re-Re distance, 2.61Å, is much shorter than the same distance in the metallic rhenium, 2.77Å and longer than in the other structures with the Re_2O_{10} groups (2.42-2.51Å).

The monoclinic structure of ReO_2 is the high temperature modification [2] and crystallizes in VO_2 structural type.

However, prior to our starting of this work, the oxygen position parameters were not well determined. The Rietveld (1969) method of profile analysis of neutron diffraction powder data is known to yield accurate structural parameters for metal oxides. The first aim of this study was in careful determination of β-ReO_2 modification crystal structure under ambient pressure by neutron powder diffraction and comparing the results with the literature data, which were obtained by X-ray diffraction experiments [1]. The second aim was to find out whether there is any significant influence of high pressure on the structure.

Neutron diffraction experiment was performed under ambient and high pressure with the high-pressure diffractometer (DN-12) at the IBR-2 pulsed reactor in Dubna. High pressure investigations of the ReO_2 oxide were carried out at six different pressures, 0.1, 0.6, 1.3, 2.3, 3.8 and 5 GPa. All neutron diffraction patterns were refined with the use of MRIA software package. The experimental points measured at ambient pressure, calculated (fitted) profile, and difference curve are shown as an example of refinement in Fig. 1. the same view of refinement fit at high pressure is shown in Fig. 2.

The final refinement results show clear difference between the refined oxygen position parameters and the same ones from literature data. The positional parameters and main interatomic distances are listed in Tables 1 and 2 respectively.

Table 1. Positional parameters of β-ReO_2.

Results of neutron diffraction pattern refinement				Literature (old, X-ray) data			
Atom	*x/a*	*y/b*	*z/c*	Atom	*x/a*	*y/b*	*z/c*
Re	0	0.1109(3)	¼	Re	0	0.11	¼
O	0.2411(4)	0.3605(4)	0.0910(3)	O	0.25	0.36	0.125

Table 2. Main interatomic distances of β-ReO_2.

Re-O	1.966(2)×2
	2.009(2)×2
	2.020(2)×2
Re-Re	2.619(1)×2

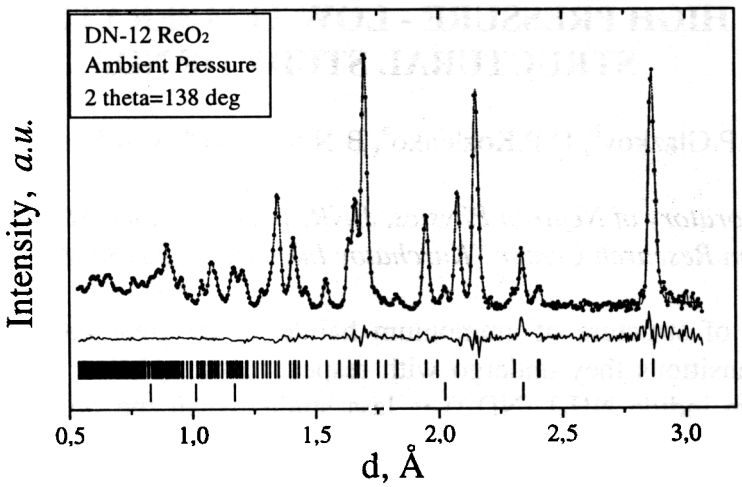

Fig. 1. Refinement fit at ambient pressure. Experimental points, calculated profile, and difference curve are shown. Tics below the curves are corresponding to the calculated positions of diffraction peaks of β-ReO_2. The "second" phase is aluminum container.

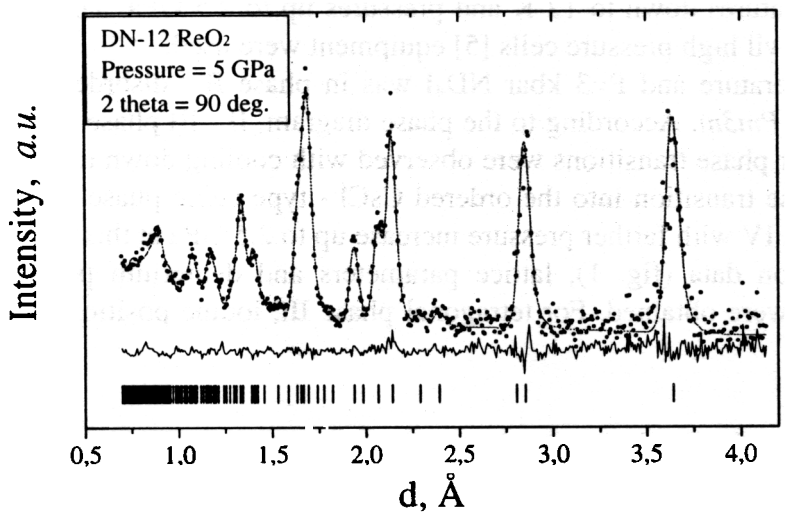

Fig. 2. Refinement fit at high pressure. Experimental points, calculated profile, and difference curve are shown. Tics below the curves are corresponding to the calculated positions of diffraction peaks of β-ReO_2.

Investigations of β-ReO_2 under pressure did not show any phase transitions up to 5GPa. No drastic changing of the structural parameters were found (at least with the accuracy available with DN-12 diffractometer). However, the determination of the ambient pressure crystal structure is the main and clear result of the experiment.

We intend to continue our high pressure study of β-ReO_2 at even higher pressures at synchrothron in Hamburg.

[1] Magneli, Acta Chem. Scand., 11, 28, (1957).
[2] Tribalot et al., Seances Acad. Sci. (Paris), 259, 2109, (1964).

HIGH PRESSURE - LOW TEMPERATURE STRUCTURAL STUDY OF ND_4I

V.P.Glazkov[b], D.P.Kozlenko[a], B.N.Savenko[a], V.A.Somenkov[b]

[a] *Frank Laboratory of Neutron Physics, JINR, 141980 Dubna Moscow Reg, Russia*
[b] *Russian Research Center "Kurchatov Institute", 123182 Moscow Russia*

Investigation of structure of ammonium halides is of great interest due to a number of orientation phase transitions they undergo with respect to the relative orientations of ammonium ions [1]. Ammonium iodide NH_4I (ND_4I) is less studied than the other ammonium halides. Its detailed phase diagram is known only at temperatures down to 100 K and pressures up to 2 GPa [2].

Recently a new high pressure phase V of ammonium halides has been discovered in Raman spectra [3]. It was found that the phase transition into the phase V occurs at P~8 GPa and ND_4I(V) phase structure has the same structural type as low temperature phase ND_4I(III) structure - tetragonal one, with antiparallel ordering of ammonium ions [1]. It was also established that pressure at which the phase transition into the phase V occurs decreases with temperature decrease [3].

To found possible differences between phases III & V structures and study the ND_4I structure at high pressures and low temperatures, we have performed neutron diffraction experiments at temperatures down to 12 K and pressures up to 2.5 GPa. The DN-12 spectrometer [4] and the sapphire anvil high pressure cells [5] equipment were used.

At room temperature and P=3 kbar ND_4I was in phase II - disordered CsCl - type cubic structure, space group *Pm3m*. According to the phase diagram, II - III phase transition has occurred at T ~ 200 K. No other phase transitions were observed with cooling down to 12 K. At T=12 K and P=5 kbar III - IV phase transition into the ordered CsCl - type cubic phase IV has occurred. ND_4I was remained in phase IV with farther pressure increase up to 2.5 GPa at this temperature.

From diffraction data (fig. 1), lattice parameters and deuterium positional parameter as functions of pressure were obtained. For tetragonal phase III, iodine positional parameter was also obtained.

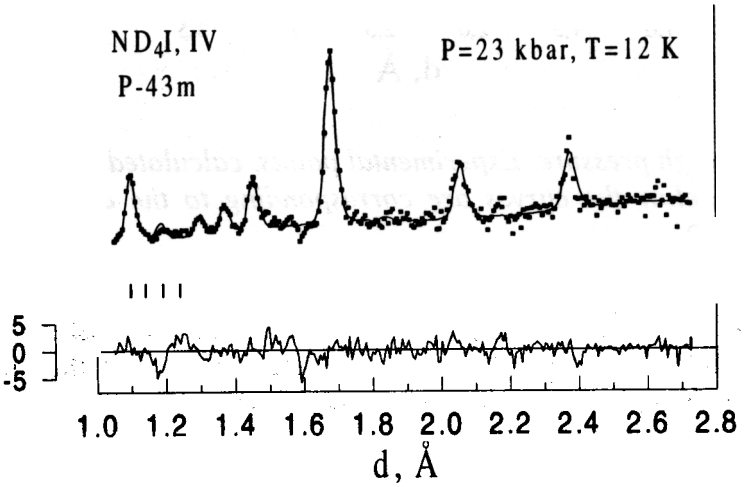

Figure 1. Diffraction pattern of ND_4I measured with the DN-12 spectrometer at pressure 23 kbar and T=12 K, normalized by the incident neutron spectrum and processed by the Rietveld method. Experimental points, calculated profile and difference curve normalized by the mean square deviation are shown.

At different pressures, D-I distance decreases with temperature decrease, and N-D bond length remains near constant $l_{N\text{-}D}$=1.03(2) Å, but shows a tendency to grow (fig. 2).

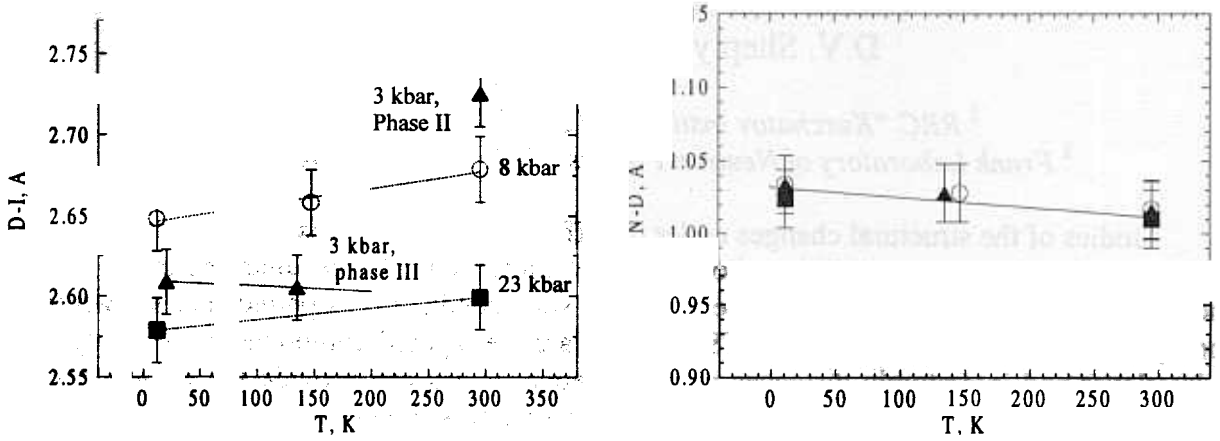

Figure 2. Temperature dependencies of D-I and N-D distances at different pressures. Triangles - data obtained at P=3 kbar, circles - data obtained at 8 kbar, squares - data obtained at 23 kbar.

If one compare phases III and V [1] structures, following differences could be found. First of all, lattice parameters ratio $a/\sqrt{2}:c > 1$ for phase V and $a/\sqrt{2}:c < 1$ for phase III. It corresponds to increase of the distance between the nearest I atoms in a-b plane for phase V and decrease of this distance for phase III in comparison with CsCl - type cubic structure of phases II and IV. Secondly, I^- ions shifted outwards the nearest deuterium atoms in phase V (increase of D-I distance, iodine positional parameter $\nu > 0.5$) and towards the nearest deuterium atoms in phase III (decrease of D-I distance, iodine positional parameter $\nu < 0.5$) in comparison with CsCl - type cubic structure ($\nu = 0.5$) - see Table 1.

Table 1. Comparison of phase III and V structures of ND_4I

Phase	Lattice parameters	$a/\sqrt{2}:c$ ratio	Iodine positional parameter
ND_4I(V), T=295 K, P=86 kbar	a=5.600(5) Å c=3.922(5) Å	1.0096	0.524(3)
ND_4I(III), T=135 K, P=3 kbar	a=6.058(5) Å c=4.317(5) Å	0.992	0.464(3)

References

1. A.M.Balagurov, D.P.Kozlenko, B.N.Savenko, V.P.Glazkov, V.A.Somenkov and S.Hull, Physica B 265, 92 (1999).
2. P.Andersson and R.G.Ross, J.Phys. C: Solid State Phys., 20, 4737 (1987).
3. S.J.Jeon, R.F.Porter, A.L.Ruoff, Journal of Raman Spectroscopy, 19, 179, (1988).
4. V.L.Aksenov, A.M.Balagurov, V.P.Glazkov, D.P.Kozlenko, I.V.Naumov, B.N.Savenko, D.V.Sheptyakov, V.A.Somenkov et al., Physica B, 265, 258 (1999).
5. V.P.Glazkov, I.N.Goncharenko, Fizika I Technika Vysokih Davlenij, 1, 56 (1991) (in Russian).

Investigation of Nd_2CuO_4 crystal structure at high pressures

V.P. Glazkov[1], B.N. Savenko[2], V.A. Somenkov[1],
D.V. Sheptyakov[2], S.Sh. Shilstein[1]

[1] *RRC "Kurchatov Institute", 123182 Moscow, Russia*
Frank Laboratory of Neutron Physics JINR, 141980 Dubna, Russia

Studies of the structural changes under the effect of high pressures and the comparison of the different bonds compressibilities allow to better understand the peculiarities of the crystal structure. The properties of many high temperature superconducting copounds are known to be strongly pressure-dependent. For the HTSC (which are the layered compounds), the analysis of the interlayer and interatomic distances pressure dependencies can provide the information on the interlayer charge exchange under the effect of external pressure [1].

The crystal structure of the electron-doped superconductors under the influence of high pressures has practically not been investigated yet. Here, the results are presented on the behavior of Nd_2CuO_4 crystal structure under high pressure. This compound is known to exhibit the electron conductivity after being doped by cerium. The aim of the study is to determine the compressibilities and the structural changes under the effect of external high pressure and to compare them to that found for the hole-doped high temperature superconductors.

The powdered sample of Nd_2CuO_4 was prepared from the single crystal, which was grown in air atmosphere by spontaneous crystallization from a melt with excess of CuO. Its structure was studied by time-of-flight neutron diffraction technique with the DN-12 diffractometer at the IBR-2 pulsed reactor in FLNP, JINR. The quasi-hydrostatic pressures up to ~5 GPa were obtained in the sapphire anvils high pressure cell with the sample volume of ~ 2.5 mm^3. The pressure was measured by the ruby fluorescence technique.

The parameters of tetragonal lattice *a* and *c* and the neodymium atom positional parameter z at ambient pressure were determined from the diffraction pattern obtained on the larger sample amount, not in the pressure cell: a=3.949 (5) Å, c=12.18(3) Å, z=0,1496(2). These values agree with those previously found for the stoichiometric Nd_2CuO_4 [2]. According to the available literature data, the violation of the stoichiometry of Nd_2CuO_4 and the substitution of Nd by Ce only cause the changes in *c* unit cell parameter, and the z(*c*) dependence is close to linear.

In the investigated pressure range, the significant shifts of the diffraction peaks and changes in their intensities are observed (Figure 1). The changes of the unit cell parameters with pressure (Figure 1) indicate that the compressibility of the unit cell along the *c* axis is approximately 1.5 times higher than that along the *a* axis. The volume compressibility of Nd_2CuO_4 is $\kappa_V=5{,}6*10^{-3}$/GPa.

In the Nd_2CuO_4 lattice, neodymium atoms occupy the (0,0,z) positions ($z\cong0.15$ at P=0), and the other atoms are situated in the non-parametric positions. Hence the changes of the relative intensities under pressure directly indicate the changes in the neodymium position parameter z. Its values were refined from the patterns at various pressures, and its pressure dependence is shown in the Figure 2 – the parameter lowers by the value of approximately 0.002.

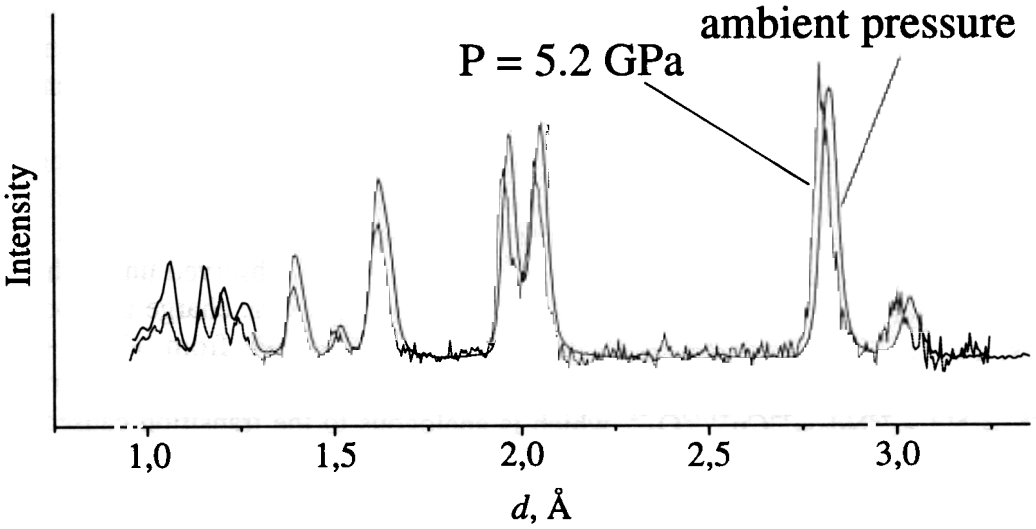

Figure 1 *The examples of neutron-diffraction patterns of Nd_2CuO_4 at different pressures.*

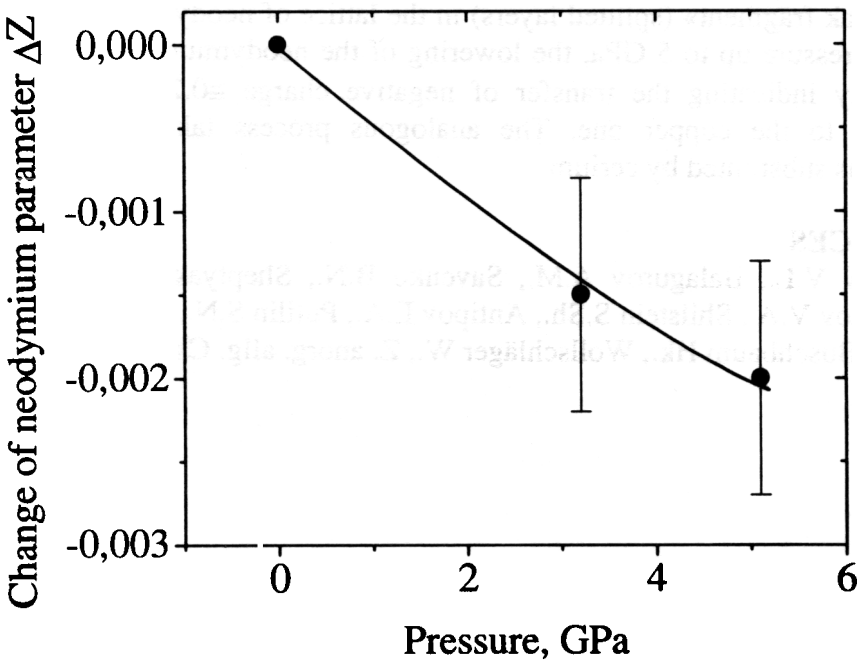

Figure 2 *Dependence of z parameter of neodymium in Nd2CuO4 on pressure – from the diffraction experiment under pressure.*

For mercury and thallium cuprates, the volume compressibility in the same pressure range is about $11+14*10^{-3}$/GPa, and its significant part is defined by the compression of the «weak fragment» – of the BaO splitted layers. The Nd_2CuO_4 lattice turns out to be much harder compressible, and this is probably due to the absence of such splitted layers in it.

The comparison of the observed changes in the structure to those caused by doping, show that the main influence on the interlayer distances & charge balance are the same. The neodimium atom z parameter lowers when Nd is partly substituted by Ce, i.e. when the average charge of ions in this layer increases. The same structural response is observed under the effect of pressure. We can therefore propose that when z parameter decreases the charge in neodymium layer increases, i.e. the part of neodymium atoms changes their state from +3 to +4. The simplified phenomenological calculations suggest that the pressure of 5 GPa causes the transition $Nd_2^{+3}Cu^{+2}O_4^{-2} \rightarrow Nd_{1.75}^{+3}Nd_{0.25}^{+4}Cu^{+1.75}O_4^{-2}$, which is analogous to the transition caused by the substitution of trivalent neodymium atoms by the four-valent cerium ($Nd_2^{+3}Cu^{+2}O_4^{-2} \rightarrow Nd_{1.82}^{+3}Ce_{0.18}^{+4}Cu^{+1.82}O_4^{-2}$). But the pressure-induced negative $\cong 0.25$ electrons charge transfer from the neodymium layers to the copper one is even higher than that caused by doping in the electron-doped superconductors, at about the same volume change. From analogy of structure changes under influence of cerium substitution and external pressure it is possible to suggest that neodymium cuprate should become metallic under the effect of external pressure.

In conclusion, the outcome of the experimental work done at DN-12 diffractometer is the following: The volume compressibility of the neodymium cuprate ($5.6.10^{-3}$/GPa) is approximately two times lower than that of the mercury cuprates. This is conditioned by the absence of the «weak fragment» (splitted layers) in the lattice of neodymium cuprate. Under the effect of external pressure up to 5 GPa, the lowering of the neodymium parameter is observed, which is apparently indicating the transfer of negative charge $\cong 0.25$ electron charge from neodymium layers to the copper one. The analogous process takes place if the part of neodymium atoms is substituted by cerium.

REFERENCES

Aksenov V.L., Balagurov A.M., Savenko B.N., Sheptyakov D.V., Glazkov V.P., Somenkov V.A., Shilstein S.Sh., Antipov E.A., Putilin S.N., Physica **C275**, 87 (1997)

2. Müller-Buschbaum Hk., Wollschläger W., Z. anorg. allg. Chemie, **414**, 76 (1975)

INFLUENCE OF TEMPERATURE AND LONG-TIME LOADING ON TEXTURE AND PHYSICAL PROPERTY OF CALCITE

T.I. Ivankina[a], A.N. Nikitin[a], G.A. Sobolev[b], V.A. Sukhoparov[c], A.S. Telepnev[a], K. Ullemeyer[a] and K. Walther[d]

[a] *Joint Institute of Nuclear Research, Frank Laboratory for Neutron Physics, 141980, Dubna, Russia*
[b] *Joint Institute of the Physics of the Earth, Russian Academy of Sciences, 123242, Moscow, Russia*
[c] *Institute for High-Pressure Physics, Russian Academy of Sciences, 142092, Troizk, Russia*
[d] *GeoForschungsZentrum Potsdam, D-14473, Potsdam, Germany*

Calcite rocks (marbles) are a good model system for experimental rock deformation because of their ductile behavior even at relatively low temperatures. Meanwhile, a large amount of experimental data on deformation mechanisms and development of calcite textures at various conditions is available (refer to [1] for a recent overview). In this study, an attempt was made to determine textural and structural changes of calcite marble samples in dependence upon the temperature and mechanical stresses [2], as well as in dependence upon the time of load.

Three cylindrical samples (height: 20 mm; diameter: 18 mm) were prepared from a fine-grained natural marble which consists exclusively of calcite. The following series of experiments was carried out at the TOF texture diffractometer at FLNP/JINR [3] using a chamber for uniaxial compression and high temperatures [4]:

(1) the texture of calcite was determined at room temperature
(2) subsequently, the texture measurements were repeated at a temperature of 250°C applying compressional stress along the sample cylinder axis
(3) after 20 weeks exposition time of the sample at room temperature (during this time span, the load decreased from 60 MPa down to 10 MPa), texture measurements were performed again

Some significant experimental pole figures of the three texture measurements are given in Figure 1. It is remarkable, that the differences in texture strength and orientation of the intensity patterns are quite small for the first and the second experimental run, *i.e.* no structural changes occured as a consequence of increased temperature and directed load. In contrast, distinct texture changes can be observed after long time exposition under load for 20 weeks. This holds true especially for the orientation of the intensity patterns (best visible in the (0006) pole figures), additionally, the contours lines become smoother which can be attributed to grain size reduction. Both observations indicate dynamic recrystallization as a response on long-acting stress at low temperatures.

For one sample, the heating period between the first two texture measurements was used to record diffraction patterns at distinct temperature levels (50-80-120-150-190-220 [°C]) and to measure the propagation velocity of ultrasonic waves along the sample axis. The data are used to calculate the directional dependence of the thermal expansion coefficient α of calcite from the observed peak shift of the BRAGG reflections, and the mechanical stresses as a reaction on temperature increase.

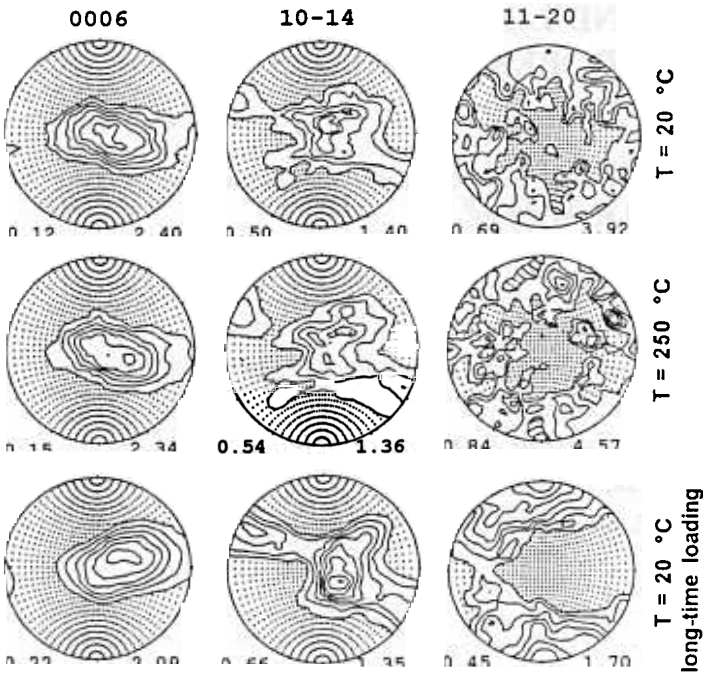

Fig. 1 Selected pole figures of texture measurements at various conditions (for explanation refer to text).

For comparison, α was determined from X-ray measurements as well. The neutron and X-ray based calculations show significant differences which will be the subject of discussion (see Table 1): the reference value d_0 is different for neutrons and X-rays, as well as the observed peak shift Δd and the calculated thermal expansion coefficient α. It is remarkable, that the neutron based d_0- values are consistently smaller for all BRAGG reflections, whereas the observed peak shift Δd and α are smaller only for the (11-20) reflection, *i.e.* the temperature dependence seems to be different for distinct lattice planes.

Table 1 Lattice spacing d_0 (T = 20°C), peak shift Δd (ΔT = 230°C) and thermal expansion coefficient $\alpha = \Delta d\ d_0^{-1}\ \Delta T^{-1}$. $_{n,\ x}$ indicate neutron and X-ray measurements, respectively.

(*hkil*)	d_0, Å	Δd, Å	$\Delta d\, d_0^{-1} \Delta T^{-1}$, K^{-1}
			$36.2\ 10^{-6}$
			$22.3\ 10^{-6}$
$(11\text{-}20)_n$	2.4883	$-0.15\ 10^{-2}$	$-2.58\ 10^{-6}$
$(11\text{-}20)_x$	2.4940	$-0.26\ 10^{-2}$	$-4.53\ 10^{-6}$
			$1.87\ 10^{-6}$
[illegible]	[illegible]	[illegible]	$0.96\ 10^{-6}$
$(11\text{-}23)_n$	2.2808	$0.046\ 10^{-2}$	$0.89\ 10^{-6}$
$(11\text{-}23)_x$	2.2840	$-0.007\ 10^{-2}$	$-0.13\ 10^{-6}$
$(10\text{-}14)_n$	3.0295	$1.02\ 10^{-2}$	$14.7\ 10^{-6}$
$(10\text{-}14)_x$	3.0351	$0.63\ 10^{-2}$	$9.0\ 10^{-6}$

Since the compressional wave velocity V_p was measured by ultrasonic sounding, the elastic module of the marble sample for the direction of wave propagation can be determined. Assuming, that the elastic module of the single crystal is close to the bulk module of the sample, also lattice stresses can be estimated. In Table 2, the calculated values are given for the (0006) and (11-20) reflection and for different temperatures. They confirm the interdependence of the elastic module from temperature

and from the lattice direction in which it is measured. This interdependence, as well as the relation to the mineral texture will be subject of discussion.

Table 2 Elastic module E and calculated macro- and micro-stresses ($\varepsilon_{lattice}$, $\sigma_{lattice}$, σ_{macro}) at different temperatures T. ρ: density.

(*hikl*)	T [°C]	ρ [kg m^{-3}]	V_p [m/s]	E [GPa]	$\varepsilon_{lattice}$	$\sigma_{lattice}$ [MPa]	σ_{macro} [MPa]
(0006)	120	$2.6 \cdot 10^3$	5840	88.67	$2.59 \cdot 10^{-3}$	229.66	25
	150	$2.61 \cdot 10^3$	5810	88.11	$3.74\ 10^{-3}$	329.53	26
	190	$2.62 \cdot 10^3$	5770	87.23	$5.50\ 10^{-3}$	479.77	27
	220	$2.63 \cdot 10^3$	5750	86.95	$6.39\ 10^{-3}$	555.61	31
(11-20)	120	$2.6 \cdot 10^3$	5840	88.67	$0.48 \cdot 10^{-3}$	42.56	25
	150	$2.61 \cdot 10^3$	5810	88.11	$0.66 \cdot 10^{-3}$	58.15	26
	190	$2.62 \cdot 10^3$	5770	87.23	$0.85 \cdot 10^{-3}$	74.15	27
	220	$2.63 \cdot 10^3$	5750	86.95	$1.13 \cdot 10^{-3}$	98.25	31

References

[1] Wenk H.-R. Typical textures in geological materials and ceramics. Texture and anisotropy: preferred orientations and their effects on materials properties. *Eds*: U.F.Kocks, C.N.Tomé, H.-R.Wenk. Cambridge University Press, 240-280 (1998).

[2] Nikitin A.N., Sukhoparov V.A., Heinitz J. and Walther K. Investigation of texture formation in geomaterials by neutron diffraction with high pressure chambers. Int. J. High Pressure Res. **14**, 155-162 (1995).

[3] Ullemeyer K., Spalthoff P., Isakov N.N., Nikitin A.N. and Weber K. The SKAT texture diffractometer at the pulsed reactor IBR-2 at Dubna: experimental layout and first measurements.- Nucl. Instr. Meth. Phys. Res. **A 412/1**, 80-88 (1998).

[4] Ivankina T.I., Nikitin A.N., Ullemeyer K., Efimova G.A., Kireenkova S.M., Sobolev G.A., Sukhoparov V.A., Tekepnev A.S. and Walther K. Investigation of structure and texture-transfomation processes in rocks. Schriftenr. f. Geowiss. **6**, 49-56 (1998).

LABORATORY INVESTIGATION OF ELASTIC ANISOTROPY AND TEXTURE OF ROCKS FROM KOLA SUPER DEEP BOREHOLE SG-3

A.N. Nikitin[a], T. I. Ivankina[a], K. Ullemeyer[a] , T. Lokajicek[b], Z. Pros[b], K. Klima[b] and Yu. P. Smirnov[c]

[a]*Joint Institute for Nuclear Research, Frank Laboratory of Neutron Physics, 141980, Dubna, Moscow Region, Russia*

[b]*Geophysical Institute, Academy of Sciences of the Czech Republic 141 31, Prague, Czech Republic*

[c]*Scientific Industrial Center, Kola Super Deep Borehole, 184200, Zapolyarny, Murmansk Region, Russia*

The interpretation of the elastic properties of the earth's crust largely depends upon the knowledge of rock anisotropies of any kind, like mineralogical composition, foliations, grain shape anisotropy and mineral textures. The influence of the texture on the elastic behavior of rocks is of interest because it affects the propagation velocity of seismic waves and therefore has consequences for the interpretation of large scale geophysical anisotropies in the earth's crust and mantle. One of the unique sources of rock material giving the information about the crustal rocks is Super Deep Borehole SG-3 at Kola peninsula (the depth of 12262 m).

The aim of this study was to determine the P-wave velocity distributions of samples from the Kola SG-3 borehole at different confining pressures, to measure the textures of the predominant rock-forming minerals by means of neutron diffraction as a basis for the modeling of the P-wave velocity distributions, and to correlate the experimental and theoretical results. From the lithotypes which are present in the drilling cores, only amphibolites were selected. We focused on a unique rock type since we mainly wanted to characterize possible *variations* of its elastic properties. Future work will concentrate on other widespread lithotypes from the Kola borehole.

The complete P-wave distribution was determined on spherical samples in 132 independent sample directions (corresponding to a regular 15° • 15° grid) for six levels of confining pressure in the interval 0.1 MPa to 400 MPa. The measurements were performed by means of ultrasonic sounding at the Geophysical Institute in Prague (for details on the measuring equipment refer to [1]). The number of considered sample directions is enough to describe the P-wave matrix with sufficient accuracy.

It is a general observation (Fig. 1), that the P-wave velocities increase with increasing confining pressure. At atmospheric pressure, the mean velocities Vp_{mean} range from 2.64 to 3.17 km/s, except sample 37172 which shows a considerably higher value of Vp_{mean} = 5.93 km/s.. At 400 MPa, the mean velocities range from 7.17 to 7.72 km/s for all samples. The observed P-wave velocity - confining pressure behaviour (see Fig. 1) which is different for the samples additionally supports the usual interpretation, that intra- and intercrystalline cracks control the P-wave velocities at low confining pressures. With increasing confining pressure, the elastic behaviour is dominated by the intrinsic properties of the minerals, i.e. the textures and the elastic constants of the rock-forming minerals. The transition between the two fields of predominance is quite different: sample 31904 shows a much wider range of crack- predominance as for example sample 9665, where the influence of cracks is neglectible at confining pressures > 40 MPa.

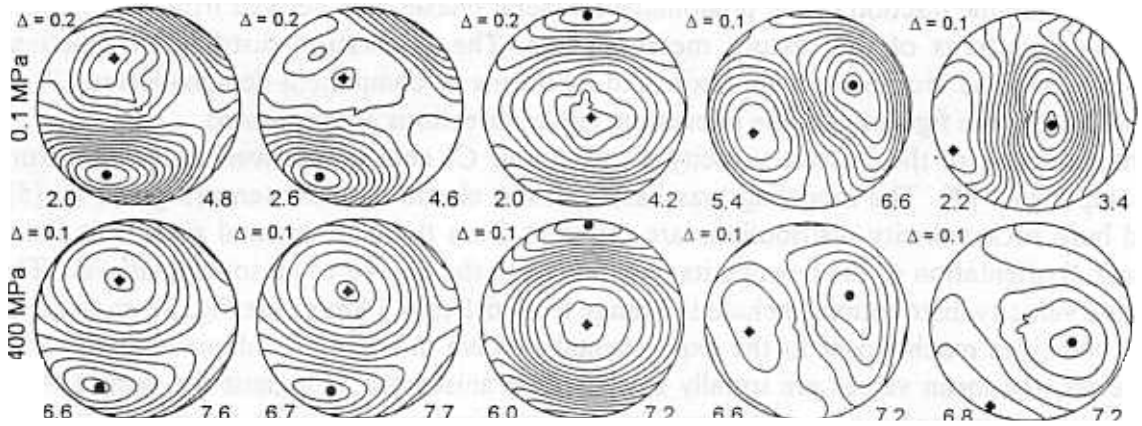

Figure 1. Experimental P-wave velocity distributions at confining pressures 0.1 and 400 MPa. The minimum and maximum directions are marked by rhombs and circles, respectively. The lowest and highest contour line is indicated at the bottom of each stereoplot, the contour spacing at the top left.

Neutron texture measurements were performed at the time-of-flight texture diffractometer at Dubna, Russia (Ullemeyer et al., 1998). The advantage of neutrons is its low absorption in matter, in addition, the beam cross section of the neutron beam at Dubna (5 cm • 8.5 cm) is large enough to allow texture measurements on exactly the same spherical samples as they were used for the P-wave measurements

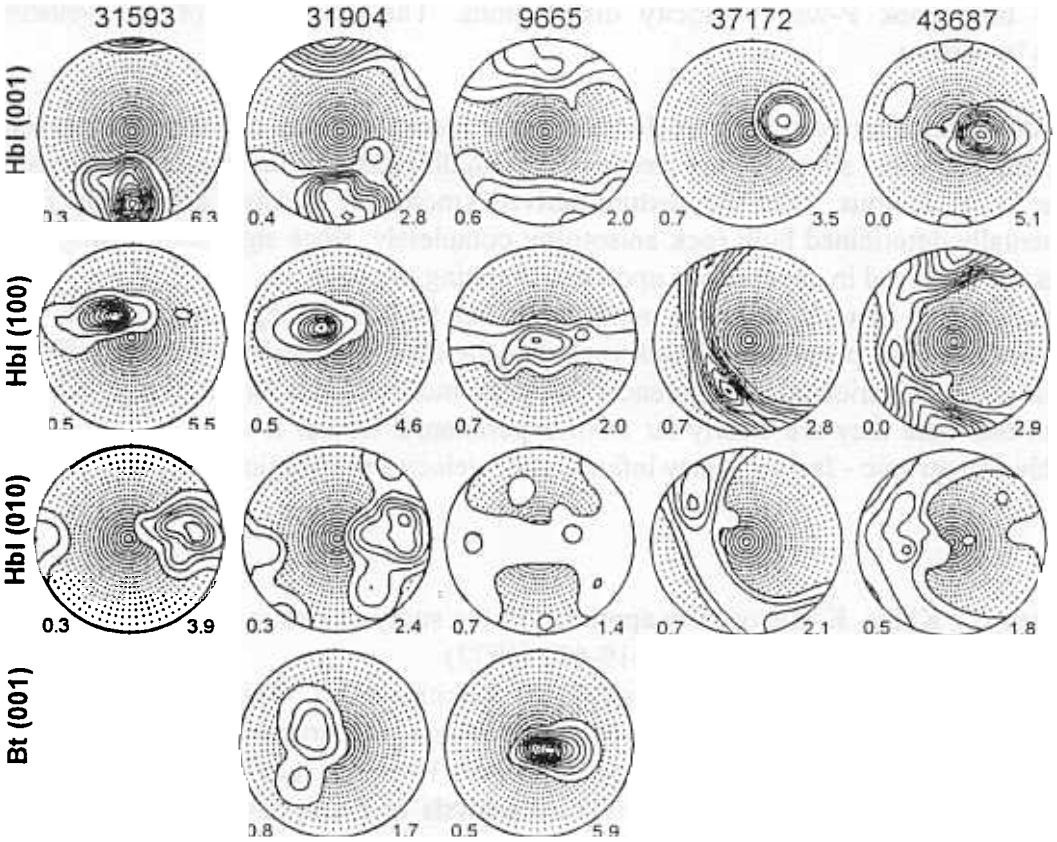

Figure 2. Pole figures of hornblende (Hbl) and biotite (Bt), recalculated from the ODF. Contouring starts at one time random, grid points with intensities smaller one time random are displayed. Minimum and maximum intensities are given at the bottom of the plots, and the orientation of the rock foliation is indicated by a dotted circle in the hornblende (100) pole figure.

An estimate of the volume fraction of the predominant mineral phases was derived from summarized neutron diffraction patterns of the texture measurements. The orientation distribution functions (ODFs) of hornblende and biotite were approximated by means of component deconvolution [3], in Figure 2, recalculated pole figures of some interesting lattice directions are presented.

For the modeling of the P-wave velocity distributions, *C*- coefficients were calculated from the texture components [4]. The modeling was based on the elastic stiffness tensors given by [5]. The averaged bulk rock velocity distributions are different from the experimental ones, this holds true for the spatial orientation of the tensors, its quantities and the degree of anisotropy as well. The modeled P-wave velocity distributions include the range from 6.1 to 6.7 km/s (see Fig. 3). In general, the calculated velocities much closer fit the experimental P-wave distributions obtained at P = 400 MPa, nevertheless, the mean values are usually smaller. The anisotropy is highest for sample 9665 because of the well-developed biotite (001) preferred orientation and the large volume fraction of biotite in this sample (30%).

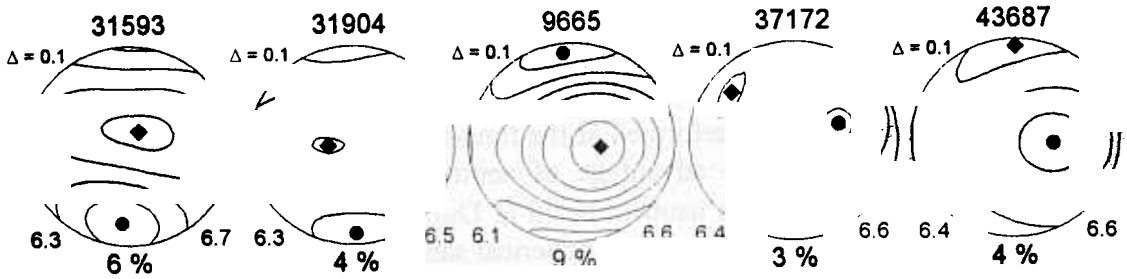

Figure 3. Modeled bulk rock P-wave velocity distributions. The anisotropy of the velocity distributions is given in percent.

Distinct orientation differences between the modeled and experimental velocity distributions are also valid, especially the sample 43687 shows a very clear orientation difference of the velocity patterns.

Furthermore, it is obvious, that the texture-derived (modeled) P-wave anisotropy can't explain the experimentally determined bulk rock anisotropy completely, since significant changes of the velocity patterns are observed in dependence upon the confining pressure.

It was concluded, that in addition to the mineral textures factors like open microcracks and open fractures control the elastic properties of bulk rock, but the closing behaviour is quite different for the samples. Furthermore, orientation differences between modeled and experimental velocity patterns are valid, in one case they are clearly far from experimental errors. It must be postulated, that unknown - highly anisotropic - factor(s) may influence the velocity distributions.

References

[1] Pros, Z., Lokajicek, T., Klima, K. Laboratory approach to the study of elastic anisotropy on rock samples. Pure and Applied Geophysics **151**, 619-629 (1977).

[2] Ullemeyer, K., Spalthoff, P., Heinitz, J., Isakov, N.N., Nikitin, A.N., Weber, K. The SKAT texture diffractometer at the pulsed reactor IBR-2 at Dubna: experimental layout and first measurements. Nuclear Instruments and Methods in Physics Research **A412**, 80-88 (1998).

[3] Helming, K., Eschner, T. A new approach to texture analysis of multiphase materials using a texture component model. Crystalline Research Technologie **25**, K203-K208 (1990)

[4] Dahms, M., Bunge, H.-J.. The iterative series-expansion method for quantitative texture analysis. I. General outline. Journal of Applied Crystallography **22**, 439-447 (1989).

[5] Aleksandrov, K.S., Ryzhova, T.V.. The elastic properties of rock forming minerals II: Layered silicates. Izvestia of the Academy of Science of the USSR, Geophysics and Physics of the Solid Earth, 1165-1168 (1961).

APPLIED AND RESIDUAL STRAIN/STRESS DETERMINATION ON QUARTZ ROCKS USING NEUTRON TOF DIFFRACTION

C.M. SCHEFFZÜK [1,2], A. FRISCHBUTTER [2], K. WALTHER [2] & R.A. ZHUKOV

[1] *Frank Laboratory of Neutron Physics, Joint Institute for Nuclear Research, 141980 Dubna, Russia*
[2] *GeoForschungsZentrum Potsdam, Telegrafenberg, 14473 Potsdam, Germany*

Introduction

Neutron diffraction *in situ* strain investigations are a suitable tool for a better understanding of the deformation behaviour and of the strain/stress relaxation behaviour of polycrystalline rock materials. In combination with the deformation apparatus ExStress, this method allows the determination of strain by external applied load, the determination of residual strain/stress behaviour and the volume-sensitive characterisation of the strain contents. Experiments were carried out on quartz rocks at the neutron time-of-flight diffractometer EPSILON, located at the beam line 7A of the pulsed reactor IBR-2.

Material and Methods

The specimens were prepared from cores of ground water holes in the Elbezone, drilled close to Königstein, a little town about 20 km SE of Dresden (E-Germany). The Elbezone is characterized by weak recent tectonic activity: In accordance with results of interpretations of repeated geodetic triangulations [1] the Elbezone is recently a 10 - 25 km wide NW-SE - trending zone, characterized by a NE-SW - directed extension, followed by small zones of compression and additionally cut by predominantly N-S directed sinistral shear zones.

Quartz is one of the best known and most frequently occurring mineral within the upper continental Earth's crust. From the mechanical point of view quartz reacts brittle, from which arises a good contrast e.g. in relation to the ductile mica in other polymineralic systems. That's why the rocks were regarded as well suitable for experiments to adapt diffraction methods for geological problems.

The Cretaceous sandstones of the Elbezone were selected because of, their quasi-monomineralic composition, the absence of crystallographic preferred orientation of quartz and different types of bedding available. Samples were taken from cores of ground water holes at a drilling depth of about 250 m below surface level. The cores were taken without orientation marks, therefore the coordinate system could be fixed only in relation to the bedding plane (xy) and perpendicular to the bedding plane [z], which direction was fixed by the core bit.

The average composition of the sandstone is: 95% quartz, accessories (5%) are potassium-feldspar, white mica, calcite, dolomite (determined by quantitative X-ray-phase analysis). The grain size varies in the range between 100-200 μm. Rarely there are rock fragments (mainly of granitic composition) which may be up to 1 mm in diameter. Quartz is mostly clastic and equigranular. The pore volume of the rocks is in the order of 10%. The sandstone is characterized by absence of crystallographic preferred orientation of quartz crystallites, but shows well developed bedding of different qualities.

The neutron diffractometer "Epsilon" is situated about 102 m from the surface of the moderator. Due to this long flight path a good spectral resolution of 0.4 % (for lattice spacings d > 0.2 nm) is achieved. This allows the measurement of samples of lower crystal symmetry (even mica and feldspar). The diffractometer is equipped with a pressure device ("ExStress"), which provides an uniaxial load of maximal 100 kN which corresponds to a maximal stress of 150 MPa for cylindrical samples with the dimensions of 30 mm ⌀ and 60 mm length. The sample is mounted inside the pressure device. Two detectors are set up with scattering angle $2\vartheta = \pm 90°$, thus one detector is able to measure the diffraction pattern in the direction of the applied load, the other one in the direction perpendicular to the load (see Fig. 1).

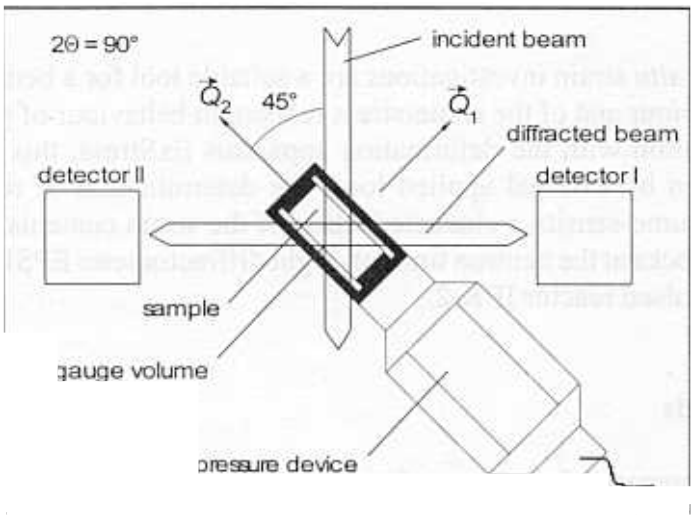

Fig. 1: Layout of the neutron time-of-flight diffractometer "Epsilon" at the reactor IBR-2 at the beam line 7A. $\vec{Q}_1$ and $\vec{Q}_2$ are the scattering vectors.

3.2 Results

In situ - deformation experiments were carried out at a quarz sample HG 7012/2/a2 up to an uniaxial pressure of σ= 56.33 MPa. Caused by the spectral distribution of the reactor pulse, the diffraction peaks can not treated like simple Gaussian. The right flank decreases slightly less than the left flank increases. For this reason the position of the Bragg reflections was determined using the asymmetrical double sigmoidal fit function described in detail by [2].

The results reflect a linear peak shift by increasing the applied load. The peak shift is an indicator of first order stresses. The linear dependence of the measured strain on the applied stress demonstrate the elastic behaviour of the rock's material, so that the observed lattice contractions are consistent with the Hooke's law. The Young's moduli were experimentally determined for the net planes $(01\bar{1}1)$, $(11\bar{2}0)$ and $(01\bar{1}2)$. The obtained Young's moduli are in all cases smaller than the "theoretical" ones, caused by possible effects from grain boundaries, accessory phases, pore volume, texture etc.

Furthermore, in addition to peak shift, peak broadening was observed too, which is an indicator for increased stresses of second order. Figure 2 (below right) shows the dependence of the peak width (FWHM) of the $(11\bar{2}0)$ Bragg reflection on the applied load. Neglecting the runaway FWHM-value at $\sigma = 40.8$ MPa a relationship between FWHM and the stress σ was determined by linear regression to be $(2.4 \pm 1.3)\cdot 10^{-2}$ time channels per MPa.

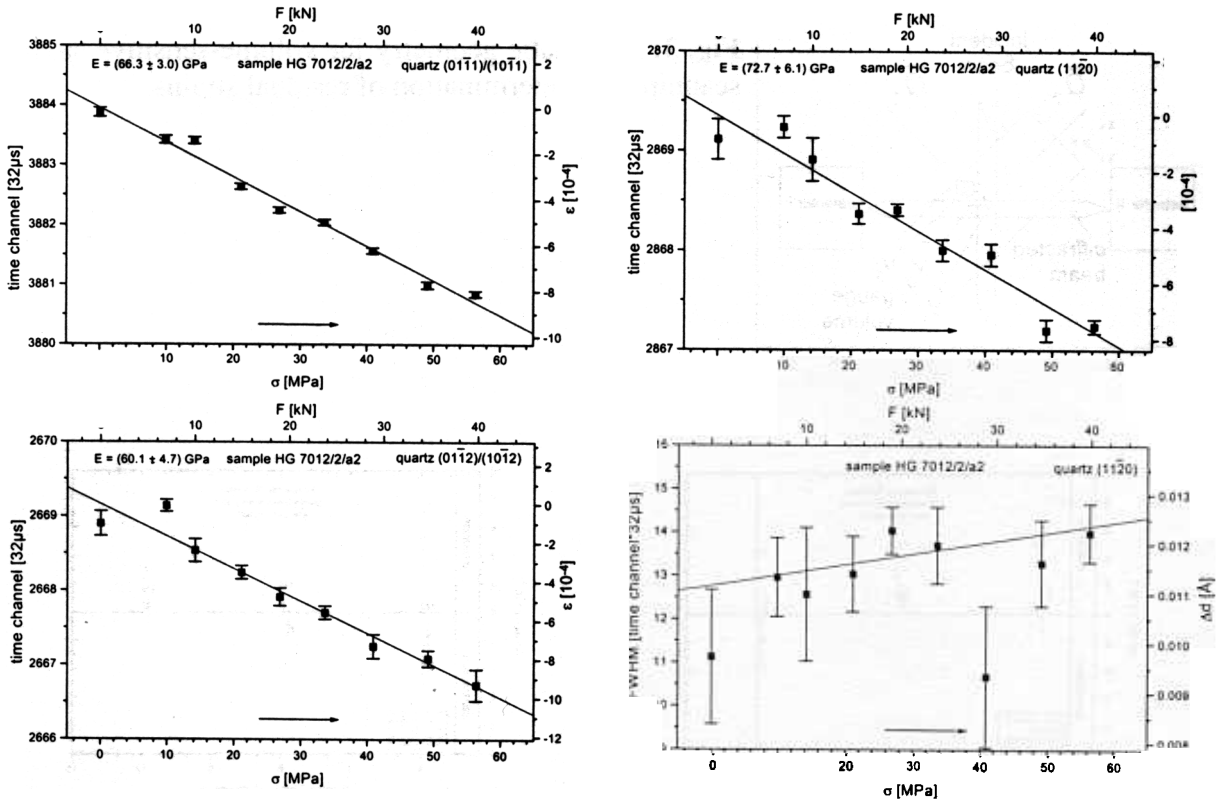

Fig. 2: Deformation of the quartz sample HG 7012/2/a2 due to the uniaxial load up to 56.33 MPa. Top left: the (01$\bar{1}$1)/(10$\bar{1}$1) Bragg reflection, the Young's modulus was determined to be E = (66.2±3.0) GPa, top right: the (11$\bar{2}$0) Bragg reflection, the Young's modulus: E = (72.7±6.1) GPa; below left: the (01$\bar{1}$2)/(10$\bar{1}$2) Bragg reflection, the Young's modulus: E = (60.1±4.7) GPa; below right: the peak broadening as full width at the half maximum (FWHM) of the (11$\bar{2}$0) Bragg reflection, the peak broadening was determined by linear regression to be $(2.4 \pm 1.3) \cdot 10^{-2}$ time channels per MPa [3].

Residual strain/stress

Residual strain was measured at the same sample six days after unloading. The strain was scanned in a radial direction, from the centre to the surface of the sandstone cylinder and arranged in the directions [x] and [y], which are perpendicular to each other and determining the bedding plane of the sandstone (Fig. 3).

It is noteworthy that the results indicate an anisotropy of residual strain distributions within the bedding plane. Figure 4 demonstrates the residual strain for the Bragg reflections (01$\bar{1}$1)/(10$\bar{1}$1), (11$\bar{2}$0) and (01$\bar{1}$2)/(10$\bar{1}$2) in [x] and [y]-direction. It is shown, that in the [x]-direction there was measured the tension in the centre (V1) of the sample and at the margin of the sample (V3). The residual strain behaviour in [y]-direction is vice versa.

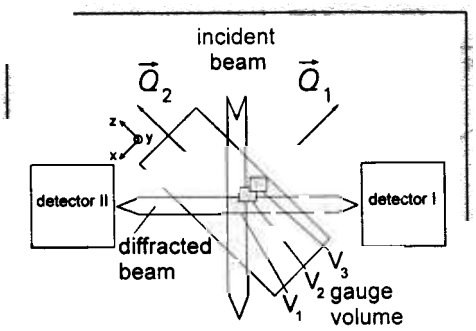

Fig. 3: Schematic geometry for volume-sensitive strain scanning for determination of residual strains.

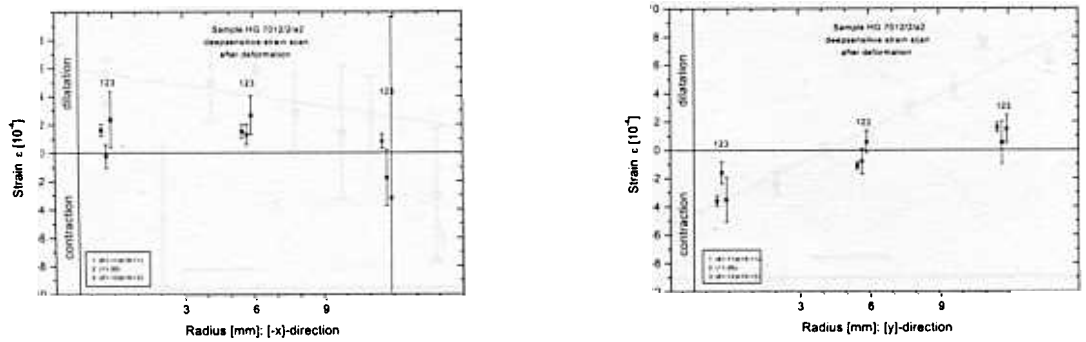

Fig. 4: Determination of the residual strain in [x]- (left) and [y]-direction (right) by scanning in radial direction. The xy-plane is the bedding plane. The strain was measured six days after unloading. 1: $(01\bar{1}1)/(10\bar{1}1)$; 2: $(11\bar{2}0)$; 3: $(01\bar{1}2)/(10\bar{1}2)$.

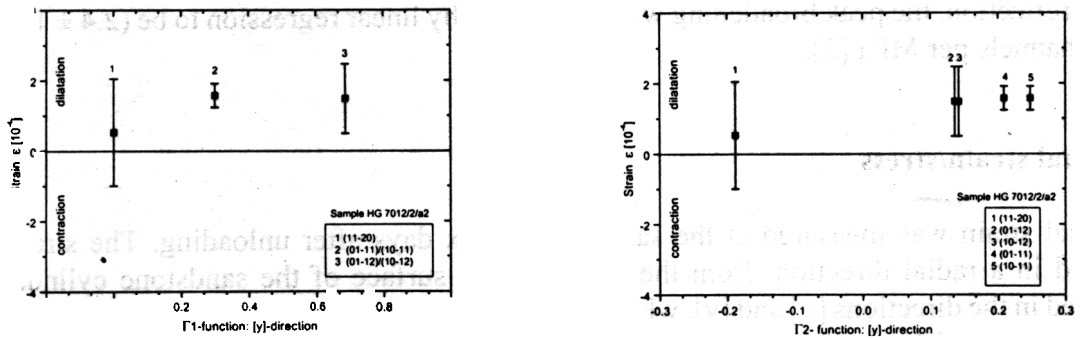

Fig. 5: Anisotropy function Γ1 (left) and Γ2 (right) for the margin at the [y]-direction.

Figure 5 demonstrate as an example only two anisotropy functions Γ1 and Γ2, determined from residual strain data at the margin of the sample HG 7012/a/a2 in [y]-direction. The relationship indicate the elastic behaviour of the sample at this point.

References

[1] Thurm, H. & Bankwitz, P. (1977), *Petermanns Geograph. Mitt.* **12** (1/4), 281-304.
[2] Scheffzük, Ch., Frischbutter, A. & Walther, K. (1998), *Schriftenr. f. Geowiss.* **6**, 39-48.
[3] Frischbutter, A. *et al.* (2000), to be published.

Residual stress study by neutron diffraction in perforator's striker

G.Bokuchava, N.Shamsutdinov, A.Tamonov

Within the framework of co-operation with the industrial enterprises of Russia (TULAMASHZAVOD) test experiments on residual stress study in perforator's striker were carried out. The knowledge of residual stress level in such components is very important for equipment production in mineral resource industry. The sample was made of steel 65C2BA (elastic constants E = 211 GPa, ν = 0.3, G= 82 GPa) and had cylindrical shape (outer diameter 24mm, inner - 8mm).

The experiment was performed at High Resolution Fourier Diffractometer [1]. For the stress measurements we used the 90°-detector with gauge volume 2x2x5mm^3. The back scattering detector was utilised for the investigation of diffraction peak broadening and the phase analysis.

Looking at the diffraction pattern one finds the presence of austenitic phase in the sample (see fig.1). After analysis of peak intensities the estimation for the volume content of austenite had been found: c_a = (11.7±0.2) %. It's a pretty large amount comparatively to the homogeneity reported by sample producers. Also the strong peak broadening can be clearly seen (fig.1). Generally, the peak width Δd behaves according to the following law:

$$(\Delta d)^2 = \left(\frac{\Delta t}{2 \cdot \frac{m}{h}}\right)^2 + (\Delta\theta \cdot ctg\theta)^2 \; d_{hkl}^2 + \varepsilon^2 \cdot d_{hkl}^2 + \alpha \cdot d_{hkl}^4$$

Here Δt and $\Delta\theta$ are the time and geometry uncertainties, α - coefficient, which takes into account the size of grains, ε - microstrain. This estimation of the microstrains gives quite a high value: ε_{micro}=0.012±0.004. The strain of this amplitude corresponds to the stresses above the yield strength of the material. But one must keep in mind the non-homogeneity of the sample, so the deformation has the limited nature, allowing stresses to exceed the yield strength.

The measured stresses are shown on fig.2. Radial and tangential components of the stress tensor are negative, i.e. compression is going on. In the sample's bulk they achieve high values. Axial component has a different behaviour. Firstly, in the places close to the edges, axial stress is positive, i.e. the material is under tension. In the core of the sample, the sign of stresses changes. Then, the sample has pretty high stress gradients. In addition to the combination of tension/compression near the edges this fact forms the complex stress state of the material. These circumstances badly damage the resistance of the sample.

After analysing of the macro- as well as micro-stress state of the sample we came to the conclusion, that material had no the optimal heat treatment. The resistance of the sample can be improved by 2-3 times by appropriate treatment.

Literature

[1] V.L.Aksenov, A.M.Balagurov, V.G.Simkin et al., JINR Communication, P13-96-164, Dubna, 1996.

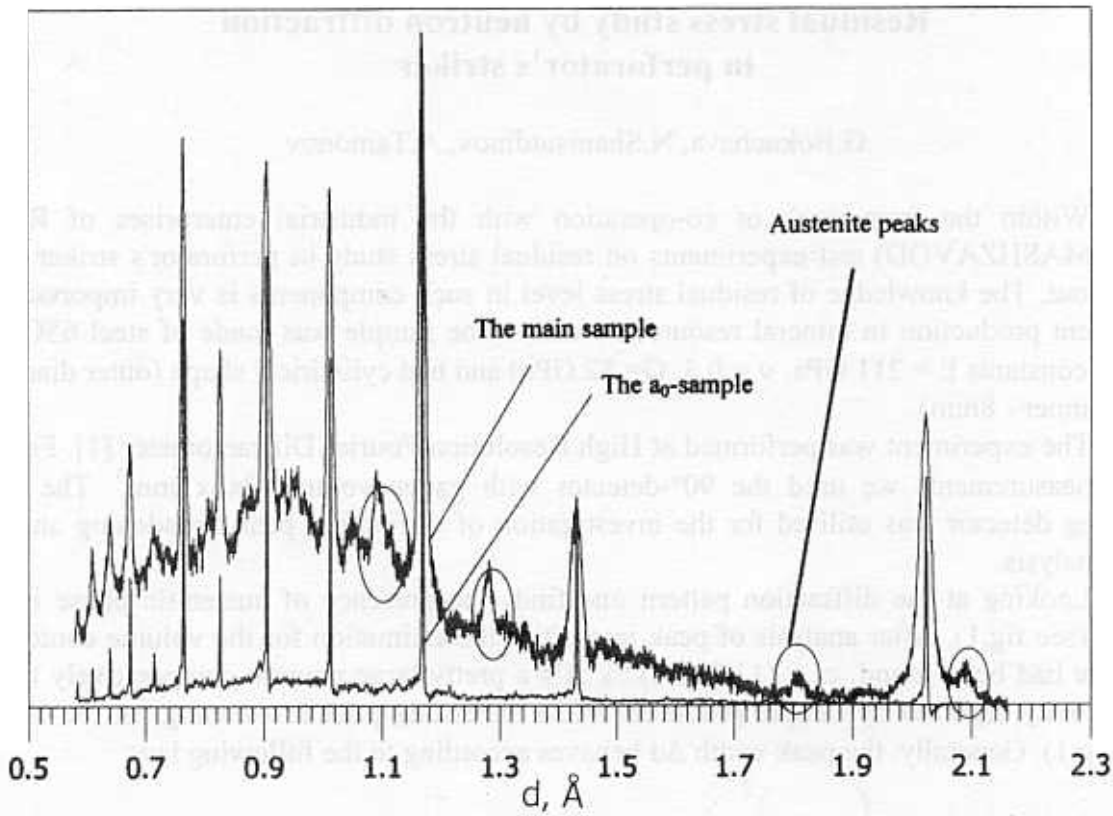

Fig. 1. The example of measured spectrum. The peak broadening compared to the unstressed sample as well as the peaks of austenite phase is well pronounced.

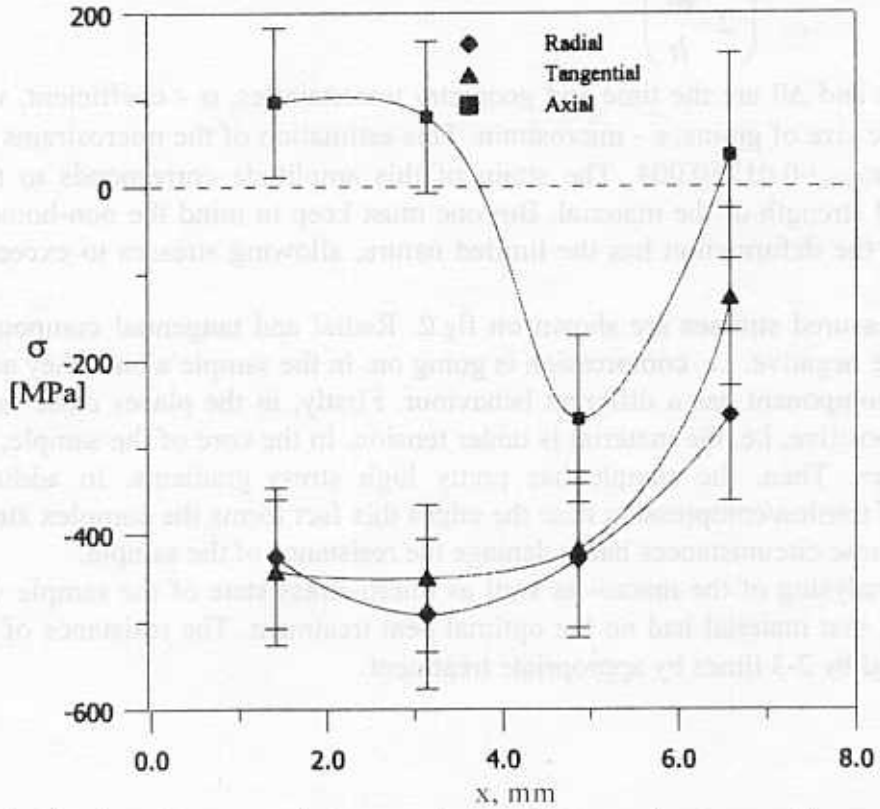

Fig.2. The distribution of measured stresses along radial coordinate x: x=0 corresponds to the surface of the outer diameter.

Light-Induced Long-Living Changes of Bacteriorhodopsin Structure

V.I. Gordeliy*[+], N. Dencher[#], T. Hauss[§], A. Kuklin[+], A. Tougan-Baranovskaya[-] J. Teixeira^, L.S. Yaguzhinskiy[$] and G. Büldt*

Frank Laboratory of Neutron Physics, Joint Institute for Nuclear Research, 141980 Dubna, Moscow District, Russia
IBI-2: Structural Biology, Research Centre Juelich, 52425 Juelich, Germany
Biochemical Institute, Technical University Darmstadt, Petersenstr. 22, 64287 Darmstadt, Germany
Laboratoire Leon Brillouin (CEA/CNRS), CE de Saclay, 91191 Gif-sur-Yvette Cedex, France
A.N. Belozersky Institute of Phisico-Chemical Biology, Moscow State University, 119899 Moscow, Russia

Purple membranes (PM) from bacterium *Halobium Salinarius* , contains only one type of the proteins - Bacteriorhodopsin (BR) . The protein catching a photon uses its energy to transport protons H^+ through the membrane. It results in electro-chemical gradient on the membrane. The energy, accumulated in this way, provides living functions of the bacterium. This first step of accumulation of energy (creation of electro-chemical gradient by proton pumping) is an universal step in energy transformation in bacteria, plants and animals. BR is widely used for investigation of mechanism of proton pumping. A major question to be answered is whether structural changes are involved in proton pumping. The photocycle of BR has been studied and it was shown that the protein pumps in its M-state.

A substantial difference between the thickness , T, of PM dark-adapted (T=50.3 Å) and exposed to continuous illumination (T=44.7 Å) has been observed by small angle neutron scattering (Fig.1). The measurements were performed at the YuMO instrument. The study was done at pH=9.6, in presence of 100 mM of guanidine hydrochloride to slow down the decay of M-state of bacteriorhodopsin (BR) in 2 wt% of PM in aqueous solutions. The observed conformational fast alterations occur within first 10 min and are irreversible for hours (Fig.1), suggesting a strong interaction of guanidine hydrochloride with PM induced by the illumination of the samples.

The reduction of the membrane thickness can be explained by the shift of BR loops and C- and N-terminates (in average by about 3 Å) toward membrane surface when PM is exposed to light. This shift can occur due to the alteration of the membrane surface potential induced by light illumination of the PM and leads to the creation of the hydrogen bonds between amino acid segments of BR loops as well as C- and N-terminates and nearest to them amino acids embedded into the membrane and stabilisation of BR in a new long-living

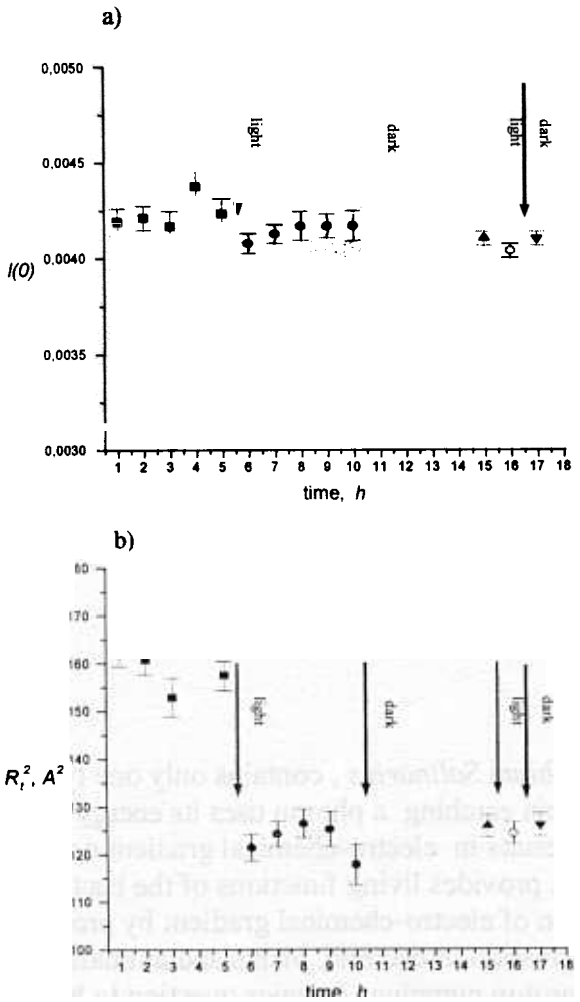

Fig.1

Fig. 5 Kinetics of the changes of (a) the intensity I(0) (b) the radius of gyration and of PM in D_2O (in presence of 100 mM of guanidine hydrochloride at T=16.8 °C in 50 mM Na_2CO_3 buffer at pH=9.6) at dark and upon illumination. The arrows corresponds to the start of a new state of the sample: (■) dark-adapted state; (●)upon first continuous illumination; (▲) at dark after the illumination; (○) under second continuous illumination; and (▼) at dark after second illumination.

structural conformation. Guanidine hydrochloride can play an important role in such a scenario due to its ability to take part in the hydrogen bonding.

In addition, the experimental data showed light-induced H/D exchange in which 52±22 hydrogen atoms are involved.

Small angle contrast variation study yields an accurate estimation of the membrane thickness, which is equal to 50.3 Å in dark-adapted state of purple membranes.

Very recently the dependence of the effect under discussion on pH has been studied. It has been shown that pH itself changes membrane structure. The pH dependence of the membrane thickness in dark and exposed to illumination displays a minimum at the same value of pH. Investigation of the molecular mechanism of the observed phenomenon is in progress.

MICROSTRUCTURAL STUDIES ON DIFFERENT TREATED ALUMINIUM ALLOYS BY SANS

F. Häußler [a], A.I. Kuklin [b], G. Zouhar [c] and H. Worch [c]

[a] *Institut für Massivbau und Baustofftechnologie, Universität Leipzig, 04109 Leipzig, Germany*

rank Laboratory of Neutron Physics, Joint Institute for Nuclear Research, 141980 Dubna, Moscow Region, Russia

[c] *Institut für Werkstoffwissenschaft, Technische Universität Dresden, 01062 Dresden, Germany*

1 Introduction

The neutron methods provide a powerful tool for the nondestructive evaluation of several material parameters inside the volume [1]. In the previous report period microstructural studies on aluminium alloy samples investigations were realized by SANS. In this paper some experimental results will be presented.

Aluminium alloys are applied in different aged conditions. Yield strength, tensile strength, uniform strain, fracture strain and the plastic flow behaviour are dependent on the microstructure, especially on grain size, distribution, nature and coherence of the precipitations, on texture and on solid solution. The integral influence of these microstructural features on the plastic behaviour can be described by means of the athermal work-hardening parameter α [2,3]. Because the SANS effect is influenced by the volume concentration and by the size distribution of the precipitations, a correlation between the scattering curve parameters and the athermal work-hardening parameter α should exist. The objective of the SANS studies is the quantitative characterization of the precipitation state caused by different heat treatments of the Al-alloys. Furthermore a quantitative relation between the precipitation state and the scattering curve parameters belonging to that sample should be elucidated.

2 Experiments and Results

The spectrometer YuMO is located on beam 4 of the pulsed reactor IBR-2 of the Frank Laboratory of Neutron Physics of the Joint Institute for Nuclear Research, Dubna. A detailed description of the SANS spectrometer YuMO is given in [4]. The SANS pattern is described by the macroscopic differential cross section $d\Sigma/d\Omega(Q)$ with Q as the scattering vector. The aluminium alloys represent polydisperse systems containing a large variety of morphological different scattering objects. Hence the SANS measurements reflect a superposition of the scattering effects of all microstructural objects.

By means of the fit program FUMILI the scattering curves d/d (Q) were fitted in the following way:

$$\frac{d\Sigma}{d\Omega}(Q) = A(1) \cdot Q^{-A(2)} + A(3) \qquad (1)$$

Here the parameter A(3) reflects the incoherent neutron scattering background. It depends on the chemical and isotopic composition of the sample under investigation. In contrast to A(3) the parameters A(2) and A(1) are caused by the microstructure. The parameter A(2) indicates the quality of the interfaces between the hydrated and non hydrated components in the sample. In the special case of A(2) = 4 (Porod-like behaviour) the parameter A(1) becomes the Porod constant which is proportional of the total inner surface. Significant deviations from this behaviour suggest the existence of fractal structures described by the fractal dimension. The parameter A(1) should be a measure of the inner surface with fractal properties.

Assuming a fractal behaviour the fractal dimension is determined by A(2), the exponent of an approximated scattering curve. Previously the decision whether a mass (volume) or a surface fractal exists is necessary. The fractal dimension d_m of mass fractals is identical with A(2) and must fulfil the condition A(2) 3. The parameter A(2) allows to describe the microstructural changes in the sample volume [5,6]. These changes are caused by different heat treatments of the aluminium alloys.

Pieces (40 x 40 x ~2 mm^3) of aluminium alloys with different content and morphology of precipitations, according to certain manufacturing conditions (thermal treatment) were prepared. Applied was an AlMgSi-alloy, naturally aged (T4). This type of alloy was also artificially aged at a temperature of 190 degrees centigrade for four hours (named also by T6).

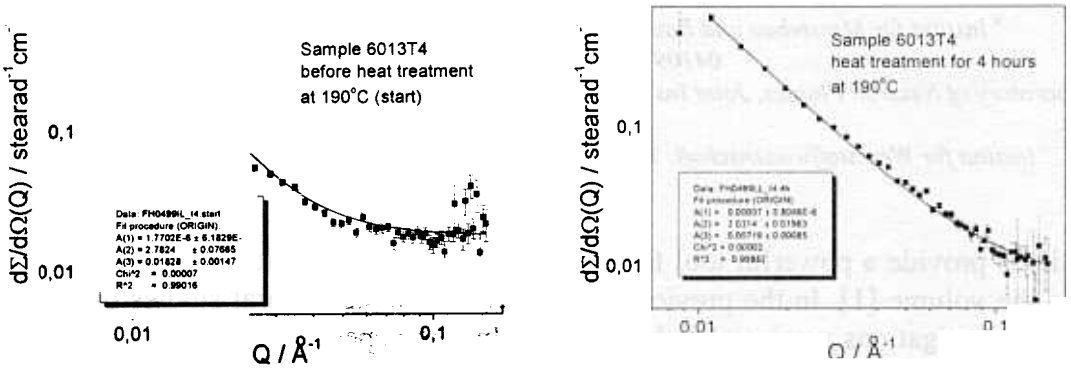

Fig. 1-2: SANS pattern of two aluminium samples with different heat treatments. The lines indicate the fitted curves according eq. (1). The fitted curve parameters A(i) and quality of the fit procedure are inside the frame.

In Fig. 1 and 2 the evolution of the microstructure caused by a different period of heat treatment is evident by the curve parameter A(i). The parameter A(2) indicates fractal behaviour. The value of A(2) is decreased from 2,78 (T4, start) to 2,03 (T4, 4 hours heat treatment) with increasing heat treatment. Investigations carried out by transmission electron microscopy (TEM) revealed rod-like or plate-like crystallographically oriented precipitations in the microstructure of sample T4, 4 hours heat treatment (also named by T6). In contrast to that, not any precipitations could be identified in the microstructure of the sample T4, start. It is assumed that the value A(2) characterizes the precipitation state of the Al-alloy under investigation. The athermal work-hardening parameter α of the T6-material is higher than the α-value of the T4-material. Because the higher magnitudes of α are correlated with higher "internal stresses" σ_i, caused by slip incompatibilities, the dimension d_m of the mass fractal seems to correspond with interface phenomena of the precipitations.

3. Conclusions

Typical processes forming the microstructure can be studied. The scattering curves reflect microstructural changes. Influences of different technologically treatments, so for instance a different duration of a thermal treatment, can be correlated to phase transitions in this aluminium alloy. Comparing the results of the microstructural studies on hydrating C_3S the following fact is evident: Although these two materials are different in their production and properties, the experimental strategy and interpretation of the SANS pattern are similarly.

4. References

[1] Allen, A.J., Time-resolved phenomena in cements, clays and porous rocks, J. Appl. Cryst. 24 (1991) pp. 624-634.

[2] Zouhar, G. et al., Modellansatz zur Voraussage des Werkstoffeinflusses auf den Ermüdungsfortschritt in Aluminiumlegierungen, Werkstoffwoche '98, München, Band VI, Symposium Metalle/Simulation, Ed. R. Kopp et al., WILEY-VCH, Weinheim 1999, pp. 869-874.

[3] Zouhar, G. et al., Ermüdungsfortschritt in Aluminiumlegierungen - Beschreibung aus Fließkurvenparametern, Materialprüfung, to be published.

[4] Ostanevich, Yu.M., Time-of-flight small-angle scattering spectrometers on pulsed neutron sources, Makromol. Chem., Macromol. Symp. 15 (1988) pp. 91-103.

[5] Allen, A. J. et al., Development of the Fine Porosity and Gel Structure of Hydrating Cement Systems, Philosophical Magazine, B56 (1987), pp. 263-288.

[6] Schmidt, P. W., Small-Angle Scattering of Disordered, Porous and Fractal Systems, J. Appl. Cryst., 24 (1991), pp. 414-435.

MICROSTRUCTURAL STUDIES ON HYDRATING TRICALCIUM SILICATE BY SANS

F. Häußler [a], A.I. Kuklin [b], S. Palzer [c], and A. Eckart [c]

[a] *Institut für Massivbau und Baustofftechnologie, Universität Leipzig, 04109 Leipzig, Germany*
[b] *Frank Laboratory of Neutron Physics, Joint Institute for Nuclear Research, 141980 Dubna, Moscow Region, Russia*
[c] *F.A. Finger-Institut für Baustoffkunde, Bauhaus-Universität, 99421 Weimar, Germany*

1 Introduction

The neutron methods provide a powerful tool for the nondestructive evaluation of several material parameters inside the volume [1]. In the previous report period microstructural studies on hydrating tricalcium silicate samples investigations were realized by SANS. In this paper some experimental results will be presented.

According to the typical composition of cement powder the cement clinker phases tricalcium silicate (C_3S) and dicalcium silicate (C_2S) are of high importance for the formation of the hydration products [2]. In the SANS experiments the hydrating C_3S paste is used for a study of the typical hydration processes forming the C-S-H phase. Macroscopic cement stone properties like strength and transport parameters (relative diffusion coefficient, permeability) depend on the structure of the interfaces and the pore volume. For that reason, the sample characterization by parameters of fractals or the application of the Porod approximation [3] is a helpful concept. Kriechbaum et al. [4] have published the results of Small Angle X-ray Scattering (SAXS). The fractal nature is one of the most important statements in this paper. Schmidt [5] emphasized the importance of SANS for studying the structure of fractals and other disordered systems.

2 Experiments and Results

The spectrometer YuMO is located on beam 4 of the pulsed reactor IBR-2 of the Frank Laboratory of Neutron Physics of the Joint Institute for Nuclear Research, Dubna. A detailed description of the SANS spectrometer YuMO is given in [6]. The SANS pattern is described by the macroscopic differential cross section $d\Sigma/d\Omega(Q)$ with Q as the scattering vector. The hydrating C_3S represent polydisperse systems containing a large variety of morphological different scattering objects. Hence the SANS measurements reflect a superposition of the scattering effects of all microstructural objects. By means of the fit program FUMILI the scattering curves d/d (Q) were fitted in the following way:

$$\frac{d\Sigma}{d\Omega}(Q) = A(1) \cdot Q^{-A(2)} + A(3) \qquad (1)$$

Here the parameter A(3) reflects the incoherent neutron scattering background. It depends on the chemical and isotopic composition of the sample under investigation. In contrast to A(3) the parameters A(2) and A(1) are caused by the microstructure. The parameter A(2) indicates the quality of the interfaces between the hydrated and non hydrated components in the sample. In the special case of A(2) = 4 (Porod-like behaviour) the parameter A(1) becomes the Porod constant which is proportional of the total inner surface. Significant deviations from this behaviour suggest the existence of fractal structures described by the fractal dimension. The parameter A(1) should be a measure of the inner surface with fractal properties.

Assuming a fractal behaviour the fractal dimension is determined by A(2), the exponent of an approximated scattering curve. Previously the decision whether a mass (volume) or a surface fractal exists is necessary. The fractal dimension d_m of mass fractals is identical with A(2) and must fulfil the condition A(2) 3. If $3 < A(2) < 4$, the fractal dimension d_S of surface fractals is calculated with

$$d_S = 6 - A(2). \qquad (2)$$

The parameter A(2) allows to describe the microstructural changes in the sample volume. These changes are caused by different w-c ratios of the C_3S samples.
Measurements were carried out using three well characterised hydrating C_3S samples [7]. Here the water-C_3S ratio was varied (0,40, 0,52, and 0,60). The samples were stored for 24 hours at 100% rel. humidity. After that the samples were sealed in plastic bags until the beginning of the SANS experiments after about two weeks. The three SANS curves measured at YuMO show a different SANS pattern. Especially there is a significant difference between the sample prepared with w/c=0,40 and the two others (see fig. 1). Different A(2) values are calculated (see eq. (1)): C3SHYD40: 3,04 +/- 0,03, C3SHYD52: 2,75 +/- 0,02, C3SHYD60: 2,62 +/- 0,01. The change of the scattering curve parameter A(2) from 2,75 to 2,62 indicates a mass fractal with decreasing density (decreasing d_m). Here a decreasing density means a more loosely packed microstructure. The increasing water-solid ratio decreases the spatial density of the C-S-H phases.

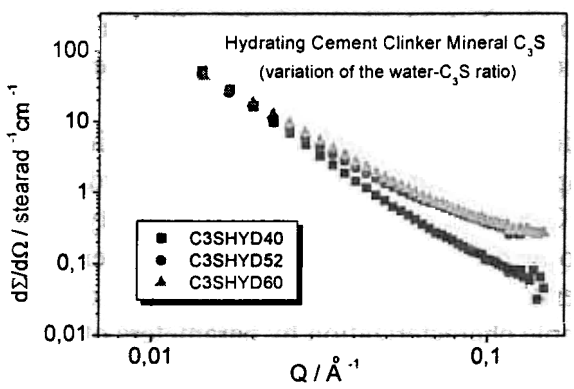

Fig. 1: Hydrating cement clinker mineral C_3S prepared with different w-c ratios (C3SHYD40: w/c=0.40; C3SHYD52:w/c=0.52; C3SHYD60: w/c=0.60).

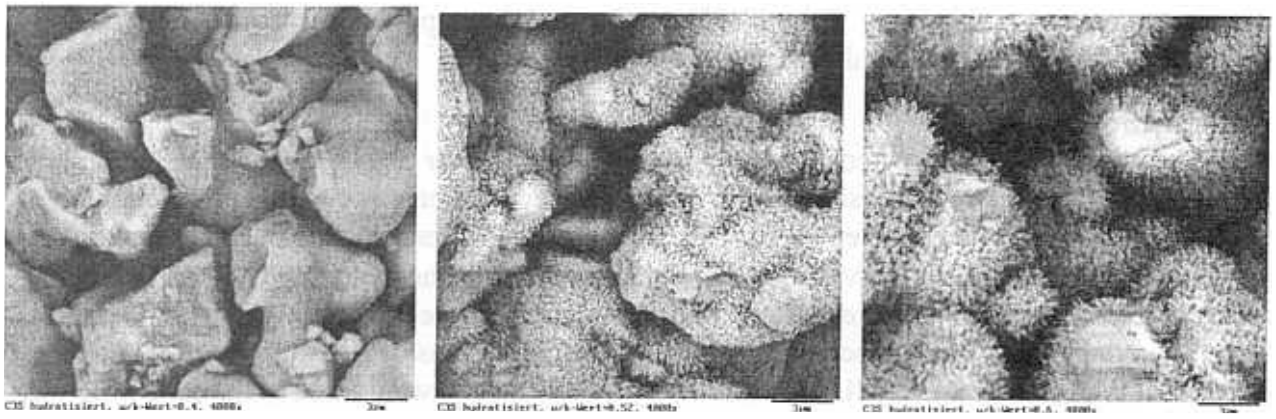

Fig. 2-4: SEM studies on the C_3S samples (M. Langenfeld, FIB Weimar, 1999)

SEM (Scanning Electron Microscopy) studies (see fig. 2-4) were realized 10 days after the SANS experiments and show significant differences in the microstructure under investigation. The sample with the lowest w-c ratio shows the lowest degree of hydration. Fig. 3 and fig. 4 show the hydration products surrounding the non hydrated clinker grain.

3. Conclusions

Typical processes forming the microstructure can be studied. The scattering curves reflect microstructural changes. In the C_3S samples these changes can be correlated to the chemical and physical processes during hydration.
Furthermore, the SANS results in combination with the SEM studies show new possibilities for a nondestructive description of the microstructure of hydrating cement paste. Tricalcium silicate as an essential cement clinker phase allows the investigation of the formation of the major hydration product (C-S-H phases).
The variation of different parameters of the sample preparation (water-solid ration, grain sizes etc.) gives the possibility to investigate the various influences to the cement paste microstructure [8]. By

applying a specially adapted mathematical and technical model of fractal structures, a very promising way of interpreting experimental results was used. These studies are described in [9].

4. References and Acknowledgements

The authors wish to acknowledge gratefully Prof. G. König for his permanent interest and the support for the work. In addition the authors want to thank Prof. J. Stark and his co-workers (FIB, Bauhaus-Universität Weimar) for their helpful discussions on the interpretation of the results, and Prof. H. Baumbach (Fraunhofer-Institut für Zerstörungsfreie Prüfverfahren Saarbrücken), Prof. J. Tritthart from TVFA Graz, and Prof. S. Roehling, Leipzig, for their kind interest in our work. This work is supported by the Deutsche Forschungsgemeinschaft (DFG) under contract No. Ha2759/3-1 and Ha2759/3-2.

[Allen, A.J., Time-resolved phenomena in cements, clays and porous rocks, J. Appl. Cryst. 24 (1991) pp. 624-634.

[2] Langenfeld, M., Stark, J., Der Einfluß von Verzögerern auf die frühe Hydratation von Portlandzementklinkerphasen, dargestellt im ESEM-FEG, Thesis, Beiträge zur Baustofforschung, Wissenschaftliche Zeitschrift der Bauhaus-Universität, 44 (1998) 1 / 2, S. 83-90.

[3] Allen, A. J. et al., Development of the Fine Porosity and Gel Structure of Hydrating Cement Systems, Philosophical Magazine, B56 (1987), pp. 263-288.

[4] Kriechbaum, M. et al., Investigations on Cement Pastes by Small-Angle X-ray Scattering and BET: the Relevance of Fractal Geometry, Advances in Cement Research, 6 (1994), pp. 93-101.

[5] Schmidt, P. W., Small-Angle Scattering of Disordered, Porous and Fractal Systems, J. Appl. Cryst., 24 (1991), pp. 414-435.

[6] Ostanevich, Yu.M., Time-of-flight small-angle scattering spectrometers on pulsed neutron sources, Makromol. Chem., Macromol. Symp. 15 (1988) pp. 91-103.

7] Häußler, F. et al., Nondestructive Microstructural Investigations on Hydrating Cement Paste and Tricalcium Silicate by Small Angle Neutron Scattering, Leipzig Annual Civil Engineering Report 1999, pp.47-64.

[8] Häussler, F. et al., H., Long-time monitoring of the microstructural change in hardening cement paste by SANS, Advances in Cement Research 9 (1997), pp. 139-147.

[9] Heinemann, A. et al. , Fractal microstructures in hydrating cement paste, Journal of Material Science Letters 18 (1999), pp. 1413-1416.

A STRUCTURE OF DMPC VESICLES IN SURCOSE/WATER SOLUTIONS

M.A. Kiselev*, P.Lesieur#, A.M. Kisselev*, D. Lombardo#, M. Killany*, S. Lesieur%

* - *Frank Laboratory of Neutron Physics, JINR, Dubna, Russia*
# - *LURE, Bat. 209-D, B.P. 34, F-91898 Orsay, France*
% - *Pharmaceutical Faculty, University Paris-Sud, Chatenay Malabry F – 92296, France*

The SANS experiment on extruded vesicles from model biological membrane is useful method for the calculation of membrane thickness[1]. Nevertheless to the importance, the radius of large unilamellar vesicles can not be determined from scattering experiment due to the great polydispersity in the vesicular radii. The methods to create of monodispersed large unilamellar vesicles (LUVs) as fast delution and temperature jump protocol were developed for mixed lipid/surfactant systems[2,3]. In these approaches, the monodispersed vesicles are created during the transformation from micellar to lamellar phase. The problem to create the LUVs with low polydispersity from pure lipid system without surfactant for SANS and SAXS experiment was not solved till now. The application of X-ray small angle scattering to the study of vesicular systems has a second problem, which is weak contrast $\Delta\rho$ between phospholipid bilayer and water. The substitution of water solutions (H_2O or D_2O) to the sucrose/water solutions is used to solve the both problems. The macroscopic cross section of vesicle can be written as[1]

$$\frac{d\Sigma}{d\Theta} = N(\Delta\rho)^2(4\pi/Q^3)^2(A_2-A_1)^2, \quad \text{with } A_i=\mathrm{Sin}(QR_i)-(QR_i)\mathrm{Cos}(QR_i) \qquad (1)$$

where N is the number of vesicles per unit volume, $\Delta\rho$- contrast for neutron or X-ray scattering, R_1 and R_2 correspond to the inner and outer radii of the vesicle, respectively. The bilayer thickness is then $d_l=R_2-R_1$.

Fig. 1 demonstrates the increase in contrast between DMPC membrane and sucrose solution as function of sucrose concentration for X-ray scattering. SAXS experiment with DMPC vesicles were carried out to test the contrast variation with sucrose buffer. The vesicles were prepared by extrusion of the solution through polycarbonate filter with pores of 500Å in diameter. Vesicles with low polydispersity were detected for sucrose concentrations from 30% to 45% (see Fig.2).

The vesicles in the sucrose/H_2O solution with sucrose concentrations below 20% (see Fig. 1) have small contrast to be measured via X-ray scattering with good statistics. The SANS at YuMO spectrometer was applied to study the region of sucrose concentrations from 0 to 20%. The neutron spectrum from the solid methane moderator was used to rich $q<0.008Å^{-1}$. Fig. 3 demonstrate the scattering cross section of extruded DMPC vesicles in D_2O, which have not oscillation and correspond to the Gaussian distribution of vesicles radii with polydispersity 72%. The addition of 5% sucrose decrease a polydispersity to the value of 40%. The value of the polydispersity decrease with further increase of sucrose concentration, the polydispersity has a minimum value of 29% at sucrose concentration 20%. The macroscopic cross section from vesicles in sucrose/D_2O solution with 20% sucrose was measured with temperature of methane moderator $T_{methane}=35^oK$ (see Fig. 4). The comparison of SAXS curve from synchrotron (Fig. 2) and SANS curve from IBR-2 reactor with cold moderator (Fig. 4) demonstrate that $q_{min}=0.005Å^{-1}$ at synchrotron are not so far from $q_{min}=0.006Å^{-1}$ at IBR-2 reactor with cold moderator. Important to note that spectra from vesicles collected at YuMO spectrometer have $q_{max}=0.15Å^{-1}$, at D22 spectrometer of DCI synchrotron $q_{max}=0.04Å^{-1}$, this difference create the advantage of SANS experiment for the correct calculation of the membrane thickness. The membrane thickness as function of sucrose concentration was calculated from Kratky-Porod plot as described in[1]. The presented in Tab. 1 results demonstrate that sucrose has not influence to the membrane thickness at the region from 0 to 40% sucrose concentration.

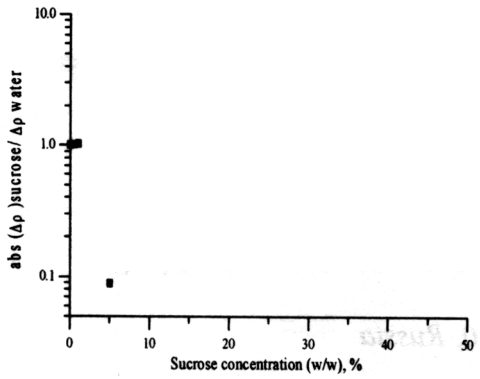

Fig. 1. Theoretical dependence of ratio $|\Delta\rho_{sucrose}|/\Delta\rho_{water}$ for DMPC membrane in L_α -phase on the sucrose concentration in H_2O (w/w). The region of sucrose concentration above 20% can create sufficient increase of the contrast for X-ray.

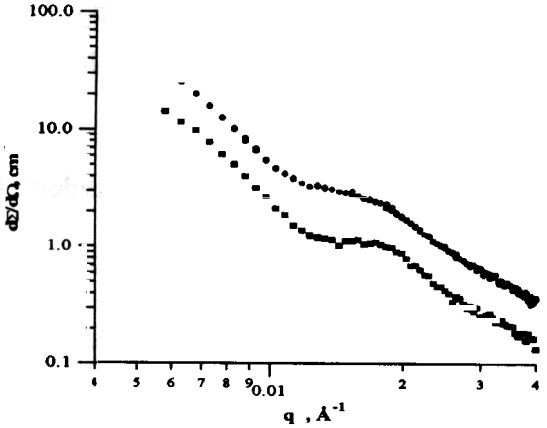

Fig. 2. SAXS curves from extruded DMPC vesicles at T=30°C in the sucrose/H_2O solution with sucrose concentration 30% (squares) and 45% (circles). The curves correspond to the scattering from the vesicles with R_1=200Å, 230Å and σ_R=65Å, 75Å for 30% and 45% sucrose concentration, respectively.

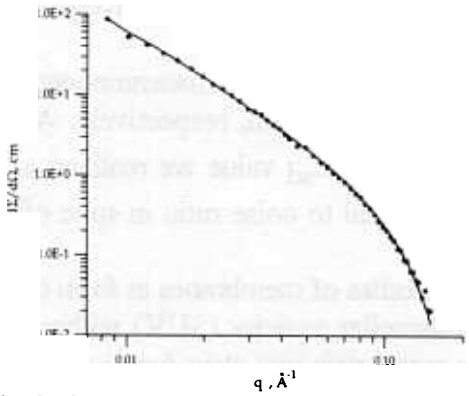

Fig. 3. SANS curve from extruded DMPC vesicles in D_2O, T=30°C (points). Fitted curve (line) with parameters: R_1=180Å, σ_R=130Å, R_2-R_1=34Å.

Sucrose concentration, %	0	20	30	40
membrane thickness, Å	44.5±1.0	44.7±0.8	43.7±0.8	43.1±0.8

Sucrose buffer has two advantages. First is the possibility to create a monodispersed population of vesicles, which sufficiently improve the experimental conditions to study the vesicles structure. Second is the increase in intensity, which is large enough to allow for the study the structure of diluted aggregates by SAXS. Sucrose/water solutions is perspective medium for the SANS and SAXS application at the investigation of vesicles structure and structure of mixed lipid/surfactant systems.

References

1 P. Balgavy, M. Dubnichkova, D. Uhrikova, S. Yaradaikin, M. Kiselev, V. Gordeliy. Bilayer Thickness in Unilamellar Extruded Egg Yolk Phosphatidylcholine Liposomes: A Small-Angle Neutron Scattering Study. Acta Physica Slovaca, 48 (1998) 509-533.

2. P. Schurtenberger, N. Mazer, W. Känzig. Micelle to Vesicle Transition in Aqueous Solutions of Bile Salt and Lecithin. J. Phys. Chem. 89 (1985) 1042-1049.

3. P. Lesieur, M.A. Kiselev, L.I. Barsukov, D. Lombardo. Temperature induced micelle to vesicle transition: kinetic effects in the DMPC/ NaC/water system. *1999, Accepted in J. Appl. Cryst.*

Determination of Structural Parameters and Hydration of Unilamellar Vesicles at high Water Excess from SANS Curves Using a Multiple-Strip Model

P. Jörchel[1], M. Kiselev[2], G. Klose[1], H. Schmiedel[1]

Institute of Experimental Physics I, University of Leipzig, Linné-Str. 5, 04103 Leipzig, Germany

2 *FLNP, Joint Institute of Nuclear Research, Dubna 141980, Russia*

Biological membranes are very complex systems. To get more information about their structure it is helpful to investigate more simple systems. For this purpose we studied the suitable system POPC (1-palmitoyl-2-oleyl-sn-glycero-3-phosphatidylcholine), $C_{12}E_4$ (tetraoxyethylene monododecylether), as well as the mixture POPC/$C_{12}E_4$. Like many other amphiphilic substances, they form membrane structures in form of liposomes at high water excess. These liposomes vary in size and number of layers. For studying the membrane structure these complex systems have to be simplified moreover. In the ideal case all vesicles would have the same size and one layer. In fact, this state is not possible to realize. Nevertheless, vesicles consisting almost exclusively of monolayers can be prepared by extrusion.

We extruded each sample before measuring 25 times with 200nm filters. The measurements were carried out at the sample-detector distances L_{sd} of 4.414m and 13.173m, respectively. At the large Lsd value the measurement time was 60 minutes. At the small L_{sd} value we realized a longer measurement time of 300 minutes for getting an acceptable signal to noise ratio in spite of the lower intensity at higher q-values.

Until now there are several publications regarding small angle studies of membranes in form of vesicles. Komura at al. /1/ determined the diameters of small unilamellar vesicles (SUV) without taking into account their size distribution and by assuming two symmetric one-strip functions as approximation for the neutron scattering amplitude density across the bilayers. The bilayer thickness of large unilamellar lipid vesicles (LUV) was deduced by means of the Kratky-Porod approximation /2/ in Refs. /3 – 6/. Further, Glatter /7/ analysed the small angle x-ray scattering (SAXS) curves by applying two symmetric two-strip functions as approximation for the electron scattering length density across the bilayer. Strip functions are also common as approximation of the neutron scattering length density calculated from diffractograms of multilamellar system by Fourier synthesis /8, 9/.

Our aim is the determination not only of the lipid bilayer thickness but also of the thickness of the hydrophobic core and of the surface requirements of the molecules as well as the extension of the hydrophobic parts of the molecules into the water subphase and of the hydration of the vesicles. For this reason the experiment was carried out with the objective to get data inclusively q-values as high as possible with an acceptable signal to noise ratio. The q-values of measurements range from 0.006 $Å^{-1}$ to 0.382 $Å^{-1}$.

The size distribution of vesicles has been determined by freeze fracture electron microscopy. That means that it is no fit parameter. An important improvement of the used model in comparison to other ones is the insertion of a parameter taking into account the presence of small amounts of multilamellar and/or non-spherical vesicles. The fit procedure using this model results in calculated spectra with very small deviations from the measured ones. An example is given in Fig.1 for vesicles of pure $C_{12}E_4$ in D_2O.

The demonstration of the efficiency of the model by its application on special vesicle dispersions and by comparison of the results obtained with other data is another aim of our experiment. Mixtures of POPC and $C_{12}E_4$ have been extensively studied at low water

concentration by SAXS /10/, SANS /11/, and NMR/12/. It was found that the structural and dynamic properties change with composition and exhibit some peculiarities.

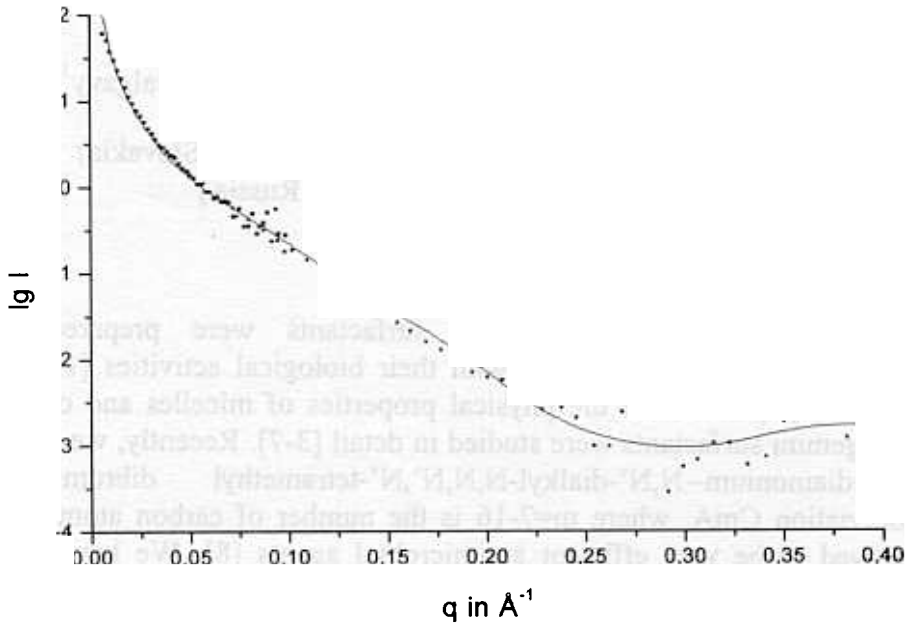

Fig. 1. Measured SANS spectrum at $C_{12}E_4$-vesicles in D_2O and fitted curve of our model. Results of fit: thickness of hydrophobic core 7.8Å, thickness of headgroup region 12.6Å, bilayer thickness 33.0Å, number of bond water molecules per $C_{12}E_4$ molecule 18, cross-sectional area per $C_{12}E_4$ molecule 69Å^2, relative amount of bilamellar vesicles 4,3%.

References:

/1/ S. Komura, Y. Toyoshima, T. Takeda, Japanese J. Appl. Phys. 21 (1982) 1370 - 1372
/2/ D. M. Sadler, D. L. Worcester, J. Biol.159 (1982) 485 – 499
/3/ D. M. Sadler, F. Reiss-Husson, E. Rivas, Chem. Phys. Lipids 52 (1990) 41 – 48
/4/ V. I. Gordeliy, L. V. Golubchikova, A. I. Kuklin, A. G. Syrykh, A. Watts, Progress Colloid Polymer Sci. 93 (1993) 252-257
/5/ P. Balgavy, M. Dubnickova, D. Uhrikova, S. Yaradaikin, M. Kiselev, V. Gordeliy, Acta physika slovaca 48 (1998) 509-533.
/6/ M. A. Kiselev, P. Lesieur, A. M. Kisselev, C. Grabielle-Madelmond, M. Ollivon, J. Alloys Compounds 286 (1999) 195 – 202
/7/ O. Glatter, Progress Colloid Polymer Sci. 84 (1991)
/8/ G. Klose, A. Islamov, B. König, V. Cherezov, L Colloid Interface Sci. 172 (1995) 438 - 446
/9/ V. I. Gordeliy, M. A. Kiselev, Biophys. J. 69 (1995) 1424 – 1428
/10/ B. König, U. Dietrich, G. Klose, Langmuir 13 (1997) 525 – 532
/11/ G. Klose, St. Eisenblätter, B. König, J. Colloid Interface Sci. 172 (1995) 438 – 446
/12/ G. Klose, B. Mädler, H. Schäfer, K.-P. Schneider, J. Phys. Chem. B 103 (1999) 3022 –3029

SANS STUDY OF AGGREGATES OF THE GEMINI SURFACTANT 1,4-BUTANEDIAMONIUM-N,N'-DIHEXADECYL-N,N,N',N'-TETRAMETHYL DIBROMIDE IN THE AQUEOUS SOLUTION

M. Dubnickova[1], M.Kiselev[2], I. Lacko[1], F. Devinsky[1], P. Balgavy[1]

[1]Faculty of Pharmacy, J. A. Comenius University, 83 232 Bratislava (Slovakia)
[2]Frank Laboratory of Neutron Physics, JINR, 141980 Dubna (Russia)

Introduction

Several years ago, different gemini surfactants were prepared and their physicochemical properties were correlated with their biological activities [1, 2]. This has stimulated a series of papers where the physical properties of micelles and other lyotropic phases formed by gemini surfactants were studied in detail [3-7]. Recently, we have prepared new 1,4-butanediamonium--N,N'-dialkyl-N,N,N',N'-tetramethyl dibromide gemini surfactants (abbreviation CmA, where m=7-16 is the number of carbon atoms in the alkyl chain) which proved to be very efficient antimicrobial agents [8]. We have studied their physicochemical properties in aqueous phases as a function of concentration and number of carbon atoms in the alkyl chain m, using the surface tension, electrical conductivity, dynamic light scattering and zeta potential measurement methods [8, 9]. These experimental data have indirectly indicated, that closely above the CmA critical micelle concentrations (cmc), the spheroidal micelles are present in the the aqueous phase at the intermediate m values ($14 \geq m \geq 10$). However, these experimental results have suggested also the presence of large aggregates for the long ($m>14$) alkyl chain CmA gemini surfactants. In the present communication, we report the results of small-angle neutron scattering (SANS) study of the C16A aggregates in the aqueous phase.

Material and Methods

The C16A gemini surfactant was prepared by reaction of tertiary N,N,N',N-tetramethyl-1,4-butanediamine with 1-bromohexadecane as described in [10]. The surfactant was purified by manifold crystallization from a mixture of acetone and methanol. Its identity and purity was confirmed by elemental analysis, thin-layer chromatography, and IR and ^{1}H NMR spectroscopies. Heavy water (99.98 % ^2H_2O) was obtained from Izotop (Moscow, Russia). Surfactant and heavy water were mixed in a glass tube, the tube was purged with gaseous nitrogen and sealed. The content was dispersed by hand shaking and sonication in a bath sonicator. The SANS measurements were performed at the small-angle time-of-flight axially symmetric neutron scattering spectrometer YuMO at the IBR-2 fast pulsed reactor. The samples were poured into quartz cells (Hellma, Müllheim, Germany) to provide the 1 mm sample thickness. The sample temperature was set and controlled electronically at 20.0±0.1°C. The sample in quartz cell was equilibrated for 1 hour at the given temperature before measurement. The sample-detector distance was set to 10.553 m.

Results and Discussion

The SANS scattering function can be written as

$$I(Q)=NP(Q)S(Q) \quad (1)$$

where Q is the scattering vector, N is the number of scattering particles in unit volume, $P(Q)$ is the particle structure factor, and $S(Q)$ is the size- and orientation-dependent interparticle structure factor. $S(Q)$ approximately equals to 1 for dilute and weakly interacting particles; we will suppose that this holds for the samples measured in the present work.

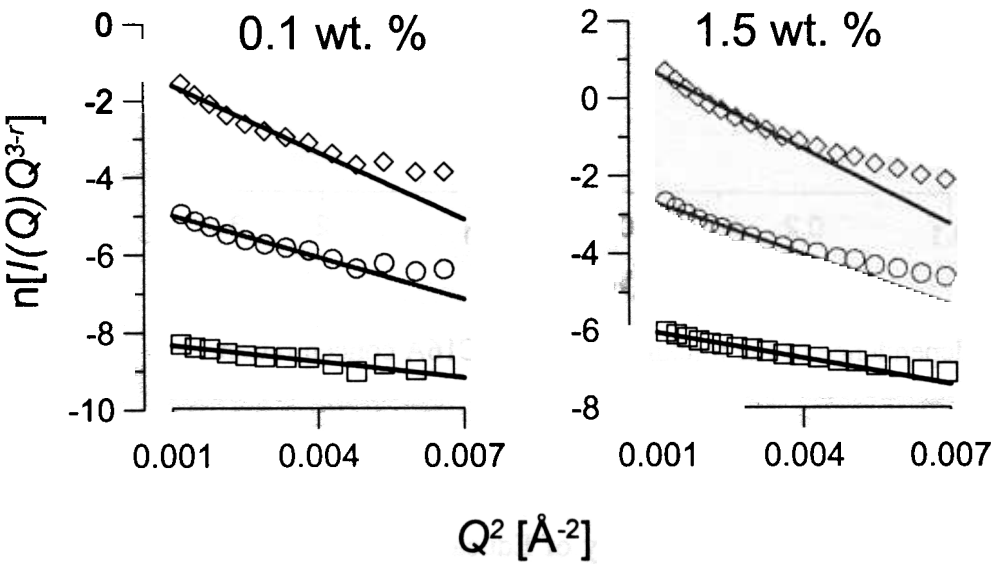

Fig.1. The dependence of SANS intensity $I(Q)$ on scattering vector Q. Squares: r=1, circles: r=2, diamonds: r=3.

According to Guinier approximation for very small scattering angles (see [11-14] for references), one rewrites then equation (1) as

$$I(Q)=I(0)\exp(-Q^2R^2/r)Q^{r-3} \qquad (2)$$

where $I(0)$ is the intensity at zero scattering vector, R is the object radius of gyration and $r\approx1$, 2, and 3 hold for infinite sheet-like object, for rod-like object of infinite length and uniform cross section, and for a globular object, respectively. Using eqn. 1 one can thus in principle discriminate between discoid, tubular and spheroidal micelles in heavy water. We have shown [15] that $r\approx1$ is a good approximation also for polydisperse hollow spheres with radii larger than the constant shell thickness, such as unilamellar liposomes. Using eqn. 2, we have fitted our SANS data in the interval of $0.004\ Å^{-2}\geq Q^2\geq 0.001\ Å^{-2}$ by the least-squares method and the fitted functions extrapolated into the interval $0.007\ Å^{-2}>Q^2\geq 0.004\ Å^{-2}$ (full lines in Fig.1). It is seen that the experimental data deviate from the fitted functions when supposing rods or globules in the C16A system, while all the experimental data are approximated rather well by the fitted function when supposing the presence of sheets and/or polydisperse liposomes. It is well known that the thickness of the infinite sheet as well as of the shell in polydisperse hollow spheres can be obtained from the radius of gyration as $d_S\approx 12^{1/2}R$ under condition that the coherent scattering length density of the solvent is substantially larger than that of scattering particle and that the scattering density within the particle can be taken as homogeneous (see [11-15] for references). This is the case of C16A aggregates in heavy water. We have thus calculated the value of d_s from the SANS curves. Its concentration dependence is shown in Fig.2. With the increase of concentration, this thickness increases. At concentrations above cmc, the value of d_s obtained corresponds to the length of two C16A molecules located in the bilayer of large discoid micelles or/and unilamellar liposomes.

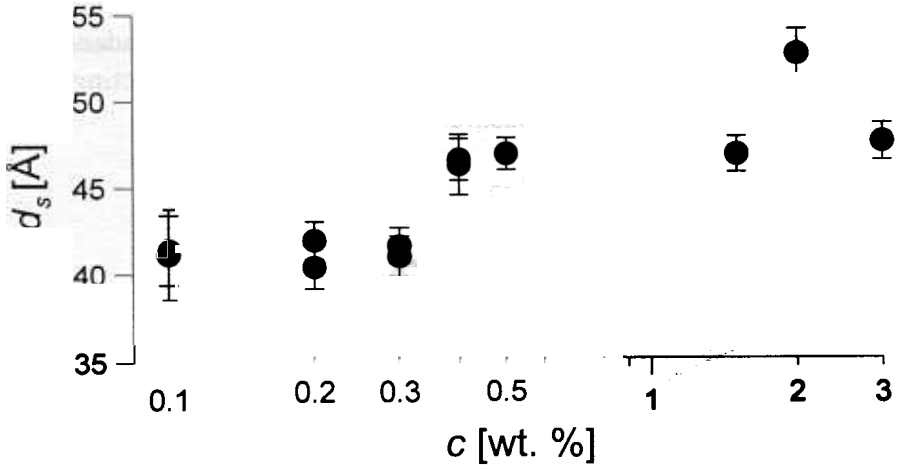

Fig.2. The dependence of the thickness d_s on the C16A concentration.

Acknowledgement

This study was supported by the Slovak Ministry of Education grants 1/4137/97 1/4187/97. The experiments in Dubna were supported within the JINR project 07-4-1031-99/03.

References

1. Devinsky, F.; Masarova, L.; Lacko, I. J. Colloid Interface Sci. 1985, 105, 235.
2. Devinsky, F.; Lacko, I; Mlynarcik, D.; Svajdlenka, E.; Masarova, L. Acta Facult. Pharm. 1990, 44, 127.
3. Zana, R.; Benrraou, M.; Rueff R. Langmuir 1991, 7, 1072.
4. Alami, E.; Beinert, G.; Marie, P; Zana R. Langmuir 1993, 9, 1465.
5. Frindi, M.; Michels, B.; Levy, H.; Zana, R. Langmuir 1994, 10, 1140.
6. Danino, D.; Talmon, Y.; Zana, R. Langmuir 1995, 11, 1448.
7. Hirata, H.; Hattori, N.; Ishida, M.; Okabayashi, H.; Frusaka, F; Zana, R. J. Phys. Chem. 1995, 12, 1149.
8. Dubnickova, M.; Pisarcik, M.; Lacko, I.; Devinsky, F.; Mlynarcik, D.; Balgavy, P. Gemini surfactants: Antimicrobial activity, micellization and interaction with phospholipid bilayers. XIIIth School on Biophysics of Membrane Transport, May 11-18, 1997, Ladek Zdroj, Poland
9. Pisarcik, M.; Dubnickova, M.; Devinsky, F.; Lacko, I.; Skvarla, J. Colloids Surfaces A: Physicochem. Eng. Aspects 1998, 143, 69.
10. Imam, T; Devinsky, F.; Lacko, I.; Krasnec, L. Pharmazie 1983, 38, 308.
11. Glatter, O.; Kratky, O. Small Angle X-ray Scattering. Academic Press, New York, 1982.
12. Kratky, O.; Laggner, P. In: Encyclopedia of Physical Science, vol. 14, Academic Press, London, 1987, p. 693.
13. Hjelm, R.P.Jr.; Thiyagaragan, P.; Sivia, D.S.; Lindner, P.; Alkan, H.; Schwahn, D. Progr. Colloid Polym. Sci. 1990, 81, 225.
14. Dubnickova, M.; Kiselev, M.; Kutuzov, S.; Devinsky, F.; Gordeliy, V.; Balgavy, P. Gen. Phys. Biophys. 1997, 16, 175.
15. Balgavy, P.; Dubnickova, M.; Uhrikova, D.; Yaradaikin, S.; Kiselev, M.; Gordeliy, V. Acta Phys. Slov. 1998, 48, 509.

SANS STUDY OF BLOCK COPOLYMER MICELLES WITH COATED CORES

J. Pleštil[1)], H. Pospíšil[1)], V. I. Gordeliy[2)]

[1)]*Institute of Macromolecular Chemistry, Academy of Sciences of the Czech Republic, Heyrovsky Sq.2, 162 06 Prague 6, Czech Republic, E-mail: plestil@imc.cas.cz*

[2)]*Frank Laboratory of Neutron Physics, Joint Institute for Nuclear Research, 141980 Dubna, Moscow Region, Russia*

Introduction

Block copolymer micelles are polymolecular particles with a dense core formed by insoluble blocks and a protective corona formed by swollen soluble blocks. Most prospective applications of the micelles are based on loading sparingly soluble compounds into micellar cores (solubilization). It is desirable to have a possibility of controlling characteristics of this process by variation of the micelle parameters. Promising candidates for such purpose are onion-type micelles. Unlike the commonly studied two-component core/corona micelles, the onion-type micelles have a three-layer structure. The so far studied multilayered micelles have been prepared using two diblock copolymers [1,2] or an ABC triblock copolymer [3,4].

This contribution demonstrates the possibility of preparing another type of multilayered particles. The procedure consists in solubilization of a monomer in micellar solution and subsequent polymerization [5].

Experimental

Materials: The micellar solution of polystyrene-*block*-poly(methacrylic acid) (PS-*b*-PMA, or SA) (M_w = 42x10^3 g/mol, weight fraction of PS = 0.58) was prepared in 0.1 M borax in H_2O. A part of the solution was transferred into 0.1 M borax in D_2O by dialysis. Methyl methacrylate (MMA) was added to the micellar solution in an amount comparable with that of the copolymer. The solutions were stored for one day and then the MMA was polymerized by γ-radiation (dose 2 kGy) at 295 K.

Small-Angle Neutron Scattering (SANS) Measurements: Scattering data measured using the YuMO spectrometers are presented as a function of the magnitude of the scattering vector, $q = (4\pi/\lambda) \sin \Theta$, where λ is the wavelength and 2Θ is the scattering angle.

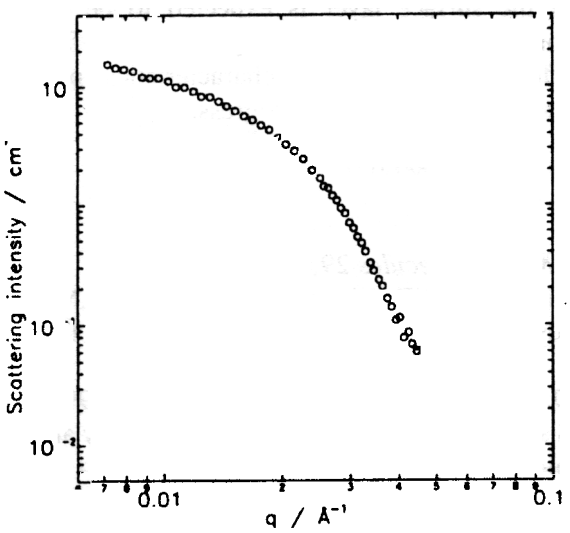

Fig.1. Changes in the SANS curve of the PS-*b*-PMA in 0.1 M borax in D_2O (c=1.92 g/L) induced by solubilization of MMA monomer and subsequent polymerization. Both normal (h-MMA) and deuterated (d-MMA) monomers are used.

Analysis of SANS data: The theoretical scattering function of spherical particles with Schulz-Zimm distribution of radii was fitted to experimental SANS data within a properly chosen q- range (bare-core approximation [6]). This fit provides the mean radius of particle core, R_{core}, and the relative standard deviation, $\sigma/R_{core} = 1/\sqrt{(Z+1)}$, where Z is the width parameter of the Schulz-Zimm distribution. Other characteristics of the particle cores (volume, aggregation number, and mass) can be calculated using the fit parameters.

Results and discussion

The PS-*b*-PMA copolymer (SA) forms micelles with PS core and PMA corona. Figure 1 demonstrates the effect of solubilization of MMA monomer in this micellar solution and subsequent polymerization on SANS curves. It can be seen that an addition of the MMA monomer to the micellar solution has only a minor influence on scattering intensities. As this is true for both the normal and deuterated monomer, we may conclude that the monomer did not penetrate into the micelle core in a large amount.

The SANS curves taken after polymerization differ significantly from that observed for the original micelles (Fig. 1). For the SA/d-PMMA system, deviation from SANS curve of simple micelles is observed only at small q's while at higher angles, the curves coincide. On the other hand, SANS curve of the SA/h-PMMA system deviates appreciably also in the region of the secondary maximum reflecting the size of the scatterer. These findings indicate that the cores of the studied particles are formed by the PS core of the original micelle and PMMA deposited on the surface of this core. Analysis of the SANS curves shows that the mean radius of PS core is 99 Å and the thickness of PMMA layer is 17 Å. These conclusions have been confirmed by the results of contrast variation experiments [5].

Polymerization process: A time-resolved SANS experiment was performed to monitor the process of polymerization of MMA in PS-*b*-PMA micellar solution. Polymerization was initiated with ammonium peroxysulfate. Figure 2 shows the time dependence of the core parameters obtained from the SANS data. We can see that a sudden increase in parameter values occurs about 30 min after the initiator was added. Our NMR experiments [7] reveal that the amount of monomer starts to decrease from the very beginning of the process. These observations suggest that in early stages of polymerization, soluble oligomers are formed. When the oligomers are long enough, they collapse onto the core surface to form a layer of the PMMA polymer.

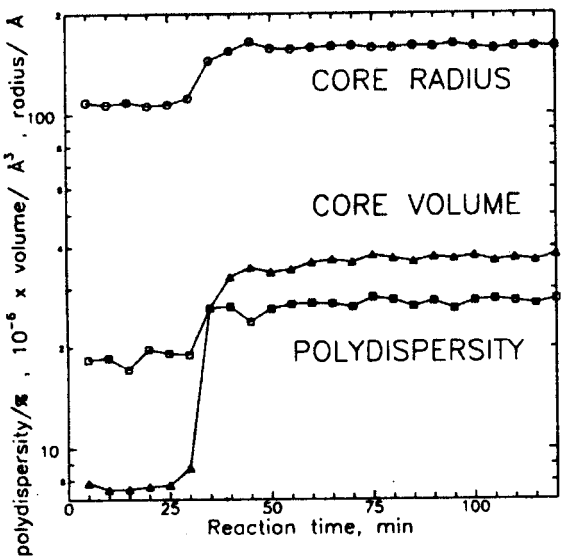

Fig.2. Variation of the core parameters with reaction time during polymerization of MMA (c=4 g/L) in a PS-*b*-PMA micellar solution (c=1.67 g/L).

Conclusions

It was demonstrated that block copolymer micelles can be modified by solubilization of a monomer and subsequent polymerization to form micelles with coated cores. The thickness of the surface layer is expected to be easily controllable. Further investigation of the factors affecting the relevant characteristics of the resulting particles is in progress.

This work was supported by the Grant Agency of the Czech Republic (grant 203/00/1317).

Reference

1. K.Procházka, T.J.Martin, S.E.Webber and P.Munk *Macromolecules* 29,6526(1996)
2. J.Pleštil, J.Kříž, Z.Tuzar, K.Procházka, Yu.B:Melnichenko, G.D.Wignall, R.Talingting, P.Munk, S..E.Webber "Small-Angle Neutron Scattering Study of Onion-Type Micelles"*Macromol. Chem. Phys.*, submitted
3. J.Kříž, B.Masař, J.Pleštil, Z.Tuzar, H.Pospíšil and D.Doskočilová *Macromolecules* 31,41(1998)
4. J. Pleštil, H.Pospíšil, B.Masař, M.A.Kiselev "SANS study of onion-type micelles formed by an ABC block copolymer with a pH-sensitive middle block", Annual Report 1998, FLNP, Joint Institute for Nuclear Research, Dubna, Russia, pp. 63-66
5. J. Pleštil, H. Pospíšil, P. Kadlec, Z.Tuzar, J. Kříž, V.I. Gordeliy "SANS study of multilayer nanoparticles based on block copolymer micelles", *Macromol. Chem. Phys.*, submitted
6. J. Pleštil "Bare-Core Approximation: A Useful Approach to SAS Data of Block Copolymer Micelles", *J. Appl. Crystallogr.*, in press
7. J. Kříž, D. Kurková,, P. Kadlec, Z. Tuzar, J. Pleštil "Interface polymerization in a polymer micelle: an NMR study radical polymerization of methyl methacrylate at the core-shell interface of polystyrene-*block*- poly(methacrylic acid) micelles", *Macromolecules*, submitted

NUCLEAR POTENTIAL OF GLASS SUBSTRATE OBTAINED FROM SPIN-FLIPPED NEUTRON TRANSMISSION THROUGH THE Co FILM

V.L. Aksenov, S.V. Kozhevnikov, Yu.V. Nikitenko

Frank Laboratory of Neutron Physics, JINR, 141980 Dubna, Moscow region, Russia

Abstract.

Transmission of a polarized neutron beam through the magnetic Co (700 Å) film on a glass substrate, where the external magnetic field was applied at an angle to the sample surface, was analyzed. The following phenomenon was observed: a neutron beam of '+-' spin transition passed through the sample without refraction at a certain value of the external magnetic field strength. This effect was used to determine the nuclear potential of a nonmagnetic substrate.

When a polarized neutron beam is transmitted or reflected from a magnetically noncollinear medium, neutron spin-flip and spatial beam-splitting take place. This effect was first predicted by Ignatovich in [1] (see also [2]) and was experimentally studied in [3-7]. In this work, a polarized neutron beam, passing through a magnetically noncollinear film, is employed to determine the nuclear potential of a nonmagnetic substrate.

Experiments were run on the polarized neutron spectrometer SPN-1 at the IBR-2 reactor in Dubna. A scheme of total polarization analysis using a multislit analyser and a position-sensitive detector was applied. The 100×50×5mm^3 sample was a magnetic Co (700 Å) film on a glass substrate; this sample was used in [4]. An external magnetic field H=0.2÷10.1 kOe was applied at an angle of 80^0 to the film surface. The grazing angle of the incident beam was equal to θ_i=3.7 mrad. Angular resolution of the spectrometer was equal to ±0.13 mrad. The neutron beam passed through the magnetic film and emerged from the edge of the substrate. Preliminary results of this study were published in [7].

As neutrons pass through the magnetic Co film, a neutron spin-flip occurs, causing an alteration in the potential energy of neutron interaction with the external magnetic field. This changes the kinetic energy of neutrons in the direction perpendicular to the sample plane. Thus, the polarized neutron beam splits in the space into two neutron beams – with and without spin-flip. In Fig.1, the grazing angle of the '+-' transmitted beam as a function of the neutron wavelength at different values of H is shown. It can be seen that with increasing H, the angle θ increases and, in the 10.1 kOe field, it becomes greater than the grazing angle of the incident beam. In Fig.2, the difference $\Delta\theta^2=\theta^2-\theta_i^2$ is shown vs. the external magnetic field strength at different wavelength values. It can be easily seen that all of the straight lines intersect at different values of the wavelength. That is, all of the straight lines intersect at a point where $\theta=\theta_i$. From here, the value of the field at which the neutron beam passes through the sample without refraction, H=7.9±0.2 kOe, was found. In this point the value of the alteration of the potential energy in the external magnetic field compensates the nuclear potential of the nonmagnetic substrate: $2\mu H=U$. Thus, the value of the nuclear potential of the substrate was determined to be U=95.3±2.4 neV.

This technique of nuclear potential measurement resembles the procedure of weighing. The magnetic field strength plays the role of the scale weight, while the neutron beam plays the role of the pointer on the 'neutron scales'. The estimates show that, using the external magnetic field, the nuclear potential of a nonmagnetic layer can be determined to an accuracy of $\Delta U/U\approx10^{-4}$. It should be emphasized that the condition of equality of the magnetic and nuclear potentials holds

for all values λ and θ_i. Therefore, it allows one to perform nuclear potential measurements on a polychromatic neutron beam with an unknown spectrum and a monodetector.

The authors wish to express their sincere gratitude to V.G.Syromiatnikov for the sample.

[1] V.K. Ignatovich, Letters to JETP 28 (1978) 311.
[2] N.K. Pleshanov, Z. Phys. 94 (1994) 233.
[3] G.P. Felcher, S. Adenwalla, V.O. de Haan, A.A. van Well, Phys. B 221 (1996) 494.
[4] H. Fredrikze, M.Th. Rekveldt, A.A. van Well, Yu.V. Nikitenko, V.G. Syromyatnikov, Phys. B 248 (1998) 157.
[5] V.L. Aksenov, E.B. Dokukin, S.V. Kozhevnikov, Yu.V. Nikitenko, A.V. Petrenko, J. Schreiber, Phys. B 234-236 (1997) 513.
[6] V.L. Aksenov, H. Fredrikze, S.V. Kozhevnikov, Yu.V. Nikitenko, M.Th. Rekveldt, J. Schreiber, JINR Commun. №E14-98-85 (1998).
[7] V.L. Aksenov, S.V. Kozhevnikov, Yu.V. Nikitenko, JINR Commun. №E14-98-373 (1998).

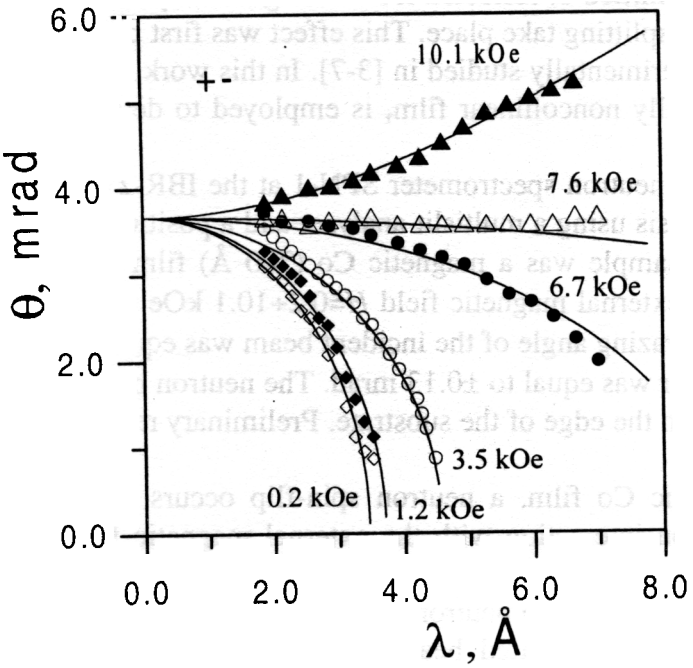

Fig. 1. The grazing angle of the transmitted neutron beam as a function of the neutron wavelength at different values of the external magnetic field (the solid line is calculation for U=95.3 neV).

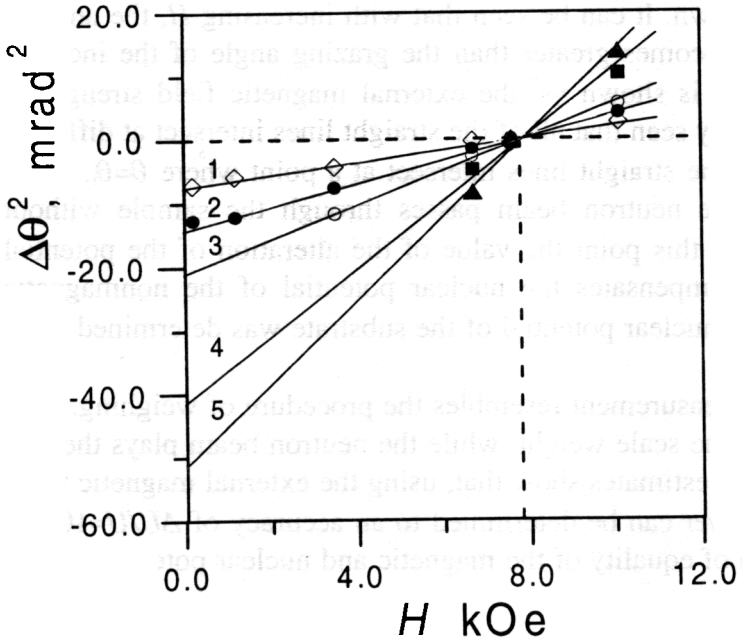

Fig. 2. The difference $\Delta\theta^2=\theta^2-\theta_i^2$ vs. the external magnetic field strength at different values of neutron wavelength: 1- 2.56; 2- 3.52; 3- 4.27; 4- 5.98 and 5- 6.66 Å.

MAGNETIC INEQUALITY OF FILM INTERFACES EXTRACTED BY POLARIZED NEUTRON REFRACTION

V.L. Aksenov, S.V. Kozhevnikov, Yu.V. Nikitenko

Frank Laboratory of Neutron Physics, JINR, 141980 Dubna, Moscow Region, Russia

Abstract.

Refraction of polarized neutrons on separate boundaries of magnetic film was investigated. The effects of neutron spin-flip and spatial splitting of a polarized neutron beam were observed. Magnetic and nuclear parameters near the interfaces were determined.

In [1], a twofold refraction of a nonpolarized neutron beam on one interface of two domains was observed. In [2], neutron refraction was employed to determine the thickness of the domain walls. Neutron spin-flip and spatial splitting of a polarized beam occur at reflection and refraction on the interface of the magnetically noncollinear medium. This effect was predicted by Ignatovich in [3] (see also [4]) and was experimentally studied in [5-7]. In this work, the refraction of a polarized neutron beam was studied separately on each boundary of a magnetic FeAlSi film.

The measurements were carried out on the SPN-1 polarized neutron spectrometer at the IBR-2 reactor in Dubna. A scheme of total polarization analysis using a multislit analyzer and a position-sensitive detector was applied. The 5×20×1 mm^3 sample was a multilayer structure of Fe(86 at%)Al(9.6 at%)Si(4.4 at%)(20 μm)/Cr(500 Å)/$CaTiO_3$. An external magnetic field of 4.5 kOe was applied at an angle $\beta=70^0$ to the sample surface. The grazing angle of the incident beam was equal to $\theta_1 = 4.7$ mrad. Angular resolution of the spectrometer was equal to ±0.13 mrad. The experiment is schematically depicted in Fig.1. The refraction on the vacuum–magnetic film interface (the first boundary) is marked as index 1, and the refraction on the magnetic film–nonmagnetic substrate interface (the second boundary) is marked as index 2.

In Fig. 2, the values of the grazing angle of the refracted beam as a function of the neutron wavelength are shown for the interval $\Delta\lambda$=0.27 Å. The probability of the neutron spin flip is 20÷30%. Four beams '+(-),+(-)' of different spin transitions is observed at refraction on the first interface (closed symbols). Only three beams can be seen at refraction on the second interface (open symbols). The fourth beam '-+' is overlapped by the direct beam. Using the experimental data from the values of the grazing angles for the refracted beams, the following parameters were calculated by formulae from [7]:

U_1=148.3±4.4 neV; B_1=11.8±0.2 kG; H_1=5.0±0.3 kOe;

(U_2-V)=108.4±3.2 neV; B_2=10.9±0.4 kG; H_2=3.0±0.7 kOe,

where $U_{1,2}$, $B_{1,2}$ and $H_{1,2}$ are the values of the nuclear potential of the magnetic film, the magnetic induction and the external magnetic field strength near the first and the second boundaries respectively; V – the nuclear potential of substrate. To determine the values of U_2 and V separately, it is necessary to carry out an experiment on neutron beam transmission through the two interfaces.

Thus, we have shown that polarized neutron refraction on separate boundaries of a magnetic film is described by different values of the magnetic parameters. This study gives us reason to hope that the method of polarized neutron refraction has considerable promise for investigation the processes of the alteration of magnetic properties on the interfaces of a magnetic film.

The authors express their deep gratitude to J. Schreiber for the sample and to H.Fredrikze and M.Th. Rekveldt for the fruitful discussions.

[1] S.Sh. Shilshtein, V.A. Somenkov, M. Kalanov, JETP 63 (1972) 2214.
[2] O. Schaerpf, H. Strothmann, Physica Scripta 24 (1988) 58.
[3] V.K. Ignatovich, Letters to JETP 28 (1978) 311.
[4] N.K. Pleshanov, Z. Phys. 94 (1994) 233.
[5] G.P. Felcher, S. Adenwalla, V.O. de Haan, A.A. van Well, Phys. B 221 (1996) 494.
[6] V.L. Aksenov, E.B. Dokukin, S.V. Kozhevnikov, Yu.V. Nikitenko, A.V. Petrenko, J. Schreiber, Phys. B 234-236 (1997) 513.
[7] V.L. Aksenov, H. Fredrikze, S.V. Kozhevnikov, Yu.V. Nikitenko, M.Th. Rekveldt, J. Schreiber, JINR Commun. №E14-98-85 (1998).

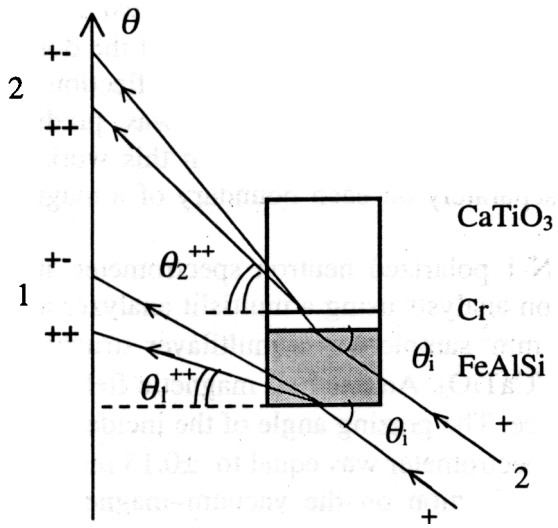

Fig. 1. Schematic representation of the experiment.

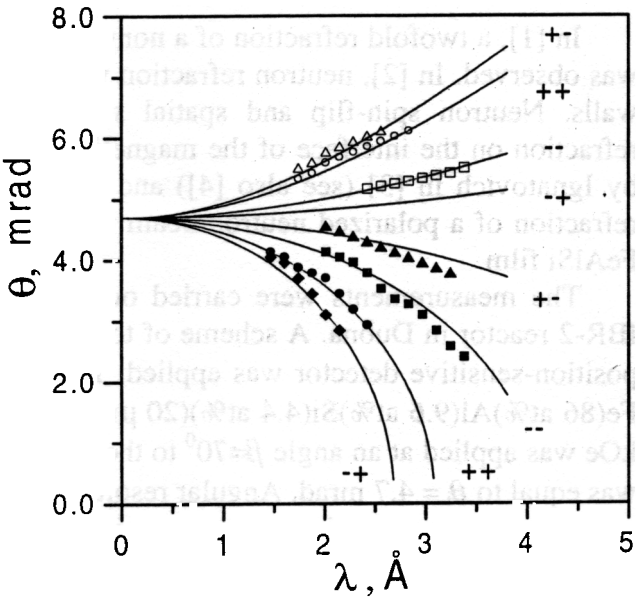

Fig. 2. The grazing angle of the refracted neutron beam as a function of the neutron wavelength (the solid lines show the calculation): closed symbols are interface 1; open symbols are interface 2.

MAGNETIC REGIME OF glass/Fe(1000Å)/Gd(50Å) LAYERED STRUCTURE EXTRACTED BY NEUTRON POLARIZATION METHODS

V.L.Aksenov, S.V.Kozhevnikov, Yu.V.Nikitenko, H. Lauter[1]

Frank Laboratory of Neutron Physics, Joint Institute for Nuclear Research, 141980 Dubna, Moscow Region, Russian Federation
[1]*Institut Laue-Langevin, Post Box 156, 38042 Grenoble, France*

In this work, a magnetic behavior of the Fe(1000Å)/Gd(50Å) layered structure has been investigated [1] using the polarization methods of generating neutron standing waves [2], spatial neutron beam-splitting [3] and full neutron polarization analysis at SPN-1 spectrometer.

The dependencies in Fig. 1+5 were obtained after the preliminary reverse magnetization of the sample with the external magnetic field up to H=4 kOe for measurement spin-flipper modes 'on,off' and 'off,on'. It can be seen in Fig. 1 that at H=110 Oe and H=277 Oe there are non-specular reflected and refracted neutron beams caused by the spin transitions in the local magnetic field H_{LOC} '-+L' and '+-L' respectively ('+-L' takes place at $\Delta E > 0$ and '-+L' at $\Delta E < 0$, where ΔE is the transmission of the energy to the neutron). At H=163 Oe, these beams are absent. In Fig. 2 it can be seen that at H=277 Oe, the spin transitions '-+' and '+-' in the external magnetic field correspond to the spin transitions '+-L' and '-+L' in the local magnetic field Hs. Thus, we can conclude that at $H > 163$ Oe, two spin-flip processes exist, which change the initial and final spin states to their opposites. The difference $\Delta R = R_{++}(\lambda) - R_{--}(\lambda)$ in Fig. 3 changes its sign with an increasing magnetic field and at H= 163 Oe, it reaches the minimum value by its absolute magnitude. The value Hs at interface in front of magnetic region is connected with perpendicular component of the magnetization Jn and the values of the tangential Ht and the perpendicular Hn components of the strength of the magnetic field : $Hs=(Ht^2+(Hn+Jn)^2)^{1/2}$. In Fig. 4 the absolute values of Hs_1 and Hs_1+Hs_2 obtained from beam-splitting angles for reflection and refraction, respectively, and its difference Hs_2 are shown. These values practically do not change and at H^*= 163 Oe are close to zero. In the range H=200+800 Oe, the Hs_1 and Hs_2 alteration occurs in the opposite phase. This may be explained by correlated changing of magnetization vector near the corresponding interfaces and (or) by neutron wave interference. From the spectral position of the maxima in the reflectivities of spin-flip neutrons, and minima connected with the adsorption of neutrons in Gd when neutron standing waves are generated, it follows that the region of flipping is located closer to the Fe-Gd interface than the region of nuclear neutron adsorption. In Fig. 5 spin-flip reflectivity is demonstrated in dependence of strength of external magnetic field. It is seen that with increasing of H the reflectivity falls. It is not excluded that it is connected with a reduction in the cross-section of the regions (domains), magnetized normal to the interface.

From the experimental results and the preliminary calculations we can conclude that there are two types of regions. In the first region (domains), the magnetization of the Gd layer (or the Fe layer) is directed normal to the sample plane. This region leads to neutron beam-splitting. At $H = H^*$, the magnetization of this region lies in the sample surface. The second region is Fe layer coated by Gd layer, or by a gadolinium oxide layer, and the magnetization is directed parallel to the direction of an external magnetic field. This region does not split the polarized beam. At $H=H^*$, the magnetization in this region lies in the sample plane and is directed normal to the direction of an external magnetic field.

[1] V.L. Aksenov, S.V. Kozhevnikov, Yu.V. Nikitenko, H. Lauter, JINR Commun. E14-99-227, Dubna, 1999.
[2] V.L. Aksenov, Yu.V. Nikitenko, Physica B 267-268 (1999) 313.
[3] V.L. Aksenov, E.B. Dokukin, S.V. Kozhevnikov, Yu.V. Nikitenko, A.V. Petrenko, J. Schreiber, Physica B 234-236 (1997) 513.

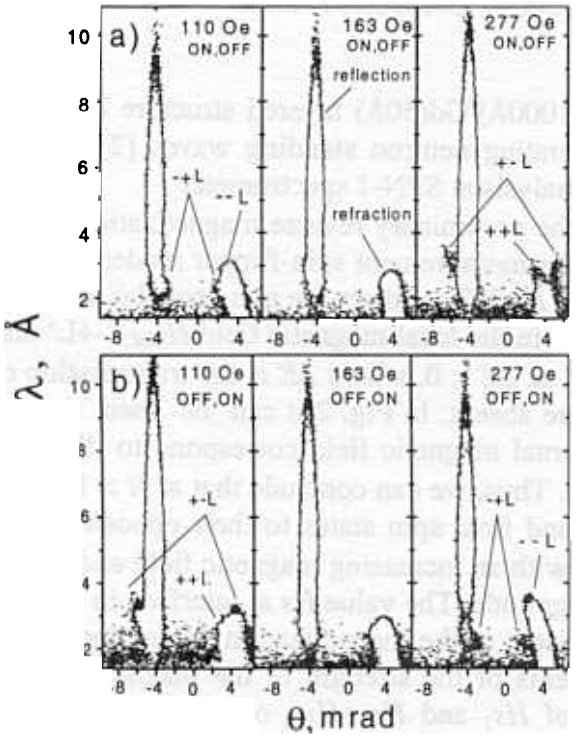

Fig. 1. Equal intensity contours on plane 'wavelength λ - output grazing angle θ' in measurement states 'on,off' and 'off,on'.

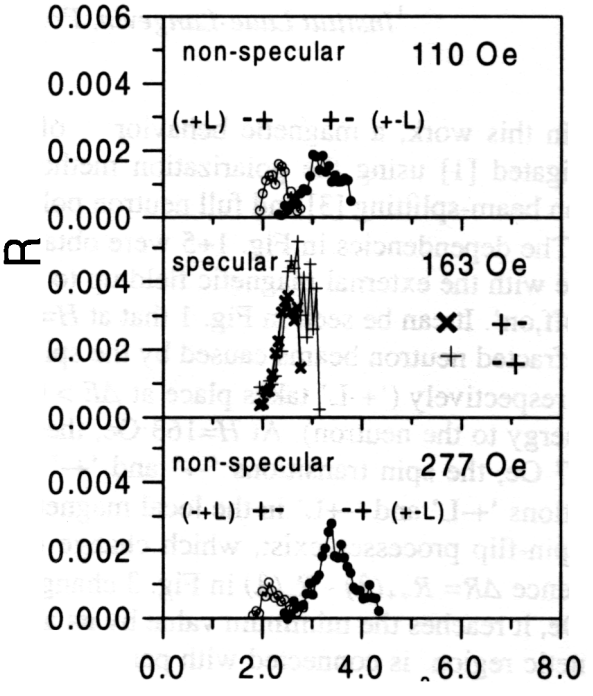

Fig. 2. Reflectivities '+-' and '-+' (closed circles are '+-L', open circles are '-+L' spin transition) on the neutron wavelength λ.

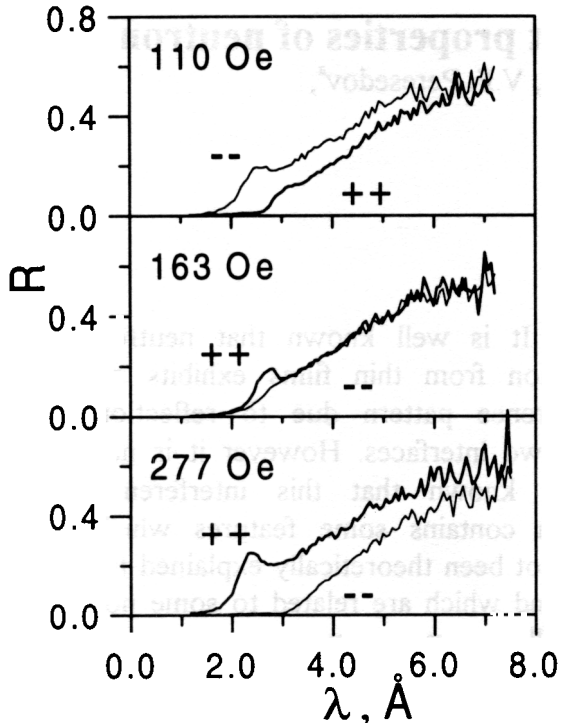

Fig. 3. Specular reflectivities '++' and '--'

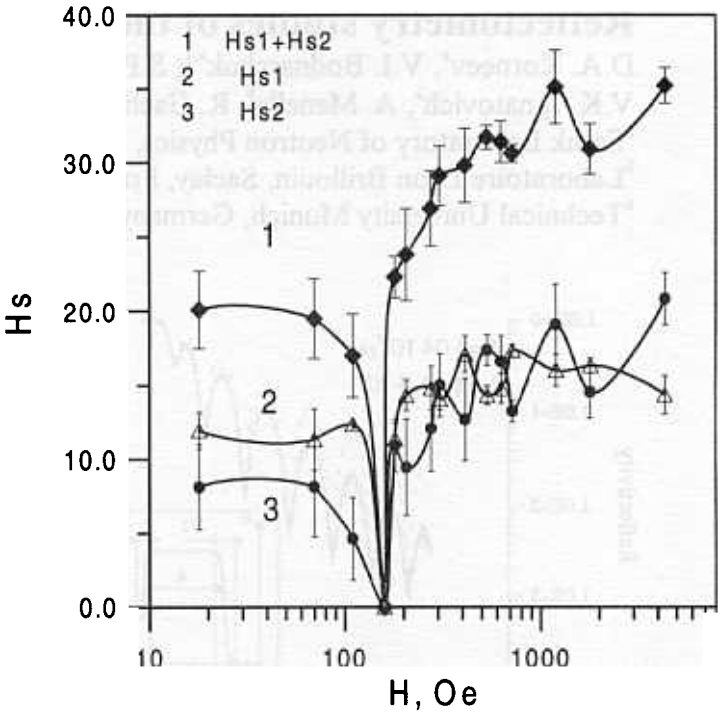

Fig. 4. The dependence of the strength of the local magnetic field at interface with vacuum Hs_1, at interface with glass Hs_2 and sum (Hs_1+Hs_2) vs. the strength of external magnetic field.

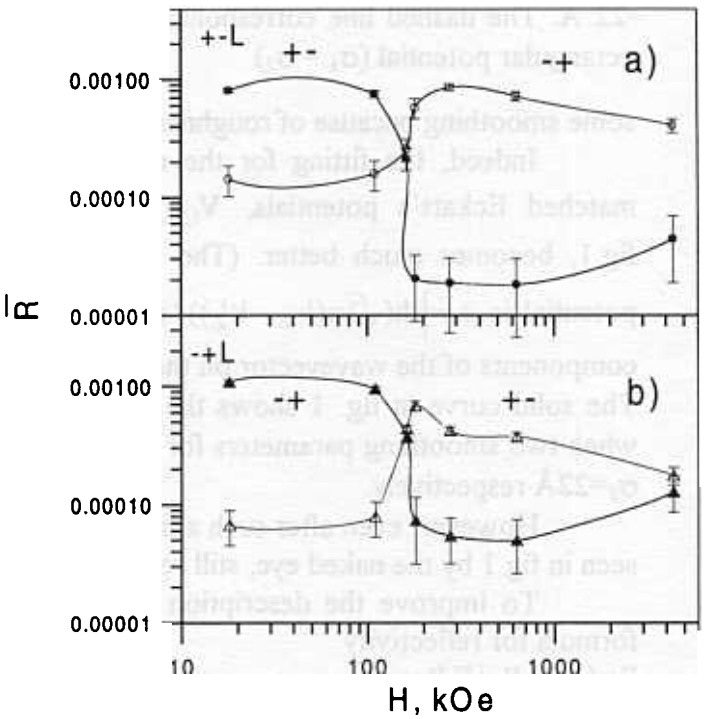

Fig. 5. The average (by a neutron wavelength) spin-flip reflectivities on the strength of external magnetic field: a) '+-L'; b) '-+L'.

Reflectometry studies of the coherent properties of neutrons

D.A. Korneev[a], V.I. Bodnarchuk[a,1], S.P. Yaradaikin[a], V.F. Peresedov[a],
V.K. Ignatovich[a], A. Menelle[b], R. Gaehler[c]
[a]Frank Laboratory of Neutron Physics, JINR, Russia
[b]Laboratoire Leon Brillouin, Saclay, France
[c]Technical University Munich, Germany

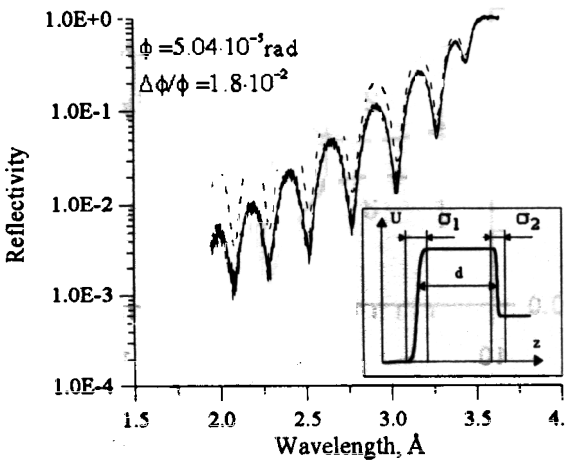

Fig. 1

Coherent plane wave approach. Experimental and theoretical reflectivities for a Cu film with d=(1796±10)Å. The solid curve is the best fit for the Eckart from potential represented in the frame with smoothing of boundaries σ_1 =70.4 Å, σ_2 =22 Å. The dashed line corresponds to the rectangular potential ($\sigma_1 = \sigma_2$)

It is well known that neutron reflection from thin films exhibits an interference pattern due to reflection from two interfaces. However it is not widely known that this interference pattern contains some features which have not been theoretically explained till now and which are related to some not yet well understood physics.

One of such precisely measured patterns is presented in fig. 1. It corresponds to the reflection from a thin Cu film of a polychromatic well-collimated neutron beam, measured with the time-of-flight technique. The model of a rectangular potential for the film gives the pattern shown by the broken line in fig.1, which is not well fitted to the experimental points. It is clear that the rectangular potential should be modified. Since both interfaces are usually not ideal, we are to introduce some smoothing because of roughnesses.

Indeed, the fitting for the model of film, described with a system of two matched Eckart's potentials, $V_{1,2}(z) = V_{0\,1,2} / (1+\exp(-z\,\pi / \sqrt{3}\sigma_{1,2}))$, as shown in fig.1, becomes much better. (The reflectivity from a single boundary with such a potential is $r = \left|\mathrm{sh}(\sqrt{3}\sigma(k_z - k'_z)) / \mathrm{sh}(\sqrt{3}\sigma(k_z + k'_z))\right|^2$, where k_z and k'_z are the z-components of the wavevector on the left and right sides of the boundary respectively). The solid curve in fig. 1 shows the best fitting (χ^2=1.39) to the experimental points when two smoothing parameters for the first and second interfaces are σ_1=70.4 Å, and σ_2=22Å respectively.

However, even after such a fitting with χ^2=1.39 some discrepancy, which is not seen in fig.1 by the naked eye, still remains.

To improve the description of the experimental data we used the modified formula for reflectivity

$$R=(1-F)\,R_c+F\,R_{inc}, \qquad (1)$$

i.e. we assume that $R(\lambda,\phi)$ (λ is the neutron wave length, ϕ=const is the grazing angle of the incident beam), consists of two parts: coherent, R_c, shown by the solid curve in fig.1, which contains interference of waves reflected from both interfaces, and

incoherent (without interference), $R_{inc}=(r_1+r_2-2r_1r_2)/(1-r_1r_2)$, which contains reflection coefficients $r_{1,2}$ from separate single smoothed boundaries (this approach was formulated in [1]). The best fit of formula (1) to the experimental points with coefficient F as a parameter gives the F about 0.04 with $\chi^2=1.15$ (see fig 2a.).

It is reasonable to assume that the coefficient F could be a function of wavelength λ. This function could be found from the following phenomenological consideration. Two rays ψ, ψ' (incident and reflected) are shifted along the film surface by the distance $l=2d/\tan\phi'$. Since the grazing angle inside the film ϕ' depends on λ, l also depends on λ. If we choose the parameter ξ as double dispersion for Gaussian like law of the suppression the interference ability of the two rays ψ, ψ' that coherent part of reflectivity will be proportional to the area of overlapping of two Gaussians and the incoherent coefficient will be $F = \mathrm{erf}(l(\lambda)/\sqrt{2}\xi)$. Because the scale of l is determined by the parameter ξ, we can identify ξ with the coherence length of the reflection process. The fraction of the incoherent reflection in (1) increases with increasing ratio l/ξ.

The fitting of formula (1) to the experimental data with $F=F(l,\xi)$ leads to $\xi\approx$ 1.5mm with considerably improved $\chi^2=1.04$ (see fig.2b), which means that our assumption of $F=F(l,\xi)$ is significant. The knowledge of the angle uncertainty $\Delta\phi/\phi$ is very important because it suppresses the interference contrast, as does the incoherent admixture. We use the value $\Delta\phi/\phi=1.8\cdot10^{-2}$.

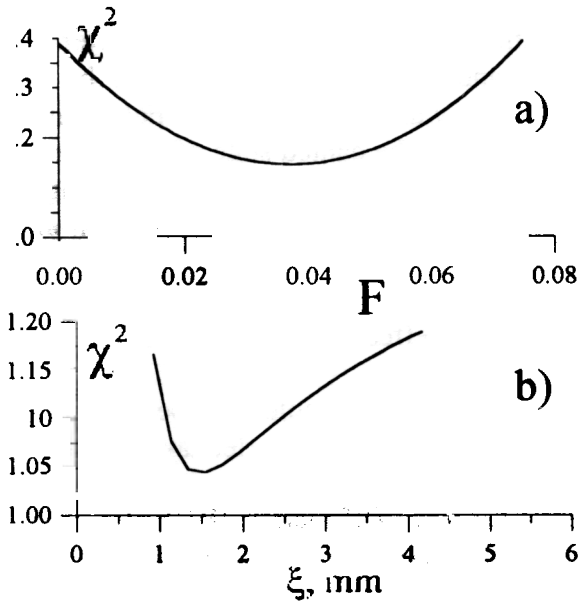

Fig.2

a) Dependence of χ^2 on the parameter F in formula (1), $\phi=5.04$mrd, $\Delta\phi/\phi=0.9\cdot10^{-2}$

b) dependence of χ^2 on the parameter ξ when $F = \mathrm{erf}(l(\lambda)/\sqrt{2}\xi)$. A deeper minimum in this curve than that in fig. 2a) indicates significance of the model with the function $F(l,\xi)$.

The question of interpretation of the parameter ξ is open at this stage of our work. It leads to two possible considerations. One is that incoherent admixture due to incoherent interaction of neutrons with film and substrate media. The other is that the parameter ξ reflects the coherent properties of the neutron itself. Supporting the latter is the fact that the incoherent diffuse scattering from roughnesses, which leads to some contribution to specular reflections, does not depend on the shift l.

However, in spite of this argument interpretation of the parameter ξ demand others experiments to check the repeatability of the incoherent effect in specular neutron reflection from thin films.

This work was supported by INTAS grant No.97-11329

References

[1] D.A. Korneev, Neutron Optics in Kumatory '96, Abstracts of Conference 1996

Magnetic off-specular neutron scattering from Fe/Cr multilayers

V.Lauter-Pasyuk[1,2], H.J.Lauter[3], B.Toperverg[3,4], O.Nikonov[2,3], E. Kravtsov[5], A.V.Petrenko[2], M.A. Milyaev[5], L. Romashev[5], V. Ustinov[5]

[1]TU München, Physik Department, D-85747 Garching, Germany

[2]Joint Institute for Nuclear Research, 141980 Dubna, Moscow Region, Russia

[3]Institut Laue Langevin, B.P.156, F-38042, Grenoble Cedex 9, France

[4]PNPI, 188450, Gatchina, St. Petersburg, Russia

[5] Institute of Metal Physics, 62019 Ekterinburg, Russia

We report about the polarised neutron scattering study of the magnetic structure of a [Cr(12Å)/^{57}Fe(68Å)]X12 multilayer on sapphire substrate carried out at the SPN reflectometer. The intensity distribution was measured over a broad range of incident and outgoing wavevectors. The specular and off-specular intensities of the first and second order Bragg-peaks (determined by the bi-layer thickness) and those at the half order positions (due to antiferromagnetic coupling) were measured. Off-specular scattering arranged into sheets running trough the antiferromagnetic half order positions is spread over an appreciable range crossing the specular line. These findings result in a picture of in-plane domains, rather than in the model of homogeneously magnetized neighboring Fe-layers, with non-collinear magnetization.

Fe/Cr multilayers are well-known systems demonstrating antiferromagnetic interlayer coupling in alternative Fe layers separated by a Cr spacer and were thoroughly studied by different techniques. Also polarised neutron reflectometry (PNR) was often applied to Fe/Cr multilayers and gave interesting results [1] in particular with respect to the canted state of the magnetisation in successive Fe layers. We will give a different interpretation due to the wide range of the measured specular and off-specular scattering. The off-specular intensity distribution along the half-order Bragg-sheets influences the interpretation of the specular scattering. This off-specular intensity cannot be simply neglected or even subtracted from the specular intensity. The presence of magnetic domains is strongly suggested as primary effect by the off-specular scattering through the half-order Bragg-positions.

The (001) superlattice [Cr(12Å)/^{57}Fe(68Å)]x12 was grown with molecular beam epitaxy. The Al_2O_3 substrate was annealed at 700°C and covered with a 70Å Cr buffer layer at 300°C. The multilayer was grown at the substrate temperature of 180°C starting with Fe layer and characterized in-situ with Reflection High Energy Electron Diffraction (RHEED) and ex-situ with X-ray Diffraction measurements. The in-plane magnetization measurements carried out at room temperature with a vibrating sample magnetometer (VSM) revealed extremely strong in-plane anisotropy in the sample with a four-fold in plane anisotropy [2].

The PNR experiments were performed on the SPN spectrometer at FLNP with the external magnetic field H applied parallel to the sample surface. A multidetector recorded the reflected intensity. The experiment was performed at an incident angle of 15.2 mrad and the external magnetic field H = 0.405 kG after having applied a negative saturation field. As an example figure 1a (for the antiparallel direction of the neutron spin and the external magnetic field) shows the scattering from the Fe/Cr multilayer in the co-ordinate system of wavelength λ and outgoing angles α_f, α_f being the angle between the surface of the film and the scattered neutrons. The scattered intensity is represented by a grey log-scale shown in the bar on the right side of the figure. Strong intensity parallel to the λ-scale corresponds to the specular line with the total reflection region around λ = 12 Å. The position of the two measured full order Bragg-peaks (at λ = 2.32 Å and λ = 1.16 Å) are determined by the thickness of Fe/Cr bi-layer. Nearly no off-

specular scattering is visible around these Bragg-peaks, that confirms that the quality of the sample was extremely good with very small interface roughness. Two half order Bragg-peaks (at $\lambda = 4.62$ Å and $\lambda = 3.47$ Å) are due to the magnetic superstructure perpendicular to the film. Additional intensity is observed going through the two half-order peaks forming superstructure Bragg-sheets. This off-specular scattering around the half-order Bragg-peak positions appears when the "magnetic" lateral order is smaller than the corresponding projection of the neutron coherence length. So, in-plane magnetization is homogeneous only within a certain, relatively small, range. Therefore the model of homogeneously magnetized layers stacked into a sequence with magnetization direction varying between next Fe-layers would be rather unsuitable. Instead one may assume that the sample is decomposed into a set of domains in which the alternating Fe layer magnetization has a component which is antiferromagnetic with respect to the next Fe layer. A small domain size is supported by electron diffraction on a similar sample [3]. The distorted wave Born approximation (DWBA) – based theory in combination with supermatrix routine for polarized neutrons was developed [4] and applied for the treatment of the off-specular scattering from antiferromagnetic domains [5]. The results of such calculation are presented in figure 1b. The agreement between theory and experiment is reached using a model of domains with average lateral dimension of 1 μm and the magnetization in alternative Fe layers non-collinear ordered through all the multilayer stack. As one can see from the figure, this simple model not only reproduces correctly the general features of the experiment, such as spin-flip off-specular scattering sheets along with the non-spin-flip reflectivity ridge, but it also describes a slight asymmetry of the superstructure sheets as well as the overall behavior of intensities along and across the sheets.

We are still analyzing the results but we assume that these magnetic domains play an essential role in the electron scattering process responsible for the GMR (giant magnetic resistance) effect. We believe the model with domains offer a more exact description than the simple explanation usually given in terms of stacks of homogeneously-ordered antiferromagnetic layers.

a)

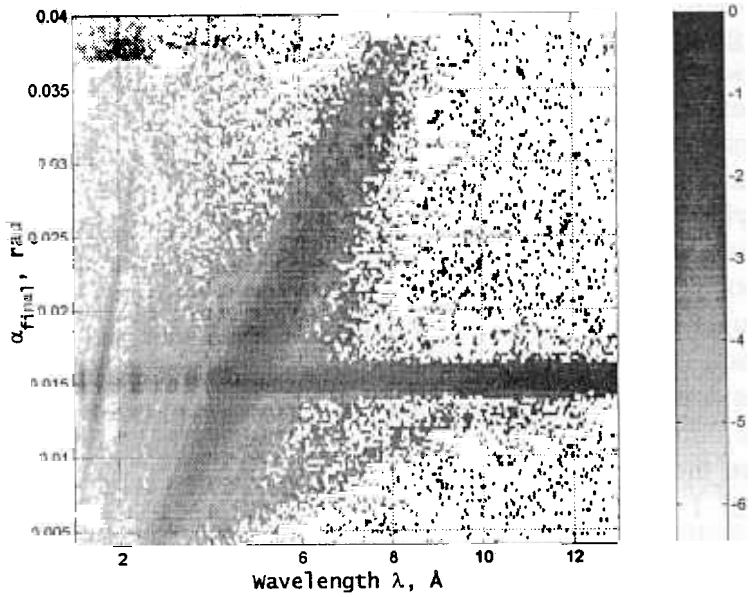

b)

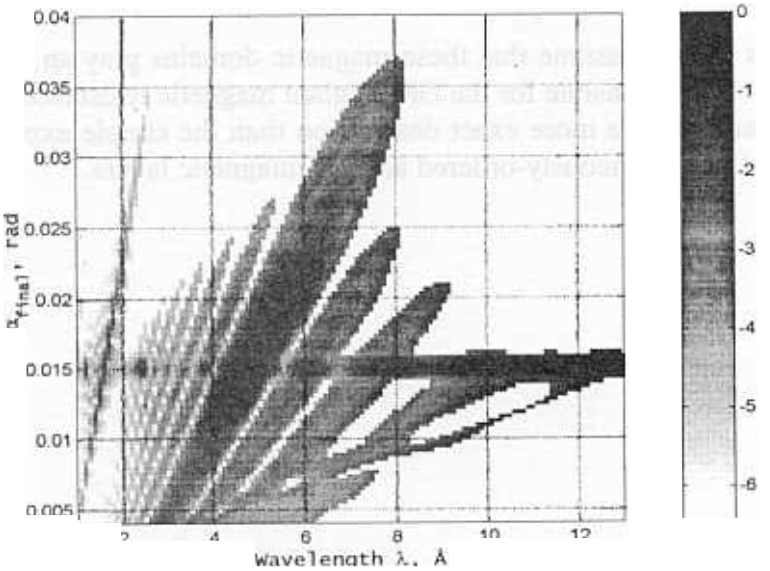

Fig.1: a) Intensity map of specular and off-specular scattered neutrons (spin-down) from the Fe/Cr multilayer at H=0.428 kG as a function of λ and α_f, the neutron wavelength and outgoing scattering angles, respectively; incident angle α_i = 15 mrad; b) result of the supermatrix calculation with the model of noncollinear domains.

A.Schreyer, J.F.Ankner, Th.Zeidler, H.Zabel, M.Schäfer, J.A.Wolf, P.Grünberg, and C.F.Majkrzak, Phs. Rev. B52 (1995)16066.

2. B.Heinrich and J.F.Cohran Adv. Phys. V42 (1993) 523.
3. T.P.Krinitsina, E.A.Kravtsov, V.V.Lauter-Passiouk, H.J.Lauter, V.V.Popov, L.N.Romashev, V.A.Tsurin, A.M.Burkhanov, V.V.Ustinov, JMMM 203 (1999) 181.
4. B.P.Toperverg, A.Rühm, W.Donner, H.Dosch, Physica B 267-268 (1999) 198.
5. V.Lauter-Pasyuk, H.J.Lauter, B.Toperverg, O.Nikonov, E. Kravtsov, M.A. Milyaev, L. Romashev, V. Ustinov, Physica B (2000), in press

COLLECTIVE DYNAMICS OF LIQUID GALLIUM STUDIED BY INELASTIC NEUTRON SCATTERING

A. Beldiman[a], M. Ion[a], Zh.A. Kozlov[b], A.G. Novikov[c], I. Padureanu[a], A. Radulescu[a] and V.V. Savostin[c]

[a]*Institute of Physics and Nuclear Engineering – Horia Hulubei, 76900, Bucharest, Romania*
[b]*Joint Institute for Nuclear Research, 141980, Dubna, Russia*
[c]*State Scientific Center – Institute of Physics and Power Engineering, 249020, Obninsk, Kaluga Region, Russia*

Atomic dynamics of liquid gallium is a matter of steady scientific interest in recent years [1 – 6]. Nevertheless some contradictions especial for abnormal liquids like gallium still exist. Gallium is the simple metal of the III-rd group in the periodic table of elements, but it exhibits several unexpected properties. One of them is the anomaly of the static structure factor $S(Q)$, known also for other elements such as Ge, Sn, Sb and Bi. The correlation between these features and dynamic properties is in a much less satisfactory state. The investigation of the short range order in liquid gallium [1] by means of neutron diffraction into the temperature range 290 – 343 K (T_m = 303 K) has shown that $S(Q)$ is a superposition of two structure factors where β-phase is present. This could explain the strange crystallisation of gallium and the physical meaning of the temperature T^* = 333 K close to Debye temperature. It was suggested that liquid gallium exhibits a kind of «memory effect», but the inelastic neutron scattering (INS) experiment [7] has shown that the dynamic properties of α-Ga do not depend on thermal history. It was also stated [4] that dynamic structure factor $S_c(Q,\omega)$ obtained from INS experiments shows sound wave peak at $\hbar\omega \approx 5 - 6$ meV and Q = 1.6 – 1.7 Å^{-1}. These collective modes could be correlated with the second structure observed on the high-Q side of $S(Q)$ main peak.

In this connection a new INS experiment was carried out at temperature 373 K aiming to get new data about the microdynamics of α-Ga. Measurements were performed with the DIN-2PI time-of-flight neutron spectrometer of the direct geometry set up at one of the neutron beams from the IBR-2 pulsed reactor (Frank Laboratory of Neutron Physics, JINR, Dubna). The incident neutron energy was 4 meV with the resolution of 4%. The wide interval of scattering angles from 6° up 134° was used within the range of Q_0 = 0.2 – 2.8 Å^{-1}. The sample container consists of twenty quartz tubes whose height is 12 cm, the inner diameter 3 mm and wall thickness 0.2 mm.

All the corrections involving the background from the empty sample holder, the attenuation factor into the sample, the detector efficiency have been applied to experimental data. As a result, the scattering function $S(Q,\omega)$ was extracted. $S(Q,\omega)$ is expressed as weighted sum:

$$S(Q,\omega) = \frac{\sigma_c}{\sigma_b} S_c(Q,\omega) + \frac{\sigma_i}{\sigma_b} S_i(Q,\omega)$$

where σ_c, σ_i σ_b stand for the coherent, incoherent and bound scattering cross section respectively. $S_i(Q,\omega)$ was evaluated from a theoretical model [8]. $S_c(Q,\omega)$ was transformed by an interpolation procedure from fixed scattering angle spectra into the representation at constant Q. The features appearing are interpreted as the evidence of the existence of propagating collective modes.

Liquid gallium is not a simple metal and quite different from alkaline metals. The calculations [9] performed with pair interaction potentials also within viscoelastic theory confirm the idea that the hardness of the repulsive part is a major factor and it depends slowly on temperature. The problem is more complicated for α-Ga at temperatures as 373 K not far from melting point where superposition of two structures exists. This feature is reflected by both the $S(Q)$ and the derived potential. Therefore both structures may have some influence on the collective excitations. Unlike molten alkali and other simple metals, the damping effect is higher for α-Ga, but the idea [3, 4] that α-Ga cannot

sustain finite-frequency excitations because of relatively high longitudinal viscosity is a questionable problem. From the analysis of $S_c(Q,\omega)$ we have build the dispersion relations (Fig. 1). The positions of the inelastic peaks plotted against corresponding Q reveal the existence of two dispersion relations which seem to be the consequence of anomalies observed in $S(Q)$ and pair interaction potential. The solid line depicts the dispersion of hydrodynamic sound velocity of 1350 m/s and the dashed line corresponds to a hydrodynamic dispersion $\omega_Q = cQ$, with c = 3300 m/s. We think that the lower frequency curve lying close to spectral moment $<\omega_0^2>^{1/2}$ is related to the main structure of the $S(Q)$ for α-Ga, while the higher frequency component is a consequence of the second structure observed in $S(Q)$, close to $<\omega_1^2>^{1/2}$. The shape and characteristic of the low frequency dispersion curve are in agreement with the results obtained in [6] from first principles molecular dynamics simulations for α-Ga at T = 702 K and 982 K. It is worth to mention here that the propagation of hypersonic waves in α-Ga was studied by Brillouin scattering of light [10]. The measured frequencies follow a hydrodynamic dispersion with an anomalous high velocity, v = 3700 m/s, which is quite near to the one derived from the high frequency dispersion curve in our results.

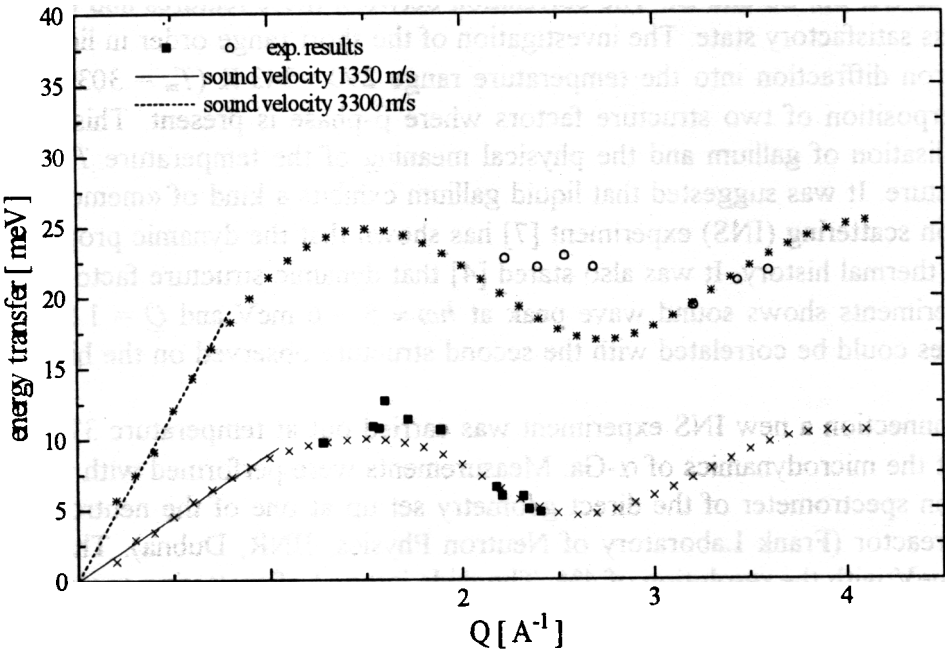

Fig. 1. The dispersion curves for α-Ga at 373 K. The empty circles and full squares represent the experimental points. The crosses and the asterisks depict $<\omega_0^2>^{1/2}$ and $<\omega_1^2>^{1/2}$.

References

1. S.N. Rapeanu and I. Padureanu, Physica Scripta T **57** (1995) 18.
2. I. Padureanu and S.N. Rapeanu, Balkan Phys. Lett. **3** (1995) 218.
3. I. Padureanu, S.N. Rapeanu, Gh. Rotarescu, I.A. Popescu, Zh.A. Kozlov and W. Voitus, Rom. J. Phys. **36** (1993) 579.
4. F.J. Bermejo, M. Garcia-Hernandez, J.L. Martinez and B. Hennion, Phys. Rev. E **49** (1994) 3133.
5. J.M. Holender, M.J. Gillan, M.C. Payne and A.D. Sympson, Phys. Rev. B **52** (1995) 967.
6. F.J. Bermejo, R. Fernandez-Perea, M. Alvarez, B. Roessli, H.E. Fischer and J. Bossy, Phys. Rev. E **56** (1997) 3358.
7. W. Luzny, S. Niziol, J. Mayer and I. Natkaniec, Phys. Stat. Sol (a) **116** (1989) K25.
8. S.W. Lovesey, J. Phys. C **6** (1973) 1856.
9. I. Padureanu, A. Beldiman and A.Radulescu, Rom. J. Phys. (in press).
10. J.G. Dill and E.M. Brody, Phys. Rev. B **14** (1976) 5218.

Some results of investigation of liquid ^{4}He dynamics.

I.V.Bogoyavlenskii, A.V.Puchkov and A.Skomorokhov

Institute of Physics and Power Engineering, 249020, Bondarenko sq.1, Obninsk, Russia

The dynamics in liquid ^{4}He at low temperatures has already been a subject of interest for many years because helium behaves in a unique way. So excitation in superfluid helium in contrast to the other "simple" liquids remain extremely sharp at wave vectors up to 3.5 Å^{-1}. Are the sharp excitations then a "signature" of the superfluid phase, connected in some way to the existence of Bose condensate in superfluid helium, or is ^{4}He just an extremely cold liquid?

The Density-Quasiparticle picture in the frame of the Field Theory and Dielectric function Formulation provides [1] a good description of the temperature dependence of neutron scattering data. In this picture, Bose condensate plays an explicit role, and the excitations at the phonon-maxon range of the dispersion curve is interpreted as a joint density/quasiparticle mode strongly coupled via the condensate. Within this description, the phonon at low Q is interpreted as a collective excitation of the Zero Sound mode (*ZS*-mode) which is not sensitive to the existence of the Bose-condensate. The sharp maxon peak is interpreted as a quasiparticle excitation of the Single Particle mode (*SP*-mode) which observed in $S(Q,\omega)$ only bellow T_λ. So the sharp maxon peak is a unique feature of the condensate and could not be observed in $S(Q,\omega)$ without one [1].

In this paper we report the results of the recent investigations [2] carried by inelastic neutron scattering to assess this relationship. Measurements were performed on the time-of-flight direct geometry DIN-2PI spectrometer at the Joint Institute for Nuclear Research in Dubna. Initial neutron energy was set about 2 meV and multi-detectors system at angle scattering range 6.3° - 71° allow us to cover Q range from 0.2 up to 1.15 Å^{-1} in one measurements. The Q-dependent resolution widths varied between 0.05 and 0.1 meV (FWHM).

The scattering function of ^{4}He was measured at eleven different temperatures in the range 0.44-2.22K at SVP. The spectra were corrected for background, detector efficiency, and interpolated from constant ϑ to constant Q. To obtain the one-phonon parameters we used simple subtraction model (SSM) [3]. The multiphonon part of $S(Q,\omega)$ was determined at lowest experimental temperature and subtracted then from experimental spectra at higher temperatures. The damped harmonic oscillator function (DHO function) was fitted to the resulting one-phonon peak taking into account the instrumental resolution.

In results we obtain data on temperature dependence of $S(Q,\omega)$ which agree in main with previous detailed study [4]. One-phonon peak is anomalously independent of temperature at the Q less than 0.3 Å^{-1}. Width of the peak slowly increases with temperature; position and intensity remain constant. We could not find any manifestations of the superfluid phase transition in the temperature dependence of the one-phonon parameters at this Q-region. At $0.3<Q<0.725$ Å^{-1} one-phonon parameters demonstrate the essential temperature dependence which is most marked at temperatures near T_λ. All one-phonon parameters have jump near T_λ. Intensity and width of peak increase smoothly with temperature up to T_λ and change set of increasing after T_λ. Position of the peak have a small dip at T=1.9 K and increases just below T_λ (see Fig.1). Changes of the one-phonon peak become more marked with Q increasing. And temperature dependence of $S(Q,\omega)$ at Q=1.15 Å^{-1} is quite different from that at the phonon region. Intensity and width of the peak increase with temperature also. Position of the peak remains constant up to 1.6 K, decreases after one and there are no indications of its rise at T_λ (see Fig.1).

We suppose that temperature dependence of peak position at $0.3<Q<0.725$ Å^{-1} with a dip bellow T_λ can be viewed as indication of strong hybridization between *ZS* and *SP* modes (If suppose that ZS energy for normal ^{4}He lies above SP energy for superfluid ^{4}He). Note, we find peculiarity in

$S(Q,\omega)$ in this Q range [5] that can be treated as indication *ZS-SP* hybridization also according prediction Glyde-Griffin model [6]. Temperature independence of one phonon peak at $Q<0.3$ Å^{-1} and its smooth dependence up to T_λ at $Q=1.15$ Å^{-1} indicate that there are no evidence *SP*-mode at $Q<0.3$ Å^{-1} and *ZS*-mode at $Q=1.15$ Å^{-1}. Wave vector range $0.3<Q<0.725$ Å^{-1} is probably a range where *SP* and *ZS* modes exist simultaneously. Note that previous detailed study of $S(Q,\omega)$ identify dip in $\omega(Q,T)$ just bellow T_λ at all $Q<1.4$ Å^{-1}, that not agree with our data completely. This disappointment may be caused by some arbitrariness of determination of the multiphonon part of $S(Q,\omega)$.

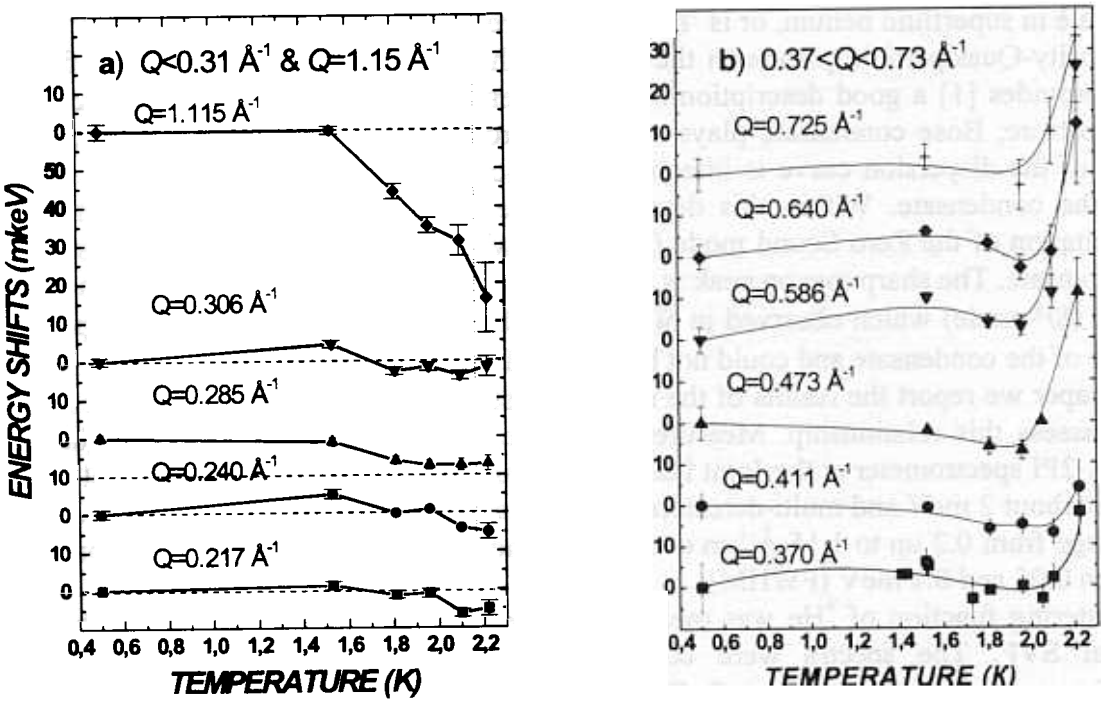

Fig.1 Energy shifts of the one-phonon peak position at SVP and various Q. Curves are simply guides to the eye.

REFERENCE

[1] H.Glyde, Journal of Low Temperature Physics, **93**(1993)862.
[2] I.V.Bogoyavlenskii, A.V.Puchkov and A.Skomorokhov, Annual report 1998, FLNP JINR, p.72
[3] A.Miller, D.Pines and P.Noziers Phys. Rev.**127**(1962)1452.
[4] K.H.Andersen, W.G.Srtiling, J.Phys. Condens Matter **6**(1994)5805.
[5] I.V.Bogoyavlenskii, A.V.Puchkov and A.Skomorokhov, Physica B, in press.
[6] A.Griffin and E.C.Svensson, Physica **B165&166**(1990)487.

Neutron spectroscopy and QC modeling of the low frequency internal vibrations of mesitylene

L. Cser[1], K. Holderna-Natkaniec[2], I. Natkaniec[3] A. Pawlukojc[3]

[1] Research Institute for Solid State Physics and Optics, H-1525, Budapest, POB 49
[2] Department of Physics, A Mickiewicz University, 61 - 614 Poznan, Poland
[3] Frank Laboratory of Neutron Physics JINR, 141980 Dubna, Russia

Mesitylene, i.e. 1,3,5-methylbenzene - $C_6H_3(CH_3)_3$ contains three methyl groups in the C_3 symmetry positions at the benzene ring. At ambient temperature this material is in liquid phase. The melting point is equal to 220.5 K. Due to the rotational freedom of methyl groups and of the high hydrogen density solid mesitylene has been proposed as an appropriate material for the cold neutron moderator [1]. Nevertheless, there is insufficient information about the dynamical behaviour of this molecule in crystal. In a simple neutron scattering experiment [2] a classification of its vibrations at different energy ranges was proposed. According to this work the spectrum around 10 meV energy transfer belongs to the CH_3 rotational an librational motion. At about 30 meV one deals with normal modes of mesitylene molecule. Above 100 meV the energy transition arises due to the C - H bending in CH_3, while highest energy transfer corresponds to the C - H streching in CH_3. In the present work the results of more detailed inelastic neutron scattering study and some results of QC modeling of vibrational spectra of mesitylene, are presented.

The IINS spectra presented in Fig. 1, were measured at temperatures 290, 100 and 18K on the NERA spectrometer [3] at the IBR-2 pulsed reactor. The spectrum at 290K is almost smooth and shows broad quasielastic wings caused by rotational and translational diffusion of molecules in liquid phase. The IINS spectrum of solid mesitylene at 100 K shows a few precursory peaks of internal vibrations of molecule and still significant quasielastic scattering caused by relatively fast reorientations of methyl groups. The quasielasic scattering is not observed at 18K. The IINS spectrum consists of broad band of the lattice vibrations and sharp peaks of the internal vibrations of molecule.

The atomic coordinates and normal modes frequencies of the isolated molecule were calculated by the AM1 semi-empirical quantum chemistry method [4] and the Hartree-Fock method using the 6 -31G basis set of the GAUSSIAN 94 program [5]. The calculated frequencies of normal modes up to 700 cm^{-1} are compared in Fig.2 with the vibrational density of states - $G(\omega)$, obtained from the IINS spectrum of mesitylene at 18K. The COSPECO program [4] based on the AM1 method allows to calculate the neutron scattering intensities of normal modes. The AM1 calculated spectrum in Fig. 2 was obtained by convolution these intensities with the resolution function of the NERA spectrometer [3]. The frequencies of normal modes calculated by the Hartree-Fock method (HF/6-31G), are presented by bars. The bars of the higher intensity correspond to the doubly degenerated modes.

Considerable deviation between the observed and calculated frequencies of methyl librations can be seen over the 20–120 cm^{-1} energy transfer range. The benzene ring deformation modes in the frequency range 150-650 cm^{-1} can be quite well approximated by the QC model calculations The discrepancies occur due to the fault of the model which can calculate only isolated molecule while the intermolecular interactions are neglected.

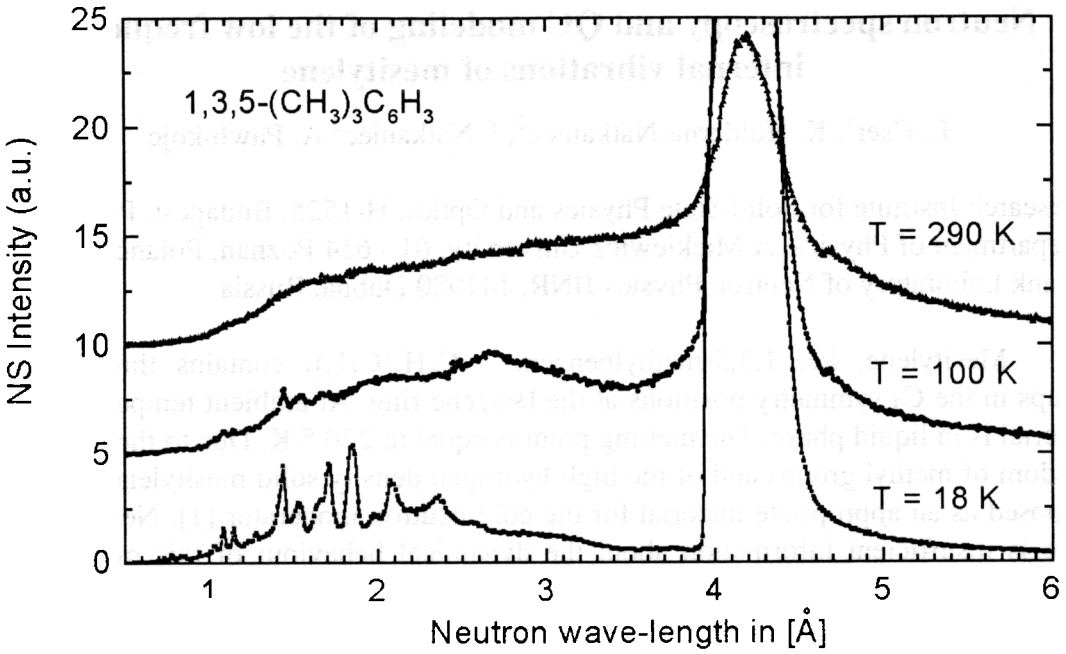

Figure The temperature dependence of the IINS spectra of liquid (T=290K) and solid (T=100 and 18K) mesitylene.

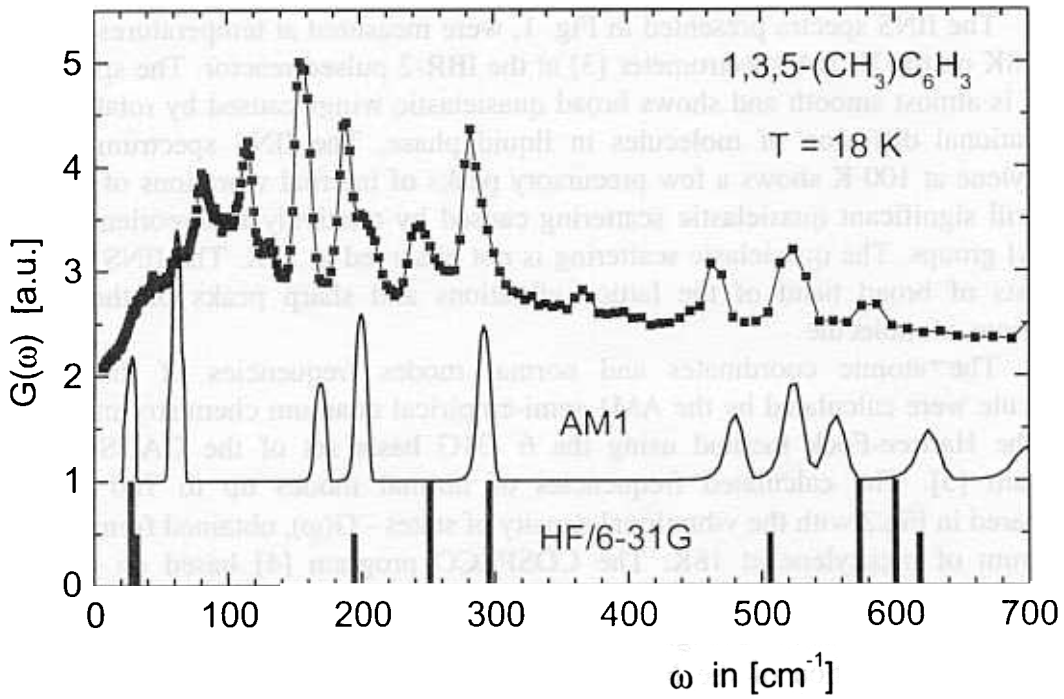

Figure 2. The comparison of the vibrational density of state G(ω) obtained from the IINS spectrum of mesitylene at 18 K with the calculated spectrum by AM1 method [4] and the frequencies of the low frequency normal modes of mesitylene molecule calculated by the HF/6-31G method [5] (bars of the higher intensity correspond to the doubly degenerated modes).

From the obtained results we can conclude that due to the presence of the methyl groups in the mesitylene molecules a number of rotational freedom is added to the lattice and internal modes. This is promising from point of view to use of solid mesitylen as a cold moderator. The QC calculations reflect many details of the molecular motions. Discrepancies between the measured and calculated spectra show the limits of this approach. It seems to be obvious to extent such investigations to other methyl-benzene compounds.

References

[1] K. Ünlü, C.Rios-Martinez and B.W. Wehring,
J.Radioanalytical and Nuclear Chemistry, 193 (1995) 145
[2] M. Utsuro, J. Phys. C: Solid state Phys., 9 (1976) L171-L175.
[3]. I. Natkaniec, S.I. Bragin, J. Brankowski, J. Mayer., in Proceedings of the ICANS XII Meeting, Abingdon 1993, RAL Report 94-025, Vol. I., p. 89-96 (1994).
[4] V.D. Khavryutchenko, COSPECO programs for vibrational spectroscopy, Institute of Surface Chemistry, Nat. Ac. Sci. of Ukraine, 252028 Kiev, Ukraine.
[5]. M.J. Frisch, G.W. Trucks, H.B. Schlegel, et all., GAUSSIAN 94, Gaussian Inc., Pittsburgh PA, 1995.

NEUTRON SPECTROSCOPY AND QUANTUM CHEMISTRY MODELING OF METHYL DYNAMICS IN 1- AND 2-METHYL-NAPHTHALENE CRYSTALS

K. Hołderna-Natkaniec[1], I. Natkaniec[2], V.D. Khavryuchenko[3]

[1]*Departament of Physics A. Mickiewicz University, 61-614 Poznań, Poland.*
[2]*Frank Laboratory of Neutron Physics, JINR, 141980 Dubna, Russia.*
[3]*Institute of Surface Chemistry, Ukrainian Academy of Science, 252028 Kiev, Ukraine.*

The CH_3 group in methylnaphthalene (MN) may be attached to the planar naphthalene rings in two different position denoted as 1 or 2 (or α, β), given compounds named as 1-MN and 2-MN (or α-MN and β-MN), respectively. The numbering of carbon atoms in naphthalene starts with the upper one in the right ring and proceed clockwise. The methyl groups in both studied materials indicate the rotational freedom. Its activation energy determined on the ground of NMR spin lattice relaxation time, was estimated as (2.4 ± 0.1) and (0.8 ± 0.1) kcal/mol in both materials, respectively.[1,2]. In present work the results of inelastic neutron scattering method was used for study a vibrational spectra as providing a link between quantum chemistry calculations and experiment. The inelastic incoherent neutron scattering (IINS) spectra were obtained at 12K on the NERA spectrometer at the IBR2 pulse reactor. After transformation (in one phonon scattering approximation) of the IINS spectra, the vibration density of states of the investigated compounds, were obtained.

On the basis of the atom coordinates and the force field matrix, the frequencies of particular modes - ωj, and their intensities in the amplitude weighted vibration density of states G(ω), were obtained by the AM1 semi-empirical quantum chemistry (QC) method. The contribution of the *n-th* atom involved in the *j-th* vibrational mode to the G(ω) spectra, were calculated as proportional to the scattering cross-section- σ_n, and the displacement – $a_{jn}(\omega_j)$. These spectra are shown in Fig's. 1 and 2 by bars, and convoluted with the resolution function of the NERA spectrometer are shown by solid lines. Disagreements between observed and calculated frequencies arise almost entirely from a free molecule approximation in the dynamical model.

It was given the various method of establishing molecular vibrational force field with their fitting, scaling and refinement procedure. New force field matrix was obtained taking into account the force field scaling factor as in naphthalene. The calculated spectra with the new fitted force field are compared with experimental ones in Fig. 1 and 2 for both studied compounds, respectively. On the grounds of presented above calculations, the assignment of internal vibration bands may be proposed.

In both studied compounds the intramolecular bands overlaps the lattice modes and naphthalene ring deformations. The bending out of plane mode χC-CH3 and methyl groups rotation indicate high amplitude and was observed at 154,192, 211 as well as at 101,119 and 146 cm^{-1} in 1-MN and 2-MN, respectively. The bending in plane modes δC-C-CH3 was observed at 263, 444 and 201,269, 293 cm^{-1} respectively in both isomeric compounds.

Literature:

1. J.U.von Schutz, H.C.Wolf, Z.Naturforch,.27a, 42 ,1972.
2. J.U. von Schutz,, F.Noack, Z.Naturforch,.27a, 645,1971.
3. I. Natkaniec, S.I. Bragin, J.Brankowski, J. Mayer, Proceeding of ICANS XII Meeting, Abington 1993, RAL Report 94-025, vol.1., p.89-96 (1994

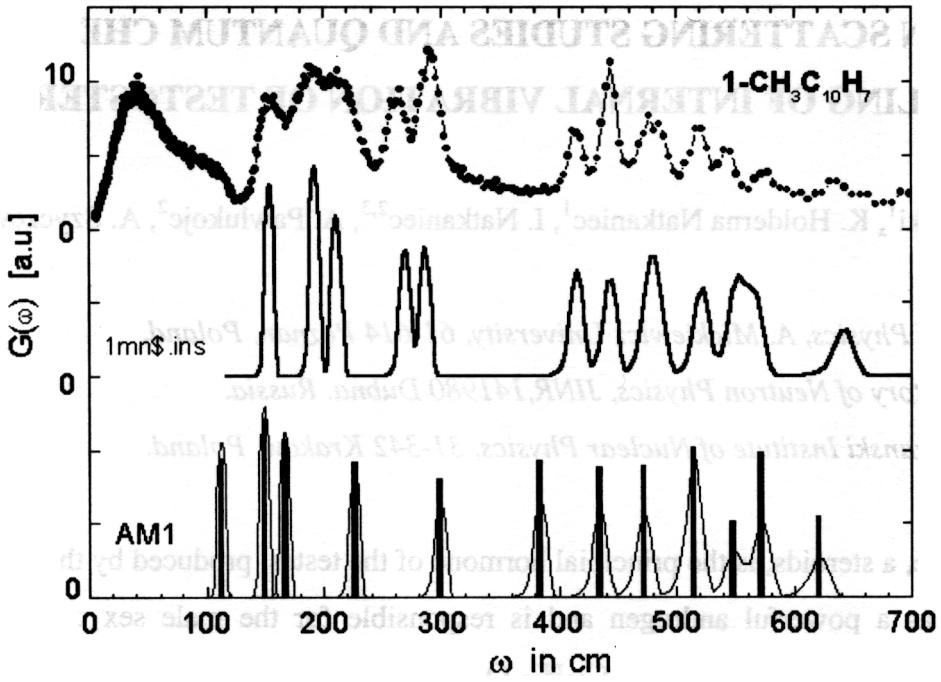

Figure 1. Phonon density of state of 1-MN versus frequency obtained experimentally from the IINS spectra at 17K, calculated by semi-empirical quantum chemistry AM1 method (bars and thin line), and after fitting the calculated frequencies to experimental ones, taking into account the force field scaling for solid naphthalene (thick solid line).

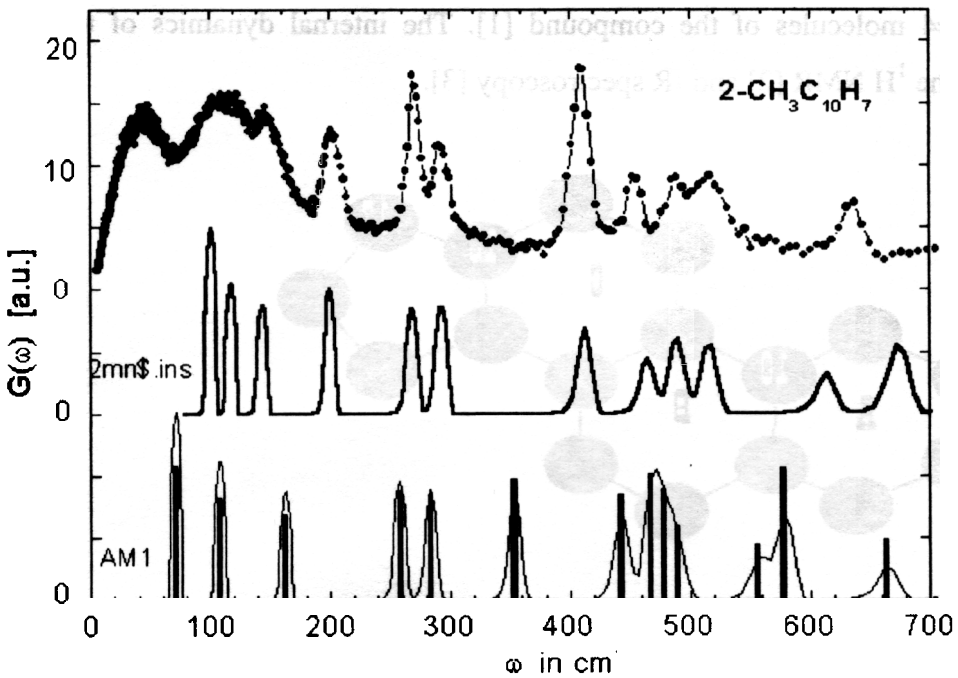

Figure 2. Phonon density of state of 2-MN versus frequency obtained experimentally from the IINS spectra at 17K, calculated by semi-empirical quantum chemistry AM1 method (bars and thin line), and after fitting the calculated frequencies to experimental ones, taking into account the force field scaling for solid naphthalene (thick solid line).

NEUTRON SCATTERING STUDIES AND QUANTUM CHEMISTRY MODELLING OF INTERNAL VIBRATION OF TESTOSTERONE

P. Klodzinski[1], K. Holderna Natkaniec[1], I. Natkaniec[2,3], A. Pawlukojc[2], A. Szyczewski[1]

[1]*Department of Physics, A. Mickiewicz University, 61-614 Poznan, Poland.*

[2]*Frank Laboratory of Neutron Physics, JINR,141980 Dubna. Russia.*

[3]*H. Niewodniczanski Institute of Nuclear Physics, 31-342 Krakow, Poland.*

Testosterone, a steroids, is the principial hormone of the testes, produced by the interstritial cells. It acts as a powerful androgen and is responsible for the male sex characteristics. Testosterone, of the chemical formula $C_{19}H_{28}O_2$, has a molecule built of sterane ring (fig.1) to which two methyl groups are bonded at the carbon atoms denoted as C10 and C13, and hydroxyl and ketone groups are bonded to the carbon atoms C17 and C3, respectively. At room temperature it crystallizes in monoclinic symmetry $P2_1$. The elementary unit cell described by the lattice constants (in A) a= 14.720(3), b=11.080(2), c=10.868(2), β= 113.34° contains Z=4 molecules of the compound [1]. The internal dynamics of testosterone was studied by the ^{1}H NMR [2] and IR spectroscopy [3].

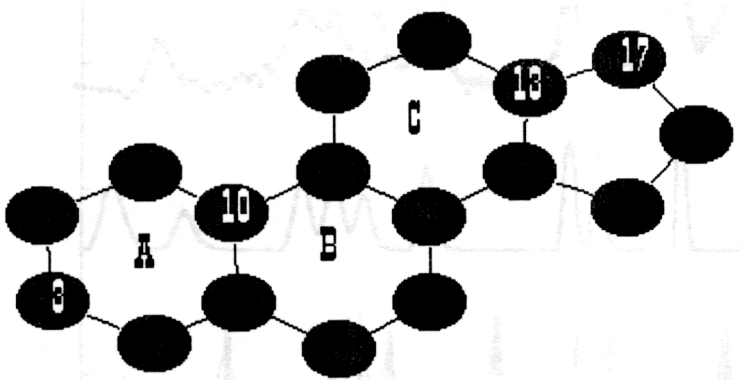

Fig.1. The sterane ring with the assumed notation of carbon atoms.

Neutron scattering experiments were performed on NERA-PR time of flight inverted geometry spectrometer at IBR-2 high-flux reactor of JINR at Dubna. The spectrometer

provides a possibility of simultaneous recording of neutron diffraction (ND) and incoherent inelastic neutron scattering (IINS) spectra. The ND spectra obtained at 20 K were recorded at the scattering angles of 68.5° and 135.0° for inter-planar distances from 2.5 to 6.5 A. The low temperature ND reflections may be indexed in the monoclinic symmetry by the least square fit method of the experimental data as a=14.40, b=10.82, c=10.61, β=110.6°. No phase transition was observed in the temperature range from 290K to 20K.

The inelastic neutron scattering spectra recorded simultaneously with ND pattern after summation over 8 detectors and subtraction of background, were transformed in one phonon scattering approximation to the amplitude weighted phonon density of state (fig.2). The energy gap between the lattice and internal modes was found. Some structure observed in the lattice band, as well as the Debye like behavior of its low frequency part i.e. $G(\omega) \sim \omega^2$ seems to be related to the ordering in low temperatures.

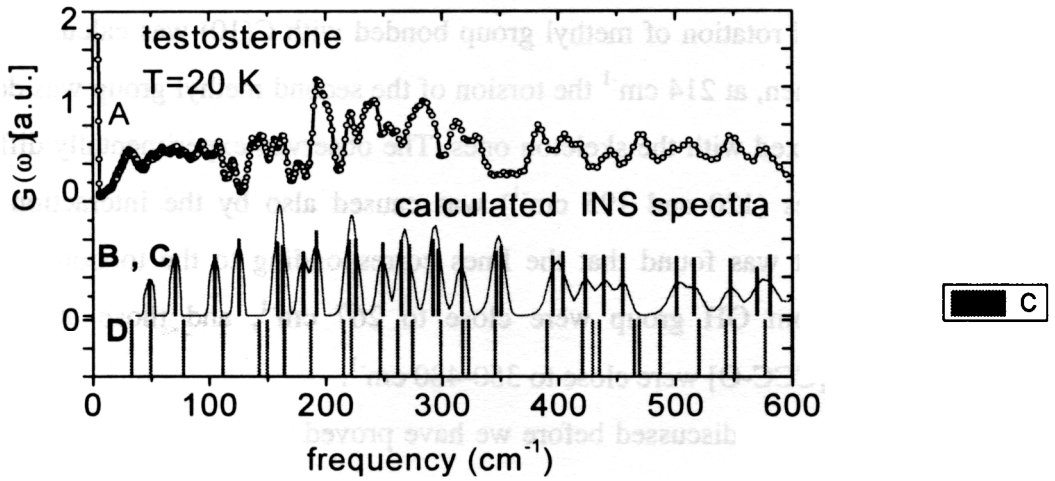

Figure 2. Phonon density of state of testosterone in one phonon scattering approximation. (details in text ,below).

In order to explain the experimental results, the calculation of the IINS spectra was performed by the semi-empirical QC AM1 method. The internal structure of an isolated molecule of testosterone was determined by this method. The force field was calculated by the QC method using different parameters proposed by Dewar in [4,5]. The intensity of normal modes of the frequency ω in the phonon density spectra, $G_n(\omega)$, was calculated as

proportional to the displacement of the *n-th* atom involved in the *j th* vibration mode a_j^n with the frequency ω and is convoluted by the spectrometers apparatus function $\delta(\omega-\omega_j)$ that provides the measurements INS intensity:

$$G_n(\omega) \sim \Sigma_j |a_j^n(\omega)|^2 \delta(\omega-\omega_j)$$

The calculated results obtained taking into regard parameters as in [4] and [5], were presented in Fig.2 by bars B and D, respectively and compare with experimental ones (curve A, fig.2). Each mode was convoluted with a broadening function that is Gaussian (exemplary presented curve C in fig.2); the line width of each Gaussian is as a resolution function of used spectrometer [6].

On the basis of the calculation results the assignment of internal modes can be proposed. In the INS spectra of testosterone the methyl torsion were observed. The methyl torsions were usually weak or inactive in optical spectroscopy, but appear strong in neutron spectroscopy. An explanation is that the three hydrogen atoms of the methyl group have the cross-section for neutron scattering of 80, so much higher then that of the other atoms in the molecule. The out of plane vibrations (symmetric or anti-symmetric) were observed in the region 170–300 cm^{-1}.As the first, the onset of rotation of methyl group bonded with C(10) was calculated at the frequency of 111 cm^{-1}. Then, at 214 cm^{-1} the torsion of the second methyl group was denoted. These vibrations were mixed with the skeleton ones. The observed experimentally difference of frequency these modes (120 and 195 cm^{-1}) was caused also by the interaction of the molecular surrounding. It was found that the lines corresponding to the torsion vibrations involving any atoms from OH group were close to 267 cm^{-1}, and those attributed to deformational modes δ [CCC-O] were close to 350-480 cm^{-1}.

On the basis of the results discussed before we have proved the different dynamics of the methyl groups.

References

[1]. P. J. Roberts, R .C. Pettersen et al., JCS Perkin II, (1973) 1978.

[2] E. R. Andrew, et al. Solid State NMR2, 57 (1993),

[3] Atlas of Steroid spectra, W. Neudert, Springer Verlag, Berlin, New York, 1965.

[4] M. J. S. Dewar et al., J.Amer.Chem.Soc.99,4,4899 ,1977,

[5] M. J .S. Dewar et al., J.Amer.Chem.Soc.107,3902-3909 (1985),

[6] I. Natkaniec et al., RAL Report 94-025, Abington 1993, vol 1.,p.89-96 (1994).

First experiments of observation of surface phonons and magnons at polarised neutron reflectometer REFLEX-P

D.A.Korneev, V.I.Bodnarchuk, V.F.Peresedov, V.V.Zhuravlev, A.F.Schebetov*, S.P.Yaradaikin

FLNP, JINR, Dubna, *PINP, Gatchina

Abstract

A new mode of the time-of-flight polarised neutron reflectometer for investigation of inelastic interaction between thermal neutrons and surface excitations via reflection by thin films is described. Using the direct inelastic method with rotating monochromator ($\Delta\lambda/\lambda=4\text{x}10^{-2}/\lambda$, $\Delta E/E=0.9\bullet10^{-2}E^{1/2}$ [λ]=Å, [E]=meV) and time-of-flight energy analysis the upper limit of the probability of thermal neutron - surface phonon inelastic collision for the Ni/Ti multilayer structure in the energy transfer region near the maximum of state density function of bulk Ni has been estimated experimentally.

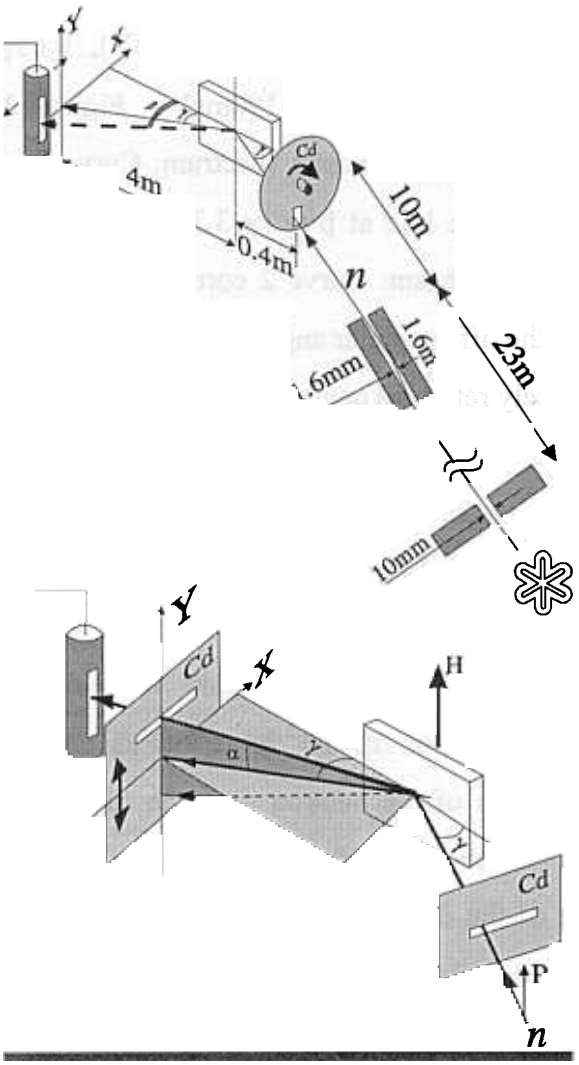

The neutron wave function damps with depth x in a medium at wave vectors k_x below the critical one: $\psi(x,y,z)\sim\exp(-x/l)\cdot\exp\{i(k_y y+k_z z)\}$, where $l=(k_c^2 - k_x^2)^{-1/2}$, k_c is the critical wave vector.

Wave vectors of surface excitations (phonons, magnons) have only surface (planar) y,z components and are also concentrated in the subsurface region. Interaction of the neutron with surface excitations must only lead to a change in k_y, k_z components of wave vector of neutron. The interaction with a surface phonon must result in a small-angle scattering. In the

Fig.1 Two ways of measuring inelastic neutron scattering on surface excitations by the reflectometer REFLEX-P: (a) The movable detector records neutrons scattered in the horizontal plane by the angle @ Two ways of measuring inelastic neutron scattering on surface excitations by the reflectometer REFLEX-P: (a) The movable detector records ne$E/E=0.9\bullet10^{-2}E^{1/2}$ ([E]=meV). The energy of scattered neutrons is analysed by the time of flight of the neutron over the distance between the sample and the detector. The best transferred energy resolution is achieved when the neutron loses energy($\beta>\gamma$). The energy gain corresponds to the region $\beta<\gamma$.

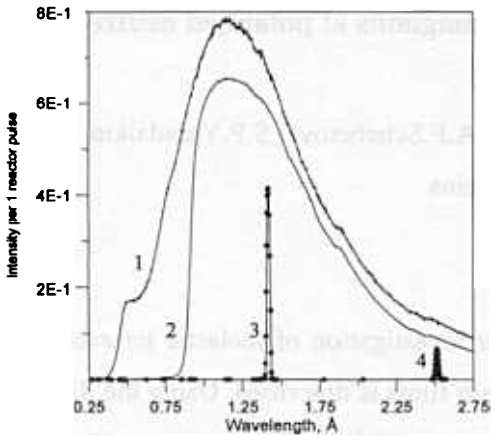

Fig.2 Neutron spectra: 1- polychromatic beam incident on mirror, 2- polychromatic beam specular reflected from mirror ($\beta=\gamma=3.3$mrd), 3,4 - specular reflected beam while the monochromator operates (various delays relative to the reactor pulse are presented).

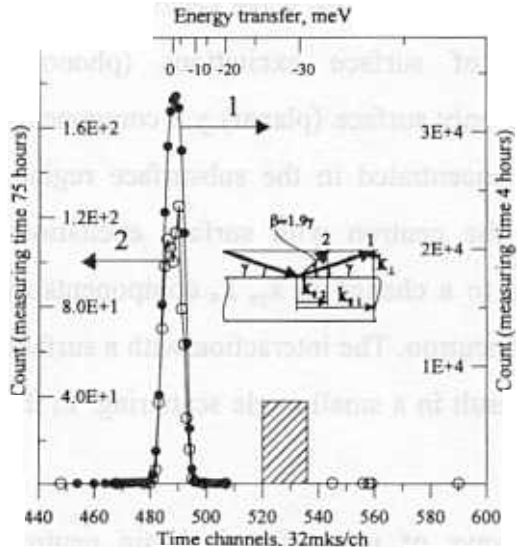

Fig.3 Curve 1 - specular beam reflected by the angle $\beta=\gamma=3.3$mrad. Curve 2 - off-specular beam reflected by the angle $\beta=1.9\gamma$ (peak on the curve 2 corresponds to the elastic diffuse scattering). The counting of the inelastic neutron in the hatched channels did not exceed the background of the setup(see the text).

case of incoherent inelastic reflection the reflected neutrons will fill the small-angle isotropic cone. The kinematics of the process is quite simple and provides a unique relation between the off-specular angle β and the energy transfer ε. A rotating monochromator is built to measure energy transfer ε at off-specular reflection (see Fig. 1). The energy ε is analysed by the time of flight of the neutron over the distance between the detector and the sample. The x coordinate and window width $\Delta x=1.4$mm of the detector unambiguously determine the expected energy $\varepsilon\pm\Delta\varepsilon$ and time $t\pm\Delta t$ regions for recording of inelastically reflected neutrons. Measurements were carried out for the off-specular angles $\beta=1.9\gamma$ ($\varepsilon\approx$-28meV), 0.65γ ($\varepsilon\approx$+20meV), and 0.25γ ($\varepsilon\approx$+190meV). Figure 3 displays the measured inelastic spectrum. Curve 1 is the monochromatic line at $\beta=\gamma$ ($\gamma=3.3$mrd), i.e. in a specular reflected beam. Curve 2 corresponds to the spectrum at the off- specular angle $\beta=1.9\gamma$. The elastic line of diffusely reflected neutrons is clearly seen. The region Δt of the expected inelastic peak is hatched. The counting in the hatched channels did not exceed the background of the setup Thus, the first results show that the inelastic process probability in the region of $\varepsilon=(28\pm3)$meV and within the vertical acceptance of detector $\Delta\beta=10^{-2}$ is as low as $1.8\cdot10^{-7}$ per one collision of the neutron with the surface of Ni, which is about 1000 times lower than the probability of the diffuse elastic process within this angle. The recalculation for $\Delta\beta=2\pi$ give us the upper estimation of the magnitude of the "inelastic" probability $< 1.1\cdot10^{-4}$ per one collision

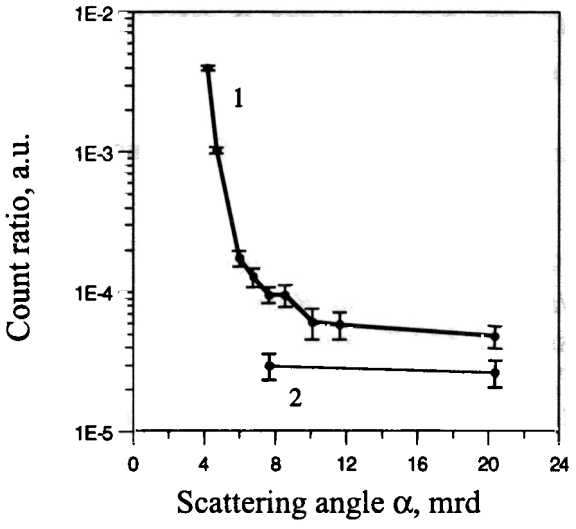

Fig. 4 1- dependence of counting of the small-angle magnetic inelastic neutron scattering on the angle α in the vertical plane (β=γ=4mrad), 2- background neutron counting when the mirror is removed from the beam. Neutrons from the spectrum region corresponding to complete external reflection are used.

The interaction of neutrons with surface magnons must lead to scattering in the vertical plane. It should be expected that neutrons inelastically reflected from the magnetic FeCo/TiZr supermirror on glass (under assumption of quadratic dispersion low of surface magnons) will concentrate within the small vertical angle $\alpha \leq \pm r$, where $r \ll 1$ is the magnon-to-neutron mass ratio. Measurements without the monochromator with polychromatic beam showed that scattering does occur and its characteristic dependence on the scattering angle α indicates inelastic reflecting of neutrons (see Fig. 4).

The work is supported by the Russian Foundation for Fundamental Research, grant № 00-02-17484.

NEUTRON SCATTERING STUDY OF THE $Cs_5H_3(SO_4)_4 \cdot 0.5H_2O$ CRYSTAL AND ITS DEUTERATED ANALOG.

S.G. Lushnikov[a], A.V.Belushkin[b], S.N.Gvasaliya[a], I.Natkaniec[b,c], L.A.Shuvalov[d], L.S.Smirnov[e] and V.V.Dolbinina[d].

[a] *A.F.Ioffe Physical Technical Institute RAS, 194021 St.Petersburg, Russia*
[b] *Frank Laboratory of Neutron Physics, JINR, 141980 Dubna, Russia*
[c] *H.Niewodniczanski Institute of Nuclear Physics, 31-342 Krakow, Poland*
[d] *Institute of Crystallography RAS, 117333 Moscow, Russia*
[e] *SSC RF Institute of Theoretical and Experimental Physics, 117259 Moscow, Russia*

The $Cs_5H_3(SO_4)_4 \cdot 0.5H_2O$ (PCTS) crystal belongs to the family of superprotonic conductors where a high protonic conductivity is due a quasi-two-dimensional dynamically disorder network of hydrogen bonds [1]. Analysis of the dynamics of the crystalline lattice of PCTS crystal reported in [2] suggests that the following sequence of phase transformations is realized: Superprotonic phase *P6/mmm* (T = 414 K) $\Leftrightarrow$ *P6$_3$/mmc* (T = 360 K) $\Leftrightarrow$ glass-like state below T_g = 260 K. Of the group of related superprotonic compounds, PCTS is now the only crystal where the glass-like state is realized with decreasing temperature (T_g = 260 K). Recent Brillouin light scattering and neutron scattering studies of $Cs_5(H,D)_3(SO_4)_4 \cdot 0.5(H,D)_2O$ (PCTS and its deuterated analog DPCTS) revealed a strong isotopic phenomenon, which results in disappearance of phase transition at T = 360 K in the deuterated crystal DPCTS[2, 3]. The goal of this work was further studies of the effect of deuteration on the structure and dynamics of the PCTS lattice at low temperatures.

Inelastic incoherent neutron scattering (IINS) and powder neutron diffraction experiments were carried out in a wide temperature range 10 - 300 K at the NERA-PR inverse geometry time-of-flight spectrometer. Powder samples of PCTS and DPCTS (two samples with different deuterium concentrations) were studied. Scattered neutron energies were measured by cooled beryllium filter and pyrographite analyzers. The elastic peak resolution was 2%. The measured IINS spectra were recalculated to the generalized density of vibrational states *G(E)* in the one-phonon incoherent approximation.

Fig.1 shows the generalized density of vibrational states *G(E)* for PCTS and DPCTS–II in the regions of transferred energies 0 – 300 cm^{-1} (Fig.1à) and 300 – 1600 cm^{-1} (Fig.1b). It is well seen that there are differences between the curves: they have the peaks at 135 and 245 cm^{-1} for PCTS which disappear on the curve G(E) for DPCTS. The consequence of deuteration is the decrease in the peak intensities which is due to a lower concentration of a strong scatterer - hydrogen atoms (the concentration of deuterium atoms estimated by the intensity decrease is $c_D \sim 60$ % for the DPCTS–II sample).

Now we turn to the discussion of neutron diffraction data for the samples studied (Fig.2). It is evident that substitution of hydrogen by deuterium noticeably affects the diffraction pattern at T = 20 K. The diffraction spectrum of DPCTS-I (with an intermediate deuterium concentration) experience only quantitative changes (in intensity) compared with the PCTS spectrum. Comparison of the diffraction spectra of PCTS and DPCTS-II shows that an increase in the deuterium concentration gives rise to several additional reflexes. The reflexes with d = 3.242, 3.110, 2.693, 2.671 Å are the most intense. The effort to describe the obtained diffraction pattern for the DPCTS-II compound in terms of space group *P63/mmc* (which corresponds to the crystal symmetry of the PCTS crystal) failed. The authors of [4] discovered that on thermal cycling a phase transition takes place in the PCTS crystal and as a result its symmetry lowers to rhombic. It can be supposed that deuteration leads to symmetry changes at low temperatures similar to those occurring in pure PCTS. Further studies are needed to understand the reasons for changes in the diffraction pattern of the

deuterated PCTS sample. However, even now we can argue that PCTS crystals exhibit the isotopic effect associated with hydrogen substitution both at high and low temperatures.

[1] Baranov A.I., Kabanov O.A., Merinov B.V. and Shuvalov L.A., Ferroelectrics **127,** 257 (1992).
[2] S.G. Lushnikov and L.A. Shuvalov Crystallography Reports **44** (1999).
[3] Lushnikov S.G., Belushkin A.V., Beskrovnyi A.I., Fedoseev A.I., Gvasaliya S.N., Shuvalov L.A.and Schmidt V.H., Sol. St. Ionics **125** (1999) 119.
[4] Merinov B.V., Melzer R., Lechner R.E., Jones D.J., Roziere J., Sol. St. Ionics **97** (1997) 161.

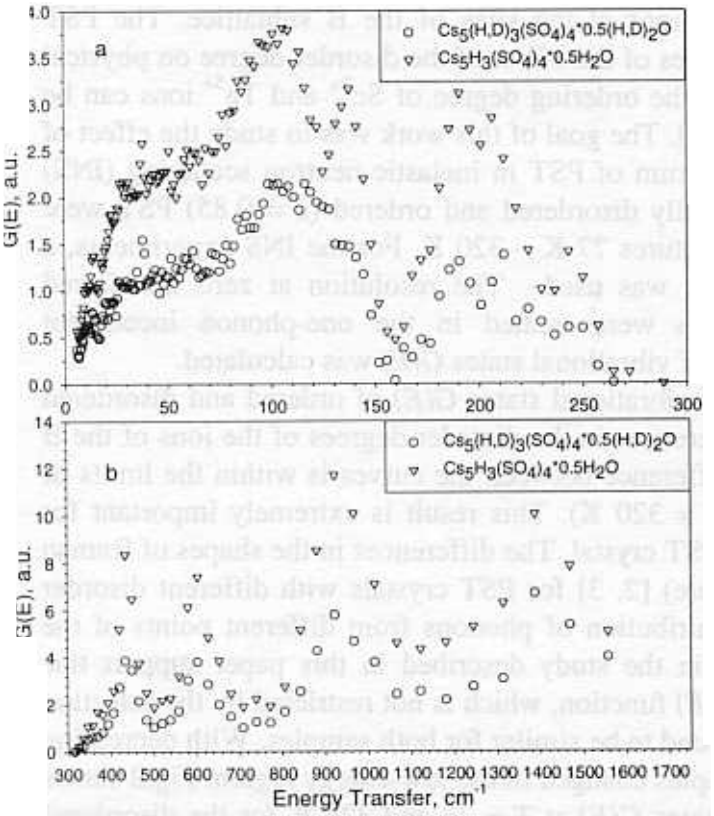

Fig.1 generalized density of vibrational states of Cs5H3(SO4)4x0.5H2O and Cs5(H,D)3(SO4)4x0.5(H,D)2O at T = 20 K.

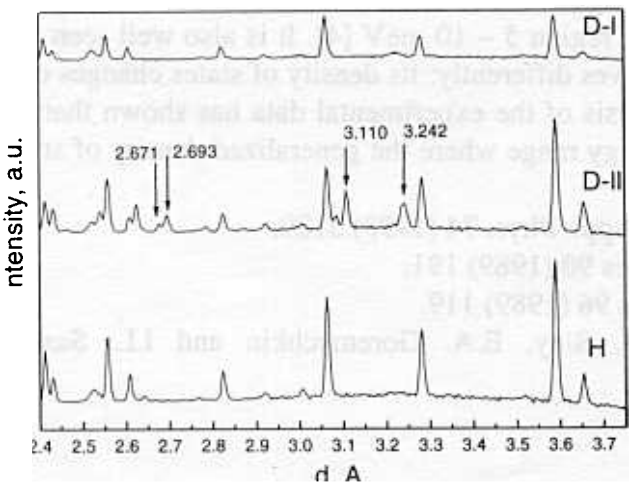

Fig.2 Diffraction spectra for all studied compounds: pure PCTS (H), sample with intermediate deuterium concentration (D-l) and with largest deuterium concentration (D-ll).

Investigation of disorder degree effect on vibrational spectra of the relaxor ferroelectrics $PbSc_{1/2}Ta_{1/2}O_3$.

S. Lushnikov[1], S. Gvasaliya[1], I.Sashin[2] and R. Blinc[3]

[1]*A.F.Ioffe Physical – Technical Institute, St. Peterburg, 194021, Russia*
[2]*Frank Laboratory of Neutron Physics, JINR, 141980, Dubna, Russia.*
[3]*Josef Stefan Institute, Lublijana, Sloveniya*

Relaxor ferroelectric $PSc_{1/2}Ta_{1/2}O_3$ (PST) belongs to perovskite-like crystals with the common formula $AB'_xB''_{1-x}O_3$, with Sc^{3+} and Ta^{5+} ions at the sites of the B sublattice. The PST compound is used as a model object in studies of the effect of the disorder degree on physical properties of relaxor ferroelectrics because the ordering degree of Sc^{3+} and Ta^{5+} ions can be changed by thermal treatment (annealing) [1]. The goal of this work was to study the effect of the disorder degree on the vibrational spectrum of PST in inelastic neutron scattering (INS) experiments. Vibrational spectra of nominally disordered and ordered (s = 0.85) PST were studied for powder PST samples at temperatures 77 K – 320 K. For the INS experiments, a KDSOG-M inverse geometry spectrometer was used. The resolution at zero transferred energy was 0.6 meV. Experimental data were treated in the one-phonon incoherent approximation and the generalized density of vibrational states *G(E)* was calculated.

Fig.1 shows the generalized density of vibrational states *G(E)* of ordered and disordered PST at T = 320 K. It is well seen that differences in the disorder degrees of the ions of the B sublattice affect *G(E)* only slightly (the difference between the curves is within the limits of experimental error which was ~ 2% at T = 320 K). This result is extremely important for understanding the lattice dynamics of the PST crystal. The differences in the shapes of Raman spectra (and also their complicated structure) [2, 3] for PST crystals with different disorder degrees was interpreted as a result of contribution of phonons from different points of the Brillouin zone [3]. The results obtained in the study described in this paper support this interpretation because the shapes of the *G(E)* function, which is not restricted by the selection rules in contrast to Raman spectra, were found to be similar for both samples. With decreasing temperature the *G(E)* function of both samples changed in the low-energy region. Fig.2 shows the low-energy region of the density of states *G(E)* at T = 77 and 320 K for the disordered (Fig.2a) and ordered (Fig.2b) PST samples. It is evident that in the region of transferred energies 6 – 10 meV a considerable change in the density of states of the disordered PST takes place. The changes in the regions 2 – 6 meV and 10 – 14 meV are small and lie within the limits of the experimental error. Therefore, the situation here is similar in many respects to the behavior of the density of states of the $PbMg_{1/3}Nb_{2/3}O_3$ (PMN) crystal in the temperature range 50 - 290 K, where *G(E)* changes in the region 5 – 10 meV [4]. It is also well seen that the *G(E)* function of the ordered sample behaves differently: its density of states changes only in the energy range 6 – 7.5 meV. Thus analysis of the experimental data has shown that the higher the disorder degree, the wider the energy range where the generalized density of states varies with temperature.

[1] F. Chu, N. Setter and A.K. Tagantsev, J. Appl. Phys. **74** (1993) 5129.
[2] I.G. Siny and T.A. Smirnova, Ferroelectrics **90** (1989) 191.
[3] I.G. Siny and C. Boulesteix, Ferroelectrics **96** (1989) 119.
[4] S.G. Lushnikov, S.N. Gvasaliya, I.G. Siny, E.A. Goremychkin and I.L. Sashin, Ferroelectrics **262** (1999).

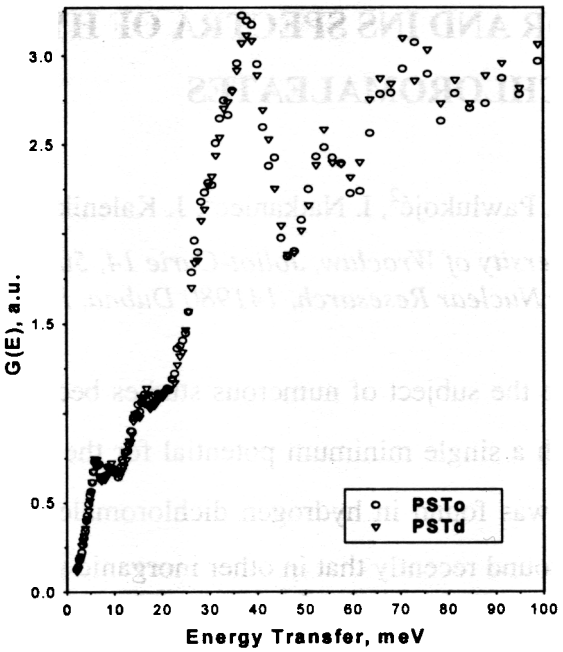

Fig.1 Generalized density of vibrational states of ordered (PSTo) and disordered (PSTd) relaxor ferroelectric PST at $T = 320$ K.

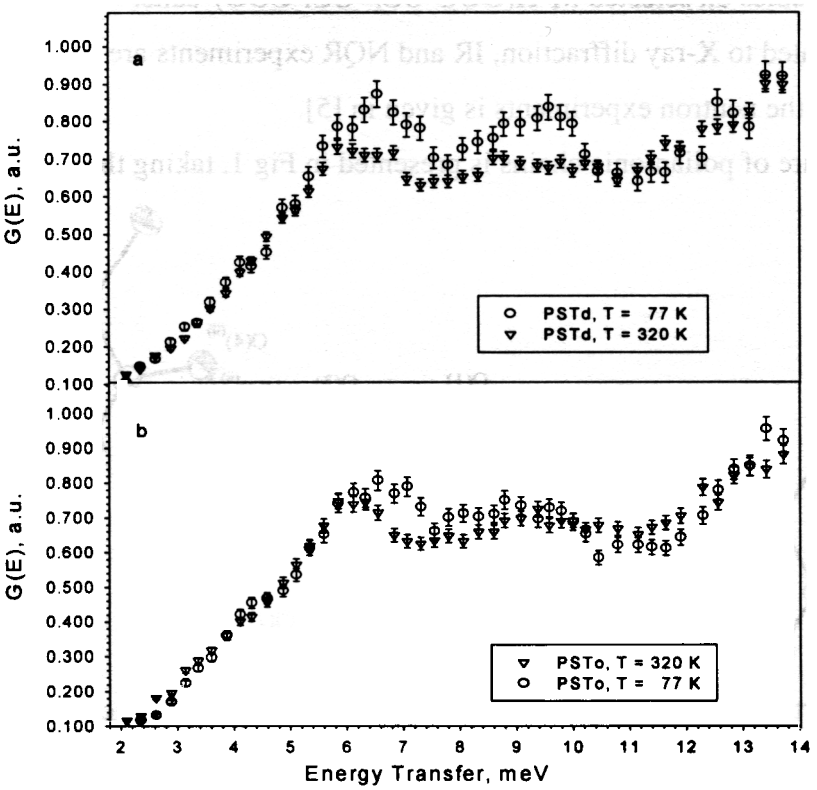

Fig.2 Density of states of disordered (2a) and ordered (2b) PST samples at T = 77 K and T = 320 K.

STRUCTURE, IR, NQR AND INS SPECTRA OF HYDROGEN DICHLOROMALEATES

I. Majerz[1,2], L. Jerzykiewicz[1], A. Pawlukojć[2], I. Natkaniec[2], J. Kalenik[1] and L. Sobczyk

1)Faculty of Chemistry University of Wrocław, Joliot-Curie 14, 50-383 Wrocław
2) Joint Institute for Nuclear Resesarch, 141980 Dubna, Russia

Hydrogen maleate anions were the subject of numerous studies because of the presence of very short OHO$^-$ hydrogen bonds with a single minimum potential for the proton motion ([and references therein). Similar situation was found in hydrogen dichloromaleate anion in the adduct with proton sponge [2]. However we found recently that in other inorganic salts infinite polyanionic chains are formed with a double minimum. In the potassium salt equal population of both minima takes place [3]. In the present raport we would like to describe preliminary results of structural and spectroscopic stududies on selected $M^+H(OOC\text{-}CCl{=}CCl\text{-}COO)^-$ salts.

Details related to X-ray diffraction, IR and NQR experiments are described in paper [4]. The information about the neutron experiments is given in [5].

The structure of polianionic chains is presented in Fig taking the potassium salt as

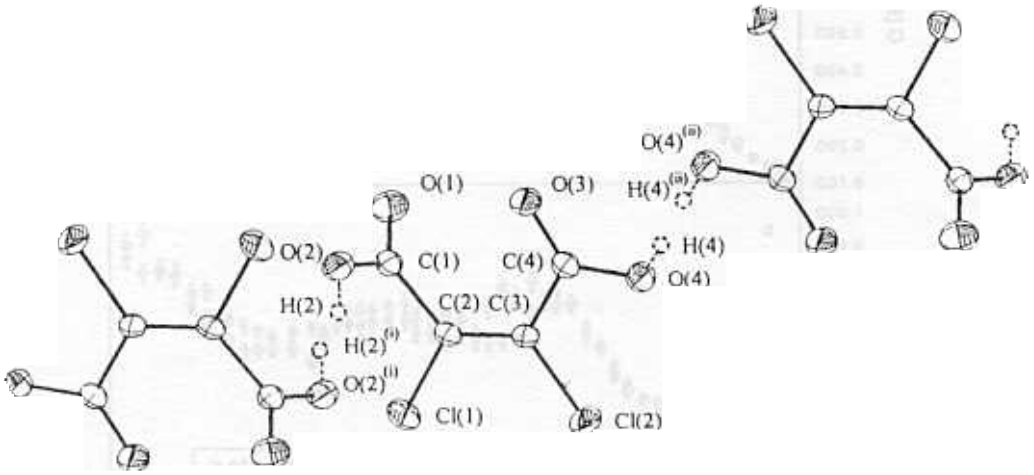

an example. Short hydrogen bonds OHO- of 2.45 **Å** are symmetric. Terminal oxygen atoms involved in hydrogen bonding are not equivalent so that the chlorine atoms Cl(1) and Cl(2) are also inequivalent what is well reflected in the NQR spectra. For the sodium salt a doublet appears with frequencies 37.384 and 38.255 MHz, for potassium salt 36.580 and 37.164, and for litium 37.407 and 38.002 MHz. In case of ammonium salt where additional differentiation due to hydrogen bonds with ammonium cation takes place one observes a quartet with frequencies 36.683, 37.142, 37.683 and 38.135 MHz. In the IR spectra one observes for all salts a highly intense broad band in the region 300 - 1600 cm^{-1} that can be treated as an evidence of double minimum hydrogen bonds with a low barrier for proton jumping.

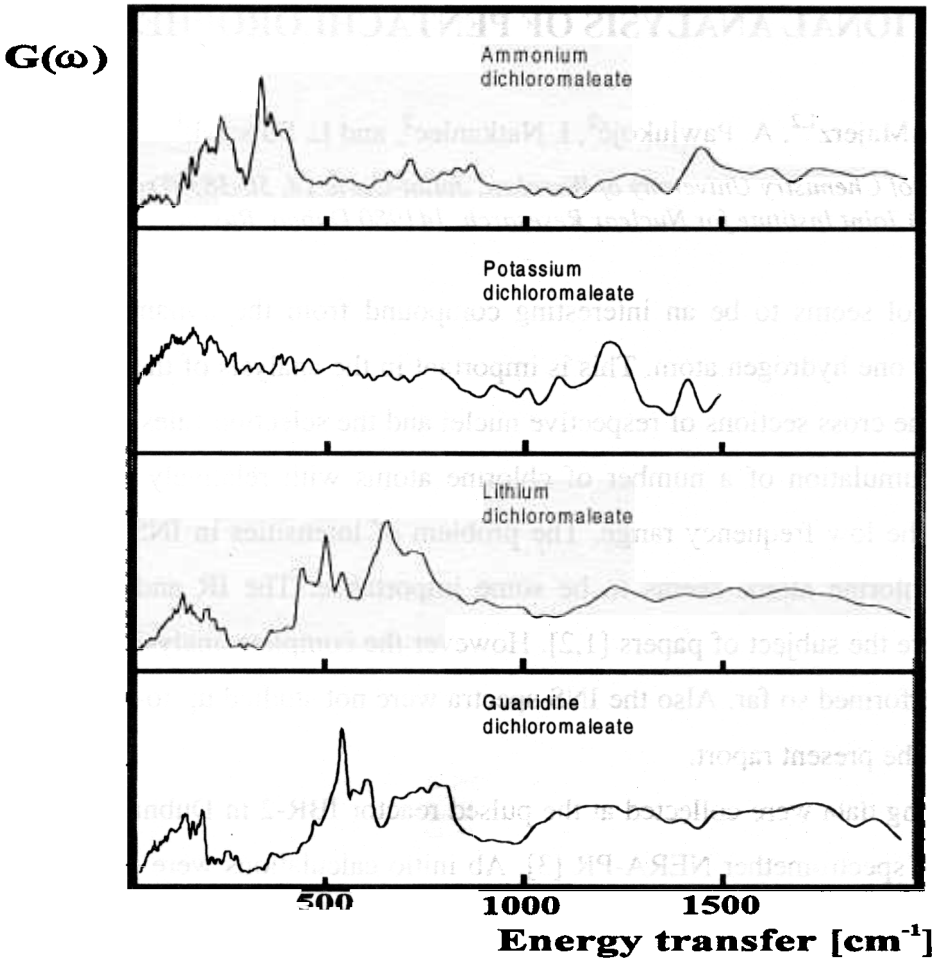

In Fig 2. there are shown INS spectra for four salts. The full analysis of these spectra at the moment is not possible without additional calculations. However on can suggest that most intense bands at low frequencies should be attributed in addition to the lattice modes to vibrations with particiaption of chlorine atoms. This relates particularly to the series of bands around 500 cm^{-1}. One should also notice dramatic differences in recorded spectra although all crystals contain similar polyanions. In the case of the potasium salt one observes strange pattern of the spectrum up to rather high frequencies that could suggest almost continuum distribution of phonons.

References.

1. F. Fillaux, N. Leygne, J. Tomkinson, A. Cousson and W. Paulus, Chem. Phys. 244 (1999) 387.

2. K. Woźniak, C.C. Wilson, K.S. Knight, W. Jones and E. Grech, Acta Cryst. B52 (1996) 691.

3. J. Baran, A. Pawlukojć, I. Majerz, Z. Malarski, L. Sobczyk and E. Grech, Spectrochim. submitted

4. I. Natkaniec, S.J. Bragin, J. Brankowski and J. Mayer, Proc. JCANS-XIII, Abingdon, 1993, RAL Report 94-025, vol. I, p. 89.

5. I. Majerz, L. Jerzykiewicz, A. Pawlukojć, I. Natkaniec, J. Kalenik and L. Sobczyk, in preparation.

VIBRATIONAL ANALYSIS OF PENTACHLOROPHENOL

I. Majerz[1,2], A. Pawlukojć[2], I. Natkaniec[2], and L. Sobczyk[1]

1)Faculty of Chemistry University of Wrocław, Joliot-Curie 14, 50-383 Wrocław
2) Joint Institute for Nuclear Resesarch, 141980 Dubna, Russia

Pentachlorophenol seems to be an interesting compound from the dynamical point of view because it contains only one hydrogen atom. This is important in the analysis of the INS spectra where a substantial role play the cross sections of respective nuclei and the selection rules are not obeyed. On the other hand the accumulation of a number of chlorine atoms with relatively large cross section should be reflected in the low frequency range. The problem of intensities in INS spectra for modes with participation of chlorine atoms seems to be some importance. The IR and Raman spectra of pentachlorophennol were the subject of papers [1,2]. However the complete analysis based on ab initio calculations was not performed so far. Also the INS spectra were not studied up-to-now. These aspects are the main subject of the present raport.

Neutron scattering data were collected at the pulsed reactor IBR-2 in Dubna using the inverted geometry time-of-flight spectromether NERA-PR [3]. Ab initio calculations were performed by using GAUSSIAN programme 94 HF/6-31G* [4].

The full vibrational analysis of pentachlorophenol will be the subject of separate paper [5] while in this report we would like to discuss the INS spectrum. It is presented in Fig. 1

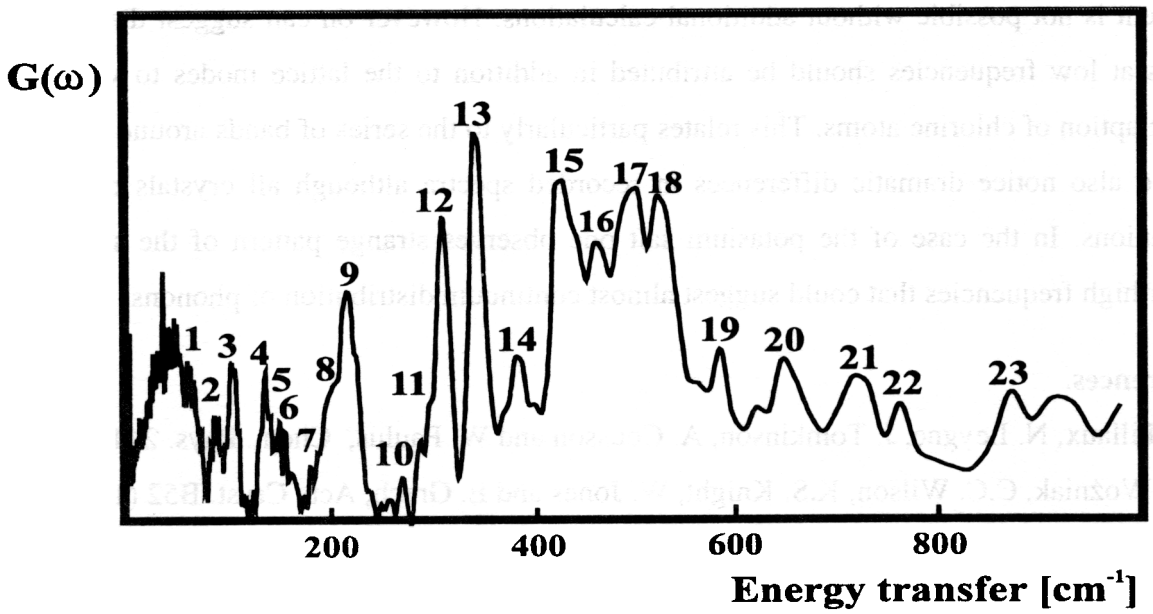

The observed frequencies (not taking into account the lattice vibration) marked from to 23 are compiled in Table with assignments based on ab initio calculations.

The comparison of data in Table 1 allows us to formulate the following conclusions. The vibrations with participation of the chlorine atoms are exposed in the spectrum with intensities comparable with those with participation of the hydrogen atom. This is well seen in the range 430 - 520 cm^{-1} which comes exclusively from the vibrations of chlorine atoms. The intensity of the components is comparable with the band at 346 cm^{-1} connected with the vibration into which the hydrogen atom is involved. We suppose that there are two reasons. Firstly as a rule participate in vibrations more than one chlorine atom that increases probability of inelastic scattering. Secondly this probability depends also on the amplitude of vibrating atoms [6] which for heavy atoms is larger than for the hydrogen atom.

In the analysis of INS spectrum of pentachlorophenol we met the problem of overtones and summation frequencies responsible for the neutron inelastic scattering. We believe that without acceptance of such scattering one can not explain the INS spectrum. It seems interesting that such overtones and summation frequencies are related to the torsional vibration of the OH group, so with participation of the hydrogen atom which, as known, is characterized by the largest cross section.

Table 1.
Frequencies observed in INS spectra and assingments

No	ν, cm^{-1}	Assignment
1	65	$C\text{-}Cl_{wagg} + OH_{tors}$ +ring def
2	90	$OH_{tors} + C\text{-}Cl_{wagg} + C\text{-}Cl_{rock}$ + ring def.
3	107	$CCl_{rock} + C\text{-}Cl_{wagg}$ + ring def.
4	138	overtones
5	152	and summation modes
6	158	of 1 and 2
7	184	
8	204	$C\text{-}O_{rock} + C\text{-}Cl_{rock}$
9	219	$C\text{-}Cl_{rock}$
10	274	summation of 8 and 1
11	290	summation of 8 and 2
12	315	$C\text{-}O_{wagg} + C\text{-}Cl_{wagg}$
13	346	$C\text{-}Cl_{wagg} + C\text{-}O_{wagg} + OH_{bend} + C\text{-}Cl_{rock}$
14	388	$C\text{-}Cl_{rock}$

15	434	$C\text{-}Cl_{stretch}$
16	468	$C\text{-}Cl_{stretch}$
17	502	$C\text{-}Cl_{stretch}$
18	527	$C\text{-}Cl_{stretch}$
19	586	summation of 17 and 2
20	652	$C\text{-}Cl_{rock} + OH_{bend}$
21	714	$C\text{-}Cl_{rock} + C\text{-}Cl_{wagg}$ + ring def.
22	764	$C\text{-}Cl_{stretch}$
23	872	$C\text{-}Cl_{stretch}$

References

[1] J.A. Faniran, Spectrochim. Acta, **35A**, 1257 (1979).

[2] J.H.S. Green, D.J. Harrison and C.P. Stockley, J. Mol. Struct., **33**, 307 (1976).

[3] I. Natkaniec, S.I. Bragin, J. Brankowski and J. Mayer, Proc. ICANS-XIII, Abingdon, 1993, R.A.L. Report 94-025, Vol.1, p. 89.

[4] Gaussian Inc., Pittsburgh, P.A., 1995.

[5] A. Pawlukojć, I. Majerz, I. Natkaniec, L. Sobczyk, in preparation

[6] J. Eckart, Spectrochim. Acta, **48A**, 271 (1992).

On diffusion of big ions in aqueous solutions

A.G.Novikov [a], M.N.Rodnikova[b], O.V.Sobolev[c].

[a]*Institute for Physics and Power Engineering, Obninsk, Russia.*
[b]*Kurnakov Institute of General and Inorganic Chemistry, Moscow, Russia*
[c]*Joint Institute for Nuclear Research, 141980 Dubna, Russia.*

In our previous inelastic neutron scattering experiments on aqueous solutions we have investigated effects of hydrophobic hydration, using as model particles tetraalkylammonium (TAA) ions Me_4N^+, Bu_4N^+ and tetraphenylphosphonium (TPP) ion Ph_4P^+[1-2]. In the course of the analysis of the experiments mentioned the main attention was paid to the dynamics of water molecules, incorporated in the hydration shells of these big ions. They contain a remarkable number of protons and contribute a sizeable portion in common neutron scattering by solutions. To separate water and ion effects supplementary experiments with heavy water solutions were performed. Now we shall use results of these experiments to infer an information concerning with the diffusion of big ions mentioned.

Due to the small contribution, introduced by water in the common neutron scattering of heavy water solutions (see fig. 4 in [1]), we can neglect with hydration effects in these solutions and consider the difference between neutron scattering by solution and water as one related to an ion:

$$S_{sol} - S_{D2O} = S_{ion} \qquad (1)$$

Then the quasielastic component of S_{ion} was extracted (detail see in [3]) and analysed in two steps. The first one was done under assumption the quasielastic scattering function to be the superposition of two Lorentzians, corresponding to the translation and rotation components of ion diffusion mobility:

$$S_{qel}^{exp}(q,\varepsilon) = \{\sum_{1,2} A_i(q)*\Delta E_i(q)/[\varepsilon^2 + \Delta E_i^2(q)]\} \oplus R(q,\varepsilon), \qquad (2)$$

where A_i and ΔE_i – are weights and halt-widths of partial curves, $R(q,\varepsilon)$ – resolution function of spectrometer, q and ε - neutron wave number and energy transfer. The results of two-Lorentzian decomposition of experimental curves according exp. (2) are presented on fig. 1. It is seen, that both components if any have similar half-widths, and neither of weights behaves like it could be expected for reorientation diffusion. This is why we have preferred the one-Lorentzian representation of experimental quasielastic scattering functions:

$$S_{qel}^{exp}(q,\varepsilon) = \{A(q)*\Delta E(q)/[\varepsilon^2 + \Delta E^2(q)]\} \oplus R(q,\varepsilon) \qquad (3)$$

The reasonable description of experimental curves by exp.(3) and straight – line q^2-dependence of intrinsic quasielastic scattering half-widths for three ions studied (fig. 2) indicate, that we deal with continuous translation diffusion, for which:

$$\Delta E(q) = 2hq^2D \qquad (4)$$

Fig. 3 gives the comparison of diffusion coefficients in heavy water at 25C° for infinite dilution, obtained from our results (fig. 2), NMR-data [4], and calculated on the basis of the conductivity (Me_4N^+ and Bu_4N^+ [5], Ph_4P^+ [6]). In the case of TAA-ions three experimental methods give similar results: the coefficients of diffusion are the smoothly falling functions of ion crystallographic radii (taken from [5]), but these radii do not coincide with the predictions of Einstein-Stokes law. TPP-

ion (crystallographic radius is taken from [7]) does not fit in with common picture and looks like more movable one compared with TAA-ions. It is not ruled out, that alkyl chains of TAA-ions fit into water structure and hinder diffusion mobility [8].

So, it can be concluded, that in heavy water the diffusion mobility of the big ions investigated obeys the continuous diffusion law without any visible evidence of reorientation.

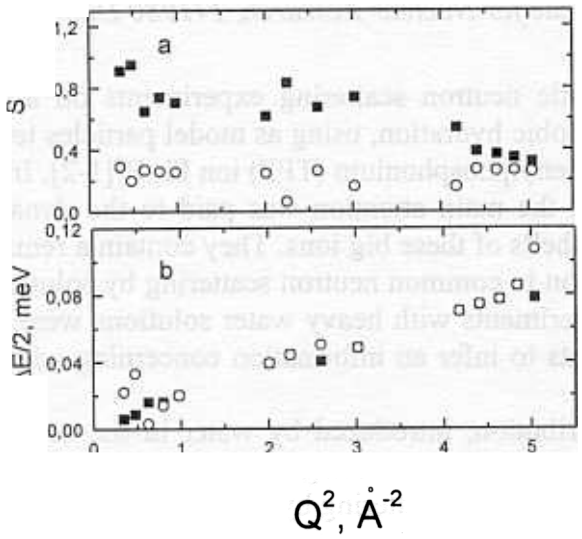

Fig. 1. The result of two-Lorentzian decomposition of quasielastic scattering functions according to exp. (2): a) intrinsic half-width of partial curves; b) weight of partial curves

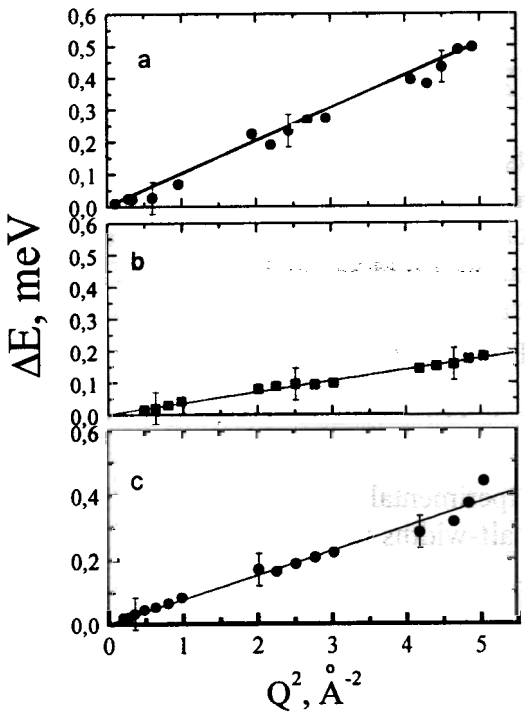

Fig. 2. Intrinsic half-width of quasielastic scattering functions for one-Lorentzian representation of experimental curves (exp. (3)): a) $\mathbf{Me_4N^+}$ ion; b) $\mathbf{Bu_4N^+}$ ion; c) $\mathbf{Ph_4P^+}$ ion.

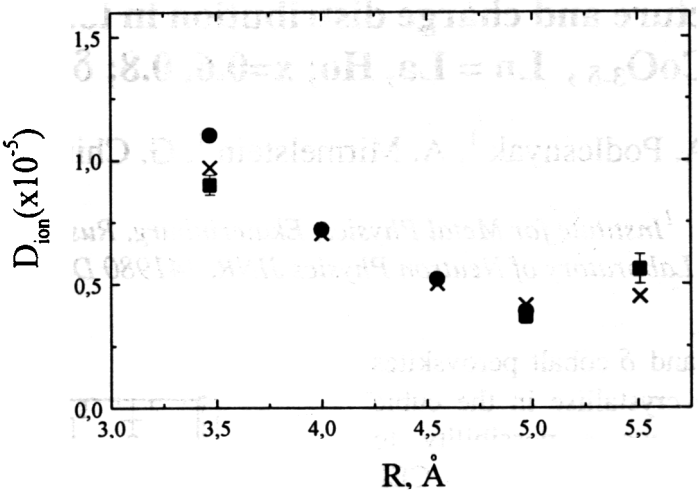

Fig. 3. The diffusion coefficients of ions as function of their crystallographic radii:
■ - this work; ● - NMR results; ✕ - conductivity results.

References

1. A. Novikov , M. Rodnikova., J. Barthel , O. Sobolev . J. Mol. Liquids. 1999, v. **79**, 203
2. A. Novikov, M. Rodnikova, O. Sobolev. Rus. J. Inorg. Chem. 1999 (in press).
3. A. Novikov, M. Rodnikova, O. Sobolev. J. Mol. Liquids. 1999, v. **82**, 83.
4. H. Hertz , B. Lindman, V. Siepe. Ber.Bunsenges. Phys.Chem. 1969, v.**73,** 542.
5. R.Kay, D.Evans. J. Phys. Chem. 1965, v. **69**, 4216.
6. M.Perie, J.Perie. J. Sol. Chem. 1989, v. **18**, 45.
7. J.Richardson, J.Ball, P.Boorman. Acta Cryst. 1986, v. C**42**, 1271.
7. B.Krumgalz. J. Chem. Soc., Faraday Trans. I, 1982, v. **78**, 437.

Local structure and charge distribution in ionic conductors $Ln_{1-x}Sr_xCoO_{3-\delta}$, Ln = La, Ho; x=0.6, 0.8; δ = 0, 0.1, 0.2.

A. Podlesnyak [1], A. Mirmelstein [1], G. Chimid [2]

[1] *Institute for Metal Physics, Ekaterinburg, Russia*
[2] *Frank Laboratory of Neutron Physics JINR, 141980 Dubna, Russia*

At certain x and δ cobalt perovskites $Ln_{1-x}Sr_xCoO_{3-\delta}$ have crystallise in the cubic structure providing thus a possibility to determine unambiguously the CEF Hamiltonian.

Inelastic neutron scattering experiments have been carried out to study the CEF interaction in the perovskite-like compounds $Ho_{0.1}Sr_{0.9}CoO_{3-\delta}$. The experiments were performed for T=10 and 50 K. The observed energy spectra at T=10 K exhibit well defined inelastic line at 3.2 meV and very broad intensities of magnetic origin around 12 and 20 meV (Fig. 1). From temperature and scattering vector dependencies one can interpret these peaks in terms of CEF transitions, since the phonon density-of-states of the non-magnetic reference compound $La_{0.6}Sr_{0.4}CoO_3$ exhibits no inelastic lines up to 30 meV (Fig. 1).

The analysis of the data involves standard techniques, which has been successfully used to interpret the observed CEF spectra in the 1-2-3 systems [1]. The 17-fold degeneracy of the ground state J-multiplet $^5I_8$ of the Ho^{3+} ions is split by cubic CEF into six levels. The values of energies of all observed and calculated ground-state transitions are given in Table 1. Estimated CEF parameters are listed in Tables 2.

Clearly more work is needed in order to check the proposed CEF Hamiltonian.

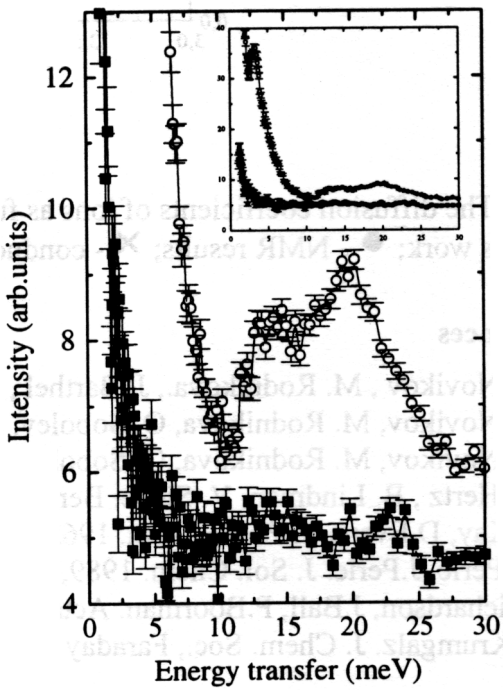

Fig. 1 Energy spectra of neutrons scattered from $Ho_{0.1}Sr_{0.9}CoO_{3-\delta}$ (opened circle), from $La_{0.6}Sr_{0.4}CoO_{3-\delta}$ (full square).

Table 1. Observed and calculated energies of Ho^{3+} in $Ho_{0.1}Sr_{0.9}CoO_{3-\delta}$, meV

Eobs	Ecalc

Table 2. CEF parameters for $Ho_{0.1}Sr_{0.9}CoO_3$, meV.

A_4^0	A_4^4	A_6^0	A_6^4

References

1. A.Podlesnyak, V.Kozhevnikov, A.Mirmelstein et al., Physica C **175**, (1991) 587.

Low-frequency collective modes in the superionic phase of lead fluoride

A.Radulescu[1], I.Padureanu[1], S.N.Rapeanu[1], A.Beldiman[1], M.Ion[1], Zh.A.Kozlov[2], V.A.Semenov

[1]*Institute of Physics and Nuclear Engineering-Horia Hulubei, Bucharest 76900, Romania*
[2]*Joint Institute of Nuclear Research, 141980 Dubna, Russia*
[3] *Institute for Physics and Power Engineering, 249020 Obninsk, Russia*

The dynamic structure factor $S(Q,\omega)$ for fluoride PbF_2 in the normal and the superionic states at T = 293 and 823 K has been investigated by cold neutron scattering [1]. A particular interest in these compounds was stimulated because some fluorite like CaF_2, $SrCl_2$, BaF_2, SrF_2, and β-PbF_2 exhibit fast-ionic conduction or "superionicity" above characteristic temperatures T_c much below the melting temperatures T_m. The ionic conductivity of these compounds increases exponentially with temperature from values smaller than 1 $\Omega^{-1}m^{-1}$, which are typical for normal ionic solids, to a value of about 100 $\Omega^{-1}m^{-1}$ comparable to those of ionic melts [2,3]. This high increase is accompanied by a fast increase in heat content, also at T_c [4,5]. It has been generally stated that the rising in the ionic conductivity and heat content are attributed to the development of a superionic phase at temperature above T_c with a thermally activated dynamic disorder in anion sublattices.

At present, according to the large volume of existing data, it seems that the conduction mechanism as well as the dynamic behaviour of anion disorder responsible for the superionic conductivity are well understood. Nevertheless, some contradictions, both in the experimental and the theoretical results exist [6].

The conduction mechanism in these materials occurs through the mobility of the ions and, at normal temperatures this is due to the anionic Frenkel disorder. It has been states that the anionic disorder must be also responsible for the conductivity in the superionic state. Both the superionic and low-temperature disorders are of the same kind but a special mechanism for the anion dynamic at high temperatures is involved. From the majority of previous studies it was concluded that a rather small fraction of anion was displaced from their regular sites, the fraction of true Frenkel defects being smaller. The high conductivity is result of the high mobility of these defects [7-10], the most important dynamic process being the diffusive motions.

Other results obtained so far contradict this general point of view. They consider that the difference between the superionic and the low-temperature disorders is one of degree, a massive disorder of the anion sublattice above T_c being assumed [11,12]. In this respect, the dynamics of the defects looks like that of the particles in a liquid where the distinction between their residence time and their flight time disappears, a sublattice melting point of view being sometimes used in association with the fast-ionic behaviour.

We consider that the fast ionic conduction mechanism via anionic diffusion defects, is not a fully elucidated problem yet. Some ion-transport mechanism [13] have not been investigated enough. A specific behaviour of the elastic constants of lead fluoride in contrast with other of fluorite has been reported when temperature is being raised above T_c [8]. In order to give some insight into the diffusion mechanism in the wave vector and energy transfer ($\mathbf{Q},\hbar\omega$) space, new investigations will be necessary. A direct proof of the diffusive mechanism in such disordered systems is provided by the investigation of the neutron quasielastic spectrum in the small energy transfers region.

Because of the insufficient investigation of PbF_2 in the range of **Q** space up to 2 $Å^{-1}$ we performed an analysis on this compound by quasielastic cold neutron scattering at the DIN-2PI time-of -flight spectrometer set up at the IBR-2 fast-pulsed reactor from JINR-Dubna. The sample of a polycristalline lead fluoride was analysed under normal and superionic state at T = 823 K. An incident neutron wave-length of 5.358 Å allowed us to perform measurements in a range of scattering vectors $0.2 = |Q| = 2.15 Å^{-1}$ with a better resolution than the previous quasielastic neutron-scattering investigations of this compound. The energy resolution $\Delta E = 0.148$ meV (full width at half maximum) was measured by means of vanadium. Thirteen batteries of He-detectors were used to detect the neutron spectra at various angles between 9°-134°.

For a fully coherent scatterer like PbF_2, the double differential cross section is related to the dynamic structure factor $S(\mathbf{Q},\omega)$ through the relation

$$\frac{d^2\sigma}{d\Omega\, dE'} = N \frac{k'}{k} \frac{1}{4\pi} \sigma_c S(\mathbf{Q},\omega) \qquad (1)$$

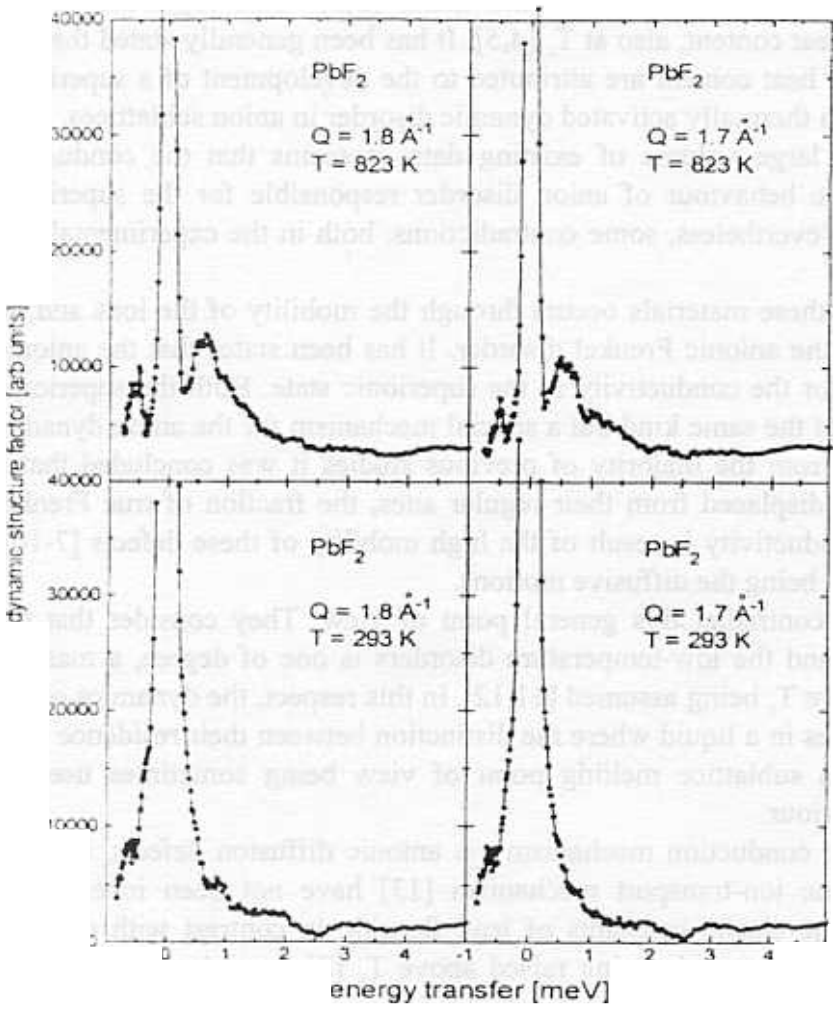

Fig. 1. Dynamic structure factor of PbF_2 at T=823 and 293 K as a function of the energy transfer for two values of Q.

were N is the number of particles in target systems, E' is the final energy of the neutrons, σ_c is the bound nucleus coherent scattering cross section and the c index denotes the coherent scattering process with $\hbar\mathbf{Q}=\hbar(\mathbf{k}-\mathbf{k}')$ the momentum transfer, and $\hbar\omega$ the energy transfer. The results obtained in uniform energy scale from the corrected time-of-flight spectra were interpolated at constant wave-vector transfer **Q** as function of energy transfer $\hbar\omega$ (Fig. 1).

In the superionic state $S(\mathbf{Q},\omega)$ at constant wave-vector transfers reveals symmetrical peaks at ~±0.5 meV in the **Q**-space range 1.55-2.05 $Å^{-1}$. This structure is similar to the long-wavelength collective excitations (Brillouin doublet) specific to some liquid metals.

Such an observation could support the idea of liquid-like behaviour at the level of the anion sublattice in the superionic state. However, the energies of these excitations are about one order of magnitude smaller and the corresponding Q values are rather high compared to those of the collective modes observed in the simple classical liquids. Therefore these excitations are of different nature from those characteristic for a classical liquid [14,15].

The results of this study lead to the conclusion that a strong correlation between the superionic transition and the low-frequency dynamics exists, raising new questions that may imply a new interest in the microscopic processes associated with the superionic transition.

References

1. A.Radulescu, I.Padureanu, S.N.Rapeanu, A.Beldiman, M.Ion, Zh.A.Kozlov, V.A.Semenov, Phys. Rev. **B5**(1999)3270.
2. C.E.Derington and M.O'Keeffe, Nature (London), Phys.Sci. **246**(1973)44.
3. V.M.Carr, A.V.Chadwik, and R.Saghafian, J. Pyis. **C11**(1978)L637.
4. C.E.Derrington, A.Navrotsky, and M.O'Keeffe, Solid State Commun. **18**(1976)47.
5. A.S.Dworkin and M.A.Bredig, J. Phys.Chem. **72**(1968)1277.
6. M.T.Hutchings, K.Clausen, M.H.Dickens, W.Hayes, J.K.Kjems, P.G.Schnabel, and C.Smith, J. Phys. **C17**(1984)3903.
7. M.J.Gillan and D.D.Richardson, J. Phys. **C13**(1979)L61.
8. C.R.A.Catlow, J.D.Comins, F.A.Germano, R.T.Harley, and W.Hayes, J. Phys. **C11**(1978)3197.
9. M.H.Dickens, W.Hayes, M.T.Hutchings, and C.Smith, J. Phys. **C12**(1979)L97.
10. M.Dixon and M.J.Gillan, J. Phys. **C11**(1978)165.
11. M.O'Keeffe, Comments Solid State Phys. **7**(1977)163.
12. A.Rahman, J. Chem. Phys. **65**(1976)4845.
13. C.R.A.Catlow, M.J.Norget and T.A.Ross, J. Phys. **C10**(1977)1627.
14. R.D.Copley and J.R.Rowe, Phys. Rev. **A9**(1974)1656.
15. I.Padureanu and S.N.Rapeanu, Rom. J. Phys. **40**(1995)1047.

HYDROGEN TRAPPING BY SOLUTE ATOMS IN NB-MO ALLOYS AS OBSERVED BY THE NEUTRON SPECTROSCOPY

V.V.Sumin,[1] G.Chimid[1],F. Mazzolai[2]

[1] -Frank Laboratory of Neutron Physics

[2] -Perugia University, Italy

The inelastic incoherent neutron scattering was measured on time-of-flight neutron spectrometer with inversed geometry KDSOG-M instelated on IBR-2 pulse reactor in Dubna, Russia. The resolution of the spectrometer is 10% for the energy transfer 100-150 meV. The Nb-Mo samples measured without and with hydrogen The difference of these spectra is a contribution of hydrogen in phonon density of state. Figure showes the hydrogen vibration in Nb-Mo(20 at.%)-H(5 at.%) solid solution at 300, 200 and 10K.

In the before studied alloy Nb-Mo(5 at.%)-H(3 at.%), hydrogen become to the hydride phase lower 150K. The hydride phase has HLM energies 116 and 165 meV (see table). We conclude from our measurement that a) Mo does not form a strong trap for hydrogen and b) hydrogen stays in usial T-site in a discripance with FIC data.

Increasing of Mo-concentration up to 20 at.% Mo- alloy the HLM energies do not change their values (table). Consiquently, hydrogen occupies the usial T-sites as for 5 at.% Mo-alloy. This is in contradiction of the FIC data also. Really the HLM energies in the octahedral site must be ca 40 and 220 meV. But we did not observed these HLM.

The temperature dependence of the HLM energies of the 20 at.% Mo- alloy differs sufficiantly from the HLM energies of the 5 at.% Mo-alloy. Indeed, the HLM energy positions are almost independ from temperature (table and figure). So we see that hydrogen does not presipitate in 20 at.% Mo- alloy. Therefore we can propose that in this alloy Mo forms a hydrogen traps and supress the hydride formation.

Table

Energies and linewidth (FWHM) (in meV) of hydrogen local modes in Nb-Mo(5at.%)-H(3at.%) and Nb-Mo(20at.%)-H(5at.%) alloys at diffrent temperatures

Nb-5%Mo-3%H				Nb-20%Mo-5%H				
T(K)	$\hbar\omega_1$	Γ_1	$\hbar\omega_2$	Γ_2	$\hbar\omega_1$	Γ_1	$\hbar\omega_2$	Γ_2
300	107±3	21	152±6	×	108±3	22	≈160	×
200	113.6±3	20	161±6	×	108±3	20	165±5	×
150	114.6±2	19	164±4	35				
100	116.7±2	18	165±4	37				
50	116.0±1.5	19	164	31				
10	116.7±1	18	164	31	107±1	17	159±2	32

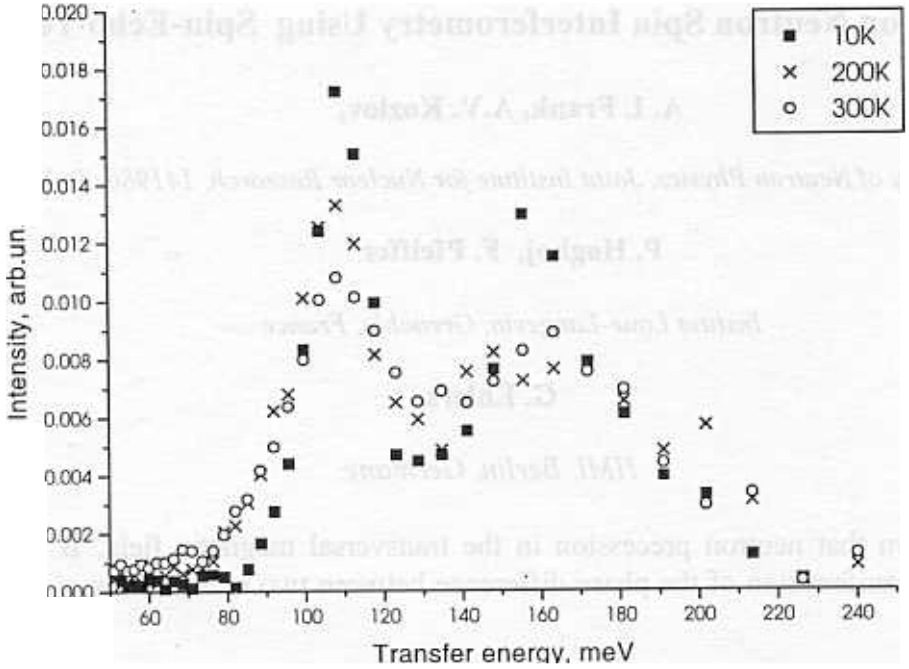

Figure. Hydrogen local modes in Nb-Mo(20 at.%)-H(5 at.%) at different temperatures

Experiments on Neutron Spin Interferometry Using Spin-Echo Technique

A. I. Frank, A.V. Kozlov,

Frank Laboratory of Neutron Physics, Joint Institute for Nuclear Research, 141980, Dubna, Russia

P. Høghøj, F. Pfeiffer

Institut Laue-Langevin, Grenoble, France

G. Ehlers

HMI, Berlin, Germany.

It is well known that neutron precession in the transversal magnetic field, **B**, may be described as the manifestation of the phase difference between two components of a spinor wave function

$$\Phi = \left(\mathbf{k}_{+} \quad \mathbf{k}_{-}\right)\mathbf{x} \quad \mathbf{k}\left[\quad \frac{\mu\mathbf{B}}{\mathbf{E}}\right)^{1/2} \quad 1+\frac{\mu\mathbf{B}}{\mathbf{E}}\right)^{1/2}\Bigg]\mathbf{x}$$

$$\mathbf{F} \cong \mathbf{k}\frac{\mu\mathbf{B}}{\mathbf{E}}\mathbf{x} = \cdot\omega_{\mathrm{L}}\frac{\mathbf{x}}{\mathbf{v}}, \qquad \omega_{\mathrm{L}} \quad \frac{2\mu\mathbf{B}}{\hbar} \tag{1}$$

where μ, **B** and **E** are neutron magnetic moment, magnetic induction and neutron energy respectively, ω_{L} is the Larmor frequency and **v** is the neutron velocity. Since two components of the spinor differ by k-numbers, the result of neutron interaction with matter is as a rule not equal phase variation of the two waves. The appearance of the extra precession angle may also be interpreted as a change of the neutron travel time, Δt, caused by the sample presence, since $\Delta\mathbf{t} = \Delta\Phi/\omega_{\mathrm{L}}$. In the simplest case of the neutron passing through the sample with thickness d and the neutron refractive index **n**, it is easy to obtain

$$\Delta\mathbf{t} \cong (1-\mathbf{n})\frac{\mathbf{d}}{\mathbf{v}}, \qquad \Delta\Phi \cong \omega_{\mathrm{L}}\frac{(\mathbf{1}-\mathbf{n})\mathbf{d}}{\mathbf{v}} \tag{2}$$

These consideration were presented in references [1] regarding to the problem of the phase contrast in neutron optics. In ref. [2] the more general case of the interaction potential was discussed. In recent works [3,4] the first experimental attempts of the observation of the extra precession angle using spin-echo technique were made.

We aimed to demonstrate with better accuracy the appearances of the additional phase precession angle when neutrons pass through the refractive sample. The experiment was done at the IN15 spin-echo spectrometer [5] of the Institute Laue-Langevin, Grenoble, France. The sample was installed inside the second precession coil of the instrument which was used together with a multi-layer monocromator. We could measure precession phases for two beams of which only one passed through the sample as it shown at the fig.1.

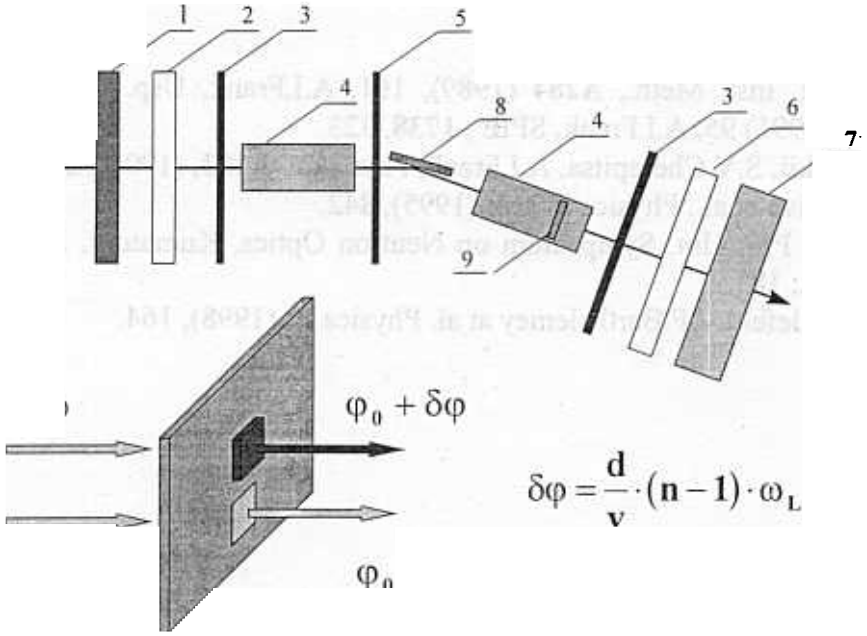

Fig.1. Scheme of the experiment. 1- velocity selector, 2- polarizer, 3- π/2 flipper, 4- precession coils, 5- π-flipper, 6- analizer, 7- position sensitive detector, 8- multi-layer monochromator, 9 - position of the diaphragm with the sample holder (shown below)

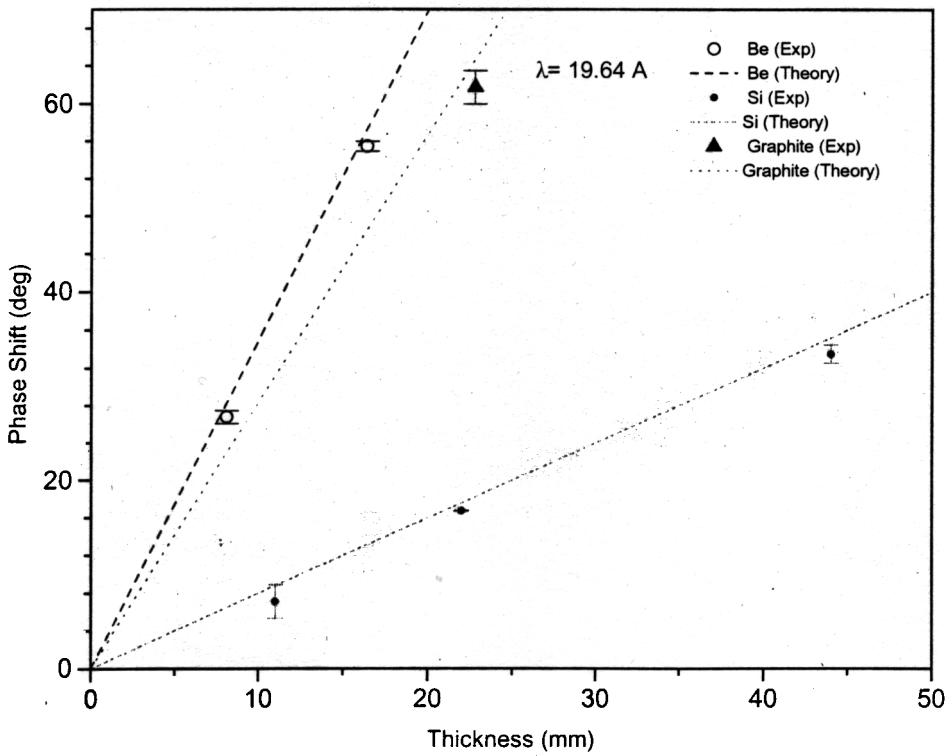

Fig.2. Measured and calculated phase precession difference between two beams.

The obtained results for the 19.6A neutrons are in an excellent agreement with theory. Similar results were obtained also with 15.5A neutrons for the Be and Si samples.

References

1. A.I.Frank, Nucl. Inst. Meth., **A284** (1989), 161, A.I.Frank, Usp. Fiz. Nauk, (Sov. Phys. Uspechy)**161** (1991) 95, A.I.Frank. SPIE , **1738**, 323.
2. V.G.Baryshevskii, S.V.Cherepitsa, A.I.Frank, Phys.Lett. **A153**, (1991), 299.
3. M.Hino, N.Achiva et.al., Physica **B 213**, (1995), 842.
4. N.Achiva et al. Proc. Int. Symposium on Neutron Optics, Kumatory. J.Phys. Soc. Jpn. **65** (1996) Suppl. A, 183.
5. P.Schleger, B.Alefeld, J.F.Barthelemey at al. Physica B, (1998), 164.

THE TECHNIQUE FOR SIMULTANEOUS ESTIMATION OF THE LEVEL DENSITY AND RADIATIVE STRENGTH FUNCTIONS OF DIPOLE TRANSITIONS AT $E_{ex} \leq B_n - 0.5$ MeV

V.A. Khitrov, A.M.Sukhovoj, E.V.Vasilieva
FLNP, JINR

Up to now the detailed and reliable information on the level density in a given J^π interval and mean probability of populating/depopulating them γ-transitions in heavy ($A > 100$) non-spherical nuclei is very pure. These parameters cannot be determined by means of traditional methods of nuclear spectroscopy from the measured spectra of γ-rays from (n_{th}, γ) reaction (or from other reactions) due to insufficient resolution of Ge detectors. The situation changed after obtaining a numerous data on the intensity distributions of the two-step cascades proceeding between the compound state and a given low-lying level. The data treatment software which allows one to derive original information from $\gamma - \gamma$ coincidences accumulated in this experiment was developed at FLNP JINR [1,2].

Using the algorithms [3,4] for analysis of $\gamma - \gamma$ coincidences registered by ordinary Ge detectors one can determine intensity distribution of cascades as a function of the excitation energy of cascade intermediate levels in the all energy region almost up to $E_{ex} \simeq B_n$ with an acceptable error which decreases as increasing an efficiency of γ-spectrometer. The measured intensity $I_{\gamma\gamma}$ of cascades is related to the unknown number of intermediate levels $n_{\lambda i} = \rho \times \Delta E$ and unknown widths of primary and secondary transitions by the relation

$$I_{\gamma\gamma} = \sum_{J,\pi} \frac{\Gamma_{\lambda i}}{\Gamma_\lambda} n_{\lambda i} \frac{\Gamma_{if}}{\Gamma_i} = \sum_{J,\pi} \frac{\Gamma_{\lambda i}}{< \Gamma_{\lambda i} > m_{\lambda i}} n_{\lambda i} \frac{\Gamma_{if}}{< \Gamma_{if} > m_{if}} \qquad (1)$$

The optimal width of interval ΔE and number N of such intervals in eq.(1) are determined by statistics of experimental data (as square of detector efficiency). A width of ΔE does not exceed 0.5 MeV even in the case of 10% efficiency detector, however. The total radiative widths Γ_λ of the capturing states are also known from corresponding experiments for all stable nuclei. The parameters $< \Gamma_{\lambda i} >$ and $m_{\lambda i}$ of the cascade γ-decay which must be found in analysis are related with the total width

$$\Gamma_\lambda = \sum_i < \Gamma_{\lambda i} > \times m_{\lambda i} \qquad (2)$$

It is clear that $N + 1$ equations (1) and (2) together with $6N$ conditions $\rho(\pi = +) > 0$, $\rho(\pi = -) > 0$, $\Gamma(E1) > 0$, and $\Gamma(M1) > 0$ restrict the interval of possible values for level density and radiative widths. This interval can be estimated with the use of two simple enough assumptions:

(a) energy dependence of level density with different J^π is determined by known and, in principle, equal for different models function;

(b) energy dependence (but not the absolute value) of widths of primary and secondary transitions is the same.

A large enough value of N, nonlinearity of eqs.(1) and (2) stipulate a choice of the way to solve the system of equations and inequalities - the Monte Carlo method. The simplest iterative algorithm was used for this aim: we set some initial values for $\Gamma(E1)$, $\Gamma(M1)$, and ρ and then distort them by means of random functions.

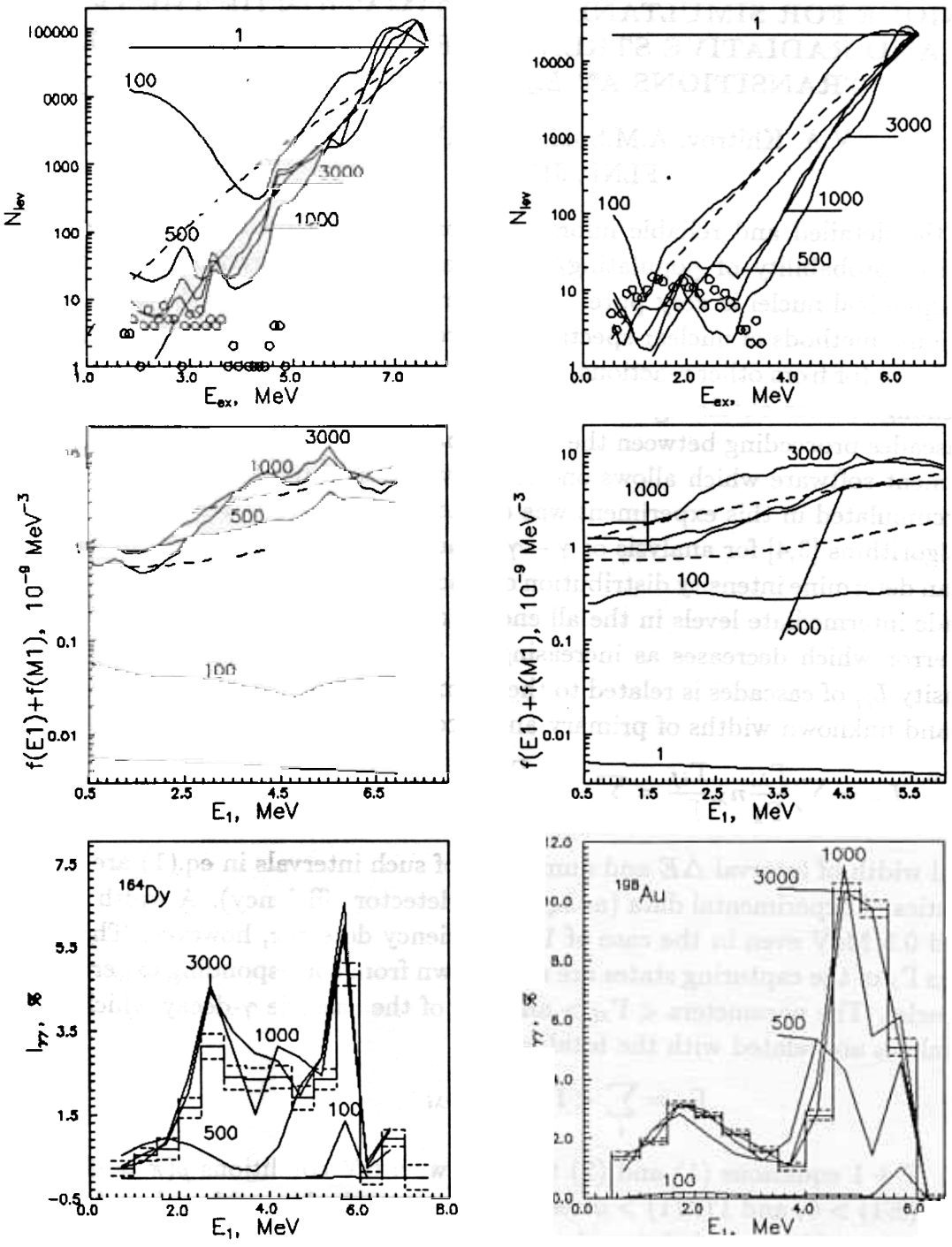

Fig. 1. The examples of the ρ and RSFs intermediate values and corresponding distributions of cascade intensities for the ^{164}Dy even-even and ^{198}Au odd-odd nuclei. Letters next to the lines mean number of iterations. Dashed curves represent predictions of the level density models [5,6] and strength function models [7,8]. Histograms show experimental cascade intensity.

If at this step of iterative procedure these distortions decrease the parameters $\Delta_1 = (I^{exp}_{\gamma\gamma} - I^{cal}_{\gamma\gamma})^2$ and $\Delta_2 = (\Gamma^{exp}_{\lambda} - \Gamma^{cal}_{\lambda})^2$ then these distorted values are used as initial parameters for the next iteration. An agreement between the experimental and calculated

cascade intensities and total radiative widths, respectively, is usually achieved after several thousands of iterations. As a result we get two random ensembles for level densities and partial widths for each of N energy intervals.

The numerous repetition of iterative calculation with different initial parameters (including obviously unreal values of Γ and ρ) for ~30 nuclei from the mass region $114 \leq A \leq 200$ showed that this algorithm gives rather narrow intervals of values for the sum level density of both parities and sum partial widths of $E1$ and $M1$ transitions. These data allow estimation of the sum radiative strength functions for $E1$ and $M1$ transitions using the following relation:

$$f = \Gamma_{\lambda i}/(E_\gamma^3 \times A^{2/3} \times D_\lambda) \tag{3}$$

The examples of intermediate results obtained within iteraive procedure for two nuclei are shown in Fig. 1. Analysis of the obtained results shows that they should be considered as probable enough estimations of level densities excited by dipole primary transitions after thermal neutron capture and radiative strength functions of these transitions. It should be noted here that no model ideas are required in this technique. Of course, the use of the reliable information on the nucleus under study decreases uncertainties of the analysis. There can be the data on energies and types of decay of known low-lying levels, mean spacings between neutron resonances, and ratio between partial widths of high-energy primary $E1$ and $M1$ transitions (although influence of two last parameters is very week).

The most critical point of the described technique is an assumption about equal energy dependence for strength functions of primary and secondary transitions. However, the assumption can be checked experimentally. This requires to measure in experiment and reproduce in calculation the intensities of two-step cascades for the maximum wide energy interval of their final level. Corresponding experiment can be realized using multidetector compton-suppressed spectrometer.

1. S.T. Boneva, E.V. Vasilieva, Yu.P. Popov, A.M. Sukhovoj,V.A. Khitrov, Sov. J. Part. Nucl. **22(2)** (1991) 232
2. S.T. Boneva et al., Sov. J. Part. Nucl. **22(6)** (1991) 698
3. Yu.P. Popov, A.M. Sukhovoj, V.A. Khitrov, Yu.S. Yazvitsky, Izv. AN SSSR, Ser. Fiz. **48** (1984) 1830
4. S.T. Boneva, V.A. Khitrov, A.M. Sukhovoj, A.V. Vojnov, Z. Phys.- A **338** (1991) 319
   S.T. Boneva, V.A. Khitrov, A.M. Sukhovoj, A.V. Vojnov, Nucl.Phys. **A589** (1995) 293
5. P. Axel, Phys. Rev. **V.126** (1962) 671
6. S.G. Kadmenskij, V.P. Markushev, W.I. Furman, Sov.J. Nucl. Phys. **V.37** (1983) 165
7. W. Dilg W. et. al., Nucl. Phys. 1973. **A217** (1973) 269
8. A.V. Ignatyuk A.V., in Proc. of IAEA Consultants meeting on the use of nulear theory and neutron nuclear data evaluation (Trieste, 1975): IAEA-190, 1976 V.1. P.211.

EXPERIMENTAL INDICATIONS OF THE PROBABLE ABRUPT CHANGE IN NUCLEAR PROPERTIES OF HEAVY NUCLEUS AT $E_{ex} \simeq 0.5B_n$

V.A. Khitrov, A.M.Sukhovoj, E.V:Vasilieva
FLNP, JINR

The cascades of two successive γ-transitions in group of nuclei from the mass region $114 \leq A \leq 200$ were studied in the framework of the program of studying nuclei with high density at FLNP JINR. Some part of the data was obtained in Riga and Rez. The observed cascades proceed between the compound state which is excited after thermal neutron capture and a group of low-lying levels. Selection of such cascades from a mass of $\gamma - \gamma$ coincidences and their analysis provided original information on nuclear properties in the excitation energy range where spacings between the levels are many times less than energy resolution of the used spectrometer.

Intensity of such cascades integrated over some interval of their intermediate levels depends on partial widths of cascade γ-transitions and number of nuclear states with $0 < E_{ex} < B_n$. A comparison between the experimental and model calculated cascade intensities shows [1] that theoretical notions of peculiarities of nuclear matter below B_n should be considerably modified. Energy dependences of level density with a given J^π and partial widths of cascade γ-transitions are the very suitable data for a comparison with the theory. The method [2,3] is developed to select the corresponding data from the cascade intensity distributions [4] built in function of the energy of the cascade intermediate levels. The results were obtained for more than 30 nuclei from the mentioned mass region.

The used data treatment software [2,3] allows one to get reliable information on the sum level density $\rho(\pi = -) + \rho(\pi = +)$ excited by $E1$ and $M1$ primary transitions and sum of their radiative strength functions $f(E1) + f(M1)$. Uncertainties of $\rho(\pi = -)$ and $\rho(\pi = +)$ as well as $f(E1)$ and $f(M1)$ separately are noticeably larger than those for corresponding sum values. It should be noted that the technique [2,3] does not use model ideas of process under study (except the shape of spin dependence of level density) and is very sensitive to minimum density of excited states. There are two most considerable differences of our technique [2,3] from known methods [5] to derive level density from the spectra obtained in the neutron induced nuclear reactions. Also, there were no methods up to now which determined strength functions for primary transitions populating the levels of heavy enough nuclei at the energy of some MeV.

The main result of the analysis [2,3] that both traditional and modern enough ideas of a nucleus at excitations from 1-3 MeV to B_n need serious corrections. Discrepancy between the level density observed by us in the (n_{th}, γ) reaction (at least in the case of the two-step cascades) and predictions of the Fermi-gas level density model which considers nucleus as a system of noninteracting fermions testifies to considerable role of phonon excitations in the wave functions of the observed states. (We do not introduce some new ideas of nuclear matter even for qualitative explanation of our results but use simple known notions). The more modern models like the generalized model of the superfluid nucleus [6,7] provides better agreement with the experimental level density, however even in this case discrepancy exceeds experimental uncertainties.

A comparison between the results [2,3] and model calculations allowed one more essential conclusion: energy dependence of level density at $E_{ex} \simeq 3-4$ MeV exhibits more or less clearly expressed "step" (see Fig. 1.). The conclusion is in complete agreement with the results [8] of approximation of random fluctuations of the cascade intensities relative to their mean value which provided estimation of the total number of levels which can be excited in the (n_{th}, γ) reaction below 3-4 MeV.

Complete explanation of the observed [2,8] effect is possible only in the framework of the strong nuclear model which reproduces experimental level density with experimental precision. However, the most probable qualitative explanation can be suggested under assumption that the thermodynamical function — specific heat of nuclear matter in the total energy region of excitation where the second order phase transition can affect nuclear properties — has the same functional dependence on energy as that which is known for a mixture of superfluid ^3He and ^4He. A well known fact of increase in specific heat of quantum liquid in the region of the second order phase transition can signify decrease in nuclear temperature and, as consequence, level density of fermion-type at certain nuclear energy. Because energy dependence of level density is exponential for both fermions and bosons then the presence of "step" requires one to postulate that at the excitation energy of several MeV in heavy nucleus the number of phonons is noticeably less than the number of quasiparticles but energy of bosons considerably exceeds energy of fermions. Such assumption follows from proportionality of the parameter a (which determines level density) to the number of excited quasiparticles or phonons. I. e., adiabatic principle – one of the basic principle of the generalized model of the superfluid nucleus – is not fulfilled. The BCS-theory [9] predicts the transition of Fermi-liquid to Fermi-gas at temperature

$$T_c \quad \frac{\delta}{1.76}, \tag{1}$$

what is approximately two times higher than the point of abrupt change in level density in our experiment. This fact can be easily explained if one take into account a decrease in temperature of phase transition in mixture of liquid ^3He and ^4He as compared with pure ^4He. Probably, more correct variant of the model of the superfluid nucleus must take into account this temperature shift, i. e., consider nucleus as a mixture of boson and fermion excitations in the wide energy interval.

The presence of phonon excitations strongly affecting nuclear properties appears as two more effects observed when studying two-step cascades:

(a) approximate harmonicity in the excitation spectra of intermediate levels (or their groups) of most intense cascades:

(b) noticeable increase in strength functions (i. e., intensities of cascade transitions) as compared with the model [10] which considers nucleus as a drop of Fermi-liquid. The estimated from the experiment and calculated according to conventional models strength functions are shown in Fig. 2. As can be seen from figure, the maximum values of the sum strength functions of $E1$ and $M1$ transitions are observed at $\sim B_n$, i. e., they conform to the energy of "step" in our level density.

So, the analysis of totality of experimental data on the two-step cascades leads to conclusion about probability of abrupt enough change in nuclear properties at $E_{ex} \simeq 3-5$ MeV and necessity of serious correction of corresponding nuclear models.

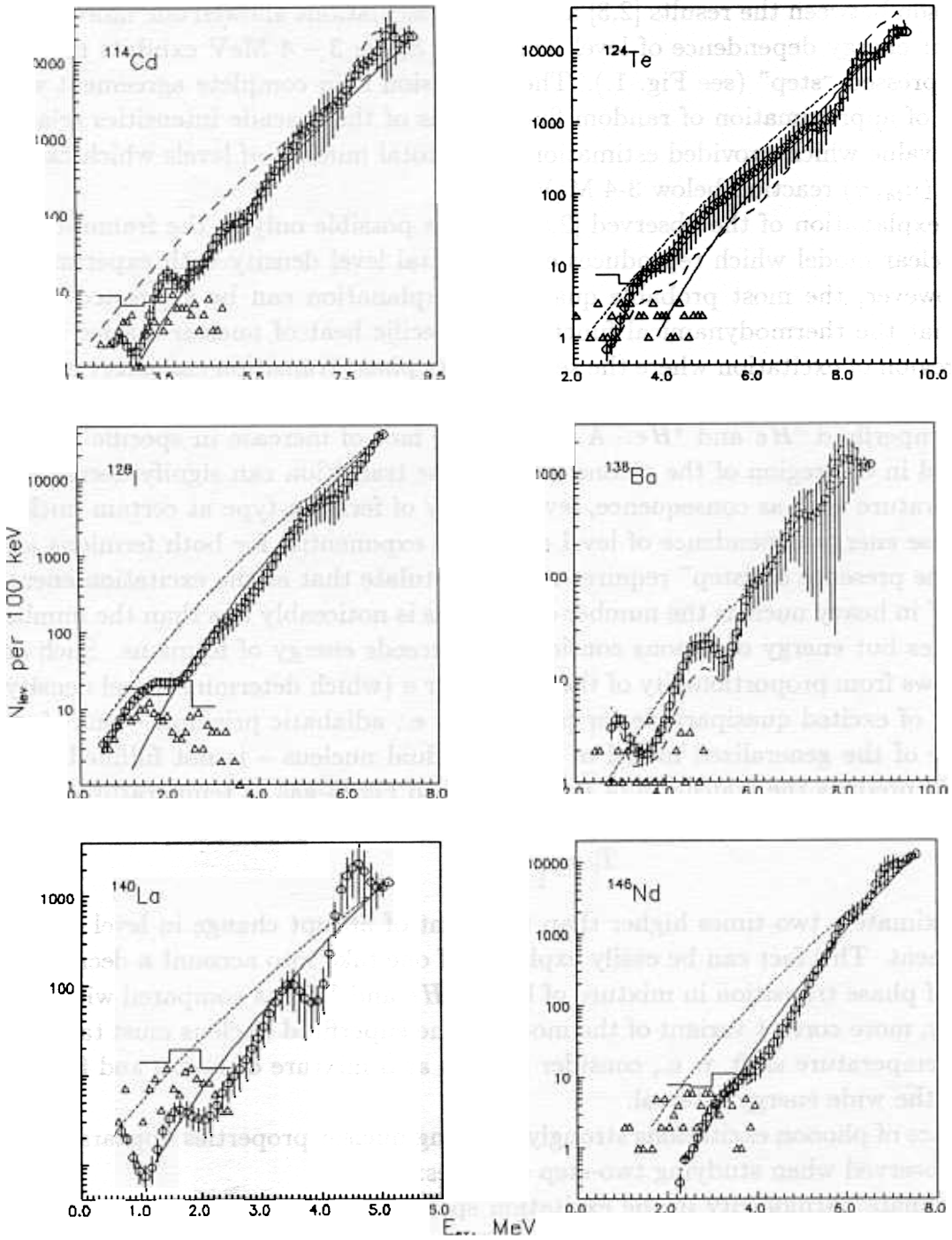

Fig. 1. The numbers of levels of both parities with errors (circles with bars) for ^{114}Cd, ^{124}Te, ^{128}I, ^{138}Ba, ^{140}La, and ^{146}Nd. Histogram - - data [8], triangles —experimental level density from the $(n, 2\gamma)$ reaction. Dashed line - · the ρ value obtained at the unreal initial parameter $\rho(E_{ex}) = \rho(B_n)$ of iterative process. The upper and lower curves represent predictions of models [11] and [7], respectively.

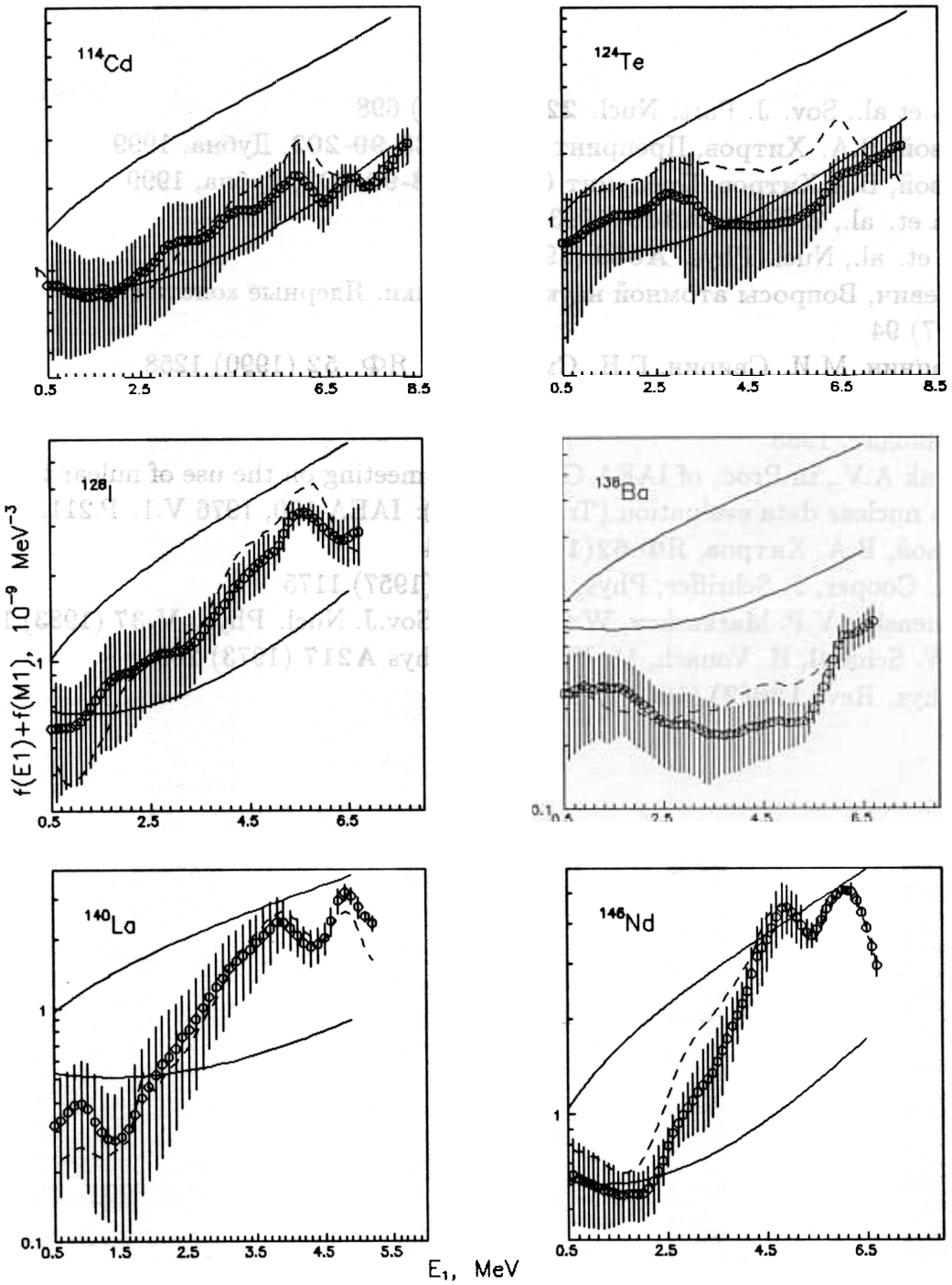

Fig. 2. The sum of the probable radiative strength functions of $E1$ and $M1$ transitions (with estimated errors) in the ^{114}Cd, ^{124}Te, ^{128}I, ^{138}Ba, ^{140}La, and ^{146}Nd nuclei. Dashed curve represents the $f(E1) + f(M1)$ mean value obtained at different initial values of strength functions and at initial level density $\rho(E_{ex}) = \rho(B_n)$ with the help of iterative procedure. Upper and lower solid curves represent predictions of models [12] and [10], respectively.

References

1. S.T. Boneva et al., Sov. J. Part. Nucl. **22(6)** (1991) 698
2. А.М. Суховой, В.А. Хитров, Препринт ОИЯИ, **Е3-99-202**, Дубна, 1999
3. А.М. Суховой, В.А.Хитров, Препринт ОИЯИ, **Е3-99-203**, Дубна, 1999
4. S.T. Boneva et. al., Z. Phys. **A346** (1993) 35
   S.T Boneva et. al., Nucl. Phys. **A589** (1995)293
5. О.Т. Грудзевич, Вопросы атомной науки и техники. Ядерные константы. **В.3-4** (1997) 94
6. Е.М. Растопчин, М.И. Свирин, Г.Н. Смиренкин, ЯФ. **52** (1990) 1258
7. А.В. Игнатюк, Статистические свойства возбужденных атомных ядер, М., Энергоатомиздат, 1983.
   A.V. Ignatyuk A.V., in Proc. of IAEA Consultants meeting on the use of nulear theory and neutron nuclear data evaluation (Trieste, 1975): IAEA-190, 1976 V.1. P.211.
8. А.М. Суховой, В.А. Хитров, ЯФ **62(1)** (1999) 24
9. J. Bardin L. Cooper, J. Schriffer, Phys. Rev. **108** (1957) 1175
10. S.G. Kadmenskij, V.P. Markushev, W.I. Furman, Sov.J. Nucl. Phys. **V.37** (1983) 165
11. W. Dilg, W. Schantl, H. Vonach, M. Uhl, Nucl. Phys **A217** (1973) 269
12. P. Axel, Phys. Rev. **126(2)** (1962) 671

NEW METHOD OF PARTIAL RADIATIVE CAPTURE CROSS SECTION MEASUREMENTS

Yu.P.Popov, A.V.Voinov, P.V.Sedyshev, S.S.Parzhitski, A.P.Kobzev, N.A.Gundorin, D.G.Serov, M.V.Sedysheva.

New method is based on the measurements of the energy shift of the primary γ-transition due to the capture of intermediate neutron with respect to its position after the thermal neutron capture. If an intense of the primary γ-transition with the energy $E^i_{\gamma 0}$ to the i-th final level of the excited nucleus after a thermal neutron capture ($E_n \cong 0$) by a nucleus with the atomic weight A, the energy of the γ-transition following the capture of an neutron with energy E_n must be:

$$E^i_\gamma = E^i_{\gamma 0} + A/(A+1)E_n$$

The method was first demonstrated in [1], where two resonances of sulfur were registered by using of reactor neutron beam with boron filter. However the authors did not manage to derive any information from the experiment beside the experimental widths of two resonances.

In our case the neutrons in the energy interval about 10 – 120 keV were generated by ^{7}Li(p,n) reaction by the Van de Graaff accelerator at proton energy exceeding the reaction threshold by ΔE_p =60 keV.

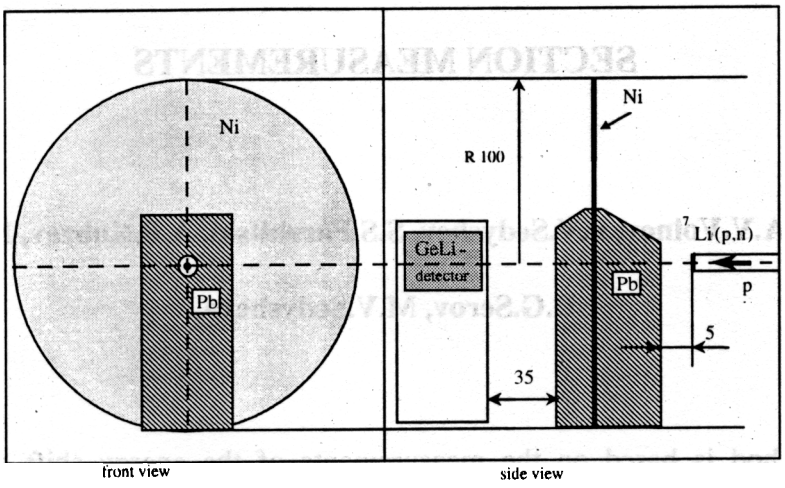

Fig. The draft of the experimental setup. The dimensions are in mm.

The draft of the experimental setup is shown in Fig. This compact geometry provided the optimum for efficiency of the γ-quanta registration and for irradiation of the sample by neutrons. According to the background measurements (without sample or with scatterer of pure graphite) the main components of background are due to the Compton effect in Ge-detector from Fe(n,γ) reaction on constructive materials (including on the turning magnet of the proton beam).

At first step of this method development we used the samples of Fe [2] and Ni [3], where the partial γ-transitions for several most intensive resonances was investigated by another methods [4,5]. It gives us possibility to standardize our relative cross sections data and check the new method.

For illustration of the method the part of experimental γ-quanta spectrum for Ni sample is presented on fig.2. One can see the structure in the spectrum due to $^{58}Ni(n,\gamma_0)^{59}Ni$ reaction with population of ground state of ^{59}Ni nucleus. Left peak belongs to the thermal neutron

capture and indicates the zero position of the neutron energy scale. The other peaks are due to the resonance neutron capture.

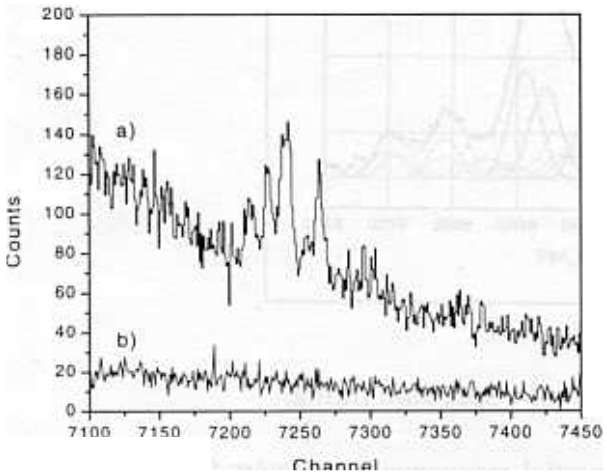

Fig.2. The experimental spectrum of $^{58}Ni(n,\gamma_0)^{59}Ni$ reaction with resonance neutrons produced by $^{7}Li(p,n)$ reaction with ΔE_p=60 keV over the reaction threshold (a), the background spectrum (b).

The experimental γ-quanta spectrum for the Fe sample is presented on the fig.3. The first two peaks are due to the thermal neutron capture by ^{56}Fe nucleus with population of ground and first excited state of ^{57}Fe. The counts to the right of the doublet are due to the γ-transitions populating these two states for the resonanse neutron capture. 16 γ-transitions (2 γ-transitions for 1 s-wave neutron resonance (27.7 keV) and 14 γ-transitions for 7 known p-wave resonances) may give the contribution to the resonance bump. For s-wave resonance these γ-transitions have E1 multipolarity, for p-wave they have M1 multipolarity. The fitting procedure (see Fig.3) and the data analysis method are described in [2].

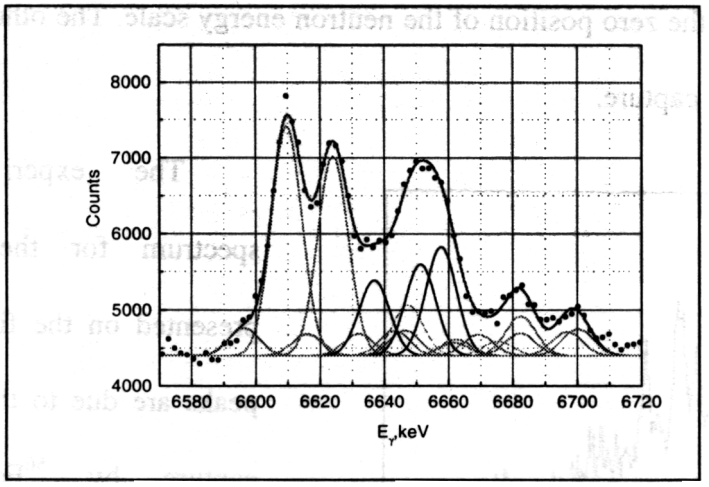

Fig.3 Graphical results of γ-spectrum fitting.

For absolute nornalization we used the known partial resonance parameters from [4,5]. Since the individual γ-transitions could overlap, we have determined only the partial radiative widths of the M1 multipolarity averaged over 7 p-wave resonances: $<\Gamma_{\gamma i}>$=69 meV.

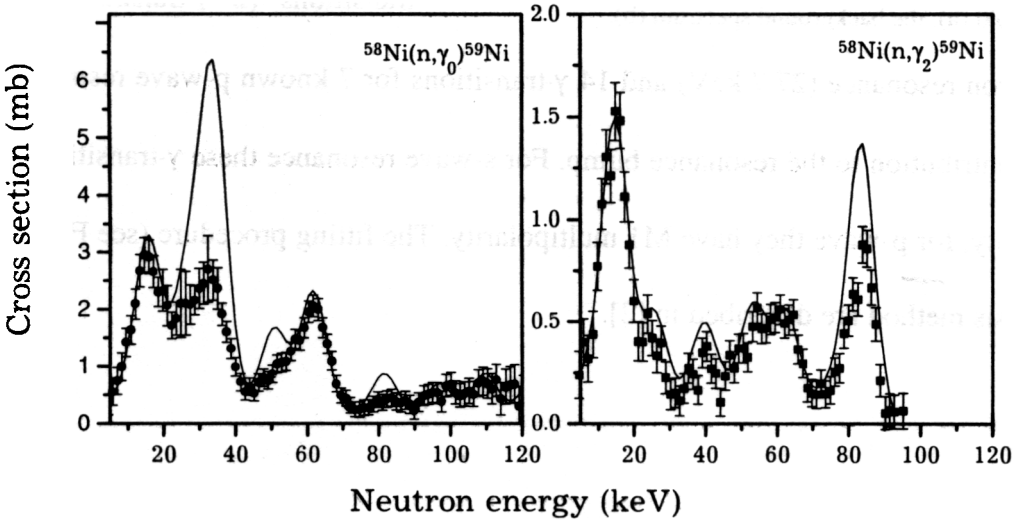

Fig.4. The partial cross sections of $^{58}Ni(n.\gamma_0)^{59}Ni$ (left) and $^{58}Ni(n.\gamma_2)^{59}Ni$ (right) reaction. The points are represented the experimental data and does not take into accounts the correction coefficients conjuncted with self-absorption and multiple scattering of neutrons in the sample. Full line are shown the corrected cross section.

The one of the first results obtained for ^{58}Ni isotope is shown in the Fig.4 where the partial cross section of ^{58}Ni(n,γ)^{59}Ni reaction for population of both the ground and second excited states of ^{59}Ni is presented. Each peak in the structure of the partial cross section is due to the contribution of a single resonance or group of the resonances. It allowed us with help of the fitting procedure to derive the partial parameters of neutron resonances and by using the partial values of radiative widths [4] make absolute normalization of our partial cross section data. It should be underlined that this result is obtained for the first time because of the high efficiency of this method in comparison with others.

New method developed in FLNP for measurements of the partial capture cross sections in the keV neutron energy region possess the record efficiency. It gave the possibility to receive the results unattainable now for the time-of-flight method not only for van de Graaff neutron sources but for the modern powerful neutron sources on the base of electron and proton accelerators. The energy dependence of the partial neutron capture cross sections was measured for the first time.

V.J.Thomson, A.V.Lopez.W.V.Prestvich, T.J,Kennett, Nucl. Instr. Meth.**126**,(1975) 263

2. Yu.P.Popov, P.V.Sedyshev, A.P.Kobzev, S.S.Parzhitski, N.A.Gundorin, D.G.Serov, M.V.Sedysheva. Phys. At. Nucl. **62** (1999) 827-831
3. Yu.P.Popov, A.V.Voinov, P.V.Sedyshev, A.P.Kobzev, S.S.Parzhitski, N.A.Gundorin, D.G.Serov. In: ISINN-7, Dubna 1999 (JINR, Dubna, 1999) 214-218.
4. H. Beer, R.R.Spenser, F.Kaeppeler, Z.Phys. A**284**, (1978) 73
5. H.Komano, M.Igashira, M.Shimizu, H.Kitasava, Phys.Rev. C**29,** (1984) 345

DETERMINATION OF THE FORWARDBACKWARD ASYMMETRY COEFFICIENT IN $^{35}Cl(n,p)^{35}S$ REACTION

Yu.M.Gledenov, R.Machrafi, A.I.Oprea, P.V.Sedyshev, V.I.Salatski, P.J.Szalanski
Joint Institute for Nuclear Research, 141980 Dubna, Russia

In the frame of mixing states with different parities model, the forward-backward α_{FB}, left-right α_{LR} and parity non-conservation α_{PN} asymmetry coefficients in the (n,p) reaction play an important role, because as is indicated in [1] the weak matrix element can be written like an expression of these three coefficients. So, in principle, if it is realized one experiment (or more) for measuring these coefficients it will be possible to obtain the weak matrix element. Recently, with resonance neutrons (up to 1keV) of the pulsed reactor IBR-30, Frank Laboratory of Neutron Physics, JINR, Dubna, it has been carried out an experiment for measuring the forward backward coefficient asymmetry on the NaCl target. Theoretically, the maximum of this coefficient is expected around E_n= 288 eV. The values of the α_{FB} have been obtained in different neutron energy intervals: 0.5-10, 150-260 and around the resonance (E_n=398 eV).

The experiment has been carried out at the 31m path of the pulsed reactor IBR-30. The neutron spectroscopy was performed by the time of flight method. It has been used a double section ionization chamber [2]. In one of its section was fixed a NaCl target of 0.5 mg/cm^2 and 200 mm in diameter onto 100 μm aluminum backing. The chamber was filled up with Ar + 4% CO_2 gas mixture at the pressure 0.35 ata. The pulse-height and time of flight spectra were registered using a multiparameter data acquisition system. The chamber has been periodically turned at 180^0 from its previous position, in one position we have measured the forward effect, while in the second position it has measured the backward effect. To normalize the neutron flux, we have used a boron counter monitor. The scheme of our experiment is shown in Fig.1.

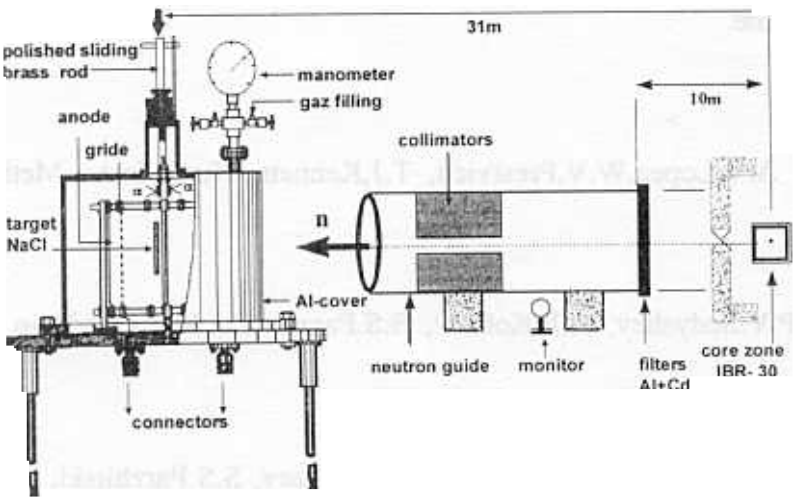

Fig.1. Experimental setup of the forward-backward asymmetry coefficient measurement

The forward-backward asymmetry coefficient was determined by the formula:

$$\alpha_{FB} = \frac{N_F - N_B}{N_F + N_B} \qquad (2)$$

Where, N_F – is the number of registered protons emitted in the forward direction, N_B – the number of registered protons emitted in the backward direction. The neutron energy dependence

of the $^{35}Cl(n,p)^{35}S$ reaction cross section is shown in Fig.2a. The theoretical evaluation of the forward-backward coefficient up to 2 keV is given in Fig.2b [3].

In Fig.3a and Fig.3b are shown the pulse-height spectra obtained in the neutron energy ranges 0.5-10 eV and 150-260 eV, while the Fig.3c illustrates a part of the time of flight spectra in the resonance region.

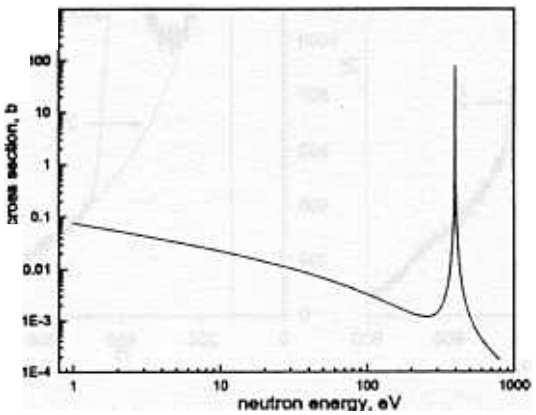

Fig.2a. The energy dependence of the $^{35}Cl(n,p)^{35}S$ cross section

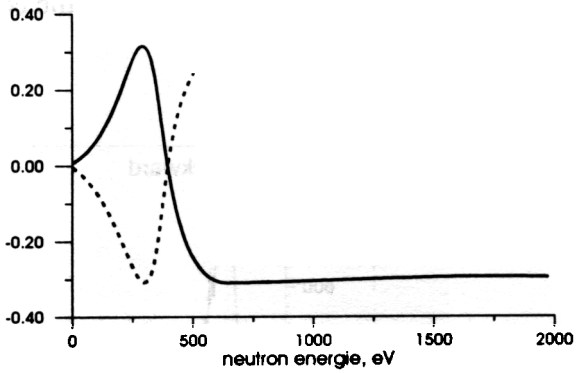

Fig.2b. Energy dependence of the forward backward asymmetry coefficients

The proton yields N_F and N_B have been obtained by the separation of the effect from the background on the pulse-height spectrum (Fig.3a and Fig.3b) for the neutron energy intervals 0.5-10 eV and 150-260 eV. But in the resonance region the value of the α_{FB} has been determined from the time spectrum shown in Fig.3c. The table 1 shows the obtained results.

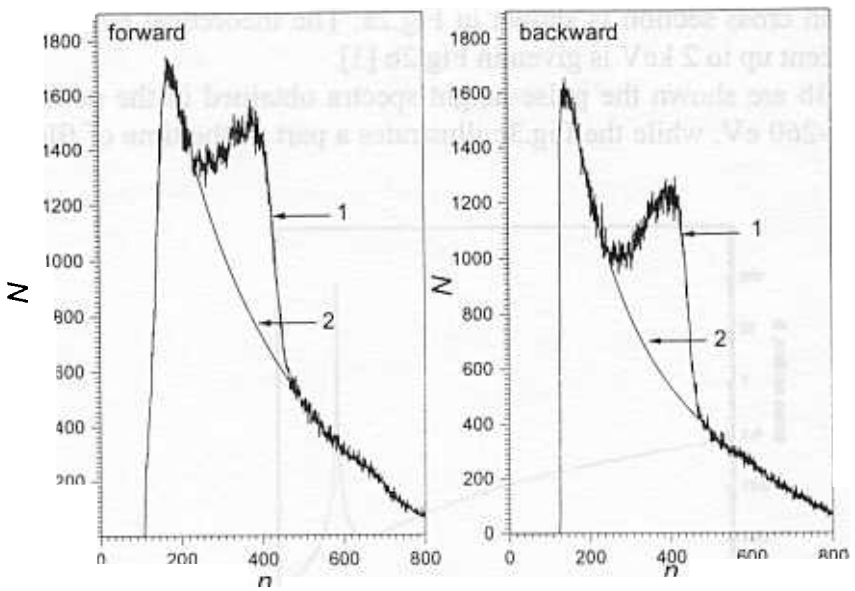

Fig.3a. The pulse height spectrum obtained in 0.5-10 eV, 1-event + background, 2- background, n- is the channel number, N- is the count per channel

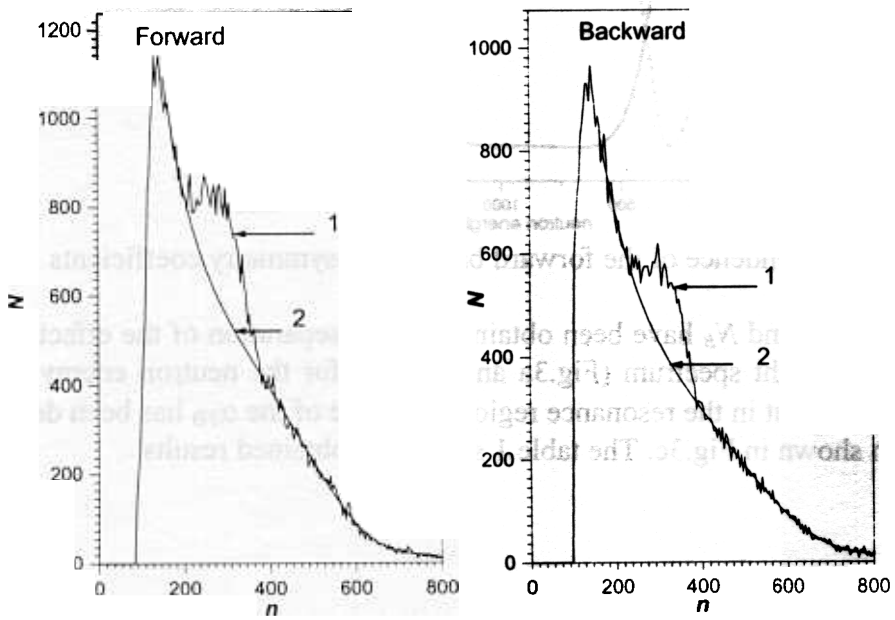

Fig.3b. The pulse height spectrum obtained in 150-260 eV, 1-event + background, 2- background, n- is the channel number, N- is the count per channel

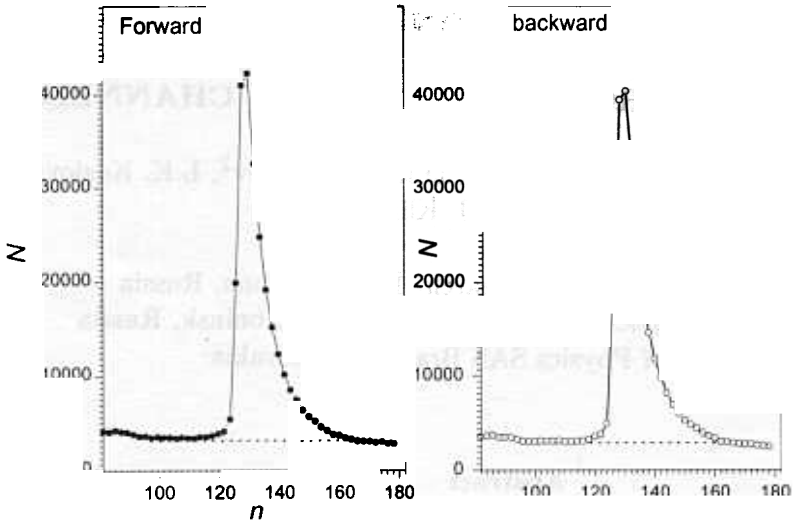

Fig.3c. Part of the time of flight spectrum for the forward backward in the resonance region n- is the channel number, N- is the count per channel

Table 1. The experimental results of the forward-backward asymmetry coefficient

The neutron energy range ,eV	$\bar{E}$,eV	α_{FB}
0.5 - 10	5.2	0.030 ± 0.005
150 - 260	205	0.17 ± 0.03
resonance region	398	0.002 ± 0.006

Using the parity non-conservation coefficient α_{PN} =-1.51x10^{-4}, the left-right α_{LR}=-2.4x10^{-4} coefficients at the thermal point energy and the forward-backward asymmetry coefficient α_{FB} = 0.17 [4,5], we obtain for the weak matrix element M_{PV}=57±17 meV.

References

[1]. Zenkin S.V., Titov N.A. Preprint INR RAS П-0367, Moscow (1984)
[2]. Yu.M.Gledenov, G.Khuukhenkhuu, M.V.Sedysheva et al., JINR Communication, E3-95- 445, Dubna (1995)
[3]. Yu.M.Gledenov, A.I.Oprea, V.I.Salatski, P.V.Sedyshev, P.I.Szalansky, Asymmetry coefficient in (n,p) reactions ISINN-6 Dubna, 1998
[4]. Yu.M.Gledenov et al., Nuclear Phys. A654 (1999) 943c-948c
[5]. A.Antonov, V.A.Vesna, Yu.M.Gledenov et al. Pis'ma ZETF. 40 (1984) 209.

ANGULAR ANISOTROPY OF FISSION FRAGMENTS FROM THE RESONANCE NEUTRON INDUCED FISSION OF ALIGNED ^{235}U TARGET AND THE ROLE OF $J^{\pi}K$ FISSION CHANNELS

Yu.N. Kopatch[1] A.B. Popov[1], W.I.Furman[1], D.I. Tambovtsev[2], L.K. Kozlovsky[2], N.N. Gonin[2], and J. Kliman[1,3]

[1]Joint Institute for Nuclear Research, 141980 Dubna, Russia
[2)]SSC Institute of Physics and Power Engineering Obninsk, Russia
[3)]Institute of Phvsics SAS Bratislava, Slovakia

Abstract

Energy dependence of the fission fragment angular anisotropy from $^{235}U(n,f)$ reaction has been measured by the FLNP-IPPE collaboration using the JINR pulsed neutron source IBR-30. Our data are analyzed together with the total neutron, total fission and spin-separated fission cross sections in energy range $0 - 30$ eV in order to obtain a new set of s-wave resonance parameters. Three fission channels ($K = 0, 1, 2$) are taken into account for both spin groups, $J = 3^-$ and $J = 4^-$. The obtained set of resonance parameters is discussed. Integral distributions of partial and total fission widths are compared with the Porter-Thomas distributions. Estimation of the degrees of openness of different $J^{\pi}K$ fission channels is made. A problem of ambiguity of the resonance parameters is also briefly discussed.

1. Fission induced by slow neutrons is one of the unique tools for studying the quantum-mechanical aspects of the fission process. It gives a possibility to obtain information about the fission amplitudes $\gamma_{f\lambda}^{J^{\pi}K}$ for a given resonance λ. These parameters form a basis for a quantitative description of the fission process induced by resonance neutrons. Here, $J^{\pi}K$ are the spin, parity and the spin projection onto the symmetry axis of the fissioning nucleus. It is known [1, 2] that such amplitudes cannot be extracted unambiguously using only data on integral fission and neutron cross sections. Additional information can be obtained from experiments on the interaction of polarized (or unpolarized) neutrons with a polarized (aligned) target.

We performed an experimental study of the energy dependence of the differential fission cross section (fission fragment angular anisotropy) of ^{235}U resonance neutron induced fission using an aligned target and unpolarized neutrons.

2. The experiment has been performed at the booster IBR-30 + LEA-40 in Dubna and is a development of the technique used by Pattenden and Postma.[3] The detailed description of the experimental set-up and of the primary data analysis can be found in.[4, 5]

The energy dependence of the A_2 coefficient, which characterizes the angular anisotropy of fission fragments, is shown in fig. 1.

For a combined analysis, we used the experimental cross sections for ^{235}U available from the National Nuclear Data Center (NNDC) at BNL.[6] The data sets selected for the analysis are summarized in Table 1.

3. The experimental data sets listed in Tab. 1 were fitted over the energy region $0 - 30$ eV using the standard R-matrix formalism in the Reich-Moore approximation [13] with the inclusion

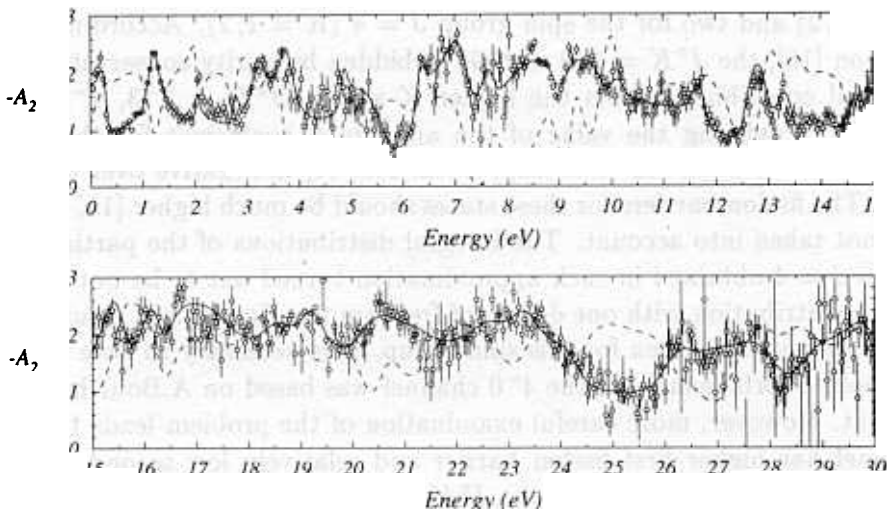

Figure 1: The results of the fit (solid curve) for $A_2(E)$, circles are experemental data. Dashed line is calculated using the resonance parameters from.[13]

of formulae for $A_2(E)$ derived in ref. [14] (see also for details ref. [5]). In the fit, each resonance λ was described by six resonance parameters: E^λ, Γ_γ^λ, γ_n^λ, γ_f^λ, ϕ^λ, and θ^λ. Such parameterization allows one to include up to 3 fission channels for each resonance λ. The partial fission amplitudes are expressed via the module of the total fission amplitude $\gamma_f^\lambda = \sqrt{\Gamma_f^\lambda}$ and two angles, ϕ^λ and θ^λ, in a spherical coordinate system:

$$\gamma_{f1}^\lambda = \gamma_f^\lambda \cdot \cos\phi^\lambda \cdot \sin\theta^\lambda, \quad \gamma_{f2}^\lambda = \gamma_f^\lambda \cdot \sin\phi^\lambda \quad \sin\theta^\lambda \quad \gamma_{f0}^\lambda = \gamma_f^\lambda \cdot \cos\theta^\lambda \tag{1}$$

Table 1: The experimental data sets selected for the evaluation

	Type of cross section	**Authors**	**Energy range**
1	$A_2(E)$	Present work	0.06 – 30 eV
2	Fission (σ_{nf})	R.Gwin et al.[7]	0.0016 – 9.7 eV
3	Fission (σ_{nf})	L.W.Weston et al.[8]	9.7 – 30 eV
4	Spin-separated fission (σ_{nf}^J)	V.L.Sailor et al.[9]	0.075 – 1.14 eV
5	Spin-separated fission (σ_{nf}^J)	M.S.Moore et al.[10]	1.6 – 30 eV
6	Total (σ_{ntot})	F.D.Brooks et al.[11]	0.035 – 1.3 eV
7	Total (σ_{ntot})	A.Michaudon et al.[12]	1.3 – 30 eV

The radiative width Γ_γ^λ was fixed and equals 0.039 eV for all resonances. All other parameters were varied. First we analyzed the data assuming that three channels are open for the spin group

$J = 3$ ($K = 0, 1, 2$) and two for the spin group $J = 4$ ($K = 1, 2$). According to the commonly used assumption [16], the $J^\pi K = 4^-0$ state is forbidden by parity conservation. We can expect no or very small contribution from the higher K states ($J^\pi K = 3^-3$, 4^-3, and 4^-4) as the geometrical factors defining the value of the anisotropy coefficient for these states have the positive sign while the observed anisotropy coefficient A_2 is negative over the whole measured energy range. The fission barriers for these states should be much higher [15, 16]. So these fission channels are not taken into account. The integral distributions of the partial fission widths for the spin group $J = 4$ obtained in such approximation turned out to be not consistent with the Porter-Thomas distribution with one degree of freedom (see fig. 3, right column). An additional fission channel seems to be open for this spin group. It is necessary to note that the conclusion [16] about absolute forbidenness of the 4^-0 channel was based on A.Bohr hypothesis [15] in its simplest variant. However, more careful examination of the problem leads to a conclusion that the 4^-0 channel has higher first fission barrier and relatively low second one for asymmetric fission modes. Thus, one would expect the $J^\pi K = 4^-0$ channel to be at least partially open for our case. So we reanalyzed the data assuming that all three channels are open for both spin groups.

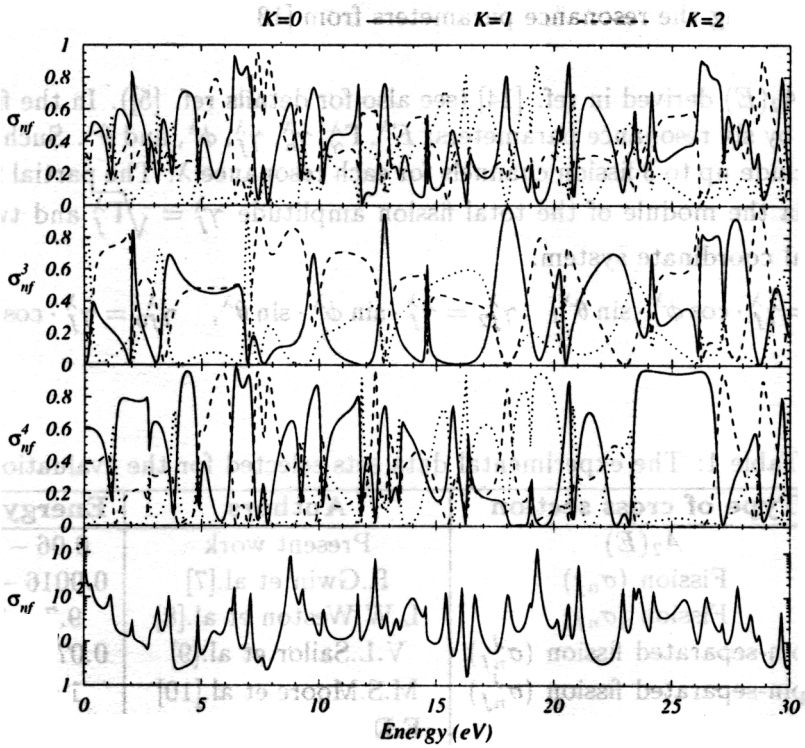

Figure 2: Decomposition of the total and spin-separated fission cross sections into K components. Energy dependence of the total fission cross section is shown in the lower plot.

The results of the final fit for $A_2(E)$ are shown in fig. 1 All other cross sections are also

well reproduced. The dashed line is calculated using a set of resonance parameters from the ENDF/B-VI library [13] which also describes all other cross sections quite well, but obviously fails to reproduce the A_2 energy dependence. It is necessary to note that the latter set of resonance parameters was obtained in the two channel approximation and without taking into account the information on $A_2(E)$.

4. Figure 2 shows the relative contributions of different K-components to the total and spin separated fission cross sections. As is expected, there are large fluctuations of weights of the K-channels for different compound states λ which result in the strong fluctuations of the relative K-contributions. It can be noted that the contribution of the $K = 0$ component is significant both in the spin-separated and the total fission cross sections.

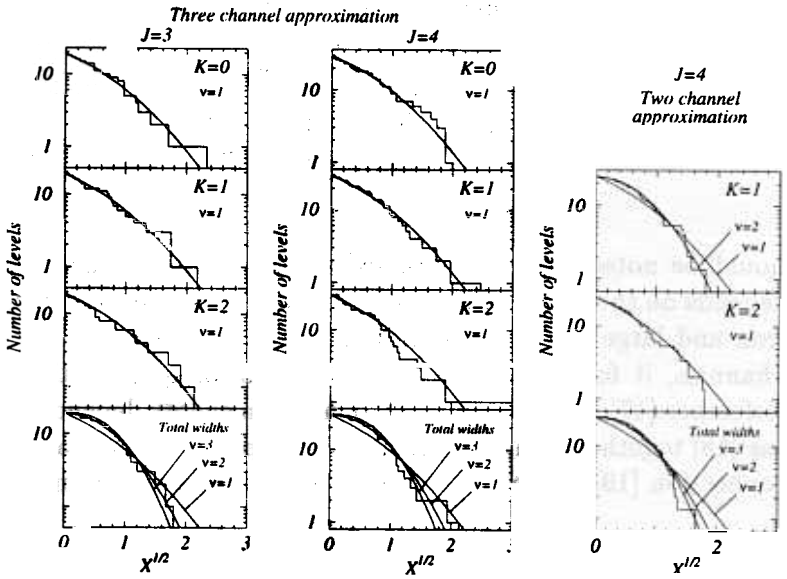

Figure 3: Integral distributions of partial and total fission widths (number of resonances with $\Gamma_{\lambda f}/\langle\Gamma_{\lambda f}\rangle > X$). Solid lines are the χ^2 distributions with ν degrees of freedom.

The integral distributions of the partial and total fission widths of resonances in the energy interval 0 – 30 eV are given in fig 3 (left and middle). The experimental distributions for each separate $J^\pi K$ channel are in good agreement with the Porter-Thomas distribution with one degree of freedom. The integral distributions of the total fission widths for both channels also fluctuate according to the Porter-Thomas distribution with the number of degrees of freedom being between 2 and 3.

The average partial ($\langle\Gamma^\lambda_{f,K}\rangle$) and total ($\langle\Gamma^\lambda_f\rangle$) fission widths for each fission channel are listed in Tab.2. The average contributions of different fission channels, defined as

$$W_K = \frac{1}{N_\lambda}\sum_\lambda \frac{\Gamma^\lambda_{f,K}}{\Gamma^\lambda_f} \qquad (2)$$

which can be regarded as a measure of the degree of openness of a given channel are shown in Tab.3. One can see that these values are almost equal for both spin groups. The $K = 0$ channel seems to be somewhat suppressed, which is consistent with modern theoretical considerations.

Table 2: Average partial and total fission widths in meV

	K=0	K=1	K=2	Total
J=3	35.0	68.1	74.0	177.1
J=4	20.4	34.0	38.0	92.4
J=3+4	26.1	47.2	51.9	125.2

Table 3: Degrees of openness of different fission channels (%)

	K=0	K=1	K=2
J=3	25	39	35
J=4	26	40	34
J=3+4	26	40	34

Finally, it should be noted that the obtained set of resonance parameters is not uniquely determined. It depends on the choice of negative resonances as well as on inclusion of resonances with small neutron and large total fission widths. However, since this parameter set includes all possible K channels, it forms the most reliable basis for quantitative analysis of $s-$ and $p-$resonance interference.[17] A combined study of neutron energy dependence of fragment mass-TKE distributions [18] together with an angular anisotropy coefficient can give new information about the interconnection [19] of the Bohr fission channels and fission modes.

References

[1] G.F.Auchampaugh, *Nucl. Phys.* **A175**, 65 (1971)

[2] D.B.Adler and F.T.Adler, *Phys. Rev.* **C6**, 985 (1972).

[3] N.J.Pattenden and H.Postma, *Nucl. Phys.* **A167**, 225 (1971

[4] D.I. Tambovtsev, L.K. Kozlovsky, N.N. Gonin, N.S. Rabotnov, Yu.N. Kopach, A.B. Popov, W.I. Furman, J. Kliman, H. Postma, A.A. Bogdzel, and M.A. Guseinov, *Phys. At. Nucl.* **60/6**, 877 (1997).

[5] Yu.N.Kopach, A.B.Popov, W.I.Furman, N.N.Gonin, L.K.Kozlovsky, D.I.Tambovtsev, and J.Kliman, *Phys. At. Nucl.* **62/5**, 900 (1999)

[6] National Nuclear Data Center, Upton, NY, 11973-500, *http://www.nndc.bnl.gov.*

[7] R.Gwin, R.R.Spencer, R.W.Ingle, J.H.Todd, and S.W.Scoles, *Nucl. Sci. Eng.* **88**, 37 (1984)

[8] L.W.Weston and J.H.Todd, *Nucl. Sci. Eng.* **88**, 567 (1984).

[9] R.I.Schermer, L.Parsell, G.Brunhart, C.A.Reynolds, V.L.Sailor, and F.J.Shore, *Phys. Rev.* **167**, 1121 (1968).

[10] M.S.Moore, J.D.Moses, G.A.Keyworth, J.W.T.Dabbs, and N.W.Hill, *Phys. Rev.* **C18**, 1328 (1978).

[11] F.D.Brooks, J.E.Jolly, M.G.Schomberg, and M.G.Sowerby, AERE-M-1670 (1966).

[12] A.Michaudon, H.Derrien, P.Ribon, and M.Sanche, *Nucl. Phys.* **69**, 545 (1965).

[13] ENDF/B-VI Summary Documentation, ENDF-201 (BNL-17541), 1991.

[14] A.L.Barabanov and W.I.Furman, in *Proc. Int. Conf. on Nuclear Data for Science and Technology*, Gatlinburg, Tenessee, USA, May 9-13, 1994 ed.J.K.Dickens, p. 448; A.L.Barabanov and W.I.Furman, *Z. Phys.* **A357**, 411 (1997).

[15] A.Bohr, in *Proc. 1st Int. Conf. Peaceful Uses At. Energy*, Geneva, Vol. 2, p. 151 (1956).

[16] J.E.Lynn, "Theory of Neutron Resonance Reactions", (Claredon Press, Oxford, 1968).

[17] A.B.Popov, W.I.Furman, and L.Lason, in *Proc. of II Int. Workshop of Fission and Fission Fragment Spectroscopy*, edited by G.Fioni *et al.*, Seissyn, France, April 21-24, 1998, p. 349 (Woodbury, New York, 1998).

[18] Sh.S.Zeinalov *et al.*, in *Proc. VI Int. Sem. on Int. Neutr. with Nucl.*, Dubna, Russia, May 25-28 1999, p. 258 (Dubna, 1999).

[19] W.I.Furman and J.Kliman, in *Proc. 17th Int. Symp. on Nucl. Phys.*, Gaussig, 1987, p. 86 (Dresden, ZfK, 1988).

RELIABILITY OF MOSSES *(HYLOCOMIUM SPLENDENS, PLEUROZIUM SCHREBERI* AND *CALLIERGON GEGANTEUM)* AS BIOMONITORS OF HEAVY METAL ATMOSPHERIC DEPOSITION IN CENTRAL RUSSIA

M.V.Frontasyeva, Ye.V. Yermakova*, E. Steinnes**

FLNP, JINR, Dubna, Moscow Region, Russia

**L.N. Tolstoy Tula State Pedagogical University*

***Department of Chemistry, Norwegian University of Science and Technology, N-7491 Trondheim, Norway*

The moss biomonitoring technique was applied to study heavy metal atmospheric deposition in the area of Yasnaya Polyana, the memorial estate of L.N.Tolstoy, which is surrounded by numerous metallurgy, chemical, power, and machine-building plants in cities to the south of Moscow (Tula, Novomoskovsk, Schekino). This is the first time that a wide spectrum of heavy metals and other toxic elements was studied in the Tula Region.

Moss samples were collected in accordance with the sampling strategy adopted in the European Moss Survey on biomonitoring heavy metal atmospheric deposition [1]. In addition to standard epigeic moss species such as *Hylocomium splendens (Hs)* and *Pleurozium schreberi (Ps)*, the epiphytic moss *Calliergon geganteum (Cg)*, which is widely distributed at the given climatic conditions, was also studied.

Epithermal neutron activation analysis at the IBR-2 rector of FLNP made it possible to identify 38 elements in the moss samples including rare-earth elements, uranium, and thorium. Interspecies ratios of elements were calculated and compared to those observed by other investigators [2] in the Northern part of Europe at different environmental conditions. The interspecies ratio (*Ps:Hs*) varies between 1.10 and 1.50 for Mg, Ti, and Mn, whereas for Ca, Sc, Ni, Rb, Sr, In, La, Ce, Sm, Gd, Tb, Dy, Ta and Th it is less than 0.80. Because of living conditions in the relatively dry climate of the Tula Region,

Hylocomium splendens shows signs of degeneration in comparison with *Pleurozium schreberi* which is probably more resistent to dry climate. Pronounced differences in interspecies ratios were observed within the area under investigation for elements characteristic of air pollution, especially for V (*Ps:Hs* 1.39; *Ps:Cg* 1.35) and Sb (*Ps:Hs* 1.28; *Ps:Cg* 1.57). This suggests that interspecies variations depend mostly on deposition level. The interspecies ratios (*Ps:Cg*) varies from 0.80 to 1.20 for elements Mg, K, Ca, Cr, Mn, Fe, Co, Zn, As, Se, Br, Rb, Sr, Zr, Cd, In, Ba, Eu, W.

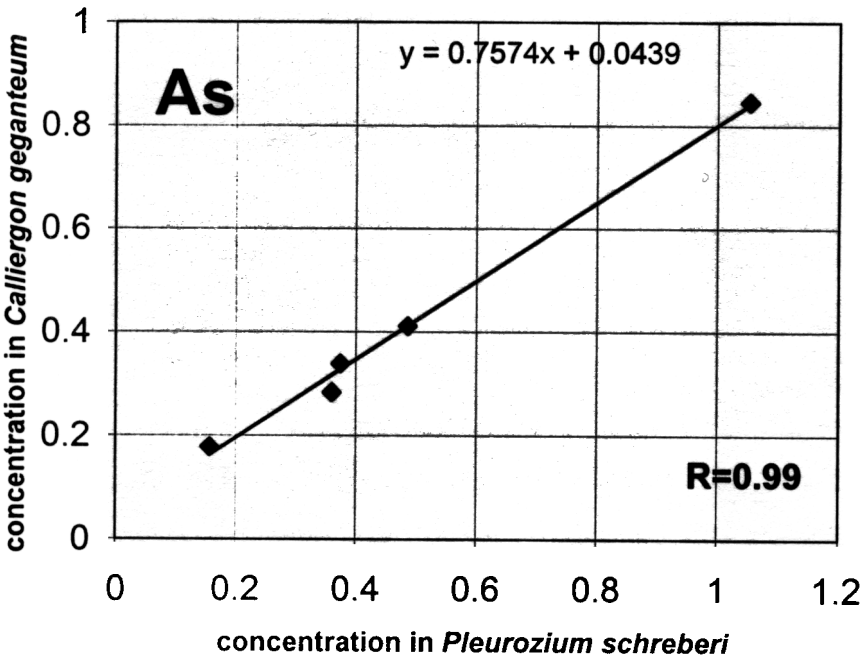

Fig 1. Concentration (ppm) of arsenic in Pleurozium schrebery versus Calliergon geganteum.

Based on this fairly extensive set of data where interspecies ratios vary within a relatively narrow range we conclude that the species *Calliergon geganteum* may replace the coventionally employed moss biomonitor species at sites where they are not found.

REFERENCES

[1] Åke Rühling. Heavy Metal Deposition in Europe – estimations based on moss analysis. Nordic Council of Ministers, Copenhagen, Nord 1994, p. 9.

[2] J.H. Hallereker, C. Reimann, P.de Catitat, T.E. Finne, G. Kashulina, H. Niskaavaara, I. Bogatyrev. Reliability of moss (Hylocomium splendens and Pleurozium schreberi) as a bioindicator of atmospheric chemistry in the Barents region: Interspecies and field duplicate variability. The Science of the Environment 218 (1998) 123-139.

SELECTION OF APPROPRIATE MOSS BIOMONITORS FOR STUDYING ATMOSPHERIC ELEMENTAL DEPOSITION IN CHINA

O. A. Stan, Zh. H. Zhang*, M.V. Frontasyeva, E. Steinnes**

FLNP, JINR, Dubna, Moscow Region, Russia

**IHEP, CAS, Beijing, China*

***Norwegian University of Science and Technology, Trondheim, Norway*

The moss biomonitoring is a well established technique widely used to study atmospheric deposition in Nordic countries [1] and in the Western Europe [2]. The present work is the first attempt to apply this technique to some areas of China. Twelve different moss species were collected during the autumn of 1998. Most of the samples were taken from highly polluted areas within the Beijing Region. The remaining ones were collected from the national park in Tianmu Mountain, Zhejiang Province, South-East China. The purpose of the present study is to find appropriate moss biomonitors growing in China, as alternatives to the species *Hyloconium splendens (HS)* and *Pleurozium schreberi (PS)* adopted in the European Moss Survey [3] which unfortunately are not found in the Beijing Region (see Table 1).

Table 1 Name and location of the Mosses in China

Name	Site	Name	Site
Myuroclada maximoviczii	BR	*Taxiphyllum taxirameum*	BR
Oxystegus cylindricus	BR	*Brachythecium plumosum*	BR
Brachythecium plumosum	BR	*Grimmia pilifera*	BR
Entodon rubicundus	BR	*Bryhnia sublaevifolia*	NP
Platyhypnidium riparioides	BR	*Entodon cf. seductrix*	NP
Taxiphyllum taxirameum	BR	*Oxyrrhynchium savatier*	NP

BR = Beijing Region; NP = National Park

A total of 49 elemental concentrations were determined by nuclear and related analytical techniques: epithermal neutron activation analysis (ENAA) at the IBR-2 reactor of JINR; hydride-generation atomic fluorescence spectrometry (HGAFS) and flame and/or graphite furnace atomic absorption spectrometry at IHEP.

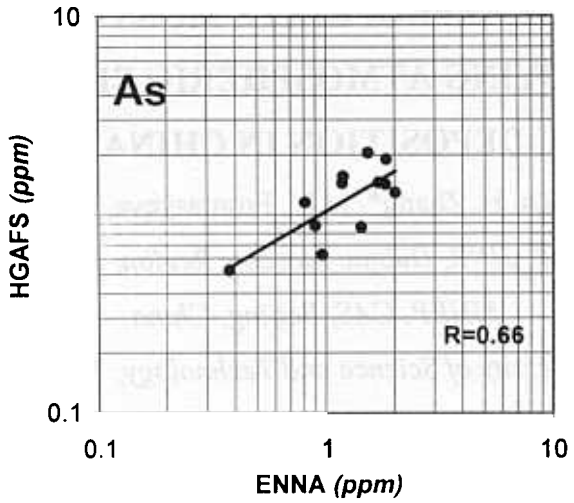

Fig.1. Arsenic concentrations in mosses obtained by ENAA versus HGAFS

A comparison of the results obtained by ENAA and HGAFS for arsenic is shown in Fig. 1. Quality assurance for element determination was provided by using IAEA standard reference material Lichen IAEA-336 in both laboratories.

In spite of the fact that all 12 moss species reflect the general level of pollution in entirely different regions of China (Fig.3), two moss species *Myuroclada maximoviczii* and *Entodon rubicundus* demonstrated the best ability to substitute each other by showing the highest correlation (Fig.2).

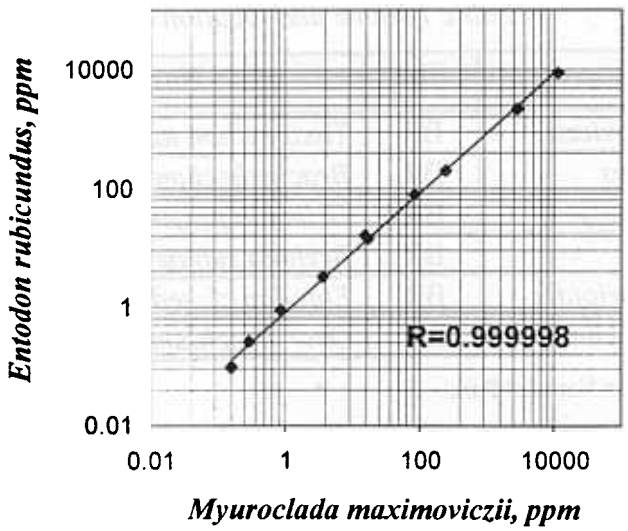

Fig 2. Comparison Myuroclada maximoviczii versus Entodon rubiundus

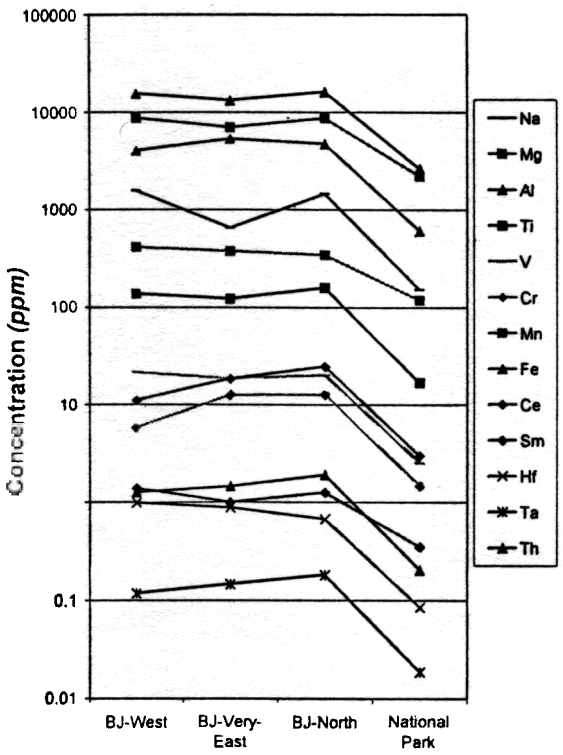

Fig. 3 Some elemental concentrations in mosses from the Beijing Region and the National Park in South-East China

Practically for all elements the concentrations are about 10 times lower in the National Park than at other sampling sites

The results obtained encourage us to plan an extended moss survey for assessment of air pollution in urban and rural areas of China.

REFERENCES

[1] M.V. Frontasyeva, E. Steinnes, Epithermal Neutron Activation Analysis of Mosses Used to Monitor Heavy Metal Deposition Around an Iron Smelter Complex, Analyst, 120 (1995) 1437-1440

[2] B. Markert, O. Wappelhorst, V. Weckert, U. Herpin, U. Siewers, K. Friese, G. Breulmann, The Use of Bioindicators for Monitoring the Heavy-Metal Status of the Environment, *J. Radioanal. Nucl. Chem.*, 240 (1999) 425-429

[3] Å. Rühling, Atmospheric Heavy Metal Deposition in Europe - estimations based on moss analysis., Nordic Council of Ministers, *NORD 1994:9* (1994) 10-13

1. PUBLICATIONS

CONDENSED MATTER PHYSICS

Reviews

1. Aksenov V.L., Shakhmatov V.S. Structural peculiatities in fullerene crystals. Correlations, coherence and order. Plenum Press, London-New-York, 1999, pp.1-28.
2. Balagurov A.M. Structural studies by neutron powder diffraction. State of the Art, Materials Science Forum, 1999, v.321-324, pp.236-245.
3. Balagurov A.M., Sikolenko V.V. Neutron Diffraction Studies in the Frank Laboratory of Neutron Physics of the Joint Institute for Nuclear Research, Surface investigations. X-ray, Synchrotron and Neutron Techniques, 1999, v.10, pp. 3 - 16
4. Nietz V.V. Investigations of crystallic matter magnetism by neutron diffraction using a pulsed field. Particles and nuclei (in press).

Diffraction

1. Aksenov V.L., Balagurov A.M., Glazkov V.P., Kozlenko D.P., Naumov I.V., Savenko B.N., Sheptyakov D.V., Somenkov V.A., Bulkin A.P., Kudryashev V.A., Trounov V.A. DN-12 time-of-flight high-pressure neutron spectrometer for investigation of microsamples. Physica B, 1999, v.265, pp.258-262.
2. Aksenov V.L., Balagurov A.M., Kozlenko D.P., Savenko B.N., Sheptyakov D.V., Glazkov V.P., Naumov I.V., Somenkov V.A. Neutron investigations of structure and dynamics of condensed matter under high pressure at IBR-2 pulsed reactor. Proceedings of Tula State University, Seria Fizika, 1999, v.2, pp.17-25.
3. Aksenov V.L., Ossipyan Yu.A., Forro L., Khasanov S., Chernyshev V.V., Shakhmatov V.S. Fullerene molecule strain in RbC_{60}. Solid State Communications, 1999 (in press).
4. Avdeev M.Yu., Nalbandyan V.B., Beskrovnyi A.I., Balagurov A.M., Volochaev V.A. Refinement of structures of two non-stoichiometric one-dimensional solid electrolytes. J. Inorganic Chemistry, 1999, v.44, pp.480-484.
5. Balagurov A.M., Beskrovnyi A.I., Pomjakushin V.Yu., Simkin V.G., Bagautdinov B.Sh., Shekhtman V.Sh., Zakharov A.A. Twinned La_2CuO_4 Structure, Crystallography Reports, 1999, v.44, pp.74-82.
6. Balagurov A.M., Kozlenko D.P., Savenko B.N., Glazkov V.P., Somenkov V.A., Hull S. Neutron diffraction study of structural changes in ammonium halides under high pressure. Physica B, 1999, v.265, pp.92-96.
7. Balagurov A.M., Pomjakushin V.Yu., Sheptyakov D.V., Aksenov V.L., Babushkina N.A., Belova L.M., Taldenkov A.H., Inyushkin A.V., Fischer P., Gutmann M., Keller L., Gorbenko O.Yu., Kaul A.R. Changes in the magnetic structure of $(La_{0.25}Pr_{0.75})_{0.7}Ca_{0.3}MnO_3$ upon the isotopic substitution of ^{18}O for ^{16}O. JETP Letters, 1999, v.69, pp.50-56.
8. Balagurov A.M., Sheptyakov D.V., Aksenov V.L., Antipov E.V., Putilin S.N., Radaelli P.G., Marezio M. The structure of $HgBa_2CuO_{4+d}$ at ambient and high pressure at 0.06JdJ0.19. Phys. Rev. B, 1999, v.59, pp.7209-7215.
9. Balagurov A.M., Pomjakushin V.Yu., Sheptyakov D.V., Aksenov V.L., Babushkina N.A., Belova L.M., Taldenkov A.H., Inyushkin A.V., Fischer P., Gutmann M., Keller L., Gorbenko O.Yu., Kaul A.R. Effect of oxygen isotope substitution on the magnetic structure of $(La_{0.25}Pr_{0.75})_{0.7}Ca_{0.3}MnO_3$. Phys. Rev. B, 1999, v.60, pp.383-387.
10. Belushkin A.V., Kozlenko D.P., McGreevy R.L., Savenko B.N., Zetterstrm P. A study of orientational disorder in ND_4Cl by the reverse Monte Carlo method. Physica B, 1999, v.269, pp.297-303.
11. Beskrovnyi A.I., Danilkin S.A., Fuess H., Jadrowski E.L., Neova-Baeva M., Wieder T. Effect of Cr content on the crystal structure and lattice dynamics of FCC Fe-Cr-Ni-N austenitic alloys. J. of Alloys and Compounds, 1999, v.291, pp.262-268.
12. Danilkin S., Beskrovnyi A., Jadrowski E. Nitrogen effect on lattice dynamics of fcc Fe-Cr-Mn (Ni) austenitic allous. Materials Science Forum, 1999, v.318-320, pp.19-24.
13. Glazkov V.P., Kozlenko D.P., Savenko B.N., Somenkov V.A., Shil'shtein S.Sh. Neutron diffraction study of structural variations in ND_4I and ND_4F ammonium halides under high pressure. Crystallography Reports, 1999, v.44, pp.50-55.
14. Lushnikov S.G., Belushkin A.V., Beskrovnyi A.I., Fedoseev A.I., Gvasaliya S.N., Shuvalov L.A., Schmidt V.H. Isotope effect in $Cs_5H_3(SO_4)_{40.5H2}O$ crystals. Solid State Ionics, 1999, v.125, pp.119-123.

15. Martinez-Sarion M.L., Mestres L., Beskrovnyi A.I, Natkaniec I., Smirnov L.S., Shelkova I.G. X-ray and neutron powder diffraction study of $Rb_{2-x}(NH4)xSO_4$ system. Poverhnost', 1999, v.2, pp.16-20.
16. Menshikov A.Z., Balagurov A.M., Beskrovney A.I., Vokhmyanin A.P., Morozov D.M. Time of flight neutron diffraction on Mn_5Si_3 magnetic structure. Materials Science Forum, 1999, v.321-324, pp.659-664.
17. Mestres L., Martinez-Sarrion M.L., Baccali A., Simkin V.G., Smirnov L.S., Balagurov A.M. X-ray and neutron powder diffraction studies of phase transition in $LiCsSO_4$. Crystallography Reports, 1999, v.44, pp.83-88.
18. Nietz V.V. Phase diagram of hematite in magnetic field below the Morin temperature. JINR communication, P17-99-14, 1999, Dubna, Russia.
19. Nietz V.V. Use of pulsed magnetic fields in neutron scattering studies of crystals. Journal of the Moscow Physical Society, 1999, v.8, pp.351-372.
20. Nietz. V.V. Magnetic solitons and neutron scattering. UFN, 1999 (in press).
21. Nikitin A.N. About a traditional method of training of high-qualification physicists for scientific organizations and universities. Proceedings of Tula State University, Seria Fizika, 1999, v.2, pp. 111-123.
22. Zlokazov V.B. Mathematical analysis of data in the experiment on the synthesis of the element 114, JINR Communication, E7-99-273, 1999, Dubna, Russia.

Texture and Stresses

1. Aksenov V.L., Nikitin A.N., Burilichev D.E. Modern texture analysis of materials. MSU Manual, 1999, 44 p., Moscow.
2. Bokuchava G.D., Luzin V.V., Schreiber J., Taran Yu.V. Residual stress investigations in austenitic steels samples with different degree of low cycle fatigue. Textures and Microstructures, 1999, v.33, pp.279-289.
3. Bokuchava G.D., Schreiber J., Stalder M. Residual stress sates of graded Cu/W materials. Materials Science Forum, 1999, v.308-311, pp.1018-1023.
4. Bokuchava G.D., Shamsutdinov N.R., Schreiber J., Stalder M. Determination of residual stresses in WCu gradient materials. Textures and Microstructures, 1999, v.33, pp.207-217.
5. Bokuchava G.D., Shamsutdinov N.R., Schreiber J. Residual stress states of graded W/Cu material. Proceedings of Tula State University, Seria Fizika, 1999, v.2, pp. 82-88.
6. Ivankina T.I., Kirilov A.S., Korobchenko M.L., Nikitin A.N., Roganov A.B., Sirotin A.P., Telepnev A.S., Ullemeyer K., Efimova G.A., Kireenkova S.M., Sobolev G.A., Sukhoparov W.A., Burilichev D.E. Experimental and measuring complex of neutronographic structure and texture analysis's for investigation of transformation processes in rocks under mechanical and thermal influences. Zavodskaya Laboratoriya. 1999, v.8, pp.26-34.
7. Ivankina T.I., Klima K., Locajicek T., Nikitin A.N., Pros Z. Study of anisotropy in an olivine xenolith using acoustic waves and neutron diffraction. Phyzika Zemli, 1999, v.35, pp.29-39.
8. Kockelmann H., Bokuchava G.D., Schreiber J., Taran Yu.V. Measurements of residual stresses in a shape welded steel tube by neutron and X-ray diffraction methods. Textures and Microstructures, 1999, v.33, pp.231-242.
9. Kockelmann H., Schreiber J., Taran Yu.V., Wright J.S. Investigation of residual stresses in a shape welded steel tube by the time-of-flight neutron diffraction technique. Materials Science Forum, 1999, v.321-324, pp.726-731.
10. Leiss B., Ullemeyer K. Texture characterisation of carbonate rocks and some implications for the modeling of physical anisotropies, derived from idealized texture types. Zeitschrift der Deutschen Geologischen Gesellschaft, 1999, v.150, pp.259-274.
11. Luzin V.V. Optimization of texture measurements. IV. The influence of the grain-size distribution on the quality of texture measurements. Textures and Microstructures, 1999, v.31, pp.177-186.
12. Niffenegger M., Taran Yu.V. Attempt of the $\sin^{2Y\text{-method}}$ application for residual stress measurements in a bimetal pipe by the time-of-flight neutron diffraction technique Proceedings of Tula State University, Seria Fizika, 1999, v.2, pp.25-32.
13. Nikitin A.N., Pereligin V.P., Burilichev D.E. An estimation of quick heavy nucleus damages in meteorites by means of neutron diffraction. Proceedings of Tula State University, Seria Fizika, 1999, v.2, pp.3-17.
14. Nikolayev D.I., Schaeben H. Calculus of the pole density function. Textures and Microstructures, 1999, v.33.
15. Nikolayev D.I., Schaeben H. Characteristics of the ultrahyperbolic differential equation governing pole density functions. Inverse Problems, 1999, v.15, pp.1603-1619.
16. Pirogov A.N., Teplyh A.E., Voronin V.I., Balagurov A.M., Pomjakushin V.Yu., Sikolenko V.V. Ferro- and antiferromagnetic structure of $LaMnO_{3+x}$. Fizika tverdogo tela, 1999, v.41, pp.103-109.

17. Siegesmund S., Weiss T., Vollbrecht A., Ullemeyer K. Marble as a natural building stone: rock fabrics, physical and mechanical properties. Zeitschrift der Deutschen Geologischen Gesellschaft, 1999, v.150, pp.237-257.
18. Taran Yu.V., Albertini G., Bruno G., Cernushi F., Rustichelli F. Residual stress investigations of a ferritic steel welded plate by nondestructive neutron diffraction technique. Proceedings of SPIE, 1999, v.3687, pp.350-359.
19. Ullemeyer K., Weber K. Texture analysis of rocks: lattice preferred orientation as an indicator of a complicated deformation history. Textures and Microstructures, 1999, v.33, pp.45-60.
20. Weiss T., Leiss B., Oppermann H., Siegesmund S. Quantitative fabric analyses of fresh and weathered marble building stones from the Marmorpalais in Potsdam, Germany. Zeitschrift der Deutschen Geologischen Gesellschaft, 1999, v.150, pp.313-332.

Small-Angle Scattering

1. Aksenov V., Avdeev M., Timchenko A., Serdyk I. General properties of protein surface of t-RNA binding priteins. Poverhnost', 1999, v.3, pp.3-9.
2. Cherezov V., Cheng A., Petit J.-M., Diat O., Caffrey M. Biophysics and synchrotron radiaion. Where the marriage fails. X-ray damage of lipid membranes and mesophases. Molecular and Cellular Biology, 1999 (in press).
3. Fan L., Svergun D., Volkov V., Aksenov V., Shcherbakova I., Koch M., May R., Serdyk I. Structural studies of the ribosome Thermus thermophilus by small-angle neutron and X-ray scattering. J.Appl.Cryst., 1999 (in press).
4. Gordeliy V., Dencher N., Hauss T., Kuklin A., Tougan-Baranovskaya A., Teixeira J., Yaguzhinskiy L., Bueldt G. Light-induced long-living hanges of bacteriorhodopsin structure in presence of guanidine hydrochloride. Biophys. Journal, 1999(in press).
5. Gorski N., Kalus J., Meier G., Schwahn D. Temperature dependence of the chemical potential of tetradecyldimethylaminoxide micelles in D_2O - a SANS study. Langmuir, 1999, v.10, pp.3476-3482.
6. Gorski N., Kalus J., Schwahn D. Pressure dependence of the chemical potential of tetradecyldimethylaminoxide micelles in D_2O - a SANS study. Langmuir, 1999, v.15, pp.8080-8085.
7. Grabcev B., Balasoiu M., Tarziu A. Kuklin A., Bica D. Application of contrast variation method in SANS experiments with ferrofluids. Journal of Magnetism and Magnetic Materials, 1999, v.201, pp.140-143.
8. Kiselev M., Lesieur P., Kiselev A., Grabiel-Madelmond C., Ollivon M. DMSO-induced dehydration of DPPC membranes studies by X-ray diffrection, small-angle neutron scattering and calorimetry. J.Alloys and Compounds, 1999, v.286, pp.195-202.
9. Kiselev M., Lesieur P., Kisselev A., Olivon M. Ice formation in model biological membranes in the presence of cryoprotectors. Nuclr. Inst&Methods, 1999 (in press).
10. Lesieur P., Kiselev M., Barsukov L., Lombardo D. Temperature induced micelle to vesicle transition: kinetic effects in the DMPC / NaCl / water system. J. Appl. Cryst., 1999 (in press).
11. Plestil J., Pospisil H., Kadec P., Tuzar Z., Kriz J., Gordeliy V. SANS study of multilayer nanoparticles based on block copolymer micelles. Macromol. Chem. Phys., 1999 (in press).
12. Serdyuk I., Ulitin A., Kolesnikov I., Vasiliev V., Aksenov V., Zaccai G., Svergun D., Kozin M., Willumeit R. Structure of a beheaded 30S ribosomal subunit from Thermus thermophilus. J. Molec. Biol., 1999, v.292, pp.633-639.
13. Shashkov S., Kiselev M., Tioutiounnikov S., Kisselev A., Lesieur P. The study of DMSO/water and DPPC/DMSO/water system by means of the IR spectroscopy, X-Ray and neutron small-angle scattering and calorimetry. Physica B, 1999 (in press).
14. Timchenko A., Trubeckaja O., Trubeckoi O., Aksenov V., Avdeev M., Obertur R., Kihara X., Serduk I. Analysis of conformation of humic substances by means of neutron and x-ray scattering. Poverhnost', 1999, v.4, pp.23-30.

Reflectometry, Pollarized Neutrons

1. Aksenov V.L, Nikitenko Yu.V., Kozhevnikov S.V., Radu F., Kruijs R., Rekveldt T. Generation of neutron standing waves at total reflection of polarized neutrons. Poverkhnost', 2000 (in press).

2. Aksenov V.L., Gundorin N.A., Nikitenko Yu.V., Popov Yu.P, Cser L. Observation of neutron standing waves at total reflection of polarized neutrons registered by precision gamma-spectroscopy methods. Poverkhnost', 2000 (in press).
3. Aksenov V.L., Nikitenko Yu.V. Neutron standing waves investigations with polarized neutrons, Physica B, 1999, v.267-268, pp.313-319.
4. Bondarenko I.V., Bodnarchuk V.I., Balashov S.N., Geltenbort P., Klein A.G., Kozlov A.V., Korneev D.A., Masalovich S.V., Nosov V.G., Frank A.I., Hoghoj P., Cimmino A. On the 90th anniversary of Frank's birthday. Neutron interference filter and fundamental experiments with ultracold neutrons. Physics of Atomic Nuclei, 1999, v.62, pp.721-737.
5. Deak L., Bayreuther G., Bottyan L., Gerdau E., Korecki J., Kornilov E.I., Lauter H.J., Leupold O., Nagy D.L., Petrenko A.V., Pasyuk-Lauter V.V., Reuther H., Richter E., Rohloberger R., Szilagyi E. Pure nuclear bragg reflection of periodic 56Fe/57Fe multilayer. J. Appl. Physics, 1999, v.85, pp.1-7.
6. Korneev D.A., Bodnarchuk V.I., Peresedov V.F., Zhuravlev V.V., Schebetov A.F. Inelastic mode of neutron reflectometer REFLEX for observation of surfase phonons and magnons. Physica B, 2000 (in press).
7. Korneev D.A., Bodnarchuk V.I., Yaradaikin S.P., Peresedov V.F., Ignatovich V.K., Menelle A., Gaehler R. Reflectivity studies of the coherent properties of neutrons. Physica B, 2000 (in press).
8. Lauter-Pasyuk V.V., Lauter H.J., Lorenz M., Leiderer P. Magnetic flux distribution inside an YBa2Cu3O7 superconducting thin film in the mixed state. Physica B, 1999, v.267-268, pp.149-153.
9. Lauter-Pasyuk V.V., Lauter H.J., Lorenz M., Petrenko A.V., Nikonov O., Aksenov V.L., Leiderer P. Magnetic field distribution around flux-lines in YBa2Cu3O7 superconducting thin films in a parallel field. Physica B, 2000 (in press).
10. Lauter-Pasyuk V.V., Lauter H.J., Toperverg B., Nikonov O., Kravtsov E., Milyaev M.A., Romashev L., Ustinov V. Magnetic off-specular neutron scattering from Fe/Cr multilayers. Physica B, 2000 (in press).
11. Toperverg B., Lauter-Pasyuk V., Lauter H., Nikonov O., Ausserre D., Gallot Y. Morphology of off-specular neutron scattering pattern from islands on a lamellar film. Physica B, 2000 (in press).

Inelastic Neutron Scattering

1. Beskrovni A., Danilkin S., Fuess H., Jadrowski E., Neova-Baeva M., Wieder T. Effect of Cr content on the crystal structure and lattice dynamics of FCC Fe-Cr-Ni-N austenitic alloys. J. of Alloys and Compounds, 2000 (in press).
2. Bobrowicz-Sarga L., Czarnecki P., Lewicki S., Natkaniec I., Wasicki J. Neutron diffraction study of thermal expansion and compressibility of piridinium nitrate and tetrafluoroborate. Materials Science Forum, 1999, v.321-324, pp.1107-1112.
3. Danilkin S., Delafosse D., Fuess H., Gavriljuk V., Ivanov A., Magnin T., Wipf H. Hydrogen vibrations in austenitic stainless steels. ILL Experimental Reports and Theory Activities, 1999.
4. Glazkov V.P., Kozlenko D.P., Savenko B.N., Somenkov V.A. INS study of vibrational spectra of ammonium halides NH_4I и NH_4F under high pressure. JINR communication, P14-99-162, 1999, Dubna, Russia.
5. Goremychkin E.A., Osborn R., Sashin I.L. Crystal field in the heavy fermion compound $CeAl_3$. Journ. of Applied Physics, 1999, v.85, pp.6046-6048.
6. Gvasaliya S.N., Lushnikov S.G., Sashin I.L., Siny I.G. Fractons in the vibrational spectra of the relaxor ferroelectric $PbMg_{1/3}Nb_{2/3}O_3$. Crystallography Reports, 1999, v.44, pp.284-288.
7. Gvasaliya S.N., Lushnikov S.G., Sashin I.L., Siny I.G., Shaplygina T.A., Blinc R. Effect of a disorder degree on the vibrational spectrum of relaxor ferroelectric $PbSc_{1/2}Ta_{1/2}O_3$. Physica B, 2000 (in press).
8. Holderna-Natkaniec K., Natkaniec I. Molecular dynamics of bicyclo 2.2.1 heptyl substituents by the NMR and neutron scattering methods. Molecular Physics Reports, 1999, v.25, pp.78-85.
9. Holderna-Natkaniec K., Natkaniec I., Khavryutchenko V.D. Low frequency internal vibrations of norbornane and its derivatives studied by IINS and quantum chemistry calculations. Neutrons and Numerical Methods - N_2M, AIP Conference proceedings 479, American Institut of Physics, Woodbury, New York , 1999, p.187-190.
10. Kozlenko D.P., Lewicki S., Wasicki J., Nawrocik W., Savenko B.N. NMR study of ammonium reorientation motion in NH_4Br at high pressure. J. Phys.: Condens. Matter, 1999, v.11, pp.7175-7183.
11. Lushnikov S.G., Gvasaliya S.N., Siny I.G., Goremychkin E.A., Sashin I.L. Anomalous behaviour of the phonon spectrum of the relaxor ferroelectric PMN at low temperatures. Ferroelectrics, 1999, v.226, pp.147 - 157.

12. Malenkov G.G., Averkiev A.A., Bobrowicz-Sarga L., Bragin S.I., Natkaniec I., Smirnov L.S. Neutron scattering by heavy water and ice under hydrostatic pressure of argon. Crystallography Reports, 1999, v.44, pp.62-68.
13. Malenkov G.G., Averkiev A.A., Bobrowicz-Sarga L., Bragin S.I., Natkaniec I., Smirnov L.S. Neutron scattering study of heavy water and ice under hydrostatic Ar pressure. Materials Science Forum, 1999, v.321-324, pp.872-877.
14. Malenkov G.G., Natkaniec I., Smirnov L.S., Bobrowicz-Sarga L., Bragin S.I. Neutron scattering investigation of ice under hydrostatic helium pressure. High Pressure Research, 1999, v.16, pp.201-214.
15. Martinez-Sarrion M.L., Mestres L., Beskrovnyi A.I., Natkaniec I., Smirnov L.S., Shelkova I.G. X-ray and neutron powder diffraction investigations of $Rb_{2-x}(NH_4)_xSO_4$ system. Poverhnost', 1999, v.2, pp.16-20.
16. Natkaniec I., Holderna-Natkaniec K., Kalus J., Khavryutchenko V.D. Neutron spectromerty and numerical simulations of low-frequency internal vibrations in solid xylenes. Neutrons and Numerical Methods -N_2M, AIP Conference proceedings 479, American Institut of Physics, Woodbury, New York, 1999, p.191-194.
17. Novikov A.G., Rodnikova M.N., Barthel J., Sobolev O.V. Quasielastic neutron scattering of aqueous tetrabutylammonium chloride solutions. J.of Mol.Liquids, 1999, v.79, pp.203-212.
18. Novikov A.G., Rodnikova M.N., Savostin V.V., Sobolev O.V. The study of hydration effects in aqueous solutions of LiCl and CsCl by inelastic neutron scattering. J. of Mol. Liquids, 1999, v.82, pp.83-104.
19. Novikov A.G., Savostin V.V., Shimkevich A.L., Zaezjev M.V. Oxygen microscopic dynamics in liquid potassium studied by inelastic neutron scattering. J. of Non-Cryst. Solids, 1999, v.250-252, pp.120-123.
20. Osborn R., Goremychkin E.A., Sashin I.L., Murani A.P. Inelastic neutron scattering study of the spin dynamics of $Yb_{1-x}Lu_xAl_3$. Journ. of Applied Physics, 1999, v.85, pp.5344-5346.
21. Pawlukojc A., Natkaniec I., Malarski Z., Leciejewicz J. The dynamical pattern of the 2-aminopyrazine-3-carboxylic acid molecule by inelastic incoherent neutron scattering, Raman spectroscopy and ab-initio calculations. Journal of Molecular Structure, 2000, v.516, pp.7-14.
22. Radulescu A., Padureanu I., Rapeanu S.N., Beldiman A., Ion M., Kozlov Zh.A., Semenov V.A. Low-frequency collective modes in the superionic phase of lead fluoride studied by quasielastic cold neutron scattering. Physical Review B, 1999, v.59, p.3270.
23. Radulescu A., Padureanu I., Rapeanu S.N., Beldiman A., Kozlov Zh.A., Semenov V.A. Low-frequency excitations in zirconium hydrides. JINR communications, E14-99-165, 1999, Dubna, Russia.
24. Shuvalov L.A., Sulyanov S.N., Natkaniec I., Smirnov L.S., Stoletova I.M. X-ray and neutron powder diffraction from $Rb_{1-x}(NH_4)_xSCN$. Poverhnost', 1999, v.2, pp.39-43.
25. Smirnov L.S., Ivanov A.N., Kolesnikov A.I., Natkaniec I. "In situ" neutron scattering studies of ice under high pressure. High Pressure Research, 1999, v.16, pp.187-199.
26. Sumin V.V., Chimid G., Muzychka A.Yu., Rashev C., Sarivanov L., Fykin L.E. The neutron spectroscopy proof of the strong Cr-N interaction in nitrogen stainless steels. Fizika metallov i metallovedenie, 1999, v.87, pp.65-71.
27. Sumin V.V., Chimid G., Muzychka A.Yu. Modelling of complexes of defects in solid solution of transition metals. Fizika metallov i metallovedenie, 2000, (in press).
28. Zaezjev M.V., Novikov A.G., Savostin V.V. Isochoric specific heat and anharmonicity for liquid potassuim. J.of Non-Cryst. Solids, 1999, v.250-252, pp.124-127.

Accelerated Ions and SR

1. Kobzev A.P. Element depth profiling in implanted samples. Nukleonika, 1999, v.44, pp. 309-315.
2. Kobzev A.P., Nikonov O.A., Peskov B.G., Uljanov V.A., Shchebetov A.F. Investigation of multilayer structures by means of charged-particle scattering. Yadernaya Fizika, 1999, v.62, pp.816-823.
3. Pogrebnjak A.D., Kobzev A.P., Gritsenko B.P., Sokolov S., Bazyl E., Sviridenko N.V., Valyaev A., Plotnikov S.V. Effect of Fe and Zr ion implantation and high-current electron beam treatment on chemical and mechanical properties of Ti-V-Al alloy. Jpn. J. Appl. Phys., 1999, v.38, pp.L248-L251.
4. Popov Yu.P., Sedyshev P.V., Kobzev A.P., Parzhitski S.S., Gundorin N.A., Serov D.G., Sedysheva M.V. Measurement of the *M*1 radiative strength function in Fe resonances by using the shift of the primary gamma line emitted upon the capture of intermediate-energy neutrons. Yadernaya Fizika, 1999, v.62, pp.886-891.

Contribution to the Conferences

1. Aksenov V.L., Gundorin N.A., Nikitenko Yu.V., Kozhevnikov S.V., Radu F. Investigation of the magnetization vector profile in a Fe-Gd bylauer. RSNE-99, May 23-27, 1999, Moscow, Russia.
2. Aksenov V.L., Gundorin N.A., Nikitenko Yu.V., Popov Yu.P., Cser L. Observation of neutron standing waves at total reflection of polarized neutrons by precision gamma-spectroscopy. ECNS'99, September 1-4, 1999, Budapest, Hungary.
3. Aksenov V.L., Kozhevnikov S.V., Nikitenko Yu.V. Refraction of polarized neutrons on boundaries of a magnetic film. ECNS'99, September 1-4, 1999, Budapest, Hungary.
4. Aksenov V.L., Kozhevnikov S.V., Nikitenko Yu.V. Spin-flipped transmission of polarized neutrons through Co film on glass. ECNS'99, September 1-4, 1999, Budapest, Hungary.
5. Aksenov V.L., Kozhevnikov S.V., Nikitenko Yu.V., Lauter H. Reflection and refraction of spin-flip neutrons in a Fe-Gd sructure. ECNS'99, September 1-4, 1999, Budapest, Hungary.
6. Aksenov V.L., Nikitenko Yu.V. Neutron standing waves and their application. RSNE-99, May 23-27, 1999, Moscow, Russia.
7. Aksenov V.L., Nikitenko Yu.V., Kozhevnikov S.V. Investigation of the refraction of polarized neutron beams in a magnetic non-collinear medium. RSNE-99, May 23-27, 1999, Moscow, Russia.
8. Aksenov V.L., Nikitenko Yu.V., Kozhevnikov S.V. Investigation of the refraction of polarized neutron beams in a FeAlSi thick magnetic film. RNIKS-99, September 13-17, 1999, Obninsk, Russia.
9. Aksenov V.L., Nikitenko Yu.V., Kozhevnikov S.V. Non-specular reflection of neutrons from a Fe-Gd film. RNIKS-99, September 13-17, 1999, Obninsk, Russia.
10. Aksenov V.L., Nikitenko Yu.V., Radu F., Gledenov Yu.M., Sedyshev P.V. Observation of resonance enchanced neutron standing waves through (n,) reaction. ECNS'99, September 1-4, 1999, Budapest, Hungary.
11. Balagurov A.M., Belushkin A.V., Kozlenko D.P., Savenko B.N. Glazkov V.P., Somenkov V.A., Syrykh G.F., Lewicki S., Wasicki J., Nawrocik W., McGreevy R.L., Zetterstrm P. Dynamics of Ammonium Halides Under High Pressure. 6th International Seminar on Neutron Scattering Investigation in Condensed Matter, April 29 - May 1, 1999, Poznan, Poland.
12. Balagurov A.M., Pomjakushin V.Yu., Sheptyakov D.V., Aksenov V.L. Neutron scattering studies of the CMR-materials: new results. RNIKS-99, September 13-17, 1999, Obninsk, Russia.
13. Balagurov A.M., Pomjakushin V.Yu., Sheptyakov D.V., Aksenov V.L., Babushkina N.A., Belova L.M., Gorbenko O.Yu., Kaul A.R. Changes in the atomic and magnetic structure of $(La_{0.25}Pr_{0.75})_{0.7}Ca_{0.3}MnO_3$ induced by the isotopic substitution of ^{18}O for ^{16}O. RSNE-99, May 23-27, 1999, Moscow, Russia.
14. Balagurov A.M., Pomjakushin V.Yu., Simkin V.G. High-resolution neutron Fourier diffraction for powders and single crystals. IUCr XVIII, August 4-13, 1999, Glasgow, Scotland.
15. BalagurovA.M. Atomic and magnetic structure of manganites. ECNS'99, September 1-4, 1999, Budapest, Hungary.
16. Belushkin A.V., Kozlenko D.P., McGreevy R.L., Savenko B.N., Zettertsrm P. A. Study of orientational disorder in ND_4Cl by the reverse Monte Carlo method. RNIKS-99, September 13-17, 1999, Obninsk, Russia.
17. Beskrovnyi A., Danilkin S., Fuess H., Jadrovski E., Neova-Baeva M., Wieder T. Crystal structure and lattice dynamics of Fe-Cr-Mn-Ni-N austenitic steels. ECNS'99, September 1-4, 1999, Budapest, Hungary.
18. Bogoyavlenskii I.V., Puchkov A.V., Skomorokhov A. Study of the Phonon-Maxon region of the liquid helium dispersion curve - the latest results. XXII Intern.Conf.on Low Temp.Physics, August 4-11, 1999, Helsinki, Finland.
19. Bogoyavlenskii I.V., Puchkov A.V., Skomorokhov A. The correlation between Bose condensation and helium excitations in neutron scattering study. ECNS-99, September 1-4, 1999, Budapest, Hungary.
20. Bokuchava G, Schreiber J., Shamsutdinov N., Stalder M. Residual stress studies in graded W/Cu materials by neutron diffraction method. ECNS'99, September 1-4, 1999, Budapest, Hungary.
21. Bokuchava G.D. Application of high resolution Fourier diffractometer at IBR-2 reactor for strain measurements. SSNS-99, August 7-13, 1999, Zuoz, Switzerland.
22. Bruno G., Albertini G., Cernushi F., Taran Yu.V., Rustichelli F. A reverse time-of-flight approach to neutron diffraction residual stress investigations on a UNI-Fe510D steel welded plate. ECNS-99, September 1-4, 1999, Budapest, Hungary.
23. Burilichev D.E., Ivankina T.I., Klima K., Locajicek T., Nikitin A.N., Pros Z. Investigation of rock samples by neutron diffraction and ultrasonic sounding. ECNS-99, September 1-4, 1999, Budapest, Hungary.
24. Burilichev D.E., Ivankina T.I., Klima K., Locajicek T., Nikitin A.N., Pros Z. Investigation of olivine xenolithes by neutron diffraction and ultrasonic sounding at various confining pressures. NSHP, September 29-October 2, 1999, Dubna, Russia.
25. Cser L., Holderna-Natkaniec K.,. Natkaniec I., Pawlukojc A. Neutron spectroscopy and QC modeling of the low frequency internal vibrations of mesitylene. ECNS-99, September 1-4, 1999, Budapest, Hungary.
26. Danilkin S., Delafosse D., Fuess H., Gavriljuk V., Ivanov A., Magnin T., Wipf H. Hydrogen vibrations in austenitic stainless steels. ECNS-99, September 1-4, 1999, Budapest, Hungary.

27. Frischbutter A., Scheffzuek C., Walther K. Deformation experiments on quartz for strain/stress-analysis by neutron time-of-flight diffraction. Int. Conf. Deformation Mechanisms, Rheology, Microstructures, March 22-24, 1999, Neustadt an der Weinstrasse, Germany.
28. Guberman D.M., Ivankina T.I., Klima K., Locajicek T., Nikitin A.N., Pros Z., Smirnov Yu.P., Ullemeyer K. Textures and elastic anisotropies of amphibolites from the Kola Superdeep Borehole. Meeting on Project No.408 (UNESCO) „Comparison of composition, structure and physical properties of rocks and minerals in the Kola Superdeep Borehole (KSDB-3) and their homologues on the surface, September 1-7, 1999, Apatity-Zapolyarny, Russia.
29. Gutberlet T., Kiselev M., Heerklotz H., Klose G. SANS study of mixed POPC/C12En aggregates. ECNS-99, September 1-4, 1999, Budapest, Hungary.
30. Holderna-Natkaniec K., Natkaniec I., Pawlukojc A., Khavryuthenko V.D. Neutron spectroscopy and QC modeling of methyl dynamics in 1- and 2-methylnaphthalene crystals. ECNS-99, September 1-4, 1999, Budapest, Hungary.
31. Ishmaev S.N., Lisichkin Y.V., Puchkov A.V., Semenov V.A., Svab E., Syrykh G.F. Neutron scattering law study of isotopic Ni-B metallic glasses. ECNS'99, September 1-4, 1999, Budapest, Hungary.
32. Ivankina T.I., Nikitin A.N., Telepnev A.S., Sukhoparov V.A., Ullemeyer K., Efimova G.A., Kireenkova S.M., Sobolev G.A., Walther K. New possibilities for investigation of physical properties and processes in geological materials under thermal deformation and simultaneous ultrasonic and neutron diffraction measurements. RNIKS-99, September 13-17, 1999, Obninsk, Russia.
33. Ivankina T.I., Nikitin A.N., Telepnev A.S., Ullemeyer K., Efimova G.A., Kireenkova S.M., Sobolev G.A., Sukhoparov V.A., Walther K. Texture and physical properties of marble deformed at 20-250°C. NSHPI, September 29 - October 2, 1999, Dubna, Russia.
34. Ivankina T.I., Nikitin A.N. Investigation of anisotropy of deep rocks by neutron diffraction and ultrasonic sounding. The Second Conference "Physical-Chemical and Petrophysical Researches in Earth's Sciences", October 25-26, 1999, Moscow, Russia.
35. Ivankina T.I., Nikitin N.N., Lokajicek T., Pros Z., Klima K., Ullemeyer K. Textures and elastic anisotropies of amphibolites from the Kola borehole. ICOTOM-12, August 9-13, 1999, Montreal, Canada.
36. Ivankina T.I., Nikitin N.N., Sobolev G.A., Sukhaparov V.A., Telepnev A.S., Ullemeyer K., Walther K. Influence of temperature and long-time loading on texture and physical property variations of a calcite marble. Int. Conf. on Textures and Physical Properties of Rocks, October 12-16, 1999, Goettingen, Germany.
37. Kiselev M.A., Kisselev A.M., Borbely S., Lesieur P. The phospholipid vesicles structure in the presence of cryoprotectors. RNIKS-99, September 13-17, 1999, Obninsk, Russia.
38. Kiselev M.A., Lesieur P., Kisselev A.M., Kutuzov S.A., Borbely S., Lombardo D., Ollivon M. Investigations of ternary phospholipid/cryoprotector/water systems. RSNE-99, May 23-27, 1999, Moscow, Russia.
39. Kiselev M.A., Lesieur P. The application of small-angle X-ray scattering to the study of model biological membranes at synchrotron source DCI. NSHP-II, September 29 - October 2, 1999, Dubna, Russia.
40. Klein H., Ullemeyer K., Brokmeier H.-G. Texture determination with X-rays and neutrons - advanced methods. Int. Conf. on Textures and Physical Properties of Rocks, October 12-16, 1999, Goettingen, Germany.
41. Kozhevnikov S.V. Neutron spectrometry and monochromatization using spin-flip and spatial beam-splitting. NOP-99, November 25-27, 1999, Villigen, Switzerland.
42. Kozhevnikov S.V. Spin-flip and beam-splitting of polarized neutrons transmitted through a Co film on glass. NOP-99, November 25-27, 1999, Villigen, Switzerland.
43. Kozlenko D.P., Balagurov A.M., Savenko B.N., Glazkov V.P., Somenkov V.A., Hull S. Neutron scattering study of structure and dynamics of ammonium halides under high pressure. IUCr XVIII, August 4-13, 1999, Glasgow, Scotland.
44. Lauter-Pasyuk V.V. Flux-lines distribution in the Ht_c films. User meeting on neutron scattering, May 25-27, 1999, Potsdam, Germany.
45. Lauter-Pasyuk V.V., Lauter H.J., Lorenz M., Petrenko A.V., Nikonov O., Aksenov V.L., Leiderer P. Magnetic field distribution around flux-lines in $YBa_2Cu_3O_7$ superconducting thin films in a parallel field. ECNS'99, September 1-4, 1999, Budapest, Hungary.
46. Lauter-Pasyuk V.V., Lauter H.J., Toperverg B., Nikonov O., Kravtsov E., Milyaev M.A., Romashev L., Ustinov V. Magnetic off-specular neutron scattering from Fe/Cr multilayers. ECRS-5, September 28-30, 1999, Delft-Noordwijkerhout, Netherlands.
47. Lesieur P., Kiselev M.A., Barsukov L. Temperature induced micelle to vesicle transition. Workshop on time resolved evolution of structure in soft condensed matter under flow, January 22-23, 1999, Leuven, Belgium.
48. Lesieur P., Lombardo D., Barsukov L.I., Kiselev M.A.. Temperature-iduced micelle to vesicle Transition in the DMPC/sodium cholate system: a synchrotron radiation SAXS study. NATO ASI on soft condensed matter, April 6-16, 1999, Geilo, Norway.

49. Lesieur P., Kiselev M.A., Barsukov L.I. Micelle to vesicle transition in the DMPC/NaC system. XI-th international conference on small-angle scattering, May 17-20, 1999, Brookhaven, USA.
50. Locajicek T., Pros Z., Klima K., Nikitin A.N., Ivankina T.I., Ullemeyer K., Smirnov Y.P., Guberman D.M., Kouznetzov Y. Laboratory investigation of elastic anisotropy and texture of rocks from Kola Super Deep Borehole SG-3. Int. Conf. on Textures and Physical Properties of Rocks, October 12-16, 1999, Goettingen, Germany.
51. Lushnikov G.S., Belushkin A.V., S.N.Gvasaliya S.N., Natkaniec I., Shuvalov L.A., Smirnov L.S., Dolbinina V.V. Inelastic neutron scattering study of the $Cs_5H_3(SO_4)_4*0.5H_2O$ crystal and its deuterated analog. ECNS'99, September 1-4, 1999, Budapest, Hungary.
52. Lychagina T., Brokmeier H.-G. Practical aspects of calculating elastic properties of textured hexagonal polycrystals. ICOTOM-12, August 9-13, 1999, Montreal, Canada.
53. Majerz I., Pawlukojc A., Sobczyk L., Dziembowska T., Grech E., Szady-Chelmieniecka A. The infra-red, raman and inelastic neutron scattering studies on 5-Nitro-N- Salicylidenethylamine. XIIIth Conference-Workshop Horizons in Hydrogen Bond Research, September 2-9, 1999, Swieradow-Zdroj, Poland.
54. Malenkov G.G., Zheligovskaya E.A., Averkiev A.A., Natkaniec I., Smirnov L.S., Bobrowicz-Sarga L., Bragin S.I. Dynamics of hydrogen bonded water frameworks under high pressure: neutron scattering and computer simulation. NSHP-II, September 29 - October 2, 1999, Dubna, Russia.
55. Morozov S.I. Band and local modes of hydrogen in V-O-H interstitial phases. ECNS'99, September 1-4, 1999, Budapest, Hungary.
56. Natkaniec I., Martinez Sarrion M.L., Mestres L., Smirnov L.S. Ammonium dynamics and structural phase transition in $Rb_{1-x}(NH_4)_xI$ mixed crystals at 20 K. ECNS'99, September 1-4, 1999, Budapest, Hungary.
57. Natkaniec I., Mikuli E., Migdal-Mikuli A. Phase transitions and water dynamics in $[Mn(H_2O)_6(ClO_4)]_2$, studied by neutron scattering methods. IUCr XVIII, August 4-13, 1999, Glasgow, Scotland.
58. Natkaniec I., Smirnov L.S., Telepnev A.S., Sukhoparov V.A., Bragin S.I. Neutron investigations of D_2O in the region of the metastable phase of ice IV. RNIKS-99, September 13-17, 1999, Obninsk, Russia.
59. Natkaniec I., Yuzyuk Yu.I., Torgashev V.I., Mestres L., Smirnov L.S. The variations of vibrational spectra of b-$LiNH_4SO_4$ at phase transitions studied by inelastic incoherent neutron and Raman scattering. ECNS'99, September 1-4, 1999, Budapest, Hungary.
60. Neova-Baeva M., Beskrovni A., Danilkin S., Fuess H., Jadrowski E., Wieder T. X-Ray and neutron study of crystal structure and lattice dynamics of Fe-Cr-Mn-and Fe-Cr-Ni-nitrogen steels with different Mn and Cr content. Deutsche Neutronenstreutagung, May 25-27, 1999, Potsdam, Germany.
61. Nikitin A.N. New possibilities for investigation of physical properties of rocks using modern methods of experimental physics. The Seminar of the Scientific Council on using of underground space and underground building (RAN), November 29, 1999, Moscow, Russia.
62. Nikolayev D.I., Luzin V.V., Lychagina T., Dzjuba A.A., Kogan V.A., Te Nijenhuis J. X'Pert texture: overview of a software package for quantitative texture analysis. ICOTOM-12, August 9-13, 1999, Montreal, Quebec, Canada.
63. Novikov A., Padureanu I., Savostin V. Atomic dynamics in liquid gallium. ECNS'99, September 1-4, 1999, Budapest, Hungary.
64. Novikov A.G., Rodnikova M.N., Sobolev O.V. The investigation of hydrophobic hydration effects. ECNS'99, September 1-4, 1999, Budapest, Hungary.
65. Pawlukojc A., Leciejewicz J. Ab-initio and DFT calculation of hydrogen bonds properties in m-amonobenzoic acid dimer. XIIIth Conference-Workshop Horizons in Hydrogen Bond Research, September 2-9, 1999, Swieradow-Zdroj, Poland.
66. Popov Yu.P., Voinov A.V., Sedyshev P.V., Parzhitski S.S., Kobzev A.P., Gundorin N.A., Serov D.G. Partial radiative capture cross section measurements on ^{58}Ni. NSHP-II, September 29 - October 2, 1999, Dubna, Russia.
67. Radulescu A., Padureanu I., Beldiman A., Rapeanu S.N., Kozlov Zh.A., Semenov V.A. Observation of low-frequency excitations of hydrogen in zirconium. ECNS'99, September 1-4, 1999, Budapest, Hungary.
68. Savenko B.N., Aksenov V.L., Balagurov A.M., Glazkov V.P., Kozlenko D.P., Sheptyakov D.V., Somenkov V.A. DN-12 - time of flight neutron spectrometer for investigation of structure and dynamics of microsamples. ECNS'99, September 1-4, 1999, Budapest, Hungary.
69. Schaeben H., Nikolayev D.I. Dual forms of texture analysis. ICOTOM-12, August 9-13, 1999, Montreal, Canada.
70. Schaeben H., Nikolayev D.I. Texture analysis of heterogeneous data. Int. Conf. on Textures and Physical Properties of Rocks, October 12-16, 1999, Goettingen, Germany.
71. Scheffzuek C. Texture and microstructure of halite at a halite-basalt contact. ICOTOM-12, August 9-13, 1999, Montreal, Canada.

72. Scheffzuek C., Frischbutter A., Walther K. Neutron diffraction strain investigation of sandstones undergoing applied stresses. ICOTOM-12, August 9-13, 1999, Montreal, Canada.
73. Scheffzuek C., Walther K., Frischbutter A. Applied and residual stress/strain measurements with neutron time-of-flight diffraction: application to sandstones. Int. Conf. on Textures and Physical Properties of Rocks, October 13-16, 1999, Goettingen, Germany.
74. Scheffzuek C., Walther K., Frischbutter, A. Strain measurements on geomaterials by neutron time-of-flight diffraction. ECRS-5, September 28-30, 1999, Delft-Noordwijkerhout, Netherlands.
75. Sheka E.F., Natkaniec I., Nikitina E., Khavryutchenko V., Barthel H. INS study of intermolecular interaction at the silicone-fumed silica interface. ECNS'99, September 1-4, 1999, Budapest, Hungary.
76. Sheptyakov D.V., Balagurov A.M., Pomjakushin V.Yu., Aksenov V.L., Babushkina N.A., Belova L.M, Gorbenko O.Yu., Kaul A.R., Fischer P., Gutmann M., Keller L. Peculiarities of atomic and magnetic structures of $(La_{1-y}Pr_y)_{0.7}Ca_{0.3}MnO_3$ (0.50 J y J0.75). IUCr XVIII, August 4-13, 1999, Glasgow, Scotland.
77. Smirnov L.S., Natkaniec I., Watanabe J., Kasahara M., Yagi T. Inelastic incoherent neutron and Raman scattering from the $[K_{1-x}(NH_4)_x]_3H(SO_4)_2$ mixed crystals. ECNS'99, September 1-4, 1999, Budapest, Hungary.
78. Stipp M., Heilbronner R., Leiss B., Stuenitz H., Ullemeyer K. Combined CIP-, X-ray and neutron diffraction texture analysis of mylonitic quartz veins from the Tonale fault. Int. Conf. on Textures and Physical Properties of Rocks, October 12-16, 1999, Goettingen, Germany.
79. Taran Yu.V., Schreiber J. The time-of-flight neutron diffraction measurements of residual stress in a shape welded steel tube. RNIKS-99, September 13-17, 1999, Obninsk, Russia.
80. Taran Yu.V., Schreiber J., Mikula P., Lukas P., Neov D., Vrana M. Neutron diffraction study of fatigue behavior of a low-carbon stainless steel. ECNS'99, September 1-4, 1999, Budapest, Hungary.
81. Taran Yu.V., Schreiber J., Mikula P., Lukas P., Neov D., Vrana M. Neutron diffraction investigation of low and high cycle fatigue austenitic stainless steels. ECRS-5, September 28-30, 1999, Delft-Noordwijkerhout, Netherlands.
82. Taran Yu.V., Schreiber J., Wright J.S. The time-of-flight neutron diffraction measurements of residual stress in a shape welded steel tube. ECRS-5, September 28-30, 1999, Delft-Noordwijkerhout, Netherlands.
83. Taran Yu.V., Wright J.S. Triaxial residual stresses measurements in a shape welded steel tube on the ENGIN stress-diffractometer. ECNS'99, September 1-4, 1999, Budapest, Hungary.
84. Toperverg B. , Lauter-Pasyuk V., Lauter H., Nikonov O., Ausserre D., Gallot Y. Morphology of off-specular neutron scattering pattern from islands on a lamellar film. ECRS -5, September 28-30, 1999. Delft-Noordwijkerhout, Netherlands.
85. Toperverg B.P., Lauter-Pasyuk V.V., Lauter H., Nikonov O.A., Aksenov V.L. Non-specular scattering of neutrons on surface inhomogeneity isles of lamelar polymers. RNIKS-99, September 13-17, 1999, Obninsk, Russia.
86. Toperverg B., Lauter-Pasyuk V.V., Lauter H., Nikonov O., Ausserre D., Gallot Y. Off-specular neutron scattering from islands on a lamellar film. ECNS'99, September 1-4, 1999, Budapest, Hungary.
87. Ullemeyer K., Braun G., Dahms M., Kruhl J.H., Olesen N., Siegesmund S. Current methods of texture analysis in geosciences: application to a muscovite-bearing quartzite. Int. Conf. on Textures and Physical Properties of Rocks, October 13-16, 1999, Goettingen, Germany.
88. Ullemeyer K., Spalthoff P., Leiss B., Weber K. TOF texture investigations of geological samples. ECNS'99, September 1-4, 1999, Budapest, Hungary.
89. Walther K, Frischbutter A., Scheffzuek C. Strain-messungen in geologischen proben mittels neutronen-flugzeitmethode am diffraktometer „Epsilon" in Dubna. Deutsche Neutronenstreutagung, May 25 -27, 1999, Potsdam, Germany.
90. Walther K., Frischbutter A., Lieckefett R., Scheffzuek C. A pressure device for strain measurements of geomaterials at the neutron diffractometer EPSILON. ICOTOM-12, August 9-13, 1999, Montreal, Canada.
91. Walther K., Frischbutter A., Scheffzuek C. Inhomogeneous strain distribution in sandstones as an effect of stratification - determined by neutron diffraction. 2nd Euroconference on World Stress Map: Deformation and Stress in the Earth's Crust, September 22-26, 1999, Aespoe-Oskarshamn, Sweden.
92. Walther K., Frischbutter A., Scheffzuek C. Intracrystalline strain measurements on Cretaceous sandstones using the TOF-method. XV. Tektonomechanik-Kolloquim, May 14-15, 1999, Universitaet Graz, Austria.
93. Walther K., Ivankina T.I., Nikitin A.N., Ullemeyer K. The influence of texture on the thermal expansion of calcite. Int. Conf. on Textures and Physical Properties of Rocks, October 12-16, 1999, Goettingen, Germany.
94. Walther K., Scheffzuek C., Frischbutter A. Neutron Time-of-Flight Diffractometer "EPSILON" for Strain Measurements: Layout and First Results. ECNS'99, September 1-4, 1999, Budapest, Hungary.
95. Watanabe J., Natkaniec I., Smirnov L.S., Kasahara M., Yagi T. Influence of pressure on the O-H...O hydrogen bond in $[K_{1-x}(NH_4)_x]_3H(SO_4)_2$ mixed crystals. NSHP-II, September 29 - October 2, 1999, Dubna, Russia.

96. Zlokazov V.B. Methods for mathematical analysis of the spectral distributions in neutron scattering studies. 6th International Seminar on Neutron Scattering Investigation in Condensed Matter, April 29 - May 1, 1999, Poznan, Poland.
97. Zlokazov V.B., Balagurov A.M. Rietveld analysis on the High Resolution Fourier Diffractometer. IUCr XVIII, August 4-13, 1999, Glasgow, Scotland.

NEUTRON NUCLEAR PHYSICS

Reviews

1. Bunakov V.E., Pikelner L.B. Parity and Time Reversal Violation in Neutron-Nucleus Reactions. Progress in Particle and Nuclear Physics. Vol.41. Oxford: Pergamon, 1998, p.337-392.
2. Nosov V.G., Frank A.I. Взаимодействие медленных нейтронов с движущимся веществом. Yad. Fiz., 1998, vol.61, No.4, p.686-696 (in Russian).

Experiments

1. Abov Yu.G., Alfimenkov V.P.., Galinskii E.M., Lason L., Mareev Yu.D., Novitsky V.V., Pikelner L.B., Tsulaya V.M., Tsulaya M.I., Chernikov A.N. Спектрометр поляризованных нейтронов. JINR, P13-99-130, Dubna, 1999, p.10 (in Russian).
2. Aksenov V.L., Nikitenko Yu.V, Radu F., Gledenov Yu.M, Sedyshev P.V., Petrenko A.V., Kozhevnikov S.V. Observation of Resonance Enhanced Neutron Standing Waves Using Charged Particle Emission After Neutron Capture. JINR, E3-98-383, Dubna, 1998, p. 6
3. Aksenov V.L.., Gundorin N.A., Nikitenko Yu.V., Popov Yu.P., Cser L. Наблюдение стоячих нейтронных волн при полном отражении нейтронов методом прецизионной гамма- спектроскопии. JINR, P3-98-374, Dubna,1998, p. 8 (in Russian).
4. Alexandrov Yu.A. О знаке и величине среднего квадрата внутреннего зарядового радиуса нейтрона. ЭЧАЯ, 1999, vol.30, issue 1, p.72-122 (in Russian).
5. Alexandrov Yu.A. Учителю. Воспоминания сотрудника Лаборатории нейтронной физики. Ф.Л. Шапиро: Человек и ученый: Книга воспоминаний, JINR, 97-377, Dubna,1998, p.176 (in Russian).
6. Alexeev A.A., Belousov Yu.V., Bergman A.A., Volkov A.N., Gledenov Yu.M., Goncharenko O.N., Grachev M.N., Kazarnovsky M.V., Matushko V.L., Mostovoi V.I.., Novikov A.V., Novoselov S.A., Parzhitskii S.S., Popov Yu.P., Ryabov Yu.V., Stavisskii Yu.Ya. Третье поколение спектрометров по времени замедления нейтронов в свинце. Первые эксперименты и перспективы. Yad.Fiz., 1999, vol.62, No.5, p.851-854 (in Russian).
7. Alfimenkov V.P. Эксперименты с поляризованными нейтронами и ядрами. VIII School on Neutron Physics, Dubna, August-September, 1998. JINR, P3-98-240, Dubna,1998, p.31 (in Russian).
8. Alfimenkov V.P., Chernikov A.N., Lason L., Mareev Yu.D., Novitski V.V., Pikelner L.B., Skoy V.R., Tsulaya M.I., Gagarski A.M., et al. Investigations of Parity Violation and Interference Effects in ^{235}U Fission Induced by Resonance Neutrons. Nucl. Phys.A.,1999, v.645, N.1, p.31-46.
9. Bagryanov B.V., Kartashov D.G., Kuvshinov M.I., Muzychka A.Yu., Nekhaev G.V., Rogov A.D., Smirnov I.G., Stoica A.D., Strelkov A.V., Shvetsov V.N. Экспериментальная проверка метода динамического конвертора ультрахолодных нейтронов на импульсном реакторе БИГР. Yad.Fiz., 1999, vol.62, No.5, p.844-850 (in Russian).
10. Belyaev S.T., Gridnev K.A., Gromov K.Ya., Dzhelepov V.P., Kalinnikov V.G., Listengarten M.A., Lobashev V.M., Mikhailov V.M., Rimski-Korsakov A.A., Soloviev V.G., Kholnov Yu.V., Tchubinskii O.V. Памяти Бориса Сергеевича Джелепова. Usp. Fiz. Nauk, 1999, vol.169, No.1, p.105-106 (in Russian).
11. Bondarenko I.V., Balashov S.N., Krasnoperov A.V., Frank A.I. и др. Экспериментальная проверка закона дисперсии ультрахолодных нейтронов. JETP Lett.,, 1998, vol.67, issue 9,10, p.746-775 (in Russian).
12. Bondarenko I.V., Bodnarchuk V.I., Balashov S.N., Geltenbort P., Klein A.G., Kozlov A.V., Korneev D.A., Masalovich S.V., Nosov V.G., Frank A.I., Hoghoi P., Chimmino A. Нейтронные интерференционные фильтры в фундаментальных экспериментах с ультрахолодными нейтронами. Yad. Fiz., 1999, vol.62, No.5, p.775-791 (in Russian).

13. Boneva S.T., Vasilieva E.V., Simonova L.I.., Bondarenko V.A., Sukhovoj A.M., Khitrov V.A. Реакция (n,) в тяжелом ядре. Наблюдаемые эффекты проявления его структуры при возбуждениях до энергии связи нейтрона. Yad. Fiz., 1999, vol.62, No.5, p.892-899 (in Russian).
14. Borzakov S.B., Pokotilovskii Yu.N. Поиск возбужденного уровня дейтрона с помощью резонансного рассеяния -квантов. JINR, P15-99-70, Dubna, 1999, p.6 (in Russian).
15. Borzakov S.B. Andreyev A.N., Dermendjiev E., Filip A., Furman W.I., Panteleev Ts., Ruskov I., Zamyatnin Yu.S., Zeinalov Sh. Measurements of Delayed Neutron Yields from Thermal Neutron Induced Fission of ^{235}U, ^{233}U, ^{239}Pu and ^{237}Np. JINR, E3-98-145, Dubna, 1998, p. 16.
16. Borzakov S.B., Zamyatnin Yu.S., Panteleev Ts., Pavlov S.S., Ruskov I. Изучение кривых распада запаздывающих нейтронов при делении ^{235}U и ^{239}Pu тепловыми нейтронами. JINR, P3-99-208, Dubna, 1999, p.14 (in Russian).
17. Borzakov S.B.., Goverdovskii A.A., Dermendjiev E., Zamyatnin Yu.S., Kalinin A.I., Konovalov V.Yu., Ruskov I., Soloviev S.M. Параметры резонансов и сечение деления ^{237}Np нейтронами с энергиями ниже 1000 эВ. Yad. Fiz., 1999, vol.62, No.5., p.933-940 (in Russian).
18. Bunakov V.E., Novikov I.S., Skoy V.R. Анализ новых предложений по измерению CP-нарушения с помощью поляризованных резонансных нейтронов. Izv. RAN, ser.. fiz., 1999, vol.63, No.1, p.20-25 (in Russian).
19. Bunakov V.E., Novikov I.S., Skoy B.P. Сравнительный анализ экспериментов по проверке T- и P-инвариантности в нейтронных ядерных реакциях. Yad. Fiz., 1999, vol.62, No.5., p.855-871 (in Russian).
20. Bystritskii V.M., Grebenyuk V.M., Parzhitskii S.S., Pen'kov F.M., Stolupin V.A., и др. Астрофизический S-фактор в dd-взаимодействиях при ультранизких энергиях. JINR, Д15-99-163, Dubna, 1999, p.14.
21. Enik T.L., Mitsyna L.V., Samosvat G.S., Kharyuzov R.V. Спектрометр УГРА для измерения электрической поляризуемости нейтрона. JINR, P13-98-317, Dubna,1998, p. 6 (in Russian).
22. Frank A.I. Учителю. Воспоминания сотрудника Лаборатории нейтронной физики. Ф.Л. Шапиро: Человек и ученый: Книга воспоминаний. ОИЯИ, 97-377, Dubna,1998, p.152-155 (in Russian).
23. Furman W.I. Воспоминания о И.М. Франке. Илья Михайлович Франк: К 90-летию со дня рождения. JINR, 98-164, Dubna,1998, p.178-179 (in Russian).
24. Furman W.I. Учителю. Воспоминания сотрудника Лаборатории нейтронной физики. Ф.Л. Шапиро: Человек и ученый: Книга воспоминаний. JINR, 97-377, Dubna,1998, p.190-195 (in Russian).
25. Geltenbort P., Kartashov D.G., Lychagin E.V., Muzychka A.Yu., Nesvizhevskii V.V., Nekhaev G.V., Serebrov A.P., Strelkov A.V., Tal'daev P.P., Kharitonov A.G., Shvetsov V.H. Исследование малых передач энергии при хранении ультрахолодных нейтронов (УХН) в вещественных ловушках. JINR, P3-99-71, Dubna, 1999, p.24 (in Russian).
26. Gledenov Yu.M., Machrafi R., Oprea A., Salatski V.I., Sedyshev P.V., Szalanski P.I., Vesna V.A., Okunev I.S.. A Search for P-odd and P-even Correlation in the ^{35}Cl(n,p)^{35}S Reaction. Nucl. Phys. A654 (1999), p. 943-948.
27. Gledenov Yu.M., Machrafi R., Oprea A., Salatski V.I., Sedyshev P.V., Szalanski P.I., Vesna V.A., Okunev I.S. A Search for P-odd and P-even Correlation in the ^{35}Cl(n,p)^{35}S Reaction. Nucl. Phys. A654 (1999), p. 943-948.
28. Gledenov Yu.M., Machrafi R., Salatski V.I., Sedyshev P.V., Andrzejewski J., Szalanski P.I.. Testing an Ionization Chamber with Gaseous Samples and Measurements of the (n,a) Reaction Cross Section. Nucl. Inst. and Meth., A431 (1999), p. 201-207.
29. Gledenov Yu.M., Sedysheva M., Khuukhenkhuu G., Tang Guoyou, Zhang Guohui, Chen Zemin, Zhang Xuemei, Chen Yingtang. Cross Section and Angular Distribution Measurements of the Fast Neutron Induced (n,a) Reaction for Medium-Mass Nuclei. JINR Communication E3-98-375. Dubna, 1998.
30. Gledenov Yu.M., Sedysheva M.V., Khuukhenkhuu G., Tang Guoyou, Zhang Guohui, Zemin Chen, Zhang Xuemei, Chen Yingtang. Cross Section and Angular Distribution Measurements of the Fast Neutron Induced (n, a) Reaction for Medium-Mass Nuclei. JINR, E3-98-375, Dubna, 1998, p. 8.
31. Gledenov Yu.M., Mashrafi R., Sedyshev P.V., Salatskii V.I., Andrzeewski Yu., Shalanski P.I. Испытание ионизационной камеры на резонансных нейтронах для исследования газовых мишеней. JINR, P15-99-211, Dubna, 1999, p.6 (in Russian).
32. Gledenov Yu.M., Salatskii V.I., Sedyshev P.V., Stempinski M., Shalanski P.I. Измерение сечения реакции ^{35}Cl(n,p)^{35}S для тепловых нейтронов и параметры резонансов при энергиях 398 и 4249 эВ. Yad. Fiz., 1999, vol.62, No.5, p.877-885 (in Russian).
33. Grigoriev E.P., Khitrov V.A., Sukhovoj A.M., Vasilieva E.V. A Search for the -Decay of the ^{168}Er Compound Nucleus in the (n,2) Reaction. JINR, E3-99-146, Dubna, 1999, p.23.
34. Gromov K.Ya., Dzhabber D.K., Malikov Sh.R., Fominykh V.I., Kholnov Yu.V., Tsupko-Sitnikov V.V., Chumin V.G. Схема уровней ядра ^{217}At при -распаде ^{221}Fr. JINR, P6-99-17, Dubna, 1999, p.14 (in Russian).

35. Gromov K.Ya., Dzhabber D.K., Malikov Sh.R., Fominykh V.I., Kholnov Yu.V., Tsupko-Sitnikov V.V., Chumin V.G. Схема уровней ядер ^{217}At при -распаде ^{221}Fr. Izv. RAN, ser. fiz., 1999, vol.63, No.5, p.860-870 (in Russian).
36. Gundorin N.A. Прецизионная гамма-спектроскопия осколков деления ядер. VIII School on Neutron Physica, Dubna, August-September 1998. JINR, P3-98-240, Dubna,1998, p.34 (in Russian).
37. Ignatovich V.K. Воспоминания сотрудника Лаборатории нейтронной физики. Ф.Л. Шапиро: Человек и ученый: Книга воспоминаний. JINR 97-377, Dubna,1998, p.112-118 (in Russian).
38. Kharyuzov R.V. Воспоминания сотрудника Лаборатории нейтронной физики. Ф.Л. Шапиро: Человек и ученый: Книга воспоминаний. JINR, 97-377, Dubna,1998, p.132 (in Russian).
39. Kholnov Yu.V., Voinov A.V. Метод увеличения разрешения в спектрах совпадений различных излучений. Izv. RAN, ser. fiz., 1998, vol.62, No.11, p.2115-2118 (in Russian).
40. Kopach Yu.N., Popov A.B., Furman W.I., Gonin N.N., Kozlovsky L.K., Tambovtsev D.I., Kliman J. Исследование угловой анизотропии осколков деления выстроенных ядер ^{235}U резонансными нейтронами и роль JK-каналов. Yad. Fiz., 1999, vol.62, No.5, p.900-914 (in Russian).
41. Kopach Yu.N., Singer P., Mutterer M., Klemens M., et al. Angular Anisotropy of Prmpt Rays and Fragment Spin Alignment in Binary and Light-Charged-Particle-Accompanied Spontaneous Fission of ^{252}Cf. Phys. Rev. Lett., 1999, N.2, p.303-306.
42. Lowie L.Y., Bowman J.D., Corvi F., Sharapov E.I., et al. Parity Violation in Neutron Resonances in ^{107,109}Ag. Phys. Rev.C., 1999.- v.59, N.2., p.1119-1130.
43. Mohr P., Beer H., Oberhummer H., Rochow W., Sedyshev P.V., Volz S., Ziges A.. Neutron Capture of ^{26}Mg at kT=52 keV and the Resonance at E_n=68.7 keV. Preprint IKDA 99/09 (1999) Iinstitut fuer Kernphysik, Technishe Universitaet Darmstadt.
44. Mohr P., Beer H., Oberhummer H., Rochow W., Sedyshev P.V., Volz S., Ziges A.. Neutron Capture of ^{26}Mg at kT=52 keV and the Resonance at E_n=68.7 keV. Phys. Rev. C60 (1999) 017603.
45. Mohr P., Beer H., Oberhummer H., Rochow W., Sedyshev P.V., Volz S., Ziges A.. Neutron Capture of ^{26}Mg at kT=52 keV and the Resonance at E_n=68.7 keV. Preprint IKDA 99/09 (1999) Iinstitut fuer Kernphysik, Technishe Universitaet Darmstadt.
46. Mohr P., Sedyshev P.V., Beer H., Stadler W., Oberhummer H., Popov Yu.P., Rochow W. Neutron Capture of ^{46}Ca at Thermonuclear Energies. Phys.Rev.C59, (1999) 3410-3417.
47. Muzychka Al.Yu., Pokotilovski Yu.N., Geltenbort P. Search for Low-Energy Upscattering of Ultracold Neutrons from a Beryllium Surface. JINR, E3-98-41, Dubna, 1998, p. 14.
48. Nesvizhevsky V.V., Strelkov A.V., Geltenbort P., Yaidzhiev P.S. Наблюдение нового механизма потерь УХН в ловушках. JINR, P3-98-79, Dubna, 1998, p. 34 (in Russian).
49. Nesvizhevsky V.V., Strelkov A.V., Geltenbort P., Yaidzhiev P.S. Наблюдение нового механизма потерь УХН в ловушках. Yad. Fiz.,1999, vol.62, No.5., p.832-843.
50. Nikolenko V.G. Учителю. Воспоминания сотрудника Лаборатории нейтронной физики. Ф.Л. Шапиро: Человек и ученый: Книга воспоминаний. JINR, 97-377, Dubna,1998, p.168 (in Russian).
51. Nosov V.G., Frank A.I. Квантовая структура нейтронных пучков и возможности ее экспериментального установления. Yad. Fiz., 1999, vol.62, No.5, p.807-815 (in Russian).
52. Parzhitskii S.S. Воспоминания сотрудника Лаборатории нейтронной физики. Ф.Л. Шапиро: Человек и ученый: Книга воспоминаний, JINR, 97-377, Dubna,1998, p.125-126 (in Russian).
53. Pikelner Л.Б. Воспоминания о И.М. Франке. Илья Михайлович Франк: К 90-летию со дня рождения. ОИЯИ, 98-164, Дубна,1998, с.157-160 (in Russian).
54. Pokotilovski Yu.N. Interaction of Ultracold Neutrons with Liquid Surface Modes as a Possible Reason for Neutron Energy Spread During Long Storage in Fluid Wall Traps. JINR, E17-98-288, Dubna, 1998, p. 11.
55. Pokotilovski Yu.N. On the Question of Possible Experimental Observation of Anderson Localization of the Neutron. Europ. Phys.J., B., v.3, N.1, 1998, p. 105-107.
56. Pokotilovski Yu.N. Quasielastic Neutron Scattering by Diffusive Adsorbed Hydrogen as a Possible Reason for Ultracold Neutrons Energy Spread During Long Storage in Closed Traps. JINR, E3-98-310, Dubna,1998, p. 14.
57. Pokotilovskii Yu.N. Воспоминания сотрудника Лаборатории нейтронной физики. Ф.Л. Шапиро: Человек и ученый: Книга воспоминаний, JINR, 97-377, Dubna,1998, p.105-106 (in Russian).
58. Popov A.B. Воспоминания о И.М. Франке. Илья Михайлович Франк: К 90-летию со дня рождения. JINR, 98-164, Dubna,1998, p.147-152 (in Russian).
59. Popov A.B. Воспоминания сотрудника Лаборатории нейтронной физики. Ф.Л. Шапиро: Человек и ученый: Книга воспоминаний. JINR, 97-377, Dubna,1998, p.110-111 (in Russian).
60. Popov Yu.P. Воспоминания о И.М. Франке. Илья Михайлович Франк: К 90-летию со дня рождения. JINR, 98-164, Dubna,1998, p.153-156 (in Russian).

61. Popov Yu.P. Учителю. Воспоминания сотрудника Лаборатории нейтронной физики. Ф.Л. Шапиро: Человек и ученый: Книга воспоминаний. JINR, 97-377, Dubna,1998, p.160-163 (in Russian).
62. Popov Yu.P., Furman W.I. Илья Михайлович Франк. (23.10.1908-22.06.1990). Yad. Fiz.,1999, vol.62, No.5, p.773-774 (in Russian).
63. Popov Yu.P., Sedyshev P.V., Gundorin N.A., Sedysheva M.V., Kobzev A.P., Parzhitskii S.S. Анализ спектров нейтронов в области энергии 2-100 кэВ с использованием g- спектрометрии высокого разрешения. Izv. RAN, ser. fiz., 1998, vol.62, No.5, p.882-886 (in Russian).
64. Popov Yu.P., Sedyshev P.V., Kobzev A.P., Parzhitskii S.S., Gundorin N.A., Serov D.G., Sedysheva M.V. Измерение радиационной силовой функции M1-переходов в резонансах Fe с использованием смещения -линии при захвате нейтронов промежуточных энергий. Yad. Fiz., 1999, vol.62, No.5, p.886-891 (in Russian).
65. Pospisil S., Telezhnikov S.A. et. al. Secondary g-Rays of ^{159}Gd After Resonance Neutron Capture. Acta Polytechnica, v.38, N.3, 1998, p.37-38.
66. Samosvat G.S. Воспоминания о И.М. Франке. Илья Михайлович Франк: К 90-летию со дня рождения. JINR, 98-164, Dubna,1998, p.164-167 (in Russian).
67. Samosvat G.S. Учителю. Воспоминания сотрудника Лаборатории нейтронной физики Ф.Л. Шапиро: Человек и ученый: Книга воспоминаний. JINR, 97-377, Dubna,1998, p.180 (in Russian).
68. Sedyshev P.V., Mohr P., Beer H., Oberhummer H., Popov Yu.P., Rochow W. Measurement of Neutron Capture on ^{50}Ti at Thermonuclear Energies. Phys. Rev. C60 (1999) 054613.
69. Shapiro S.M., Strelkov A.V. Федор Львович Шапиро. Страницы биографии. Ф.Л. Шапиро: Человек и ученый: Книга воспоминаний. JINR, 97-377, Dubna,1998, p.5-20 (in Russian).
70. Sharapov E.I. Воспоминания о И.М. Франке. Илья Михайлович Франк: К 90-летию со дня рождения. JINR, 98-164, Dubna, 1998, p.185-187 (in Russian).
71. Sharapov E.I. Воспоминания сотрудника Лаборатории нейтронной физики. Ф.Л. Шапиро: Человек и ученый: Книга воспоминаний. JINR, 97-377, Dubna,1998, p.119-120 (in Russian).
72. Sharapov E.I., Bowman J.D., Crawford B.E., Delheij P.P.J, et al. Parity Nonconservation in Neutron Resonances in ^{133}Cs. Phys. Rev.C., 1999, v.59, N.3, p.1772-79.
73. Sharapov E.I., Bowman J.D., Crawford B.E., Delheij P.P.J., et al. Search for Parity Violation in ^{93}Nb Neutron Resonances. Phys. Rev.C., 1999, v.59, N.2, p.1131-1135.
74. Shevchenko N.V., Rakityansky S.A., Sofianos S.A., Belyaev V.B. Non-Radiative Synthesis of ^{7}Be in Solar Plasma. J.Phys.G: Nucl. Part. Phys., 1999, v.25, N.1, p.95-106.
75. Smith D.A., Bowman J.D., Crawford B.E., Sharapov E.I., et al. Neutron Resonance Spectroscopy of ^{117}Sn from 1 eV to 1.5 keV. Phys. Rev.C., 1999, v.59, p.2836-2843.
76. Strelkov A.V. Воспоминания сотрудника Лаборатории нейтронной физики. Ф.Л. Шапиро: Человек и ученый: Книга воспоминаний. JINR, 97-377, Dubna,1998, p.144-148 (in Russian).
77. Strelkov A.V. Федор Львович и история открытия ультрахолодных нейтронов. Ф.Л. Шапиро: Человек и ученый: Книга воспоминаний. JINR, 97-377, Dubna,1998, p.196-217 (in Russian).
78. Sukhovoj A.M., Khitrov V.A. Экспериментальная оценка плотности уровней тяжелого ядра, реально возбуждаемых в реакции (n,) при $E_{возб}$ < 3-4 МэВ. Yad. Fiz., 1999, vol.62, No.1, p.24-36 (in Russian).
79. Utsuro M., Ignatovich V.K. Experimental Test of the de Broglie Wave-Packet Description of the Neutron. Phys. Lett. A., 1998. v.246, N.1,2. p.7-15.
80. Varlamov V.E., Panteleev Ts.Ts., Strelkov A.V., Shvetsov V.N. Исследование нагрева ультрахолодных нейтронов на поверхности бериллия. JETP, 1998, vol.114, issue 3, p.786-797 (in Russian).
81. Vasilieva E.V., Sukhovoj A.M., Khitrov V.A. Экспериментальная оценка параметров, определяющих каскадный -распад компаунд-состояний тяжелых ядер. Наиболее вероятная энергетическая зависимость суммы радиационных силовых функций дипольных переходов для 0,52МэВ < E < B_n. JINR, P3-99-203, Dubna, 1999, p.16 (in Russian).
82. Vasilieva E.V., Sukhovoj A.M., Khitrov V.A. Экспериментальная оценка параметров, определяющих каскадный -распад компаунд- состояний тяжелых ядер. Наиболее вероятная плотность возбужденных состояний в интервале от 1-2 МэВ до B_n. JINR, P3-99-202, Dubna, 1999, p.22 (in Russian).
83. Vesna V.A., Gledenov Yu.M., Lebedev-Stepanov P.V., Okunev I.S., Sinyakov A.V., Tchuvilskii Yu.M., Shul'gina E.V. Поиск эффектов нарушения пространственной четности в g-переходе ^{7}Li*®g(M1)®^{7}Li (Eg=0.478 МэВ). Yad. Fiz., 1999, vol.62, p.565-576 (in Russian).
84. Zamyatnin Yu.S. Воспоминания о И.М. Франке. Илья Михайлович Франк: К 90-летию со дня рождения. JINR, 98-164, Dubna,1998, p.126-127 (in Russian).
85. Zamyatnin Yu.S. Воспоминания сотрудника Лаборатории нейтронной физики. Ф.Л. Шапиро: Человек и ученый: Книга воспоминаний, JINR 97-377, Dubna,1998, p.142-143 (in Russian).

86. Zeinalov Sh.S., Zeinalova O.V., Smirnov V.I. Приложение корреляционного метода к измерениям запаздывающих нейтронов при индуцированном тепловыми нейтронами делении ^{237}Np. JINR, P3-98-17, Dubna,1998, p.19 (in Russian).
87. Zhang Guohui, Tang Guoyou, Chen Jinxiang, Shi Zhaomin, Gledenov Yu.M., Khuukhenkhuu G., Sedysheva M., Chen Zemin, Chen Yingtang, Zhang Xuemei. Measurements of Double Differential Cross Sections for ^{40}Ca(n,a)^{37}Ar Reaction at 5.0 and 6.0 MeV. Communication of Nuclear Data Progress N19 (1998) (China Nuclear Information Centre, Atomic Energy Press, Beijing 1998) p. 4-6.
88. Zhang Guohui, Tang Guoyou, Chen Jinxiang, Shi Zhaomin, Liu Guangzhi, Zhang Xuemei, Chen Zemin, Gledenov Yu.M., Sedysheva M., Khuukhenkhuu G. Differential Cross Section Measurements for the ^{6}Li(n,t)^{4}He Reaction at 3.67 and 4.42 MeV. In Communication of Nuclear Data Progress N21 (1999), China Nuclear Information Centre, Atomic Energy Press, Beijing 1999.
89. Пикельнер Л.Б. Воспоминания сотрудника Лаборатории нейтронной физики. Ф.Л. Шапиро: Человек и ученый: Книга воспоминаний, ОИЯИ, 97-377, Дубна,1998, с.107-109 (in Russian).

Theory

1. Bunatian G. Inguiry for the p^+- p^- Bound State Conversion into Two p^0 as Being due to the Weinberg p^+- p^- Interaction. Hadronic Atoms and Positronium in the Standard Model: Proc. of the Intern. Workshop, Dubna, Russia, May 1998. JINR, E2-98-254, Dubna, 1998, p.85-90.
2. Bunatian G.G. Inquiry for the (p^+- p^-) Bound State Conversion into Two p^0 as Being due to the Weinberg p - p Interaction. Nucl. Phys.A., 1999, v.645, N.2, p.314-328.
3. Bunatian G.G. Inquiry for the Conversion on the (p^+- p^-) Bound State into Two p^0. JINR, E4-98-177, Dubna, 1998, p. 16.
4. Bunatian G.G. Inquiry Into Antineutrino Angular Distribution in the Experiments on Polarized Neutron - Decay. JINR, E4-99-62, Dubna, 1999, p.23.
5. Bunatian G.G. On Radiative Corrections to the Strangeness-Conserving -Decay of Free Baryons. ЯФ, 1999, т.62, N.4, p.697-714.
6. Ignatovich V.K., Masahiko Utsuro, Ignatovich Ph.V. Neutron-Electron Interaction: Transmission and Scattering Amplitudes and Interference Corrections. Phys. Rev.C., 1999, v.59, N.2, p.1136-1148.
7. Ignatovich V.K., Radu F., Generalized Matrix Method for the Transmission of Neutrons Through Multilayer Magnetic Systems with Noncollinear Magnetization. PNCMI'98: Proc.of the Second Intern.Workshop on Polarised Neutrons for Condensed Matter Investigations, Grenoble, Sept.1998. Physica B., 1999, Vol.267-268)
8. Ignatovich V.K., Utsuro M. Review of Inelastic Losses of UCN and Quantum Mechanics of the de Broglie Wave Packet. JINR, E4-98-327, Dubna,1998, p. 10.
9. Ignatovich V.K. Принцип инвариантности, или расслоения, в нейтронной оптике и фундаментальные свойства нейтрона. Yad. Fiz., 1999, vol.62, No.5, p.792-806 (in Russian).
10. Lyuboshitz V.V., Lyuboshitz V.L. Замечания о Т-инвариантности и поляризационных эффектах при упругом рассеянии частицы со спином 1/2 на неполяризованной мишени. JINR, P4-98-88, Dubna,1998, p. 10 (in Russian).

Applied Research

1. Cherchintsev V.D., Frontasyeva M.V., Lyapuniv S.M., Smirnov L.I. Biomonitoring air pollution in Chelyabinsk region (Ural mountains, Russia) through trace-elements and radionuclides: temporal and spatial trends, IAEA Report, NAHRES-43, Vienna, 1999, p. 136-154.
2. Frontasyeva M.V. Atmospheric Deposition of Heavy Metals in Some Areas of Russia, Poland and Romania (Project REGATA). In the Book of Abstracts: Workshop «Monitoring of Narural and Man-Made Radionuclides and Heavy Metal Waste in Environment» (2-5 November, 1999, Dubna, Russia), p.23.
3. Frontasyeva M.V., Gorbunov A.V., Gundorina S.F., Lyapunov S.M. and Oprea C., Nuclear and Related Analytical Techniques Used for Workplace Monitoring and Occupational Health Studies. (Part 2). Preprint JINR, E14-99-68, Dubna, 1999.
4. Frontasyeva M.V., Gorbunov A.V., Lyaponov S.M., Oprea C.D. Workplace Monitoring and Occupational Health Studies at the Center for Production of Phosphorus Mineral Fertilizers, Voskresensk (Moscow Region, Russia), Using Nuclear and Related Analytical Techniques. Part I. JINR, E14-98-392, Dubna, 1998, p. 14.
5. Frontasyeva M.V., Grodzinska K., Steinnes E.. Atmospheric deposition of heavy metals in two of the most polluted areas in the world: the copper basin in Poland and the South Ural mountains in Russia. In Proceedings, Int. Conf. Modern Trends in Activation Analysis, MTAA-10, 19-23 April, 1999, Bethesda, Maryland, USA, p. 117.

6. Frontasyeva M.V., Pavlov S.S. Regata Experimental Setup for Air Pollution Studies. Юбилейный сборник СГУ, Дубна, Д-99-123, с.185-193.
7. Frontasyeva M.V., Smirnov L.I., Steinnes E., Cherchintsev V.D., Lyapuniv S.M.. Heavy metal atmospheric deposition study in Chelyabinsk region (South Ural Mountains , Russia) using moss biomonitoring technique and applying ENAA and AAS. Prepint JINR, E14-899-257, Dubna, 1999 (Submitted to the Journal of Radioanalytical and Nuclear Chemistry).
8. Frontasyeva M.V., Steinnes E., Lyapunov S.M., Cherchintsev V.D., Smirnov L.I. Биомониторинг загрязнения промышленных зон Южного Урала тяжелыми металлами с использованием ядерно-физических методов анализа. В Сб. «Экология промышленных регионов на рубеже XXI века», Magninogorsk, 1999, p. 7-13 (in Russian).
9. Lavdansky P.A., Engovatov I.A., Frontasyeva M.V. Activation of Shielding and Construction Materials in the Problem of Nuclear Power Plant Decommissioning. In the Book of Abstracts: Workshop «Monitoring of Narural and Man-Made Radionuclides and Heavy Metal Waste in Environment» (2-5 November, 1999, Dubna, Russia), p. 64.

Contribution to the Conferences & Schools

1. Beer H., Sedyshev P.V., Popov Yu.P., Mohr P., Stadler W., Oberhummer H., Rochow W. Neutron Capture of ^{22}Ne, ^{30}Si, and ^{40}Ar at Thermonuclear Energies. 10th Int. Symposium on Capture Gamma-Ray Spectroscopy and Related Topics, Santa Fe, New Mexcio, USA, 30. 8.-3. 9. 1999 (Abstracts).
2. Boneva S.T., Vasilieva E.V., Sukhovoj A.M., Khitrov V.A. Двухквантовые гамма- каскады после захвата тепловых нейтронов в ^{187}Os. Международное совещание по физике атомного ядра: Тезисы докладов 48 совещания по ядерной спектроскопии и структуре атомного ядра, Moscow, June 1998. St-Petersburg, 1998, p.72.
3. Boneva S.T., Vasilieva E.V., Sukhovoj A.M., Khitrov V.A. Каскадный гамма-распад компаунд-состояния ^{190}Os. Международное совещание по физике атомного ядра: Тезисы докладов 48 совещания по ядерной спектроскопии и структуре атомного ядра, Moscow, June 1998. St-Petersburg, 1998, p.73.
4. Bunatian G.G. Inquiry for the (p^+- p^-) Bound State Conversion into Two p^0 as Being due to the Weinberg p - p Interaction. Mesons and Light Nuclei '98: Proc. of the 7th Conf., Prague-Pruhonice, Czech Republic, Aug. - Sept. 1998., Singapore etc.: World Sci., 1999, p.56-61.
5. Ermakova E.V., Frontasyeva M.V., Pavlov S.S. Эпитепловой нейтронный активационный анализ мхов биомониторов, используемых для определения атмосферных выпадений тяжелых металлов в районе Ясной Поляны (Тульская область). Тезисы в Трудах «Третья открытая научная конференция молодых ученых и специалистов ОИЯИ», Dubna, 15-19 February 1999, Д-99-94, p. 59.
6. Furman W.I. Ядерное деление резонансными нейтронами. VIII School on Neutron Physics, Dubna, August- September 1998. JINR, P3-98-240, Dubna,1998, p.39 (in Russian).
7. Galinskaya T.E., Frontasyeva M.V., Ramadan A.B. Изучение недельных циклов элементов-загрязнителей в Великой Каирской долине Египта. Тезисы в Трудах , «Третья открытая научная конференция молодых ученых и специалистов. JINR, Dubna, 15-19 February 1999», Д-99-44, с. 27.
8. Gledenov Yu.M., Machrafi R., Oprea A., Salatski V.I., Sedyshev P.V., Szalanski P.I.. Determination of the Forward Backward Asymmetry Coefficient in the ^{35}Cl(n,p)^{35}S Reaction. In: E3-99-212, ISINN-7, p. 229-232.
9. Gledenov Yu.M., Machrafi R., Oprea A.I., Sedyshev P.V., Salatski V.I., Andrzejewski J., Szalanski P.I.. Characteristics of an Ionization Chamber for (n,p) and (n,a) Reaction on Gaseous Targets. In:E3-99-212, ISINN-7, p.303-307.
10. Gledenov Yu.M., Mashrafi R., Oprea A., Popov Yu.P., Sedyshev P.V.. A Study of Angular Correlation in (n,p) Reaction. In:E3-99-212, ISINN-7, p.295-302.
11. Gledenov Yu.M., Oprea A., Salatski V.I., Sedyshev P.V., Szalanski P.I., Vesna V.A., Okunev I.S.. A Search for P-odd and P-even Correlation in the ^{35}Cl(n,p)^{35}S Reaction. In: Intern.Nucl.Phys.Conf., August 24-28, Paris, France, 1998, Abstracts of contributed papers, p.716.
12. Gledenov Yu.M., Salatski V.I., Sedyshev P.V., Szalanski P.I., Andrzejewski J., Zak A.. Test of GIC with Gaseous Samples and Measurements of (n,a) Cross Sections. In: Intern. Nucl. Phys. Conf., August 24-28, Paris, France, 1998, Abstracts of Contributed Papers, p.769.
13. Gledenov Yu.M. et al. Нейтронные исследования для ядерной астрофизики. Международное совещание по физике атомного ядра: Тезисы докл. 48 совещ. по яд. спектроскопии и структуре ат. ядра, Moscow, June 1998. St-Petersburg, 1998, p.202 (in Russian).
14. Gledenov Yu.M. Нейтронные реакции с вылетом заряженных частиц. VIII Shool on Neutron Physics, Dubna, August-September 1998. JINR, P3-98-240, Dubna, 1998, p.32 (in Russian).

15. Gledenov Yu.M., Sedyshev P.V., Keler P., Bar N. Коэффициенты асимметрии в реакции $^{35}Cl(n,p)^{35}S$. 2-я Открытая научная конференция молодых ученых и специалистов ОИЯИ,. Dubna, March 1998. Труды конференции, JINR Д-98-224, Dubna,1998, p.12-14.
16. Kuharska A., Grodzinska R., Frontasyeva M.V., Gundorina S.F., Ostovnaya T.M. Изучение атмосферных выпадений тяжелых металлов в Центральной Европе (Медный бассейн в Польше) с помощью мхов-биомониторов и ядерно-физических методов (нейтронный активационный анализ и атомная абсорбция). Тезисы в Трудах: «Третья открытая научная конференция молодых ученых и специалистов. JINR, Dubna, 15-19 February 1999», Д-99-44, p. 62 (in Russian).

Nikonov V.V., Lukina N.V., Frontasyeva M.V., Steinnes E. Trace Elements in Al-Fe Humus Podzols of Boreal Forests. In the Book of Abstracts: Workshop «Monitoring of Narural and Man-Made Radionuclides and Heavy Metal Waste in Environment» (2-5 November, 1999, Dubna, Russia), p. 55.

1. Oprea C., Shorenkova O. and Komkova L., GIS -gestuzte Datenprasentation fur Umweltdaten. Okosystemare Ansatze in der Okotoxikologie, 18-19 May 1998, Zittau, Germany, p.176.
2. Oprea C., Timofte L., Cozma F., Frontasyeva M.V., Steinnes E., et.al. Heavy Metal Atmospheric Deposition in Transilvania Studied by Moss Biomonitoring Technique Using ENAA and AAS. In the Book of Abstracts: Workshop «Monitoring of Narural and Man-Made Radionuclides and Heavy Metal Waste in Environment» (2-5 November, 1999, Dubna, Russia), p. 54.
3. Oprea K., Frontasyeva M.V., Gundorina S.F., Gorbunov A.V., Lyapunov S.M. Ядерно-физические методы, используемые в решении задач мониторинга на рабочих местах и здоровья человека. Тезисы в Трудах , «Третья открытая научная конференция молодых ученых и специалистов ОИЯИ, Dubna, 15-19 February 1999», Д-99-44, p. 65.
4. Oprea K.D. GIS-представление данных для изучения окружающей среды. 2-я Открытая научная конференция молодых ученых и специалистов ОИЯИ, Dubna, March 1998. Труды конференции, JINR, Д-98-224, Dubna, 1998, p.146-147.
5. Oprea K.D. Подвижность и доступность ^{137}Cs и его отношение к стабильному Cs в дельте Дуная: озеро Надежды. 2-я Открытая научная конференция молодых ученых и специалистов JINR, Dubna, March 1998. Труды конференции, JINR, Д-98-224, Dubna, 1998, p.146.
6. Protopopescu D. Deformation of Nuclei Near the Top of Potential Barrier. 2-я Открытая научная конференция молодых ученых и специалистов ОИЯИ, Дубна, март 1998. Труды конференции, ОИЯИ, Д-98-224, Дубна,1998, с.61-63.
7. Samosvat G.S. Рассеяние нейтронов ядрами и фундаментальные свойства нейтрона. VIII School on Neutron Physics, Dubna, August-September 1998. JINR, P3-98-240, Dubna,1998, p.36 (in Russian).
8. Serov D.G. Многопараметрический анализ данных при гамма- спектроскопии осколков деления на импульсном источнике нейтронов. 2-я Открытая научная конференция молодых ученых и специалистов ОИЯИ, Dubna, March 1998. Труды конференции, JINR, Д-98-224, Dubna, 1998, p.38.
9. Shvetsov V.N. Ультрахолодные нейтроны и фундаментальные проблемы физики. VIII School on Neutron Physics, Dubna, August-September 1998. JINR, P3-98-240, Dubna,1998, p.20 (in Russian).
10. Smirnov L.I. ЭНАА мхов-биомониторов для определения атмосферных выпадений тяжелых металлов (район магнитогорского металлургического комбината, Челябинская область). 2-я Открытая научная конференция молодых ученых и специалистов ОИЯИ, Dubna, March 1998. Труды конференции, JINR, Д-98-224, Dubna, 1998, p.147.
11. Strelkov A.V. Эксперименты с УХН. VIII School on Neutron Physics, Dubna, August-September 1998. JINR, P3-98-240, Dubna,1998, p.37 (in Russian).
12. Sukhovoj A.M. Каскады гамма- лучей радиационного захвата нейтронов. VIII School on Neutron Physics, Dubna, August-September 1998. JINR, P3-98-240, Dubna,1998, p.38 (in Russian).
13. Tretyakova T.Yu., Lanskoy D.E. L Binding Energy in Neutron-Rich Hypernuclei. Heavy Ion Physics: Proc. VI Intern. School Seminar, Dubna, Sept. 1997. Singapore etc.: World Sci., 1998, p. 187-189.
14. Vasilieva E.V., Sukhovoj A.M., Khitrov V.A., Honzatko J., Tomandl I., Bondarenko V.A., Simonova L.I. Спектроскопия состояний деформированных ядер до энергии возбуждения E_{ex}~3-4 МэВ. Международное совещание по физике атомного ядра: Тезисы докладов 48 совещания по ядерной спектроскопии и структуре атомного ядра, Moscow, June 1998.St-Petersburg, 1998, p.44.
15. Vesna V.A., Okunev I.S., Shul'gina E.V., Gledenov Yu.M., Popov Yu.P., Lebedev-Stepanov P.V., Sinyakov A.V., Tchuvil'sky Yu.M.. Parity Violation in B and Li Nuclei in Reactions with Polarized Thermal Neutrons. In: Intern.Nucl.Phys.Conf., August 24-28, Paris, France, 1998, Abstracts of Contributed Papers, p.717.
16. Zeinalov Sh.S. Регистрация и идентификация заряженных частиц при делении атомных ядер. VIII School on Neutron Physics, Dubna,August-September. 1998. JINR, P3-98-240, Dubna,1998, p.33 (in Russian).

17. Zhang Guohui, Tang Guoyou, Chen Jinxiang, Shi Zhaomin, Liu Guangzhi, Zhang Xuemei, Chen Zemin, Gledenov Yu.M., Sedysheva M., Khuukhenkhuu G.. Differential Cross Section Measurements for the $^{6}Li(n,t)^{4}He$ Reaction at 3.67 and 4.42 MeV. In: ISINN-7 (Dubna 1999), 1999, p.219-224.
18. Пикельнер L.B. Нейтронная спектроскопия. VIII School on Neutron Physics, Dubna, August-September 1998. JINR, P3-98-240, Dubna,1998, p.35 (in Russian).

THE IBR-2 SPECTROMETER COMPLEX AND COMPUTATION INFRASTRUCTURE

1. Chkhalo N., Gebauer B., Levchanovsky F. et al. Development of Large-Area Hybrid Low-Pressure 2D-MSGC Detectors for Neutron Imaging. Proc. of Intern. Workshop on Micro-Pattern Gas Detectors, Orsay, France, June 28-30, 1999.
2. Fromme M., Hoffman-Schulz G., Litvinenko E., Zeim R. «BEAN - A New Standard Program for Data Analysis at BER-II». Proc. of Intern. Conf. RT'99 (June 1999, Santa Fe, USA).
3. IvankinaT.I., Kirilov A.S. et al. An Experimental and Measuring Complex of Neutronography Structure and Texture Analysis to Investigate the Transitional Processes and Physical Properties of Geomagnetic Materials under the Action of Mechanical and Thermal Effects. «Zavodskaya Laboratoriya, Diagnostica Materialov (Industrial laboratory, Diagnostics of materials)», 1999, No. 8, v.65, p. 26-33 (in Russian).
4. Kirilov A.S. et al. A VME-Based Accumulation, Control and Supervising System for Neutron Texture Measurements. Textures and Microstructures, 1999, vol. 33, p. 329-336.
5. Litvinenko E.I., Zhidkov E.P. "Some Methods of Neutron Scattering Data Analysis". Computer Physics Communications, 1999 (in press).
6. Litvinenko E.I.. Methods and Programs for Express-Analysis of Neutron Scattering Data. JINR, 10-99-219, Dubna, 1999.

6. PRIZES

JINR Prizes:

In Experimental Physics:

Second Prize:

A.A.Bogdzel, J.Kliman, Yu.N.Kopach, A.B.Popov, W.I.Furman, N.N.Gorin, L.K.Kozlovsky, D.I.Tambovtsev, A.L.Barabanov. «Investigations of the angular anisotropy of fission fragments from the resonance neutron induced fission of ^{235}U aligned nuclei and the role of JK-channels»

In Scientific and Technical Applied Field:

Second Prize:

V.V.Golikov, L.B.Golovanov, S.M.Golubykh, E.N.Kulagin, V.V.Kukhtin, K.Lerua, V.I.Luschikov, V.F.Minashkin, H.Oberlak, A.P.Cheplakov. «An installation for radiation research at the IBR-2 reactor»

FLNP Prizes:

In Nuclear Physics:

First Prize:

D.G.Kartashov, E.V.Lychagin, A.Yu.Muzychka, G.V.Nekhaev, A.V.Strelkov, V.N.Shvetsov. «Discovery and investigation of supersmall UCN energy transfers from the walls of the vessel»

Second Prize:

E.V.Vasilieva, A.M.Sukhovoj, V.A.Khitrov. «Direct experimental estimate of the parameters determining the gamma-decay of the compound states of heavy nuclei»

Third Prize:

A.V.Voinov, N.A.Gundorin, A.P.Kobzev, S.S.Parzhitskii, Yu.P.Popov, P.V.Sedyshev, M.V.Sedysheva, D.G.Serov. «Pdevelopment of a new method of neutron spectroscopy and the first measurements of partial cross sections of radiative neutron capture»

In Condensed Matter Physics:

First Prize:

V.L.Aksenov, A.M.Balagurov, V.Yu.Pomyakushin, D.V.Sheptyakov. «Magnetic atomic structure of CMR-magnetics»

Second Prize:

T.I.Ivankina, A.N.Nikitin, A.S.Telepnev, K.Ullemeier. «Texture neutronography and anisotropic properties of rocks at high pressure»

Third Prize:

A.V.Belushkin, D.P.Kozlenko, B.N.Savenko. Investigations of the dynamics of ammonium ions in ammonium halides»

In Applied Physics:

Third Prize:

Yu.G.Abov, V.P.Alfimenkov, E.M.Galinskii, L.Lason, Yu.D.Mareev, V.V.Novitskii, L.B.Pikelner, V.M.Tsulaya, M.I.Tsulaya, L.P.Chernenko. «Spectrometer of polarized neutrons»;

V.B.Zlokazov. «Programs of automated processing of physical information»

The JINR young scientists contest in condensed matter and nuclear physics with neutrons:

Scientific Research:

First Prize:

D.E.Burilichev. «Investigations of olivine-containing xenolites by meams of neutron diffraction and ultrsounding»

7. SEMINARS

Date	Authors	Title
25.02.99	A.P.Khokhlov (MSU, Moscow)	Nanostructures in ion-containing polymeric systems
26.03.99	S.T.Belyaev (RRC KI, Moscow)	Interaction of ultracold neutrons and matter (theory)
15.04.99	B.V.Vasiliev	Astrophysical effects related to electric polarization of matter
12.05.99	V.P.Skulachev (MSU, Moscow)	Some problems of the biology of the XXI century
10.06.99	A.A.Vazina (Inst. of Theor. and Exper. Biology, Pushchino)	Use of synchrotoron radiation for the investigation of the structure of biological objects
19.10.99		Seminar on the occasion of the awarding of the Frank Prize for 1998. Prize winners: Prof. Yu.Ya.Stavissky (INR RAS, Moscow, Russia) Prof. J.Carpenter (ANL, USA)

8.1. STRUCTURE OF LABORATORY AND SCIENTIFIC DEPARTMENTS

Directorate:
Director:
V.L.Aksenov
Deputy Directors:
A.V.Belushkin
W.I.Furman
Scientific Secretary:
V.V.Sikolenko

Reactor and Technical Departments
Chief engineer: V.D.Ananiev
IBR-2 reactor
Chief engineer: A.V.Vinogradov
IBR-30 booster + LUE-40
Head: S.A.Kvasnikov
Mechanical maintenance division
Head: A.A.Belyakov
Electrical engineering department
Head: V.P.Popov
Design bureau
Head: V.I.Konstantinov
Experimental workshops
Head: A.N.Kuznetsov

Scientific Departments and Sectors
Condensed matter department
Head: V.L.Aksenov
Nuclear physics department
Head: V.N.Shvetsov
Department of IBR-2 spectrometers complex
Head: A.V.Belushkin
Department of IREN
Head: A.P.Sumbaev
Nuclear Safety and applied research
Head: V.I.Luschikov

Administrative Services
Deputy Director: S.V.Kozenkov
Secretariat
Finances
Personnel

Scientific Secretary Group
Translation
Graphics
Photography
Artwork

CONDENSED MATTER DEPARTMENT

Sub-Division	Title	Head
Diffraction sector. Head: A.M.Balagurov		
Group No.1	HRFD	V.Yu.Pomjakushin
Group No.2	DN-2	A.I.Beskrovnyi
Group No.3	DN-12	B.N.Savenko
Group No.4	NSVR	K.Ullemeyer
Small-angle neutron scattering group. Head: V.I.Gordeliy		
Neutron optics sector.		
Group No.1	SPN-1	Yu.V.Nikitenko
Group No.2	REFLEX	D.A.Korneev
Inelastic scattering group. Head: I.Natkaniec		

NUCLEAR PHYSICS DEPARTMENT

Sub-Division	Title	Head
Group No.1	Polarized neutrons and nuclei	Yu.D.Mareev
Group No.1	Neutron spectroscopy	A.B.Popov
Group No.3	Nuclear fission	Sh.S.Zeinalov
Group No.4	Thermal polarized neutrons	M.I.Tsulaya
Group No.5	Proton and α-decay	Yu.M.Gledenov
Group No.6	Properties of γ-quanta	A.M.Sukhovoy
Group No.7	Neutron structure	G.S.Samosvat
Group No.8	Ultra-cold neutrons	V.N.Shvetsov
Group No.9	Neutron optics	A.I.Frank
Group No.10	Neutron activation analysis	M.V.Frontasyeva
Group No.11	Theory	Yu.A.Alexandrov

DEPARTMENT OF IBR-2 SPECTROMETERS COMPLEX

Sub-Division	Title	Head
Sector No.1	Electronics	V.I.Prikhodko
Group No.1	Analogous electronics	A.A.Bogdzel
Group No.2	Digital electronics	V.F.Levchanovsky
Group No.3	Software	A.S.Kirilov
Group No.4	Local networks	G.A.Sukhomlinov
Group No.5	Technology	A.B.Melnichuk
Sector No.2	Spectrometers	V.V.Zhuravlev
Group No.1	Development	G.A.Varenik
Group No.2	Samples environment	A.P.Sirotin
Group No.3	Detectors	J.Sokolovsky

8.2. USER POLICY

The IBR-2 reactor usually operates 10 cycles a year (2500 hrs.) to serve the experimental programme. A cycle is established as of 2 weeks of operation for users, followed by a one week period for maintenance and machine development. There is a long shut-down period between the end of June and the middle of October.

All experimental facilities of IBR-2 are open to the general scientific community. The User Guide for neutron experimental facilities at FLNP is available by request from the Laboratory's Scientific Secretary.

Condensed matter studies at IBR-2 have undergone some changes in accordance with the experience gained during the last several years. It was found to be necessary to establish specialized selection committees formed of independent experts in their corresponding fields of scientific activities. The following four committees were organized:

1. Diffraction *Chairman* - V.A.Somenkov - Russia	3. Neutron optics *Chairman* - A.I.Okorokov - Russia
2. Inelastic scattering *Chairman* - J.Janik - Poland	4. Small angle scattering *Chairman* - L.Cser - Hungary

Dr. Vadim V. Sikolenko, Scientific Secretary of FLNP, is responsible for the user policy. Two deadlines for proposal submission are: May 16 - for the experimental period from October through February; and October 16 - for the period from March through June.

Scientific Secretary is responsible for:

- distribution of "Application for Beam Time" forms to potential users;
- registration of submitted proposals;
- reviewing of the proposals by instrument scientists to estimate the technical feasibility of the proposed experiment;
- sending of the approved proposals to Members of Selection Committees and registration of their comments and recommendations.

The IBR-2 beam schedules are drawn up by the head of the Condensed Matter Department together with instruments responsibles on the basis of experts recommendations and are approved by the FLNP Director or Deputy Director for condensed matter physics. The schedules are sent to Chairmen of Selection Committees.

After the completion of experiments, "Experimental Report" forms are filled out by experimenter(s) and submitted to the Scientific Secretary.

The Application Form and other information about FLNP are available by WWW: http://nfdfn.jinr.ru/~sikolen/usepol.html

Contact address:
***Dr. V.Sikolenko**, Frank Laboratory of Neutron Physics*
Joint Institute for Nuclear Research
141980 Dubna, Moscow region, Russia
Tel.: (+7)-095-926-22-53, (+7)-09621-65096, Fax: (+7)-09621-65085; (+7)-09621-65484;
E-mail: sikolen@nf.jinr.ru

8.3. MEETINGS AND CONFERENCES

In 1999, FLNP organized the following meetings:

1.	VII International Seminar on Interaction of Neutrons with Nuclei (ISINN-7)	May 25-28	Dubna
2.	II International Seminar on Neutron Scattering at High Pressure (NSHP-II)	September 29-October 2	Dubna

In 2000, FLNP will organize the following meetings:

1.	VIII International Seminar on Interaction of Neutrons with Nuclei	May 16-19	Dubna
2.	II International Workshop on Data Taking Systems in Neutron Source Experiments (DANEF'2000)	June 5-7	Dubna
3.	III International Seminar on Relaxor Ferroelectrics	June 14-17	Dubna

8.4. COOPERATION

List of Visitors from Non-Member States of JINR in 1999

Name	Organization	Country	Dates
Magdy Ibrahim Khalil El-Shareqawy	NRC, AEA, Cairo	Egypt	01.01-01.04
R.Machrafi	Univ.Mohamed V.Rabat	Marocco	01.01-25.08
	IzfP, Dresden		15.01-05.02
	ILL, Grenoble		17.01-30.01
	ILL, Grenoble		17.01-30.01
M.Janich	Univ. Halle-Saale	Germany	20.01-28.01
J.Lange	Univ. Halle-Saale	Germany	20.01-28.01
M.Jung	Univ. Darmstadt	Germany	23.01-30.01
K.Walther	GeoFRZ, Potsdam	Germany	08.03-19.03
M.Rudalics	Johannes Kepler University, Linz	Austria	19.03-30.04
A.Zidansek	J.Stefan Institute, Ljubljana	Slovenia	21.03-28.03
F.Haeussler	Univ. Leipzig	Germany	11.04-17.04
G.Klose	Univ. Leipzig	Germany	16.04-27.04
	ILL, Grenoble	France	19.04-27.04
	ILL, Grenoble		19.04-24.04
B.Gross	Firme TUMTECH, Muenchen	Germany	27.04-30.04
T.Hecks	Firme TUMTECH, Muenchen	Germany	27.04-30.04

P.Joerchel	Univ. Leipzig	Germany	16.05-23.05
H.-J.Lauter	ILL, Grenoble		
A.Bogdan		Finland	
Kim Guinyun		Korea	
M.Stalder	IzfP, Dresden	Germany	17.05-30.05
T.Wieder	TU Darmstadt	Germany	22.05-28.05
Zhang Guohui	Peking University, Beijing	China	24.05-31.05
T.Decker	Univ. Muenchen	Germany	26.05-30.05
F.Reinold	Univ. Muenchen	Germany	26.05-30.05
V.Lauter	ILL, Grenoble	France	01.06-11.06
H.Barthel	WH Burghausen		12.06-18.06
		Japan	29.06-04.07
Shanker Saxena Siddharth	University of Groningen	The Netherlands	30.06-03.07
D.N.Argyriou	Argonne National Laboratory	USA	30.06-03.07
I.Soloviev	JRC for Atom. Technology, Tsukuba	Japan	30.06-04.07
G.E.Biotteau	LLB, Saclay	France	30.06-05.07
B.Guettler	Univ. Braunschweig	Germany	30.06-07.07
B.Dorner	ILL, Grenoble	France	07.07-14.07
J.Gimaret	ILL, Grenoble		
H.Yasuda	JAERI	Japan	29.09-29.01.2000
Jichen Li	UMIST, Manchester	UK	
	Argonne National Lab.	USA	16.10-20.10
R.De Cardy Carpenter	Argonne National Lab.	USA	16.10-20.10
O.Steinsvoll	Inst. for Energy Technology, Kjeller	Norway	17.10-01.11
L.Steinsvoll	Inst. for Energy Technology, Kjeller	Norway	17.10-01.11
Kim Guinyun	Pohang Accelerator Laaboratory	Korea	24.10-30.10
Zhang Zhaohui	IHEP, Beijing	China	29.10-20.12
E.Steinnes	Univ. of Sc. & Technology, Trondheim	Norway	01.11-07.11
H.-J.Lauter	ILL, Grenoble	France	10.11-18.11
V.Lauter	ILL, Grenoble	France	10.11-18.11
A.Frischbutter	GeoFRZ, Potsdam	Germany	10.11-18.11
K.Walther	GeoFRZ, Potsdam	Germany	12.11-18.11
A.Bogdan	University of Helsinki	Finland	17.11-19.11
K.G.Bramnik	TU Darmstadt	Germany	21.11-27.11
P.Jorchel	Univ. Leipzig	Germany	05.12-17.12
F.Haeussler	Univ. Leipzig	Germany	07.12-13.12

8.5. EDUCATION

The education programme of FLNP is based on the chairs of Lomonosov Moscow State University and Moscow Engineering Physics Institute and admits students of the last two years in higher education institutions who have attended introductory specialized courses or lectures in nuclear physics and investigation of condensed matter at nuclear reactors and accelerators. These specializations are in line with research performed in FLNP which has at its disposal a good experimental base for both sectors comprising the IBR-2 reactor and the IBR-30 booster pulsed neutron sources.

The education and training courses for students affiliated with FLNP have been organized, to a large extent, to prepare specialists in neutron physics for the Laboratory and other Russian neutron centres.

For illustration we present the list of courses taught by lecturers of the Interfaculties Center of Lomonosov Moscow State University «Structure of Matter and New Materials» (Head: Prof. V.L.Aksenov):

- theoretical methods in condensed matter physics
- methods of investigation of condensed matter at nuclear reactors and accelerators
- fundamentals of neutron physics and neutron sources
- methods for structure analysis of ideal and real crystals
- synchrotron radiation spectroscopy of solid matter
- methods of experimental data processing.

A number of leading FLNP scientists take part in delivering these courses. Each student has access to the Laboratory computer network. An obligatory condition for successful completion of the 4th year is skillful to use of modern personal computers. Students are included in research groups led by their instructors. This makes it possible for undergraduate students working on their theses to take part in preparing or performing experiments.

In 1999, the training proceeded successfully. Six students who had their training course at FLNP were employed by JINR and other scientific centers in Russia.

The Interfaculties Center gave graduation certificates to its seventh group of students in the reported year. The group had 2 students making the total number of students who graduated from the Center equal 47. One of them has been employed by FLNP and joined the young scientists who have renewed the staff of the FLNP Scientific Department of Condensed Matter Physics to a noticeable degree.

8.6. PERSONNEL

Distribution of the Personnel per Department as of 01.01.2000

Theme	Departments	Main staff
-0974-	Nuclear Physics Department	58
-1031-	Condensed Matter Physics Department	54
-1012-	IBR-2 Spectrometers Complex Department	50.5
-0993-	IREN Department	33
-1007-	Nuclear Safety Sector	15
-0851-	IBR-2 Department	51
	Mechanical and Technical Department	61
	Electric and Technical Department	34
	Central Experimental Workshops	39
	Design Bureau	8
	FLNP infrastructure:	
	Directorate	5
	Services and Management Department	18
	Scientific Secretary Group	7
	Staff Management Group	5.5
	Supplies Group	3
Total		**442**

Personnel of the Directorate as of 01.01.2000

Country	People
Azerbaijan	1
Armenia	1
Bulgaria	8
Egypt	1
Germany	4
Georgia	2
Kazakhstan	1
Mongolia	3
Poland	8
Romania	3
Russia	18
Ukraine	1
TOTAL	**51**

8.7. FINANCE

Financing of the FLNP Scientific Research Plan in 1999 (th. USD)

No.	Theme	Financing plan, $ th.	Expenditures for 12 months, $ th.	In % of FLNP budget
I	**Condensed matter physics**	**4059.1**	**1376.3**	**33.9**
	-1031-	2357.4	808.0	34.3
	-0851-	1182.8	333.8	28.2
	-1012-	518.9	234.5	45.2
II	**Neutron nuclear physics**	**1119.1**	**1180.0**	**105.4**
	-0974-	619.1	377.4	60.9
	-0993-	500.0	802.6	160.5
III	**Elementary particle physics**			
	-1007-	**6.1**	**22.3**	**365.6**
IV	**Relativistic nuclear physics**			
	-1008-	**41.6**	7.0	**16.8**
V	**TOTAL:**	**5225.9**	**2585.6**	**49.5**